

# **Multi-incidence angle soil moisture retrieval using passive microwave data at L-band**

by

**Sandy Peischl**

Diplom-Geoökologin (M.Sc.)

Thesis submitted in total fulfillment  
of the requirements of the degree of

Doctor of Philosophy

Department of Civil Engineering  
Monash University  
Australia

---

**Multi-incidence angle soil moisture retrieval using passive microwave data at L-band**

Sandy Peischl

Department of Civil Engineering, Monash University, Australia

Ph.D. Thesis, Melbourne

Supervision:

Prof. Jeffrey P. Walker and Dr Christoph Rüdiger, Monash University, Australia

Dr Dongryeol Ryu, The University of Melbourne, Australia

Dr Yann H. Kerr, Centre d'Etudes Spatiales de la Biosphère (CESBIO), France

This research has been funded by the Australian Research Council grant DP0879212 in the framework of the MoistureMap project.

© 2017 by S. Peischl

All Rights Reserved.

---

Für Euch hoch oben, Oma Ilse & Opa Karl.

Für Dich hier bei mir, Olaf.



---

**Declaration**

I hereby declare that this thesis contains no material which has been accepted for the award of any other degree or diploma in any university or equivalent institution, and that, to the best of my knowledge and belief, this thesis contains no material previously published or written by another person, except where due reference is made in the text of the thesis.



.....

Sandy Peischl (March 2017)



---

## Abstract

**T**HIS thesis investigates the potential of multi-incidence angle L-band measurements to enhance the retrieval process of near-surface soil moisture information from passive microwave data. In particular, it examines remotely sensed multi-angle observations collected over Australia by both airborne and spaceborne systems at varying spatial and temporal resolution. Initial work focussed on the adaption of one of the current state-of-the-art retrieval algorithms called L-band Microwave Emission of the Biosphere (L-MEB) to multi-angle measurements. Subsequently, the modified model was applied to three independent sets of field data to evaluate different aspects of the retrieval mechanism. Two out of the three available datasets were collected prior to the Soil Moisture and Ocean Salinity Mission (SMOS) launch in 2009. However, the third field experiment named Australian Airborne Cal/val Experiments for SMOS (AACES) was specifically designed for calibration and validation of SMOS. The design and realisation of this intensive field campaign, which was conducted twice in summer and winter, was a vital part of this Ph.D. The multi-incidence angle research included an initial assessment on the performance of specific model parameterizations by comparison with ground data. Further analysis focussed on partly synthetic studies on the accuracy of simultaneously derived model parameters at various angular groups and parameter combinations. Findings from the previous research were then tested on the newly available AACES dataset, which in turn was used to evaluate the performance of the spaceborne L-band sensor of SMOS. The findings from the synthetic study and the field measurements were compiled and ultimately aim at supporting a better understanding and utilization of multi-incidence angle observations for the purpose of large scale soil moisture mapping.



---

## Acknowledgements

There are a lot of people that I'm thankful for being part of this journey and significant milestone in my life.

First of all, I would like to thank my principal supervisor Jeffrey Walker. You were the one who made the adventure of OZ possible in the first place. Thank you for this opportunity! Through your guidance, patience and persistent motivation this work has come a long way. During all that time you didn't give up on me, so how could I?

The start of a new period of life on the other side of the world might be challenging but I instantly felt welcome - especially when I learnt, there is someone who speaks my language - not my dialect though. Christoph Rüdiger, I also want to say "Dankeschön" for your help, discussions and advice throughout my research. Moreover, I would like to thank my supervisor at Melbourne University, Dongryeol Ryu, who more than once opened my eyes to look at things at a different viewing angle.

A special "thank you" goes to my supervisor, Yann Kerr. I'm grateful that you accepted my nomination as international supervisor even though you probably already had a lot of work with the upcoming launch of SMOS just a few months later. I highly appreciate your valuable and encouraging input in my research. You gave me the chance to come over to Toulouse for several occasions to work closely with you and your wonderful team at CESBIO. Speaking of, I want to acknowledge Phillippe Richaume and François Cabot for the time they spent to explain to me the technical and mathematical background of some of the algorithms over and over again. Further, I'm grateful to have shared the experience of that huge Australian field experiment with some people of the CESBIO team who I call friends by now: "Delphine, let's shake off that mud.", "Simone, let's make time stand still.", and "Arnaud, let's write a handbook on Matlab!". Over these past years you all became big supporters. Merci beaucoup!

In terms of the field work and all the people that voluntarily participated in such an extensive experiment and got up at 4 am in the morning. Thank you for all those memorable moments out there in the outback. A special thanks goes to Rodger Young

whose creativity in repairing and fixing instruments was a valuable asset for the success of the field experiments.

And back in the office, what would I be without you, Ye Nan, Ranmalee, Rocco? Ye Nan, my lifetime friend with your indispensable programming skills. Ranmalee, the one and only queen of coconut rice. Rocco, the scientist and master of the art of living. In general at the department the “motley crew”: Sandra, Gayani, Anja, Stefania, Ying, Ling and Narelle, I always enjoyed your company and positive energy.

I also want to say “Danke” to my family and friends. Your postcards/little surprise parcels and skype calls made the time difference and spatial distance insignificant. It was so great to even have you, Sven & Mirka, with me on the southern hemisphere; and to find my special place like home with my little Colombian family around me. Last but not least, Olaf, you deserve the spotlight for being a vital part of this adventure and your continuous support throughout all these years.

---

## Declaration for thesis by publication

*General Declaration for thesis based or partially based on conjointly published or unpublished work*

In accordance with Monash University Doctorate Regulation 17 / Doctor of Philosophy and Master of Philosophy (MPhil) regulations the following declarations are made:

This thesis includes 3 original papers published in peer reviewed journals and 1 publication which is currently in press. The core theme of the thesis is “Multi-incidence angle soil moisture retrieval using passive microwave data at L-band”. The ideas, development and writing up of all the papers in the thesis were the principal responsibility of myself, the candidate, working within the Department of Civil Engineering under the supervision of Prof Jeffrey Walker, Dr Christoph Rüdiger, Dr Dongryeol Ryu and Dr Yann Kerr.

The inclusion of co-authors reflects the fact that the work came from active collaboration between researchers and acknowledges input into team-based research. In the case of chapters 3-6 my contribution to the published work involved the following:

**Table 1:** Details on candidates journal publications

Thesis Chapter	Publication Title	Publication Status	Nature and Extent of candidate’s contribution
3	Wheat canopy structure and surface roughness effects on multi-angle observations at L-band	published	Review of literature, data processing and interpretation, and write up.
4	Sensitivity of multi-parameter soil moisture retrieval to incidence angle configuration	published	Idea, data processing and interpretation, and write up.
5	Analysis of data acquisition time on soil moisture retrieval from L-Band observations	in press	Idea, data processing and interpretation, and write up.
6	The AACES field experiments: SMOS calibration and validation across the Murrumbidgee River catchment	published	Experimental design, data collection, data processing and interpretation, and write up.

Declaration signature:



.....

Sandy Peischl

---

Following a full list of all publications that have resulted from the studies undertaken for this degree:

#### **Peer-reviewed Journal Paper**

1. **Peischl, S.**, Walker, J., Ryu, D., and Kerr, Y. (2017): Analysis of data acquisition time on soil moisture retrieval from L-Band observations, *IEEE Transactions on Geoscience and Remote Sensing*, *IEEE Transactions on Geoscience and Remote Sensing*, accepted for publication.
2. **Peischl, S.**, Walker, J., Ye, N., Ryu, D. and Y. Kerr (2014): Sensitivity of multi-parameter soil moisture retrievals to incidence angle configurations, *Remote Sensing of Environment*, 143(0), 64-72, doi: <http://dx.doi.org/10.1016/j.rse.2013.11.019>.
3. **Peischl, S.**, Walker, J., Ryu, D., Kerr, Y., Panciera, R. and C. Rüdiger (2012): Wheat canopy structure and surface roughness effects on multi-angle observations at L-band, *IEEE Transactions on Geoscience and Remote Sensing*, 50(5), pp. 1498-1506, doi: 10.1109/TGRS.2011.2174644.
4. **Peischl, S.**, Walker, J., Rüdiger, C., Ye, N., Kerr, Y., Kim, E., Bandara, R. and M. Allahmoradi (2012): The AACES field experiments: SMOS calibration and validation across the Murrumbidgee River catchment, *Hydrology and Earth System Sciences Discussions*, 16(6), 1697-1708, doi: 10.5194/hess-16-1697-2012.

#### **Peer-reviewed Conference Paper**

1. **Peischl, S.**, Walker, J., Ryu, D., Ye, N. and Kerr, Y. (2011). Soil moisture retrieval from multi-incidence angle observations at L-band. In Chan, F, Marinova, D. and Anderssen, R.S. (eds) *MODSIM2011, 19th International Congress on Modelling and Simulation*. Modelling and Simulation Society of Australia and New Zealand, Perth, December 2011, pp. 1987-1993. ISBN: 978-0-9872143-1-7. invited paper (see appendix A).
2. **Peischl, S.**, J. Walker, M. Allahmoradi, D. Baret, R. Gurney, Y. Kerr, E. Kim, J. LeMarshall, C. Rüdiger, D. Ryu, and N. Ye (2009). Towards Validation of SMOS using Airborne and Ground Data over the Murrumbidgee Catchment. In Anderssen, R.S., Braddock, R.D. and L.T.H. Newham (eds) *18th World IMACS Congress and MODSIM09 International Congress on Modelling and Simulation*.

---

Modelling and Simulation Society of Australia and New Zealand and International Association for Mathematics and Computers in Simulation, Cairns, July 2009, pp. 3733-3739. ISBN: 978-0-9758400-7-8 (see appendix B).

3. Rüdiger, C., J.P. Walker, M. Allahmoradi, D. Barrett, J. Costelloe, R. Gurney, J. Hacker, Y. Kerr, E. Kim, J. Le Marshall, W. Lief, A. Marks, **S. Peischl**, D. Ryu and N. Ye (2009). Identification of Spaceborne Microwave Radiometer Calibration Sites for Satellite Missions. In Anderssen, R.S., R.D. Braddock and L.T.H. Newham (eds) 18th World IMACS Congress and MODSIM09 International Congress on Modelling and Simulation. Modelling and Simulation Society of Australia and New Zealand and International Association for Mathematics and Computers in Simulation, Cairns, July 2009, pp. 3740-3746. ISBN: 978-0-9758400-7-8 (see appendix C).

#### **Conference Presentation/Poster**

1. **Peischl, S.**, J. Walker, C. Rüdiger, D. Ryu and Kerr, Y. (2013): Assessing the angular density of passive microwave L-band data, IEEE International Geoscience and Remote Sensing Symposium (IGARSS), Melbourne, Australia, 21-26 July 2013.
2. **Peischl, S.**, J. Walker, C. Rüdiger, D. Ryu and Kerr, Y. (2012): SMOS multi-incidence angle observations over Australia, IEEE International Geoscience and Remote Sensing Symposium (IGARSS), Munich, Germany, 22-27 July 2012.
3. Rüdiger, C., Walker, J., **Peischl, S.**, Merlin, O., Mialon, A., Kerr, Y. and Kim, E. (2012): SMOS Validation in Australia, AGU Chapman Conference on Remote Sensing of the Terrestrial Water Cycle, Hawaii, USA, 19-22 February 2012.
4. **Peischl, S.**, Walker, J., Rüdiger, C., Ye, N., Ryu, D. and Kerr, Y. (2011): Estimation of soil moisture from multi-angle airborne observations, Monash Postgraduate Conference, Department of Civil Engineering, Monash University, Melbourne, Australia, 22 November 2011.
5. **Peischl, S.**, Walker, J., Rüdiger, C., Ye, N., Ryu, D. and Kerr, Y. (2011): Validation of SMOS multi-incidence angle L1C and L2 products over Australia, SMOS Science Workshop, Arles, France, 27-29 September 2011.
6. **Peischl, S.**, Walker, J., Ryu, D. and Kerr, Y. (2011): Towards soil moisture retrieval using multi-incidence angle observations, European Geosciences Union (EGU) General Assembly, Vienna, Austria, 3-8 April 2011.

- 
7. **Peischl, S.**, J. Walker, D. Ryu, Y. Kerr, C. Rüdiger (2010): Towards multi-incidence angle passive microwave retrieval of soil moisture, 30th IEEE International Geoscience and Remote Sensing Symposium (IGARSS), Honolulu, 25-30 July 2010.
  8. Kim, E., Walker, J, Rüdiger, C., Costelloe, J., Ye, N., **Peischl, S.**, Allahmoradi, M.; Marks, A. (2010): SMOS/MIRAS Calibration Using Earth Surface Targets, ESA Living Planet Symposium, Bergen, Norway, 28 June to 2 July 2010.
  9. **Peischl, S.**, J. Walker, D. Ryu, Y. Kerr, C. Rüdiger (2009): Multi-angle Soil moisture retrieval from SMOS, Civil and Environmental Engineering Postgraduate Conference, The University of Melbourne, Australia, November 2009.
  10. Walker, J., Allahmoradi, M., **Peischl, S.**, Ye, N., Rüdiger, C., Barrett, D., Gurney, R., Kerr, Y., Kim, E., LeMarshall, J., Ryu, D., Calvet, J. (2009): Towards an Australian Validation of SMOS, European Geosciences Union (EGU) General Assembly, Vienna, Austria, April 2009.
  11. Walker, J., Rüdiger, C., Allahmoradi, M., Barrett, D., Costelloe, J., Gurney, R., Hacker, J., Kerr, Y., Kim, E., LeMarshall, J., Lieff, W., Marks, A., **Peischl, S.**, Ryu, D., Ye, N (2009): A Potential Ground Calibration Target for SMOS, European Geosciences Union (EGU) General Assembly, Vienna, Austria, April 2009.
  12. **Peischl, S.**, J. Walker, D. Ryu, C. Rüdiger, R. Panciera, R. Gurney (2008): Moisture Map - Effects of Sensor Look Angle on Soil Moisture Retrieval, Civil and Environmental Engineering Postgraduate Conference, The University of Melbourne, Australia, October 2008.

## Report

1. Walker, J. P, Rüdiger, C., **Peischl, S.**, Allahmoradi, M., Ryu, D., Kerr, Y., Kim, E., Gurney, R., Barrett, D. and Le Marshall, J. (2010): Australian Airborne Cal/val Experiments for SMOS (AACES-2) Winter campaign: Experiment Plan. Department of Civil Engineering, Monash University. 167pp.
2. Rüdiger, C. and **Peischl, S.** (2010): Addendum to the Australian Airborne Cal/val Experiments for SMOS (AACES-2) Winter campaign: Experiment Plan. Department of Civil Engineering, Monash University.
3. Walker, J. P, Rüdiger, C., **Peischl, S.**, Allahmoradi, M., Ryu, D., Kerr, Y., Kim, E., Gurney, R., Barrett, D. and Le Marshall, J. (2010): Australian Airborne

---

Cal/val Experiments for SMOS (AACES-1) Summer campaign: Experiment Plan. Department of Civil Engineering, Monash University. 167pp.

4. Rüdiger, C. and **Peischl, S.** (2010): Addendum to the Australian Airborne Cal/val Experiments for SMOS (AACES-1): Experiment Plan. Department of Civil Engineering, Monash University, 33pp.

### Website

- AACES Summer Campaign: <http://www.moisturemap.monash.edu.au/aaces-1>
- AACES Winter Campaign: <http://www.moisturemap.monash.edu.au/aaces-2>



# Contents

<b>Declaration</b>	<b>V</b>
<b>Abstract</b>	<b>VII</b>
<b>Acknowledgements</b>	<b>X</b>
<b>Declaration for thesis by publication</b>	<b>XV</b>
<b>List of Figures</b>	<b>XXV</b>
<b>List of Tables</b>	<b>XXVII</b>
<b>List of Symbols</b>	<b>XXIX</b>
<b>I Motivation and Background</b>	<b>1</b>
<b>1 Introduction</b>	<b>3</b>
1.1 Relevance . . . . .	3
1.2 Objective and scope . . . . .	8
1.3 Organisation of the thesis . . . . .	10
References for Chapter 1 . . . . .	11
<b>2 Literature review</b>	<b>17</b>
2.1 Soil moisture . . . . .	17
2.1.1 Definition . . . . .	18
2.1.2 Measurement techniques . . . . .	19
2.2 Remote sensing of soil moisture . . . . .	21
2.2.1 Passive microwave sensing principles . . . . .	24
2.2.2 L-band Microwave Emission of the Biosphere - L-MEB . . . . .	27
2.2.3 Soil Moisture and Ocean Salinity Mission - SMOS . . . . .	32
References for Chapter 2 . . . . .	34
<b>II Analysis on airborne multi-incidence angle L-band data</b>	<b>41</b>
<b>3 Evaluation of L-MEB for vegetation and roughness effects [Paper 1]</b>	<b>43</b>
3.1 Introduction . . . . .	46

3.2	Wheat canopy structure and surface roughness effects on multi-angle observations at L-band . . . . .	46
3.3	Summary . . . . .	56
<b>4</b>	<b>Evaluation of L-MEB for angular retrieval preferences [Paper 2]</b>	<b>59</b>
4.1	Introduction . . . . .	62
4.2	Sensitivity of multi-parameter soil moisture retrieval to incidence angle configuration . . . . .	62
4.3	Summary . . . . .	72
<b>5</b>	<b>Evaluation of data acquisition time on angular observations [Paper 3]</b>	<b>73</b>
5.1	Introduction . . . . .	76
5.2	Analysis of data acquisition time on soil moisture retrieval from L-Band observations . . . . .	76
5.3	Summary . . . . .	83
<b>III</b>	<b>Analysis on spaceborne multi-incidence angle L-band data</b>	<b>85</b>
<b>6</b>	<b>Australian Airborne Cal/val Experiments for SMOS (AACES) [Paper 4]</b>	<b>87</b>
6.1	Introduction . . . . .	90
6.2	The AACES field experiments: SMOS calibration and validation across the Murrumbidgee River catchment . . . . .	90
6.3	Summary . . . . .	103
	References for Chapter 6 . . . . .	104
<b>7</b>	<b>Evaluation of SMOS data products for the Australian validation site</b>	<b>107</b>
7.1	Overview of SMOS L0 to L3 products . . . . .	107
7.2	Comparison of SMOS brightness temperature data products . . . . .	109
7.2.1	SMOS L1C data . . . . .	109
7.2.2	SMOS L3TB data . . . . .	113
7.3	Summary . . . . .	118
	References for Chapter 7 . . . . .	121
<b>8</b>	<b>Evaluation of multi-incidence angle soil moisture retrieval using AACES</b>	<b>123</b>
8.1	Analysis of canopy structure effects with respect to paper 1 . . . . .	123
8.2	Analysis of angular moisture retrieval with respect to paper 2 . . . . .	126
8.3	Summary . . . . .	128
	References for Chapter 8 . . . . .	130
<b>IV</b>	<b>Resume and Perspective</b>	<b>133</b>
<b>9</b>	<b>Conclusion</b>	<b>135</b>
9.1	L-MEB related key findings . . . . .	135
9.2	AACES related key findings . . . . .	137
<b>10</b>	<b>Future Work</b>	<b>139</b>

<b>V</b>	<b>Appendix</b>	<b>141</b>
<b>A</b>	<b>Conference Proceeding I</b>	<b>143</b>
<b>B</b>	<b>Conference Proceeding II</b>	<b>151</b>
<b>C</b>	<b>Conference Proceeding III</b>	<b>159</b>



# List of Figures

2.1	Schematic illustration of an electromagnetic wave. . . . .	22
2.2	The electromagnetic spectrum with designated spectral regions, corresponding wavelengths [ $\mu\text{m}$ to $\text{m}$ ] and frequencies [Hz]. UV: ultraviolet, NIR: near infrared, MIR: middle infrared, FIR: far infrared (thermal), (source: after Albertz, 2001). . . . .	23
2.3	Variation in electromagnetic signal attenuation from none= 0 to full= 1 depending of media and frequency(source: Kerr, 1996). . . . .	24
2.4	Relation between calculated TB and $\theta$ for a homogeneous soil medium with a specular surface at three moisture conditions (source: Ulaby et al., 1986). . . . .	26
2.5	Contribution of vegetation and soil components to the detected TB signal. . . . .	28
2.6	Relation between TB and look angle for bare soil (left) and vegetated/grassland conditions (right). . . . .	30
3.1	Locations of the three focus farms covered by multiangle L-band observations in NAFE'05. Overlaid are the flight lines of the aircraft, the location of nearby monitoring stations, and the grid of HDAS surface soil moisture measurements. The high-resolution spatial sampling area of nearsurface surface soil moisture (6.25–125 m) is displayed by a cluster of points in contrast to the coarser sampling scale (250–500 m), where each individual sampling location is marked. (Inset) Distribution of all NAFE'05 focus farms within the Goulburn River catchment, located in New South Wales, Australia. (in publication: Fig. 1) . . . . .	48
3.2	Dual-polarized brightness temperature estimates plotted against incidence angle and compared to multiangle PLMR observations over wheat canopy for the Merriwa Park and Cullingral study sites. The measured soil moisture (SM) and the VWC are individually displayed for each observation day. (in publication: Fig. 2) . . . . .	51
3.3	Scatterplot of the L-MEB model simulations in comparison with independent ground data from Merriwa Park on different observation dates using (dots) the default model parameterization 'M1_def' [15], (crosses) the sitespecific roughness parameterization 'M2_HR' [26], and (circles) the optimized model parameterization 'M3_opt'. Additionally, results based on a nonlinear daily-optimized $\text{HR} = f(\text{SM})$ approach are shown in red for days where model predictions were improved by more than 0.1 K compared to 'M2_HR' and 'M3_opt' results. The rmse calculated between the observed and simulated brightness temperatures is given for all model approaches on all days. (in publication: Fig. 3) . . . . .	52

- 
- 3.4 Scatterplot showing the retrieved against measured surface soil moisture values at the Merriwa Park focus farm for the four available observation days. The inverse application of the L-MEB model was made for all model parameterizations discussed in Section IV. (in publication: Fig. 4) . . . . . 53
- 4.1 Schematic of simulating synthetic multi-angular brightness temperature data (TB) using the forward model L-MEB. Part 1 illustrates the simulation of synthetic TB<sub>ref</sub> based on NAFE'05 ground measurements. Part 2 describes the simulation of synthetic TB<sub>sim</sub> based on NAFE'05 ground measurements and a matrix of two parameter value combinations depending on the scenario chosen (scenario: SM-VWC; SM-HR; SM-Tsurf; or SM-Tveg). The final iterative comparison considers inclusion of a random TB error of maximum  $\pm 2$  K for TB<sub>ref</sub> and calculates the root mean square error between the varying TB<sub>ref</sub> and TB<sub>sim</sub> for each iteration step to arrive at a mean TB rmse map. (in publication: Fig. 1) . . . . . 64
- 4.2 Plots of mean TB rmse distribution [K] for four scenarios of two-parameter combinations (SM-VWC, SM-HR, SM-Tveg, SM-Tsurf). The rmse was calculated from the iterative difference in TB<sub>ref</sub> and TB<sub>sim</sub> considering all dual-polarized TB data within 0–50° incidence angle range. The contour lines indicate the level of rmse in the parameter space. The top row represents wet conditions ( $SM = 0.43 \text{ m}^3/\text{m}^3$ ,  $VWC = 1.9 \text{ kg}/\text{m}^2$ ) and the bottom row dry conditions ( $0.14 \text{ m}^3/\text{m}^3$ ,  $VWC = 0.7 \text{ kg}/\text{m}^2$ ). (in publication: Fig. 2) . . . . . 65
- 4.3 Evolution of the mean dual-polarized TB rmse distribution [K] across varying ranges of incidence angle for four scenarios of two-parameter combinations (rows 1 & 5: SM-VWC, rows 2 & 6: SM-HR, rows 3 & 7: SM-Tveg, rows 4 & 8: SM-Tsurf). The black contour line indicates an rmse level of 1.5 K. Panel (a) illustrates moist conditions with  $SM = 0.43 \text{ m}^3/\text{m}^3$ ,  $VWC = 1.9 \text{ kg}/\text{m}^2$ , and panel (b) illustrates dry conditions with  $SM = 0.14 \text{ m}^3/\text{m}^3$  and  $VWC = 0.7 \text{ kg}/\text{m}^2$ . (in publication: Table III) 66
-

- 
- 4.4 Comparison of two-parameter retrieval results derived from the airborne dual-polarized NAFE'05 TB measurements, which were classified into five angular groups as shown on the x-axis (1: 0–10°; 2: 10–20°; 3: 20–30°; 4: 30–40°; 5: 40–50°). The shaded area depicts the standard deviation of the NAFE'05 ground measured soil moisture with the average value indicated by the blue line. Note that in each plot the left y-axis corresponds to the retrieved soil moisture and the right y-axis relates to the additionally retrieved parameter indicated at the top of each column: i) VWC [ $\text{kg}/\text{m}^2$ ], ii) HR [?], iii) Tveg [K], and iv) Tsurf [K]. Panel (a) illustrates wet conditions with  $\text{SM} = 0.43 \text{ m}^3/\text{m}^3$  and  $\text{VWC} = 1.9 \text{ kg}/\text{m}^2$ , while panel (b) illustrates dry moisture conditions with  $\text{SM} = 0.14 \text{ m}^3/\text{m}^3$  and  $\text{VWC} = 0.7 \text{ kg}/\text{m}^2$ , respectively. The index of each row relates to a different parameterization (P) used for the vegetation structure characterization in the retrieval model: i) P1:  $\text{tt}_H = 1$ ,  $\text{tt}_V = 8$ ; ii) P2:  $\text{tt}_H = 0.2$ ,  $\text{tt}_V = 1.4$ ; iii) P3:  $\text{tt} = 1$ ,  $\text{tt}_V = 1$ . (For interpretation of the references to color in this figure legend, the reader is referred to the web version of this article.). (in publication: Fig. 4) . 67
- 4.5 Comparison of two-parameter retrieval results (blue diamond: SM, green circle: secondary parameter) against NAFE'05 ground measurements (blue line: measured SM; green line: second parameter ground truth) obtained from synthetic, dual-polarized TB data. Different angular group combinations (x-axis) were tested for the retrieval as given in Table 3. Note that in each plot the left y-axis corresponds to soil moisture and the right y-axis relates to the additionally retrieved parameter. The top four panels represent wet conditions and the bottom four panels illustrate dry conditions, respectively. (For interpretation of the references to color in this figure legend, the reader is referred to the web version of this article.). (in publication: Fig. 5) . . . . . 68
- 5.1 Top: Location of the NAFE'06 focus farms Y1, Y7 and Y10 and the OzNet monitoring network (green dots) within the Yanco study area. Bottom inset: Y7 focus farm which was covered by multi-angle transect flights (grey), location of the corresponding monitoring station Y7 and distribution of the intensive soil moisture sampling grid (black points). (in publication: Fig. 1) . . . . . 78
- 5.2 Linear regression applied to ground measured thermal infrared (TIR) and surface soil temperature (Tsurf) from 1cm depth measurements considering three types of vegetation cover. (in publication: Fig. 2) . . 79
- 5.3 Comparison of 1P retrieved soil moisture values (SMret) across the focus farm Y7 per PLMR pixel (green shades) with the farm-averaged ground measured HDAS (Avg. SMground in grey) observations per sampling day. AM: morning flight; PM: afternoon flight. (in publication: Fig. 3) . . . . . 79
-

5.4	Comparison of retrieved soil moisture values across the focus farm Y7 per PLMR pixel with the ground measured HDAS information classified into morning (6 A.M.) and afternoon (6 P.M.) observations. (in publication: Fig. 4) . . . . .	80
5.5	Comparison of polarization ratios between the vertical and horizontal brightness temperature observations measured during the course of the NAFE'06 field campaign. Overlain is the HDAS soil moisture information averaged from all samples taken across focus farm Y7. (in publication: Fig. 5) . . . . .	81
6.1	Overview of the Murrumbidgee River catchment in Australia (inset), with AACES-1 covering all ten flight patches and AACES-2 focusing on the central half of the study area. SMOS footprints within each flight patch and the location of ground sampling activities as well as the existing long-term soil moisture network sites (OzNet) are indicated on the map. (in publication: Fig. 1) . . . . .	93
6.2	Overview of the Murrumbidgee River catchment and its climatic, topographic and soil diversity. Overlain is the outline of the AACES study area with the course of the Murrumbidgee River and the location of the 20 focus farms, where the ground sampling activities took place. The spatial dataset is publicly available through Australian Bureau of Rural Science (2001, 2006) and Geoscience Australia (2008). (in publication: Fig. 2) . . . . .	94
6.3	Schematic of the airborne sampling strategy showing the flight lines for each individual patch flight (P) and the transect flight (T) across the AACES study area, with the latter designed to include as many ground sampling farms and OzNet monitoring sites as practical. (in publication: Fig. 3) . . . . .	95
6.4	Schematic of the temporary monitoring station instrumentation during the AACES field campaigns (left panel) and the permanent instrumentation at the new OzNet monitoring sites in the Murrumbidgee River catchment (right panel). (in publication: Fig. 4) . . . . .	96
6.5	Left panel: schematic of the ground sampling strategy concentrating on two focus farms per patch. Each focus farm was instrumented with two temporary monitoring stations and covered by six soil moisture sampling lines. Right panel: example of ground sampled, near-surface soil moisture data using the HDAS system. (in publication: Fig. 5) . . . . .	97
6.6	Example of airborne L-band data collected at H-polarization during the summer (AACES-1) and winter (AACES-2) field campaigns with the brightness temperatures given in Kelvin. Note, each flight patch represents a single flight day. (in publication: Fig. 6) . . . . .	99
6.7	Temporal and spatial patterns of H-polarized SMOS L1C brightness temperature data [K] collected during the summer field campaign (AACES-1). Overlain are the Murrumbidgee catchment boundary and the individual flight patch of that particular day, where airborne L-band data is available. (in publication: Fig. 7) . . . . .	99

---

6.8	Example of airborne L-band data collected at H-polarization during the AACES-1 campaign in transect flight mode (brightness temperatures given in Kelvin). (in publication: Fig. 8) . . . . .	99
6.9	Comparison of 1 km PLMR observations with L-MEB simulated brightness temperature data for AACES-1. (in publication: Fig. 9) . . . . .	100
7.1	Comparison of SMOS L1C (V346) and airborne brightness temperature (TB) observations at three groups of incidence angles extracted for all AACES patches (A-1: AACES-1, A-2: AACES-2) . . . . .	110
7.2	Comparison of SMOS L1C (V620) and airborne brightness temperature (TB) observations at three groups of incidence angles extracted for all AACES patches (A-1: AACES-1, A-2: AACES-2). . . . .	111
7.3	Comparison of SMOS L1C (V620) and PLMR TB observations for all AACES patches with v-polarization in blue and h-polarization in red, respectively. PLMR TB data are given by three correspondingly coloured angular focus points with its standard deviation indicated by black error bars. Top two rows: AACES-1; bottom row: AACES-2. . . . .	112
7.4	Comparison of SMOS L3TB data and PLMR TB observations at three groups of incidence angles extracted for the AACES-1 study area. Top: L3TB ascending data, bottom: L3TB descending data. . . . .	115
7.5	Comparison of SMOS L3TB data and PLMR TB observations at three groups of incidence angles extracted for the AACES-2 study area. Top: L3TB ascending data, bottom: L3TB descending data. . . . .	115
7.6	Comparison of SMOS L3TB and PLMR TB observations for all patches covered by AACES-1. PLMR TB data are given by three angular focus points with the standard deviation for each indicated by error bars. Underlain are the SMOS L3TB data as red (h-polarization) and blue dots (v-polarization). Top rows: SMOS L3TB ascending data. Bottom row: SMOS L3TB descending data. . . . .	117
7.7	Comparison of SMOS L3TB and PLMR TB observations for all patches covered by AACES-2. PLMR TB data are given by three angular focus points with the standard deviation for each indicated by error bars. Underlain are the SMOS L3TB data as red (h-polarization) and blue dots (v-polarization). Top rows: SMOS L3TB ascending data. Bottom row: SMOS L3TB descending data. . . . .	118
8.1	Overview of the land surface conditions and sampling strategy of patch 06 farm 12. . . . .	124
8.2	Comparison of PLMR TB for P06F12 with simulated brightness temperatures using vegetation structure parameters with $tt_h=1$ and $tt_v=8$ by Wigneron et al. (2007) (left) or vegetation structure parameterization as given in chapter 3 (right). . . . .	125

---



# List of Tables

1	Details on candidates journal publications . . . . .	XI
3.1	Characteristics of selected NAFE'05 focus farms with multi-incidence angle observations (in publication: Table I) . . . . .	49
3.2	Parameterization of the forward models studied (in publication: Table II)	50
3.3	Comparison of ground-measured surface soil moisture (standard deviation in brackets) with surface soil moisture values retrieved using different surface roughness and vegetation structure parameterizations. (in publication: Table III) . . . . .	53
4.1	Overview of the L-MEB input parameter values for the two experiment days. (in publication: Table 1) . . . . .	64
4.2	Range of values (min-max) tested in multi-parameter retrieval combinations. (in publication: Table 2) . . . . .	65
4.3	Classification of angular groups according to incidence angle [°] and polarization (d — dual, h — horizontal, v — vertical). (in publication: Tab. 3) . . . . .	68
5.1	Daily variable L-MEB input parameters for farm Y7. (in publication: Table I) . . . . .	79
5.2	Fixed L-MEB input parameters for farm Y7. (in publication: Table II) .	80
5.3	RMSE of the retrieval results for soil moisture compared to measurements at farm Y7. (in publication: Table III) . . . . .	80
6.1	Multispectral and thermal infrared instrument characteristics. (in publication: Table 1) . . . . .	94
6.2	Characteristics of all focus farms sampled during AACES-1 and AACES-2 (shaded rows). (in publication: Table 2) . . . . .	98
6.3	Overview of total ground data collected during the AACES field campaigns. (in publication: Table 3) . . . . .	98
7.1	Overview of SMOS data products . . . . .	108
8.1	Results of angular soil moisture retrieval P06F12. Ground measured soil moisture: $SM=0.34 [m^3/m^3]$ . . . . .	127



# List of Symbols

$\epsilon_c$ .....	complex dielectric constant [-]
$\epsilon_r$ .....	dielectric constant relative to free space [F/m]
$\epsilon'_r$ .....	real part of dielectric constant [-]
$\epsilon''_r$ .....	imaginary part of dielectric constant [-]
$\Gamma_p$ .....	smooth surface reflectivity at polarization p [-]
$\Gamma_{sp}$ .....	rough surface reflectivity at polarization p [-]
$\omega$ .....	single scattering albedo of the vegetation [-]
$\rho_b$ .....	dry bulk density [1 g dry soil/cm <sup>3</sup> soil]
$\rho_w$ .....	water density [1 g water/cm <sup>3</sup> water]
$\sigma$ .....	standard deviation of surface height [-]
$\tau_{NAD}$ .....	vegetation optical depth at nadir [-]
$\theta$ .....	incidence angle [degree]
$\theta_{grav}$ .....	gravimetric soil moisture [g/g]
$\theta_{vol}$ .....	volumetric soil moisture [v/v]
$\Upsilon_{veg}$ .....	transmissivity of the vegetation layer [-]
$e_h$ .....	smooth surface emissivity at horizontal polarization [-]
$e_p$ .....	smooth surface emissivity at polarization p [-]
$e_v$ .....	smooth surface emissivity at vertical polarization [-]
$h_s$ .....	soil roughness parameter [-]
$k$ .....	electromagnetic wavenumber [-]
$p_t$ .....	total porosity [v/v]
$R_s$ .....	water saturation [v/v]
$T_{soil}$ .....	effective soil temperature [K]
$T_{veg}$ .....	physical vegetation temperature [K]

$TB_p$ .....	brightness temperature at polarization $p$ [K]
$tt_p$ .....	angular correction parameter for opacity [-]
$tt_p$ .....	angular correction parameter for opacity [-]
$V_a$ .....	fraction of air of the total soil volume [v/v]
$V_s$ .....	fraction of soil of the total soil volume [v/v]
$V_t$ .....	total soil volume [v/v]
$V_w$ .....	fraction of water of the total soil volume [v/v]
VWC .....	vegetation water content [kg/m <sup>2</sup> ]

# **Part I**

## **Motivation and Background**

---

# 1

## Introduction

**W**ATER resources on our planet are driving forces across the various ecosystems supporting life and biodiversity on Earth. During the last decades public ecological awareness has increased tremendously, after globally facing rising numbers of extreme climatic events (e.g. floods and extended periods of drought) along with a dramatic growth in population. While reliable prediction of such natural disasters still poses a challenge for state-of-the-art models, imminent availability of continuous global observations from remote sensing provide valuable information in time and space for sophisticated climate modelling, water monitoring and management strategies.

### 1.1 Relevance

---

One crucial environmental parameter in the assessment of water resources is the top layer soil moisture content. It controls energy fluxes and water processes near the soil surface making it a significant variable in meteorological and climate modelling applications (Robinson et al., 2008). It governs not only the interactions at the land surface-atmosphere interface by regulating the partitioning of rainfall into infiltration and runoff (Beven, 2003; Houser, 2003), but also the evapotranspiration and photosynthetic activity of plants (Western et al., 1999; Wetzel and Chang, 1987). The soil moisture content is highly variable in space and time due to the spatial variability of

the environmental conditions such as topography, soil and vegetation properties as well as climate, land use and land cover. The relative impact of these factors in turn is influenced by the local conditions and their temporal behaviour. Some of the influencing factors such as soil texture, soil structure, slope and relative elevation are regarded static whereas the others such as vegetation and meteorological conditions feature temporal dynamics (Famiglietti et al., 1998). These aspects cause the quantification of the soil moisture content in weather forecast, flood modelling and other hydrological algorithms to be highly difficult to estimate, introducing additional uncertainties that need to be accounted for. Thus, in-situ data of the soil moisture content is preferred.

While ground measurements of soil moisture at a large spatial scale are cumbersome and time-consuming, remote sensing offers the advantage of frequent observations not only in space but also in time. The **Soil Moisture and Ocean Salinity (SMOS)** satellite, launched by the **European Space Agency (ESA)** on the 2<sup>nd</sup> November 2009, is the first spaceborne mission dedicated to global mapping of surface soil moisture (Kerr et al., 2000). After decades of research amongst available remote sensing techniques including visible and thermal infra-red, the concept of passive microwave imaging is currently understood to be the most promising approach to observe surface soil moisture evolution and hence has been adopted for SMOS. The sensor wavelength of 1400-1427 MHz was specifically chosen in order to operate within a protected region of the electromagnetic spectrum (L-band), which is supposed to be entirely clean of radio frequency interferences. Moreover, the measured brightness temperature response at L-band is highly sensitive to near-surface soil moisture and less affected by contributions induced by the surface roughness conditions and the presence of vegetation. With a desired spatial resolution of better than 50 km, requiring an antenna size around 8 m diameter for this wavelength, an innovative Y-shaped radiometer that unfolded in space was deployed. This antenna relies on a 2-dimensional interferometric synthetic aperture synthesis utilizing the 69 individual receivers distributed along the three arms. The novel design of this sensor also enables quasi-simultaneous acquisition of full-polarized (four stokes parameters) microwave observations at a range of incidence

angles 0-55° for any location of the earth surface, while the satellite moves along its track.

The passive microwave technology is based on the relationship between the measured brightness temperature and the dielectric constant of the target medium (for instance soil), which in turn can be related to its moisture content. However the retrieval of soil moisture from L-band microwave observations over vegetated areas is relatively complex compared to bare soil conditions, since the additional vegetation contribution on the emission signal needs to be accounted for within the model. Thus, with the increasing number of input parameters, even more ground information is needed to ensure accurate soil moisture estimates from remote sensing instrument. On the basis of numerous tower experiments, field campaigns and synthetic data, studies have shown that estimates of ancillary model parameters (such as vegetation water content) can be retrieved for the same SMOS footprint in addition to the soil moisture information using angular dependencies of the observed brightness temperature (Wigneron et al., 2000).

This so-called multi-parameter retrieval significantly enhances the soil moisture retrieval since there is less reliance on input parameters from other sources. The multi-incidence angle observations are therefore understood to facilitate the overall soil moisture retrieval process and to improve the final SMOS soil moisture product - considering a SMOS target accuracy of 0.04 m<sup>3</sup>/m<sup>3</sup> for bare or low-vegetated soil. However, this theoretically valid innovative approach of soil moisture mapping needs to be rigorously and constantly validated using in-situ data across a range of surface conditions around the globe. That way the retrieval algorithm and hence the soil moisture product are steadily improved.

Apart from the spatial and temporal variability of the topsoil moisture content, the aspect of scale considering point-wise ground measurements in contrast to large-scale satellite footprints is challenging. Hence, for validation purpose one requires a large quantity and representative distribution of ground measurements with respect to the satellite scale (Cosh et al., 2004). Over the past decades two concepts of ground measurements have proved acceptable for satellite validation: i) short-term

field campaigns, and ii) long-term soil moisture network stations. Latter have the advantage of data time series depicting the evolution of soil moisture during the daily as well as seasonal cycles across the spatial coverage. Moreover, mostly the stations are equipped with additional soil moisture and soil temperature sensors at different depths as well as rainfall and vegetation monitoring information. These ancillary data in turn can be integrated into the soil moisture retrieval model. With respect to SMOS calibration and validation (Cal/Val) activities numerous soil moisture networks are available across the whole globe (e.g. Australia: OzNet (Smith et al., 2012), Africa: AMMA-CATCH (De Rosnay et al., 2009), France: SMOSMANIA (Albergel et al., 2008; Calvet et al., 2007), Germany (Dall'Amico et al., 2013), Spain: REMEDHUS (Martinez-Fernandez and Ceballos, 2003), USA: COSMOS (Zreda et al., 2012). Note, most of these stations are also part of the International Soil Moisture Network (Dorigo et al., 2011) which represents a global in-situ soil moisture data base freely available to the scientific community.

The drawback of the network stations is the single scale level of the available point data, i.e. a small number of soil moisture measurements represent a large areal extent, which needs to be up-scaled and converted for comparison with the satellite observations. Here, the second approach with the field campaigns represents a crucial link between the two methods. Often field campaigns are designed such as that intensive ground measurements are accompanied by airborne observations which i) adds a second spatial scale level to the data set, and ii) offers the direct comparison of the brightness temperature data. Preferably all ground and airborne measurements are conducted coincident with the satellite overpass for best validation results.

The overall challenge for microwave soil moisture retrieval is to reconstruct the desired environmental parameter from the measured signal with a minimum set of auxiliary data. Previous studies describe various techniques to model and validate soil moisture using synthetic studies and/or field data from ground, airborne and space experiments (Wigneron et al., 2003). Early retrieval techniques focussed on the statistical approach by establishing a linear relationship between the measured brightness temperature and the surface soil moisture (Choudhury et al., 1987; Teng

et al., 1993; Theis et al., 1984). Here the slope and intercept of the regression line were interpreted in terms of land cover variables estimated from ancillary data. The drawback of this model is its restricted applicability, as the regression usually only holds for the time and regions the data were obtained from. Moreover, the first generation of soil moisture retrieval methods was developed for airborne observations with instruments operating at one polarization/frequency channel and nadir view angle. This mono-configuration and the resulting single measurement constrains the retrieval to a single parameter. Thus, in order to retrieve accurate surface soil moisture the parameterization of the soil and vegetation media is crucial. Usually this information is provided by land cover classification maps to account for vegetation and temperature effects in the model. For well-defined and well-controlled areas this approach has proven to be acceptable. However, considering the adaptation to satellite data, where detailed ancillary data on the vegetation effects might be limited, other approaches are generally more appropriate. Studies by Van de Griend and Owe (1994a) and Chanzy et al. (1997) described a method to obtain information on the vegetation attenuation from remote sensing indices such as NDVI (Normalized Difference Vegetation Index). Moreover Magagi et al. (2000) used a polarization difference index to derive the optical depth of the vegetation layer. The obtained retrieval results for the indices based methods were overall satisfying. The obtained retrieval results for the indice based methods were overall satisfying. However, indices obtained from satellite data are sensitive to atmospheric absorption and scattering effects, and in terms of visible and near-infrared signatures, the presence of clouds. Moreover, the sensitivity of the vegetation indices to biomass depends on the wavelength of the satellite sensor since the penetration depth within the canopy strongly decreases with decreasing wavelength.

Another retrieval technique is the use of neural networks by transferring input variables (brightness temperature measurements) into output variables (land surface data) (Liou et al., 2001). This has been tested by Del Frate et al. (2003) with reasonable results for agricultural areas. However, due to the huge amount of data that are needed to train the system and to create an explicit inverse function which produces satisfying

results, the challenge is not always feasible. A third type of algorithms are based on parameterization of the land surface variables as model input in order to simulate remotely sensed signatures as output. Through an iterative minimization routine in terms of the root mean square error (rmse) between the forward simulations and the actual observations this approach becomes an inverse model. The relation between the brightness temperature and moisture content can be modelled in different ways. Some approaches are more easily inverted (e.g. radiative transfer), whereas others are more complex and require the complete information about the temperature of the soil and its moisture profile (e.g. coherent wave theory, non-coherent radiative transfer). The physical basis of the retrieval algorithms adopted by SMOS is the radiative transfer equation.

The capability of SMOS to obtain multi-angular observations at dual/full polarization mode is a major asset for the potential of multi-parameter retrieval. Estimation of the vegetation ancillary data as model input such as vegetation water content (VWC) and the empirical parameter  $b$ , which describes the canopy type and structure, is not easy at large spatial scale, which vary both spatially and temporally. Consequently, the multi-angular approach provides an opportunity to retrieve ancillary data together with soil moisture. However several studies showed that there might be polarization as well as angular dependencies in ancillary data due to, for example, the structure of the canopy and the resulting scattering and attenuation effects on the brightness temperature (Davenport et al., 2008; Hornbuckle et al., 2003; Owe et al., 2001; Pardé et al., 2003; Ulaby and Wilson, 1985; Van de Griend and Owe, 1994b; Van de Griend et al., 1996; Wigneron et al., 1995). Additional validation of these preliminary results with airborne and SMOS scale data is required.

## 1.2 Objective and scope

---

In the context of the novel design of SMOS and the associated newly developed soil moisture retrieval algorithms this thesis investigates the potential of multi-incidence angle L-band measurements to enhance the modelling of near-surface soil moisture

---

information from passive microwave data. In particular, it examines remotely sensed multi-angle observations collected over Australia by both airborne and spaceborne systems at varying spatial and temporal resolution.

Part of the available airborne data were collected during two intensive field campaigns conducted prior to the SMOS launch: NAFE'05 (Panciera et al., 2008) and NAFE'06 (Merlin et al., 2008). Both campaigns covered a variety of soil moisture and vegetation conditions at two different test sites in Eastern Australia and were accompanied by extensive ground measurements. The ground data included soil moisture network stations plus ancillary vegetation and soil data, as well as transects of soil moisture measurements made by the ground crew. The resulting ground and airborne datasets formed the initial work basis of this thesis which focussed on the adaption of one of the current state-of-the-art SMOS retrieval algorithms to multi-angle L-band observations. This thesis is the first to work with the multi-angular airborne data from these two field campaigns.

With respect to the SMOS Cal/Val activities further work of this research focussed on the planning and realisation of the globally first-ever validation campaign conducted shortly after the successful launch of the SMOS satellite. The AACES field experiment (Peischl et al., 2012a) was specifically designed to meet the SMOS requirements on complete footprint coverage across several hundreds of kilometres for an optimal comparison of satellite, airborne and in-situ data. The ground measurements included near-surface soil moisture, vegetation and soil properties and were supported by long-term profile soil moisture and soil temperature network stations. The airborne L-band observations were collected in such a way that they covered a minimum of two independent/four dependent SMOS footprints ( $\approx 44$  km) per sampling day. The AACES validation campaign was conducted in summer and winter to provide a representative dataset with a wide range of soil moisture, vegetation and climatic conditions. Both seasonal data sets were intensively examined to test and validate the research findings regarding multi-angle soil moisture retrieval drawn from the previous NAFE campaigns.

### 1.3 Organisation of the thesis

---

This thesis is organized in four main parts with the first part including i) an introduction chapter on the purpose, background and scope of the proposed research, and ii) an overview on the significance of soil moisture and remote sensing applications, with a more detailed description of the SMOS mission and the soil moisture retrieval algorithm. This is followed by two parts, which include the field and synthetic studies that have been conducted during the course of the Ph.D, with the individual chapters presenting work that has been published in high-ranking journals. Throughout the thesis the focus shifts from the evaluation of the core retrieval algorithm using previous field campaigns before SMOS was launched towards the final validation of SMOS L1C and L3TB brightness temperature products over Australia.

In the last part of this thesis, lessons are drawn from the collected study results and inter-comparison with SMOS and ultimately implemented into recommendations for the utilization of multi-incidence angle L-band observations with respect to airborne and spaceborne soil moisture mapping. Furthermore, suggestions for future works are addressed in order to take full advantage of the potential of multi-angular L-band measurements to facilitate the soil moisture retrieval process.

# References for Chapter 1

- Albergel, C., C. Rüdiger, T. Pellarin, J.-C. Calvet, N. Fritz, F. Froissard, D. Suquia, A. Petitpa, B. Piguet, and E. Martin (2008), “From near-surface to root-zone soil moisture using an exponential filter: an assessment of the method based on in-situ observations and model simulations,” *Hydrology and Earth System Sciences Discussions*, 12, pp. 1323–1337 (cited on p. 6).
- Beven, K. (2003), *Surface Runoff Generation*, vol. 1, 29, John Wiley & Sons Inc. Hoboken, 527–541, ISBN: 978-0-471-21489-2 (Electronic ISBN: 978-1-60119-600-2) (cited on p. 3).
- Calvet, J.-C., N. Fritz, F. Froissard, D. Suquia, A. Petitpa, and B. Piguet (2007), “In situ soil moisture observations for the CAL/VAL of SMOS: The SMOSMANIA network,” in: *IEEE International Geoscience and Remote Sensing Symposium (IGARSS) 2007*, IEEE, pp. 1196–1199 (cited on p. 6).
- Chanzy, A, T. Schmugge, J.-C. Calvet, Y Kerr, P Van Oevelen, O Grosjean, and J. Wang (1997), “Airborne microwave radiometry on a semi-arid area during HAPEX-Sahel,” *Journal of Hydrology*, 188, pp. 285–309 (cited on p. 7).
- Choudhury, B., C. Tucker, R. Golus, and W. Newcomb (1987), “Monitoring vegetation using Nimbus-7 scanning multichannel microwave radiometer’s data,” *International Journal of Remote Sensing*, 8(3), pp. 533–538 (cited on p. 6).
- Cosh, M. H., T. J. Jackson, R. Bindlish, and J. H. Prueger (2004), “Watershed scale temporal and spatial stability of soil moisture and its role in validating satellite estimates,” *Remote sensing of Environment*, 92(4), pp. 427–435 (cited on p. 5).
- Dall’Amico, J. T., F. Schlenz, A. Loew, W. Mauser, J. Kainulainen, J. E. Balling, and C. Bouzinac (2013), “The SMOS Validation Campaign 2010 in the Upper Danube Catchment: A Data Set for Studies of Soil Moisture, Brightness Temperature, and Their Spatial Variability Over a Heterogeneous Land Surface,” *IEEE Transactions on*

- Geoscience and Remote Sensing*, 51(1), pp. 364–377, DOI: 10.1109/tgrs.2012.2196523 (cited on p. 6).
- Davenport, I. J., M. J. Sandells, and R. J. Gurney (2008), “The effects of scene heterogeneity on soil moisture retrieval from passive microwave data,” *Advances in Water Resources*, 31(11), pp. 1494–1502, DOI: 10.1016/j.advwatres.2008.06.002 (cited on pp. 8, 31).
- De Rosnay, P., C. Gruhier, F. Timouk, F. Baup, E. Mougou, P. Hiernaux, L. Kergoat, and V. LeDantec (2009), “Multi-scale soil moisture measurements at the Gourma meso-scale site in Mali,” *Journal of Hydrology*, 375(1), pp. 241–252 (cited on p. 6).
- Del Frate, F., P. Ferrazzoli, and G. Schiavon (2003), “Retrieving soil moisture and agricultural variables by microwave radiometry using neural networks,” *Remote Sensing of Environment*, 84(2), pp. 174–183 (cited on p. 7).
- Dorigo, W. A., W. Wagner, R. Hohensinn, S. Hahn, C. Paulik, A. Xaver, A. Gruber, M. Drusch, S. Mecklenburg, P. van Oevelen, A. Robock, and T. Jackson (2011), “The International Soil Moisture Network: a data hosting facility for global in situ soil moisture measurements,” *Hydrology and Earth System Sciences*, 15(5), pp. 1675–1698, DOI: 10.5194/hess-15-1675-2011 (cited on p. 6).
- Famiglietti, J. S., J. W. Rudnicki, and M. Rodell (1998), “Variability in surface moisture content along a hillslope transect: Rattlesnake Hill, Texas,” *Journal of Hydrology*, 210(1), 136LU Times Cited:146 Cited References Count:29, pp. 259–281 (cited on pp. 4, 20).
- Hornbuckle, B. K., A. W. England, R. D. De Roo, M. A. Fischman, and D. L. Boprie (2003), “Vegetation canopy anisotropy at 1.4 GHz,” *IEEE Transactions on Geoscience and Remote Sensing*, 41(10), pp. 2211–2223, DOI: 10.1109/tgrs.2003.817192 (cited on pp. 8, 30).
- Houser, P. (2003), *Infiltration and Soil Moisture Processes*, vol. 1, 27, John Wiley & Sons Inc. Hoboken, 493–506, ISBN: 978-0-471-21489-2 (Electronic ISBN: 978-1-60119-600-2) (cited on p. 3).
- Kerr, Y. H., J.-P. Wigneron, P. Ferrazzoli, and P. Waldteufel (2000), “Soil moisture and vegetation biomass retrievals using L-band, dual polarised and multi angular radiometric data in preparation of the SMOS mission,” in: *IEEE International Geoscience and*

- Remote Sensing Symposium (IGARSS)*, vol. 3, The Institute of Electrical and Electronics Engineers, Inc. (IEEE), pp. 1244–1246, DOI: 10.1109/IGARSS.2000.858081 (cited on p. 4).
- Liou, Y.-A., S.-F. Liu, and W.-J. Wang (2001), “Retrieving soil moisture from simulated brightness temperatures by a neural network,” *IEEE Transactions on Geoscience and Remote Sensing*, 39(8), pp. 1662–1672 (cited on p. 7).
- Magagi, R. D., Y. H. Kerr, and J.-C. Meunier (2000), “Results of combining L-and C-band passive microwave airborne data over the Sahelian area,” *IEEE transactions on geoscience and remote sensing*, 38(4), pp. 1997–2008 (cited on p. 7).
- Martinez-Fernandez, J. and A. Ceballos (2003), “Temporal stability of soil moisture in a large-field experiment in Spain,” *Soil Science Society of America Journal*, 67(6), pp. 1647–1656 (cited on p. 6).
- Merlin, O., J. P. Walker, J. D. Kalma, E. J. Kim, J. Hacker, R. Panciera, R. Young, G. Summerell, J. Hornbuckle, M. Hafeez, and T. Jackson (2008), “The NAFE’06 data set: Towards soil moisture retrieval at intermediate resolution,” *Advances in Water Resources*, 31(11), pp. 1444–1455, DOI: 10.1016/j.advwatres.2008.01.018 (cited on p. 9).
- Owe, M., R. A. M. de Jeu, and J. P. Walker (2001), “A methodology for surface soil moisture and vegetation opticaldepth retrieval using the microwave polarization difference index,” *IEEE Transactions on Geoscience and Remote Sensing*, 39(8), pp. 1643–1654, DOI: 10.1109/36.942542 (cited on pp. 8, 128).
- Panciera, R., J. P. Walker, J. D. Kalma, E. J. Kim, J. Hacker, O. Merlin, M. Berger, and N. Skou (2008), “The NAFE’05/CoSMOS Data Set: Toward SMOS Soil Moisture Retrieval, Downscaling, and Assimilation,” *IEEE Transactions on Geoscience and Remote Sensing*, 46(3), 270QB Times Cited:18 Cited References Count:18, pp. 736–745, DOI: 10.1109/Tgrs.2007.915403 (cited on p. 9).
- Pardé, M., J.-P. Wigneron, A. Chanzy, P. Waldteufel, Y. H. Kerr, and S. Huet (2003), “Retrieving surface soil moisture over a wheat field: comparison of different methods,” *Remote Sensing of Environment*, 87(2), pp. 334–344, DOI: 10.1016/j.rse.2003.08.002 (cited on pp. 8, 30).

- Peischl, S., J. P. Walker, C. Rüdiger, N. Ye, Y. H. Kerr, E. J. Kim, R. Bandara, and M. Allahmoradi (2012a), “The AACES field experiments: SMOS calibration and validation across the Murrumbidgee River catchment,” *Hydrology and Earth System Sciences Discussions*, 9(3), pp. 2763–2795, DOI: 10.5194/hessd-9-2763-2012 (cited on p. 9).
- Robinson, D. A., C. S. Campbell, J. W. Hopmans, B. K. Hornbuckle, S. B. Jones, R. Knight, F. Ogden, J. Selker, and O. Wendroth (2008), “Soil moisture measurement for ecological and hydrological watershed-scale observatories: A review,” *Vadose Zone Journal*, 7(1), 288BJ Times Cited:55 Cited References Count:335, pp. 358–389, DOI: 10.2136/Vzj2007.0143 (cited on pp. 3, 19).
- Smith, A. B., J. P. Walker, A. W. Western, R. I. Young, K. M. Ellett, R. C. Pipunic, R. B. Grayson, L. Siriwardena, F. H. S. Chiew, and H. Richter (2012), “The Murrumbidgee soil moisture monitoring network data set,” *Water Resources Research*, 48(7), n/a–n/a, DOI: 10.1029/2012wr011976 (cited on p. 6).
- Teng, W., J. Wang, and P. Doraiswamy (1993), “Relationship between satellite microwave radiometric data, antecedent precipitation index, and regional soil moisture,” *International Journal of Remote Sensing*, 14(13), pp. 2483–2500 (cited on p. 6).
- Theis, S. W., B. J. Blanchard, and R. W. Newton (1984), “Utilization of vegetation indices to improve microwave soil moisture estimates over agricultural lands,” *IEEE Transactions on Geoscience and Remote Sensing*, (6), pp. 490–496 (cited on p. 7).
- Ulaby, F. T. and E. A. Wilson (1985), “Microwave attenuation properties of vegetation canopies,” *IEEE Transactions on Geoscience and Remote Sensing*, (5), pp. 746–753 (cited on p. 8).
- Van de Griend, A. and M. Owe (1994a), “Microwave vegetation optical depth and inverse modelling of soil emissivity using Nimbus/SMMR satellite observations,” *Meteorology and Atmospheric Physics*, 54(1), pp. 225–239 (cited on p. 7).
- Van de Griend, A. and M. Owe (1994b), “The influence of polarization on canopy transmission properties at 6.6 GHz and implications for large scale soil moisture monitoring in semi-arid environments,” *IEEE Transactions on Geoscience and Remote Sensing*, 32(2), pp. 409–415 (cited on p. 8).

- Van de Griend, A. A., M. Owe, J. de Ruiter, and B. T. Gouweleeuw (1996), "Measurement and behavior of dual-polarization vegetation optical depth and single scattering albedo at 1.4-and 5-GHz microwave frequencies," *IEEE Transactions on Geoscience and Remote Sensing*, 34(4), pp. 957–965 (cited on p. 8).
- Western, A. W., R. B. Grayson, and T. R. Green (1999), "The Tarrawarra project: high resolution spatial measurement, modelling and analysis of soil moisture and hydrological response," *Hydrological Processes*, 13(5), pp. 633–652 (cited on pp. 3, 20).
- Wetzel, P. J. and J. T. Chang (1987), "Concerning the relationship between evapotranspiration and soil moisture," *Journal of Climate and Applied Meteorology*, 26(1), pp. 18–27 (cited on pp. 3, 18).
- Wigneron, J.-P., A. Chanzy, J.-C. Calvet, and N. Bruguier (1995), "A simple algorithm to retrieve soil moisture and vegetation biomass using passive microwave measurements over crop fields," *Remote Sensing of Environment*, 51(3), pp. 331–341, DOI: 10.1016/0034-4257(94)00081-w (cited on pp. 8, 29, 32).
- Wigneron, J.-P., P. Waldteufel, A. Chanzy, J.-C. Calvet, and Y. H. Kerr (2000), "Two-dimensional microwave interferometer retrieval capabilities over land surfaces (SMOS Mission)," *Remote Sensing of Environment*, 73(3), 347GH Times Cited:75 Cited References Count:37, pp. 270–282, DOI: 10.1016/S0034-4257(00)00103-6 (cited on pp. 5, 29, 126).
- Wigneron, J.-P., J.-C. Calvet, T. Pellarin, A. A. Van de Griend, M. Berger, and P. Ferrazzoli (2003), "Retrieving near-surface soil moisture from microwave radiometric observations: current status and future plans," *Remote Sensing of Environment*, 85(4), pp. 489–506, DOI: 10.1016/S0034-4257(03)00051-8 (cited on pp. 6, 29).
- Zreda, M, W. Shuttleworth, X Zeng, C Zweck, D Desilets, T Franz, and R Rosolem (2012), "COSMOS: the cosmic-ray soil moisture observing system," *Hydrology and Earth System Sciences*, 16(11), pp. 4079–4099 (cited on p. 6).



# 2

## Literature review

**I**N recent decades the continuous development of new measurement technologies induced a broad understanding of the soil moisture evolution across time and space. Apart from the direct estimation of the soil moisture by determining the soil water weight as a fraction of the total soil weight, a range of non-destructive devices have been employed to estimate the amount of soil water without removing the actual soil sample from the field and analysing it in the laboratory. Moreover, the approach of remote sensing offers spatially extended and more frequent observations of soil moisture. Thus given the wide variety of available means for soil moisture measurements, the field of application of soil moisture information continuously expands and gains more attention in different scientific disciplines.

### **2.1 Soil moisture**

---

Among the major global water bodies such as oceans, ice sheets/glaciers, groundwater, lakes and rivers, the proportion of soil moisture constitutes only about 0.005 % to the global water storage (Strahler and Strahler, 2002). Despite this tiny fraction, it represents a significant environmental parameter in the evolution of near-surface atmospheric variability and the atmosphere-biosphere-hydrosphere interactions (Legates et al., 2010).

Soil moisture regulates the energy and water fluxes between the soil surface and the atmosphere by partitioning net radiation into latent and sensible heat components. The impact on both short-term (weather) and long-term (climate) atmospheric conditions results from the interaction of the moist/dry land surface and the corresponding decrease/rise in the daily surface temperature as well as air temperature amplitude (Chen et al., 2011; Timbal et al., 2002). This behaviour among other factors might induce convective processes and thunderstorms. Consequently, information on the soil moisture variability is essential for representative weather forecasting skills.

In terms of the biosphere-hydrosphere interactions soil moisture affects the plant health and its water stress in times of dry soil conditions, which ultimately lead to reduced evapotranspiration and photosynthetic activity of the vegetation (Sellers et al., 1997; Wetzel and Chang, 1987). Moreover, the availability of water in the root zone controls the ecosystem productivity considering plant growth as well as the supply with important solved nutrients such as carbon, nitrogen and methane with respect to the biochemical cycle of the Earth's system.

### 2.1.1 Definition

As per definition the soil moisture content describes the quantity of water in the soil. Considering the soil medium there are three components that need to be taken into account: the solid soil particles as well as voids in between these particles which are filled by either water or air that altogether make up the total soil volume  $V_t$ :

$$V_t = V_a + V_w + V_s, \quad (2.1)$$

with  $V_a$ ,  $V_w$ ,  $V_s$  representing the air, water and soil component, respectively. The soil moisture content being the liquid phase in the soil volume can be expressed in terms of volumetric soil moisture:

$$\theta_{vol} = \frac{V_w}{V_t}, \quad (2.2)$$

or in terms of mass  $M$ :

$$\theta_{grav} = \frac{M_w}{M_s}, \quad (2.3)$$

which is also known as gravimetric soil moisture content. The volumetric soil moisture can easily be related to the gravimetric soil moisture by introducing the density of water  $\rho_w$  and dry soil bulk  $\rho_b$ :

$$\theta_{vol} = \theta_{grav} \cdot \frac{\rho_b}{\rho_w}, \quad (2.4)$$

with

$$\rho_b = \frac{M_s}{V_t}. \quad (2.5)$$

Since the amount of voids for water  $V_w$  and air  $V_a$  is limited by the soil porosity, the volumetric soil moisture content may also be expressed as:

$$\theta_{vol} = p_t \cdot R_s = \left( \frac{V_a + V_w}{V_t} \right) \cdot \left( \frac{V_w}{V_a + V_w} \right) = \frac{V_w}{V_t}, \quad (2.6)$$

with  $p_t$  as the total porosity and  $R_s$  representing the water saturation defined as the ratio of the volume of water  $V_w$  to the volume of the pore space ( $V_a + V_w$ ). Depending on the soil texture the volumetric soil moisture may range in general between  $0.1 \text{ m}^3/\text{m}^3$  (permanent wilting point) and  $0.5 \text{ m}^3/\text{m}^3$  (saturated soil equivalent to effective porosity).

### 2.1.2 Measurement techniques

A thorough review of available soil moisture measurements is presented by Bittelli (2011) and Robinson et al. (2008). Here, the focus is set on the techniques relevant for this research. Basically there are two approaches to measure the spatial and temporal variability of soil moisture: i) in-situ point measurements and ii) observations by remote sensing sensors. The former may be further distinguished by considering a direct versus indirect measurement of the soil moisture content.

The traditional method of direct soil moisture measurements is the gravimetric sampling. The taken soil samples will be processed at the laboratory by oven-drying the soil sample at 105 °C for 24 hours and calculating the actual water content (gravimetric moisture) by recording the difference between its wet and dry weight, respectively. The volumetric soil moisture content can then be determined by taking into account the volume of the soil sample (see equation (2.2)). While this method is a rather time-consuming and requires destructive sampling - which obviously can not be repeated for the same soil sample - there is also the minimal invasive option of in-situ measurements by using soil moisture sensors. The sensing probes are inserted into the soil and measure the dielectric constant, which in turn may be related to the amount of water stored in the soil. This indirect measurement approach is based on the significant difference in the real part of the dielectric constant of liquid water ( $\approx 80$ ) compared to that of the surrounding soil components ( $< 4$ ). Consequently, through soil dielectric models the soil moisture content can be retrieved (Dobson et al., 1985; Mironov et al., 2004; Wang and Schmugge, 1980). The soil moisture probes are often permanently installed (as part of numerous network stations) and usually at different depths to acquire moisture information across soil profiles. Consequently, valuable information on the vertical water distribution and for example the migration of a wetness front after a rainfall or irrigation event may be monitored over time. These long-term records are important to advance our understanding of the small-scale temporal variability of soil moisture especially with respect to the involved hydrological processes (Western et al., 1999).

Considering the confined spatial correlation of soil moisture, the sensors need to be placed within a dense sampling pattern to provide a representative coverage of the spatial soil moisture heterogeneity. The key factors influencing the soil moisture include the vegetation cover/land use, soil properties, topography and climatic conditions (Famiglietti et al., 1998). Despite this, the lack of large-scale coverage of in-situ measurements due to the cost-intensive realisation of a high-density instrumentation as well as the issue of inaccessibility of some regions makes spatial interpretations and modelling difficult (Western et al., 2004). At this point, the remote sensing technique

using air- or spaceborne devices proves complementary to the in-situ measurements. The remote sensing soil moisture estimation is based on a similar principle by taking advantage of the dielectric properties of the soil-water-compound and the subsequent application of dielectric mixing models.

Remote sensing is a non-invasive soil moisture observation and offers the advantage of the spatial coverage that the in-situ measurements are lacking of. However it needs to be distinguished between airborne and spaceborne observations. Most airborne observations are part of a field campaign and usually capture at maximum a few hundreds of kilometres depending on the research objective and budget. Hence, they provide a detailed snapshot of the soil moisture condition for a given region. In contrast, satellite observations may be obtained on a frequent basis with a long-term, global coverage. Especially, in the context of climate and hydrological modelling this is very crucial and helps to further advance the monitoring of areas that are hardly accessible for in-situ measurements. The drawback of remote sensing is the indirect measurement approach which constantly needs to be validated to account for influencing factors such as topography, vegetation cover, vegetation type and soil texture. Moreover, it suffers from the shallow measurement depth of the very topsoil surface layer, the low spatial resolution and, also in the case of spaceborne sensors, there is the limited life span of often only a couple of years of such satellite missions.

Hence, a combination of ground, airborne and spaceborne observations is the ideal setting to obtain the wealth of temporal and spatial soil moisture products that is requested by the scientific community for weather forecast, climate modelling, sustainable water management and further applications (Vereecken et al., 2008).

## **2.2 Remote sensing of soil moisture**

---

Remote sensing describes a type of data acquisition where the sensing device is mounted to a tower, air-plane or spacecraft and has no physical contact to the observed object. The measurement principle of this technique is based on radiometry

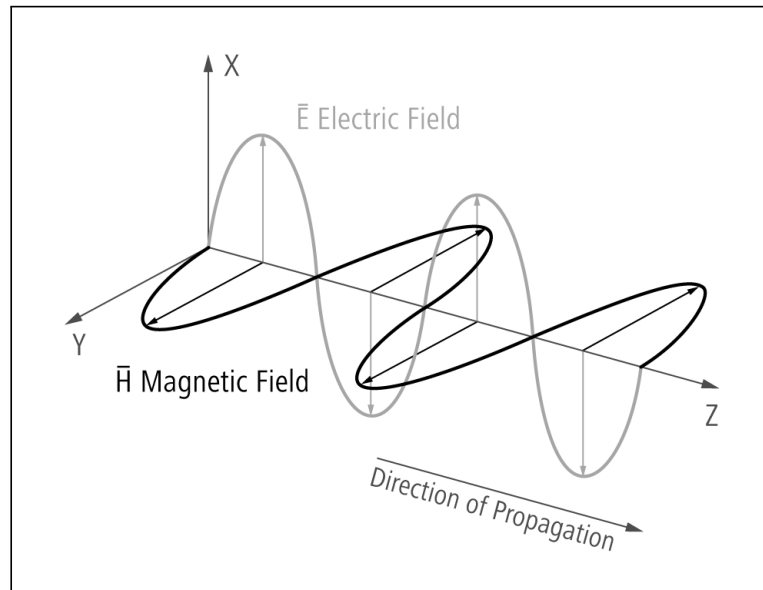


**Figure 2.1:** Schematic illustration of an electromagnetic wave.

which considers each body at a non-zero absolute physical temperature to emit electromagnetic radiation (energy) in terms of a wave. An electromagnetic wave is composed of its propagation direction vector and an amplitude vector perpendicular to it (see Figure 2.1). The transverse waves correspond to an electric and magnetic field which oscillate orthogonal to each other (Lo, 1986). The polarisation of an electromagnetic wave is thus linked to the displacement of the wave in x- or y-direction, usually expressed as “h” and “v” for horizontal and vertical polarization, respectively.

The electromagnetic spectrum spans from x-rays, ultraviolet (UV), to visible, infrared and micro- as well as radio-waves (see Figure 2.2) corresponding to increasing wavelength while decreasing the frequency (energy). The microwave region is further differentiated into bands commonly referred to by a capital letter.

Means of soil moisture remote sensing include visible, thermal infrared and microwave observations. Considering the short-wave observations the main concept focuses on the colour of the soil, i.e. soil appears darker when wet. However, this approach is deemed to fail the demand for dense temporal monitoring due to the dependence on weather conditions (no cloud cover and atmospheric effects) as well as sunlight illumination. Another method is linked to the effects of latent heat of the soil surface. The temperature approach stems from the fact that dry soils are warmer

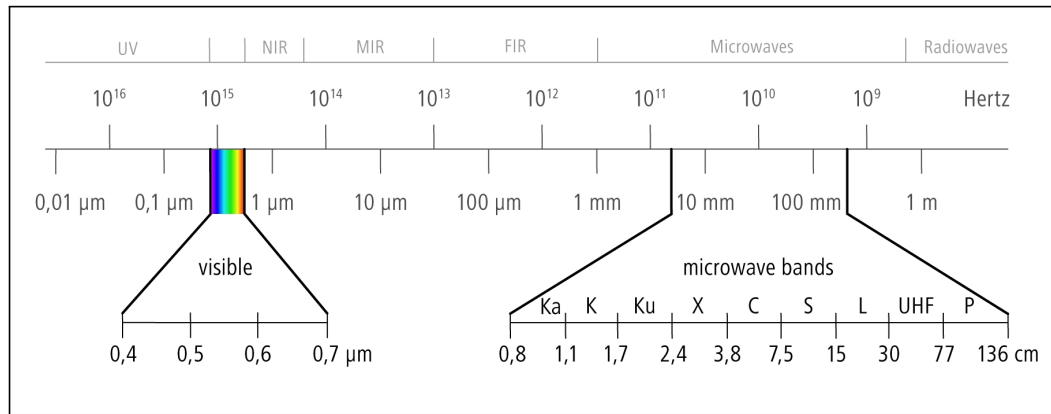


**Figure 2.2:** The electromagnetic spectrum with designated spectral regions, corresponding wavelengths [ $\mu\text{m}$  to m] and frequencies [Hz]. UV: ultraviolet, NIR: near infrared, MIR: middle infrared, FIR: far infrared (thermal), (source: after Albertz, 2001).

due to the low thermal inertia compared to wet soils. However, in addition to the above mentioned factors inherent to optical sensors there is also the opacity of the vegetation cover which interacts with the soil skin effects. Consequently, in order to derive soil moisture information from these methods the small scale forcing near the soil surface need to be exactly accounted for, which makes it difficult to translate this technique to larger spatial scales.

A different approach of soil moisture remote sensing is provided by the microwave domain. The basic principle of microwave measurements is based on the large contrast between the dielectric properties of liquid water and that of soil matter (Schmugge et al., 1986). In response to an electromagnetic field the permanent dipole and the alignment of the water molecules lead to the rather high dielectric constant of water (Behari, 2006), which influences the natural emission of the soil-water medium. The microwave technique offers especially at low frequencies the advantage of i) being operational independent of daylight, and ii) measurements that are least affected by cloud cover or atmospheric effects. Note, the microwave sensors may be distinguished into active and passive sensors. The active sensors such as scatterometer and synthetic aperture radar (SAR) send pulses and receive the reflected signal whereas passive sensors also known as radiometers are solely receivers that detect the naturally emitted or reflected radiation from the earth surface. Over the past 30 years each remote sensing method has been tested extensively for measuring the spatial and temporal

variations of soil moisture (Jackson et al., 1996; Kerr, 2007; Newton and Rouse Jr, 1980), and L-band ( $\approx 1-2$  GHz) passive microwave remote sensing has proven to be the most promising (Njoku and Entekhabi, 1996; Wang and Choudhury, 1981). As previously mentioned there is a fundamental distinction between the dielectric constant of soil with around 4 while that of pure water is about 20 times higher at 1.4 GHz frequency. Furthermore, low-frequency sensors are least affected by surface roughness, vegetation and atmospheric effects (see Fig. 2.3), and measure a deeper layer of soil with a higher moisture sensitivity (Jackson, 2005). Though in the L-band domain the monitored penetration depth slightly varies comparing studies from Laymon et al. (2001) who found an emission depth of 3 - 5 cm, whereas Raju et al. (1995) and Escorihuela et al. (2010) tended for a more shallow penetration depth in the range of around 2 - 2.5 cm. Nevertheless the overall consensus of all the above together with the fact that the 1.4 GHz frequency is a protected band for scientific applications renders it an ideal frequency range for the assessment of soil moisture by means of remote sensing.

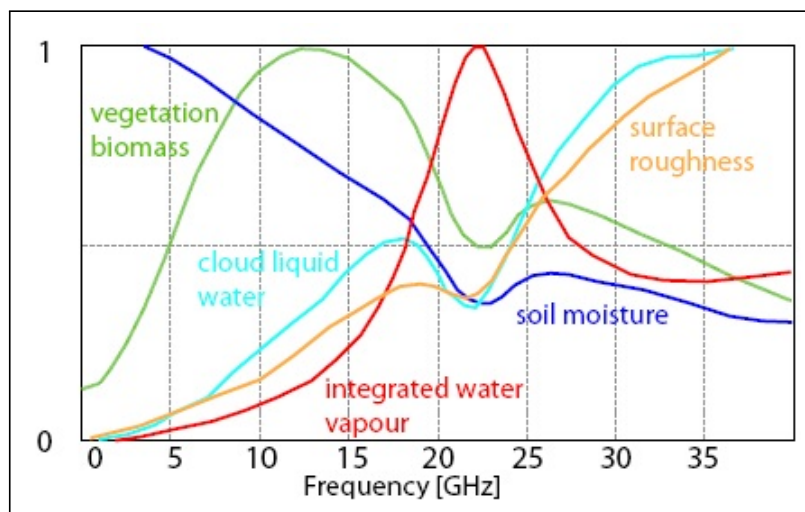


**Figure 2.3:** Variation in electromagnetic signal attenuation from none= 0 to full= 1 depending of media and frequency(source: Kerr, 1996).

### 2.2.1 Passive microwave sensing principles

Passive microwave radiometers detect the radiation emitted and/or reflected by the earth surface, which can be quantified in terms of the brightness temperature  $TB_p$  [K]

(Rayleigh-Jeans Law). Note, in case of spaceborne microwave sensor the measurement depicts a sum of contributions from the reflected cosmic radiation, the atmosphere and the land surface. While the cosmic energy is known, the atmospheric impact is rather small and may be safely neglected considering the lower microwave frequencies ( $< 5$  GHz) used in soil moisture sensing.

Assuming a bare soil, the brightness temperature of the soil surface is related to the effective temperature of the soil  $T_{soil}$  [K] and its emissivity for a given polarization  $e_p$ , where  $p$  stands for horizontal ( $h$ ) or vertical ( $v$ ) by:

$$TB_p = e_p \cdot T_{soil}. \quad (2.7)$$

The emissivity may also be related to the fraction of the incident radiation reflected by a surface

$$e_p = 1 - \Gamma_p \quad (2.8)$$

with  $\Gamma_p$  depicting the surface reflectivity. Note, the emissivity itself is characterized by the soil dielectric properties of the soil volume, and can be quantified using the Fresnel equations for a smooth, bare surface according to:

$$e_h = 1 - \left| \frac{\cos \theta - \sqrt{\epsilon_r - \sin^2 \theta}}{\cos \theta + \sqrt{\epsilon_r - \sin^2 \theta}} \right|^2 \quad (2.9)$$

$$e_v = 1 - \left| \frac{\epsilon_r \cos \theta - \sqrt{\epsilon_r - \sin^2 \theta}}{\epsilon_r \cos \theta + \sqrt{\epsilon_r - \sin^2 \theta}} \right|^2 \quad (2.10)$$

where  $\epsilon_r$  is the dielectric constant relative to free space [F/m] and  $\theta$  represents the incidence angle [degree] between the line of sight of the sensor and the local normal to the land surface. The dielectric constant is a complex number that is composed of a real and an imaginary part ( $\epsilon_c = \epsilon'_r + j\epsilon''_r$ ) together depicting the soil response to an electromagnetic wave. In detail, as the energy travels through the soil column the real part affects the propagation characteristics of the wave, whereas the imaginary part of the dielectric constant determines the loss of energy. Thus, considering a heterogeneous medium such as soil - with its different components of air, soil and

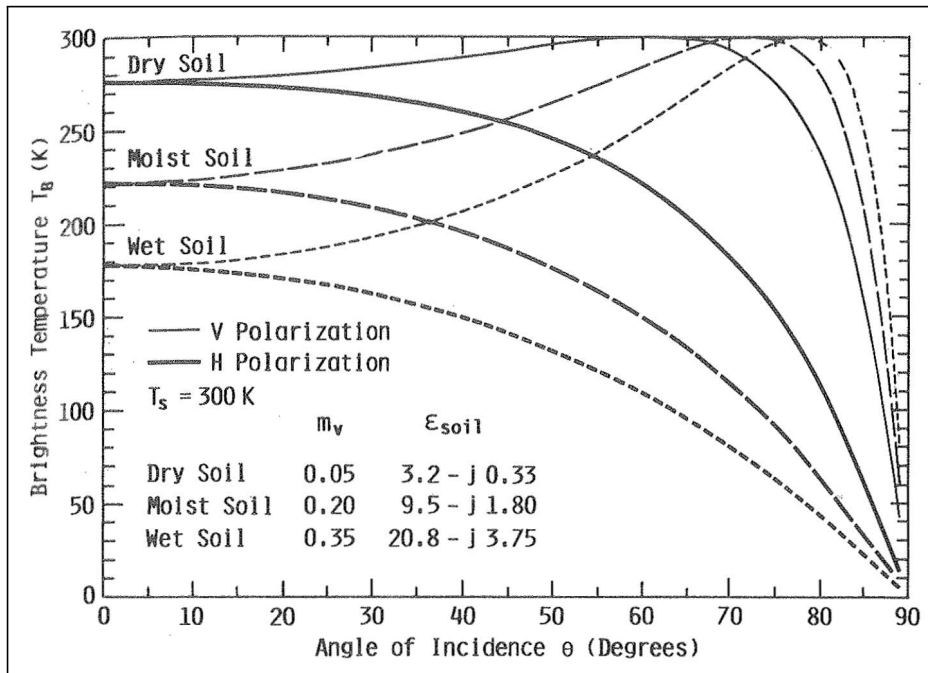


**Figure 2.4:** Relation between calculated TB and  $\theta$  for a homogeneous soil medium with a specular surface at three moisture conditions (source: Ulaby et al., 1986).

water particles - the complex dielectric constant represents a combination of all these constituents. Additional factors which impact the dielectric properties include the salinity, wavelength and temperature. In order to determine the dielectric constant and consequently link it to the soil moisture content numerous semi-empirical dielectric mixing models have been developed to account for the varying contributions of soil and electromagnetic wave components (Dobson et al., 1985; Mironov et al., 2004; Wang and Schmugge, 1980).

Equation 2.9 and 2.10 clearly demonstrate that the emissivity and accordingly the measured brightness temperature are also influenced by the incidence angle of the detected radiation. Assuming constant soil conditions but varying incidence angles, the resulting brightness temperature dependence on incidence angle is illustrated in Figure 2.4 for both vertical and horizontal polarizations. With increasing incidence angle the brightness temperature values decrease for horizontally polarized observations, while for vertically polarized observations brightness temperature values rise with increasing look angles. Thus, if the correct incidence angle is not taken into account, the observed surface would be assumed wetter than it actually is for horizontal polarized

observations (Burke and Simmonds, 2001) or drier for vertically polarized observations. However, the overall behaviour of the brightness temperature response to the incidence angle plotted in Figure 2.4 does not change with varying soil moisture. Rather, there is simply an upward translation of the curves with decreasing moisture content (Ulaby et al., 1986).

Considering the natural conditions the assumption of a smooth surface in the Fresnel equation does not hold well. Numerous study results suggest that the emissivity of a surface increases with its surface roughness due to the extended soil area interacting with the radiation; while the sensitivity of emissivity to the soil moisture content declines with the increased surface roughness with respect to the reduced range in measurable emissivity between the moisture extremes of dry and wet soils (Newton and Rouse Jr, 1980; Wang, 1983). Hence various approaches exist in literature to account for these roughness effects, with Choudhury et al. (1979) proposing a relatively simple, semi-empirical equation for the rough surface reflectivity  $\Gamma_{sp}$ :

$$\Gamma_{sp} = \Gamma_r^{-h_s \cos^2(\theta)} \quad (2.11)$$

with  $h_s$  defined as soil roughness parameter corresponding to the wavenumber  $k$  and the standard deviation of the surface height  $\sigma$  in terms of  $h_s = 4k^2\sigma^2$ .

### 2.2.2 L-band Microwave Emission of the Biosphere - L-MEB

With the presence of a vegetation layer over the soil surface, the emission process becomes more complex and so does the brightness temperature model. The **L-band Microwave Emission of the Biosphere** (Wigneron et al., 2007) is based on a simplified radiative transfer equation (zero<sup>th</sup> order model) to approximate the impact of the overlying vegetation layer. The resulting brightness temperature TB can be described as a composite which will be hereafter referred to as tau-omega model (Mo et al.,

1982):

$$TB_p = e_p \cdot T_{soil} \cdot \Upsilon_{veg} + (1 - \omega) \cdot T_{veg} \cdot (1 - \Upsilon_{veg}) + (1 - e_p) \cdot (1 - \omega) \cdot T_{veg} \cdot (1 - \Upsilon_{veg}) \cdot \Upsilon_{veg} \quad (2.12)$$

where  $\Upsilon_{veg}$  is the transmissivity of the vegetation layer,  $T_{veg}$  is the physical temperature of vegetation [K] and  $\omega$  is the single scattering albedo of the vegetation. Consequently,

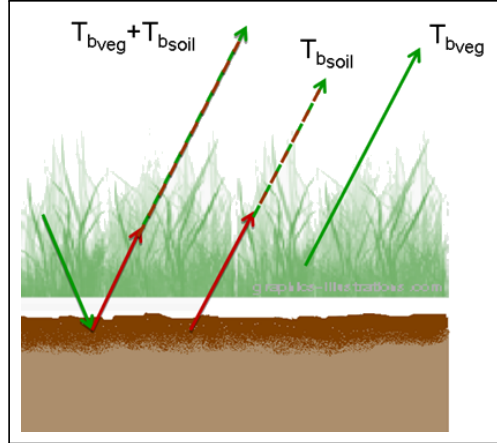


**Figure 2.5:** Contribution of vegetation and soil components to the detected TB signal.

the overall brightness temperature response is the sum of three main terms: i) the soil emission which is attenuated by the vegetation layer, ii) the direct emission of the vegetation itself and iii) the downward vegetation emission which is reflected by the soil and again attenuated by the canopy layer. Figure 2.5 shows the various types and sources of microwave emission of the soil surface and the overlying vegetation layer. The basic principle of soil moisture retrieval and the approach chosen for SMOS is to find the best-suited set of soil moisture and vegetation parameters by minimizing a cost function while considering the differences between modelled direct and measured brightness temperature data.

The vegetation transmissivity  $\Upsilon_{veg}$  describes the impact of attenuation within the canopy layer and may be computed from the optical depth/vegetation opacity at nadir  $\tau_{NAD}$ :

$$\Upsilon_{veg}(p, \theta) = \exp(\tau_{NAD} / \cos(\theta)) \quad (2.13)$$

Past research has shown that the vegetation opacity in turn can be parameterized through a simple linear relationship by the total vegetation water content (VWC) using

the so-called  $b$ -parameter:

$$\tau_{NAD} = b \cdot VWC. \quad (2.14)$$

Several studies considered the vegetation parameter  $b$  to be a function of canopy type and structure; though values between  $0.12 \pm 0.03$  were found representative of most agricultural land use.

Regarding the scattering effects within the canopy layer the single scattering albedo  $\omega$  was found to be rather low leading to the general agreement across the research community to neglect this parameter in the algorithm by postulating  $\omega = 0$ . Moreover, since no dependency on the incidence angle could be demonstrated so far, the impact of the single scattering albedo of the low vegetation layer is likely to be minor. In contrast, for the optical depth of standing vegetation (excluding litter) with dominant vertically structured canopy an additional pair of correction factors  $tt_p$  were introduced to account for the dependency of the opacity to the incidence angle:

$$\tau(p, \theta) = \tau_{NAD} \cdot (\sin^2(\theta) \cdot tt_p + \cos^2(\theta)). \quad (2.15)$$

The complexity of the soil-vegetation system and the different contributions to the measured brightness temperature makes soil moisture retrieval challenging. Past studies by Wigneron et al. (1995, 2000, 2003) tested especially the potential of dual-polarised, multi-angle observations for multi-parameter retrievals (soil moisture, optical depth, effective surface soil temperature...). In particular, two-parameter retrievals of multi-angle SMOS data proved to provide useful information about soil moisture and optical depth when the range of look angles was sufficiently large (Wigneron et al., 2003). However, the quality of this information from multi-angle systems depends on having an accurate characterization of the ratio  $\tau_h/\tau_v$  and the angular dependency of this vegetation parameter especially for vertical vegetation structures (Ulaby et al., 1986).

Given a simple example of brightness temperature response signatures from vegetated versus bare as shown in Figure 2.6. Even though the soil conditions are set equal, the behaviour of a vegetated surface may differ strongly to that of a bare soil due to

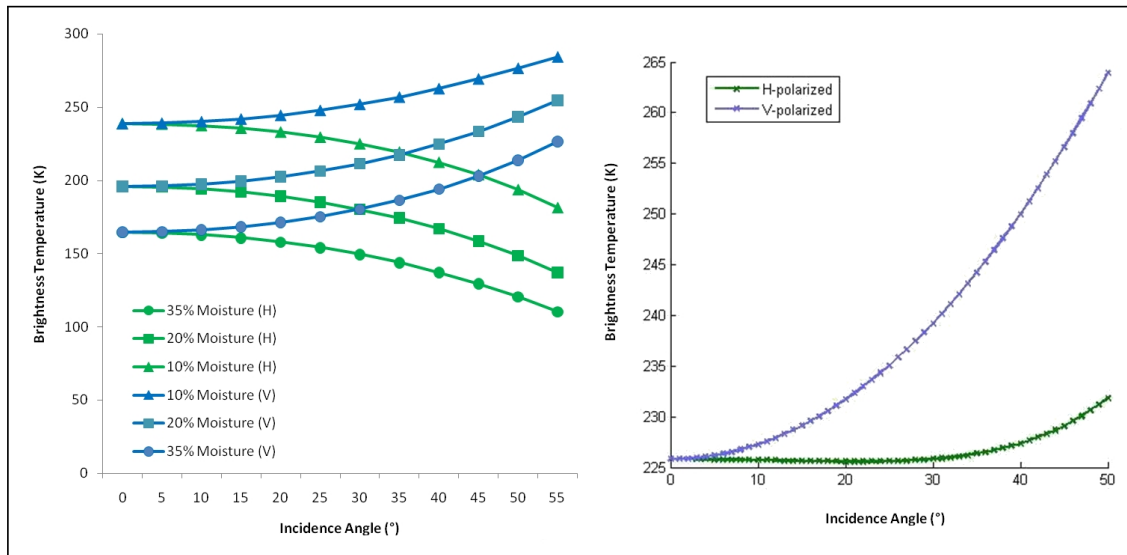


**Figure 2.6:** Relation between TB and look angle for bare soil (left) and vegetated/grassland conditions (right).

the interference of the electromagnetic signal with the canopy. For the depicted test case the vertically polarized microwave trend shows a rise with larger incidence angles - though the incline is much stronger for the vegetated area. In contrast to bare soil conditions the horizontally polarized microwave curve clearly demonstrates an upward trend by increasing brightness temperatures with larger angles. The additional vegetation layer significantly affects the soil emission through scattering and attenuation processes, which on its own additionally depend on the look angle configuration. With respect to the range of surface conditions and the variety of land use across the Earth, a better understanding of angular dependencies of the components in the soil moisture retrieval process is crucial for satisfying results. Moreover, it clearly demonstrates that there is a strong need to explore the magnitude of the individual impact - even at different spatial scales - to assess the application of multi-angle retrieval techniques and provide sophisticated L-band soil moisture mapping.

Previous studies have identified various incidence angle dependencies of surface variables which are essential for the model parameterization: vegetation optical depth, single scattering albedo and soil surface roughness. The research conducted by Hornbuckle et al. (2003), Pardé et al. (2003) and Wigneron et al. (2004) particularly focused on the canopy structure and incidence angle relationship over agricultural

areas. However, dependency of the single scattering albedo on the viewing angle is not yet clearly demonstrated. Thus, angular dependency of the optical depth needs to be understood at larger scales, such as those of airborne and satellite observations, as well as the angular dependency of the optical depth of special features of natural environments (rarely/never ploughed) such as litter and necromass (Wigneron and Hornbuckle, 2006).

Shi et al. (2002) demonstrated that it is crucial to account for roughness effects as they differ strongly at varying incidence angles. Correspondingly, Saleh et al. (2009) investigated the performance of the retrieval process with a focus on available roughness information. The study is based on multi-angle data to simultaneously obtain the main roughness parameter and the optical depth, which quantifies the energetic opacity of the vegetation. Based on the data set, they were able to develop an approach which could provide first estimates of roughness information for the SMOS soil moisture retrieval algorithm. However, the results were obtained over a confined area and for a spatial resolution of maximum 375 m (at nadir). Hence, this small scale approach needs to be tested and verified for different environmental conditions and larger scales to assess its suitability for application to SMOS. Moreover, according to the study by Davenport et al. (2008), which is based on synthetically generated space borne microwave data, the multi-angle system is more likely to be affected by the sub-pixel soil roughness heterogeneity than single-angle retrieval algorithms. Thus, the globalized effect of soil roughness on the SMOS soil moisture product still needs to be investigated for a clearer understanding.

Past research has shown that there are significant look angle dependencies of land surface variables on the measured brightness temperature, meaning that the other ancillary data required for soil moisture retrieval can also be estimated, resulting in a more accurate soil moisture retrieval. However, due to the absence of comparable spaceborne products, retrieval algorithms such as L-MEB have been developed from synthetic simulations and high-resolution data from towers, with the development of multi-incidence angle relationships constrained to only a subset of the possible parameters. Consequently, the derived relationships and model interactions between

land surface variables and observed brightness temperature response need to be verified at larger spatial scales, for a wider range of land surface conditions, and be extended to include further land surface multi-incidence angle relationships.

### **2.2.3 Soil Moisture and Ocean Salinity Mission - SMOS**

The Soil Moisture and Ocean Salinity (SMOS) mission (Kerr et al., 2001, 2010) has been operational since its launch on the 2<sup>nd</sup> November 2009 led by the European Space Agency (ESA). Initially proposed in 1998 the project was chosen for one of ESA's Earth Explorer Missions as part of the Living Planet Programme. The SMOS mission is the very first specifically dedicated to the global observation of soil moisture over land and the salinity over the ocean. Identified as a key project by the scientific community the mission was set to advance the development and evolution of hydrological, meteorological and climatological models.

The single payload of the spacecraft is an innovative two-dimensional synthetic radiometer known as **Microwave Interferometric Radiometer with Aperture Synthesis (MIRAS)**. Equipped with 69 antenna receivers distributed on a Y-shaped deployable array and central hub, the instrument operates at 1.4 GHz within the protected L-band at full polarization (McMullan et al., 2008). The satellite orbits at a quasi-circular, sun-synchronous, dusk-dawn orbit allowing observations at moderate spatial resolution (30-50 km) and a revisit time of approximately three days at the equator. The target soil moisture product accuracy is set to be better than  $0.04 \text{ m}^3/\text{m}^3$  when the vegetation biomass is lower than  $4 \text{ kg}/\text{m}^2$  (Barre et al., 2008). The second objective of mapping ocean salinity aims to monitor salinity down to 0.1 practical salinity units (psu), averaged over 10 - 30 days in areas covering 200 km x 200 km.

One novel aspect of this innovative spaceborne sensor is the utilization of the multi-incidence angle observations for soil moisture retrieval (Kerr et al., 2011). There are two approaches for acquiring multi-angle observations from satellite; along-track or across-track (Wigneron et al., 1995). The across-track method relies upon measurements from different orbits to obtain a range of incidence angles. The disadvantage of

this multi-angular observation approach is that there are generally temporal variations of the surface parameters during the time interval of the measurements. In contrast, the along-track method uses measurements from within a single orbit thus allowing simultaneous acquisition of data for a range of incidence angles. Due to the unique instrument characteristics of SMOS, this is the type of satellite data that are provided by the MIRAS sensor with incidence angles between 0-55° (from nadir).

The spaceborne multi-angle observation technique of SMOS is an innovative concept based on the aperture synthesis (Kerr et al., 2001). Therefore expectations were high that the multi-angular data which SMOS provides would significantly improve the soil moisture retrieval compared to traditional techniques that have only vertical and/or horizontal polarization observations for a single incidence angle. In this regard, scientists have constantly been challenged to develop and modify retrieval concepts especially adapted to the SMOS technique to be able to fully utilize its multi-angle potential.

Due to the satellite's unprecedented performance so far, unforeseen utilizations of the SMOS data are reflecting its versatility in terms of research opportunities in weather forecast, climate modelling, sustainable water management and beyond its original scientific brief. Even though originally designed as a five-year project, the mission meanwhile has been extended until at least 2017.

## References for Chapter 2

- Barre, H. M.J. P., B. Duesmann, and Y. H. Kerr (2008), “SMOS: The Mission and the System,” *IEEE Transactions on Geoscience and Remote Sensing*, 46(3), pp. 587–593, DOI: 10.1109/tgrs.2008.916264 (cited on p. 32).
- Behari, J. (2006), *Microwave dielectric behaviour of wet soils*, vol. 8, Springer Science & Business Media (cited on p. 23).
- Bittelli, M. (2011), “Measuring Soil Water Content: A Review,” *Horttechnology*, 21(3), pp. 293–300 (cited on p. 19).
- Burke, E. J. and L. P. Simmonds (2001), “A simple parameterisation for retrieving soil moisture from passive microwave data,” *Hydrology and Earth System Sciences*, 5(1), pp. 39–48 (cited on p. 27).
- Chen, F., W. T. Crow, P. J. Starks, and D. N. Moriasi (2011), “Improving hydrologic predictions of a catchment model via assimilation of surface soil moisture,” *Advances in Water Resources*, 34(4), pp. 526–536, DOI: 10.1016/j.advwatres.2011.01.011 (cited on p. 18).
- Choudhury, B. J., T. J. Schmugge, A. Chang, and R. Newton (1979), “Effect of surface roughness on the microwave emission from soils,” *Journal of Geophysical Research*, 84 (C9), pp. 5699–5706, DOI: 10.1029/JC084iC09p05699 (cited on p. 27).
- Davenport, I. J., M. J. Sandells, and R. J. Gurney (2008), “The effects of scene heterogeneity on soil moisture retrieval from passive microwave data,” *Advances in Water Resources*, 31(11), pp. 1494–1502, DOI: 10.1016/j.advwatres.2008.06.002 (cited on pp. 8, 31).
- Dobson, M., F. Ulaby, M. Hallikainen, and M. El-rays (1985), “Microwave Dielectric Behavior of Wet Soil-Part II: Dielectric Mixing Models,” *IEEE Transactions on Geoscience and Remote Sensing*, GE-23(1), pp. 35–46, DOI: 10.1109/tgrs.1985.289498 (cited on pp. 20, 26).

- Escorihuela, M. J., A. Chanzy, J. P. Wigneron, and Y. H. Kerr (2010), "Effective soil moisture sampling depth of L-band radiometry: A case study," *Remote Sensing of Environment*, 114(5), pp. 995–1001, DOI: 10.1016/j.rse.2009.12.011 (cited on pp. 24, 56).
- Famiglietti, J. S., J. W. Rudnicki, and M. Rodell (1998), "Variability in surface moisture content along a hillslope transect: Rattlesnake Hill, Texas," *Journal of Hydrology*, 210(1), 136LU Times Cited:146 Cited References Count:29, pp. 259–281 (cited on pp. 4, 20).
- Hornbuckle, B. K., A. W. England, R. D. De Roo, M. A. Fischman, and D. L. Boprie (2003), "Vegetation canopy anisotropy at 1.4 GHz," *IEEE Transactions on Geoscience and Remote Sensing*, 41(10), pp. 2211–2223, DOI: 10.1109/tgrs.2003.817192 (cited on pp. 8, 30).
- Jackson, T. J., J. Schmugge, and E. T. Engman (1996), "Remote sensing applications to hydrology: soil moisture," *Hydrological Sciences Journal*, 41(4), pp. 517–530, DOI: 10.1080/02626669609491523 (cited on p. 24).
- Jackson, T. J. (2005), "Remote Sensing: Soil Moisture," in: *Encyclopedia of Soils in the Environment*, ed. by D. Hillel, Elsevier, pp. 392–399 (cited on p. 24).
- Kerr, Y. H., P. Waldteufel, J.-P. Wigneron, J. M. Martinuzzi, J. Font, and M. Berger (2001), "Soil moisture retrieval from space: The Soil Moisture and Ocean Salinity (SMOS) mission," *IEEE Transactions on Geoscience and Remote Sensing*, 39(8), pp. 1729–1735, DOI: 10.1109/36.942551 (cited on pp. 32, 33).
- Kerr, Y. H., P. Waldteufel, J.-P. Wigneron, S. Delwart, F. Cabot, J. Boutin, M.-J. Escorihuela, J. Font, N. Reul, C. Gruhier, S. E. Juglea, M. R. Drinkwater, A. Hahne, M. Martín-Neira, and S. Mecklenburg (2010), "The SMOS Mission: New Tool for Monitoring Key Elements of the Global Water Cycle," *Proceedings of the IEEE*, 98(5), pp. 666–687, DOI: 10.1109/jproc.2010.2043032 (cited on p. 32).
- Kerr, Y. H., P. Waldteufel, P. Richaume, J.-P. Wigneron, P. Ferrazzoli, and R. J. Gurney (2011), *SMOS level 2 processor for soil moisture - Algorithm Theoretical Based Document (ATBD)*, Report ESA No.: SO-TN-ESL-SM-GS-0001, CESBIO, p. 121 (cited on p. 32).

- Kerr, Y. (2007), "Soil moisture from space: Where are we?" *Hydrogeology Journal*, 15(1), pp. 117–120, DOI: 10.1007/s10040-006-0095-3 (cited on p. 24).
- Laymon, C. A., W. L. Crosson, T. J. Jackson, A. Manu, and T. D. Tsegaye (2001), "Ground-based passive microwave remote sensing observations of soil moisture at S-band and L-band with insight into measurement accuracy," *IEEE Transactions on Geoscience and Remote Sensing*, 39(9), pp. 1844–1858 (cited on p. 24).
- Legates, D. R., R. Mahmood, D. F. Levia, T. L. DeLiberty, S. M. Quiring, C. Houser, and F. E. Nelson (2010), "Soil moisture: A central and unifying theme in physical geography," *Progress in Physical Geography*, 35(1), pp. 65–86, DOI: 10.1177/0309133310386514 (cited on p. 17).
- Lo, C. P. (1986), "Applied remote sensing" (cited on p. 22).
- McMullan, K. D., M. A. Brown, M. Martin-Neira, W. Rits, S. Ekholm, J. Marti, and J. Lemanczyk (2008), "SMOS: The Payload," *IEEE Transactions on Geoscience and Remote Sensing*, 46(3), 270QB Times Cited:39 Cited References Count:10, pp. 594–605, DOI: 10.1109/tgrs.2007.914809 (cited on p. 32).
- Mironov, V. L., M. C. Dobson, V. H. Kaupp, S. A. Komarov, and V. N. Kleshchenko (2004), "Generalized refractive mixing dielectric model for moist soils," *IEEE Transactions on Geoscience and Remote Sensing*, 42(4), pp. 773–785 (cited on pp. 20, 26).
- Mo, T., B. J. Choudhury, T. J. Schmugge, J. R. Wang, and T. Jackson (1982), "A model for microwave emission from vegetation-covered fields," *Journal of Geophysical Research*, 87 (C13), pp. 11,229–11,237, DOI: 10.1029/JC087iC13p11229 (cited on p. 27).
- Newton, R. W. and J. W. Rouse Jr (1980), "Microwave radiometer measurements of soil moisture content," *IEEE Transactions on Antennas and Propagation*, AP-28(5), Data indicate that dense vegetation to a height of 125 cm has little effect on measured emission at a 21.4-cm wavelength for incident angles out of 35deg. Above 35deg the effect on the emission becomes noticeable. However, even at 20°, the data indicate that a vegetation increase from 125-cm height to 188-cm height has a measurable effect on the microwave emission., pp. 680–686, DOI: 0018-926X/80/0900-0680 (cited on pp. 24, 27).

- Njoku, E. G. and D. Entekhabi (1996), "Passive microwave remote sensing of soil moisture," *Journal of Hydrology*, 184(1), pp. 101–129, DOI: 10.1016/0022-1694(95)02970-2 (cited on p. 24).
- Pardé, M., J.-P. Wigneron, A. Chanzy, P. Waldteufel, Y. H. Kerr, and S. Huet (2003), "Retrieving surface soil moisture over a wheat field: comparison of different methods," *Remote Sensing of Environment*, 87(2), pp. 334–344, DOI: 10.1016/j.rse.2003.08.002 (cited on pp. 8, 30).
- Raju, S., A. Chanzy, J.-P. Wigneron, J.-C. Calvet, Y. Kerr, and L. Laguerre (1995), "Soil moisture and temperature profile effects on microwave emission at low frequencies," *Remote sensing of environment*, 54(2), pp. 85–97 (cited on p. 24).
- Robinson, D. A., C. S. Campbell, J. W. Hopmans, B. K. Hornbuckle, S. B. Jones, R. Knight, F. Ogden, J. Selker, and O. Wendroth (2008), "Soil moisture measurement for ecological and hydrological watershed-scale observatories: A review," *Vadose Zone Journal*, 7(1), 288BJ Times Cited:55 Cited References Count:335, pp. 358–389, DOI: 10.2136/Vzj2007.0143 (cited on pp. 3, 19).
- Saleh, K., Y. H. Kerr, P. Richaume, M. J. Escorihuela, R. Panciera, S. Delwart, G. Boulet, P. Maisongrande, J. P. Walker, and P. Wursteisen (2009), "Soil moisture retrievals at L-band using a two-step inversion approach (COSMOS/NAFE'05 Experiment)," *Remote Sensing of Environment*, 113(6), pp. 1304–1312, DOI: 10.1016/j.rse.2009.02.013 (cited on p. 31).
- Schmugge, T. J., P. O'Neill, and J. R. Wang (1986), "Passive microwave soil moisture research," *IEEE Transactions on Geoscience and Remote Sensing*, GE-24(1), pp. 12–22, DOI: 10.1109/TGRS.1986.289584 (cited on p. 23).
- Sellers, P. J., M. D. Heiser, F. G. Hall, S. B. Verma, R. L. Desjardins, P. M. Schuepp, and J. I. MacPherson (1997), "The impact of using area-averaged land surface properties- Topography, vegetation condition, soil wetness- In calculations of intermediate scale (approximately 10 km<sup>2</sup>) surface-atmosphere heat and moisture fluxes," *Journal of Hydrology*, 190(3), pp. 269–301 (cited on p. 18).
- Shi, J., K. S. Chen, Q. Li, T. J. Jackson, P. E. O'Neill, and L. Tsang (2002), "A parameterized surface reflectivity model and estimation of bare-surface soil moisture with

- L-band radiometer,” *IEEE Transactions on Geoscience and Remote Sensing*, 40(12), pp. 2674–2686 (cited on p. 31).
- Strahler, A. H. and A. N. Strahler (2002), *Physical geography: science and systems of the human environment*, vol. 3, Wiley New York (cited on p. 17).
- Timbal, B., S. Power, R. Colman, J. Viviani, and S. Lirola (2002), “Does soil moisture influence climate variability and predictability over Australia?” *Journal of Climate*, 15(10), pp. 1230–1238 (cited on p. 18).
- Ulaby, F., R. Moore, and A. Fung (1986), *Microwave remote sensing: active and passive, Vol. III: From theory to applications*, vol. 3, Norwood, MA: Artech House (cited on pp. 26, 27, 29).
- Vereecken, H., J. A. Huisman, H. Bogaert, J. Vanderborght, J. A. Vrugt, and J. Hopmans (2008), “On the value of soil moisture measurements in vadose zone hydrology: A review,” *Water Resources Research*, 44 (W00D06), 365ER Times Cited:34 Cited References Count:297, p. 21, DOI: 10.1029/2008WR006829 (cited on p. 21).
- Wang, J. R. (1983), “Passive microwave sensing of soil moisture content: The effects of soil bulk density and surface roughness,” *Remote sensing of environment*, 13(4), pp. 329–344 (cited on p. 27).
- Wang, J. R. and T. J. Schmugge (1980), “An empirical model for the complex dielectric permittivity of soils as a function of water content,” *IEEE Transactions on Geoscience and Remote Sensing*, (4), pp. 288–295 (cited on pp. 20, 26).
- Wang, J. and B. J. Choudhury (1981), “Remote Sensing of Soil Moisture Content Over Bare Field at 1.4 GHz Frequency,” *Journal of Geophysical Research*, 86 (C6), pp. 5277–5282, DOI: 10.1029/JC086iC06p05277 (cited on p. 24).
- Western, A. W., R. B. Grayson, and T. R. Green (1999), “The Tarrawarra project: high resolution spatial measurement, modelling and analysis of soil moisture and hydrological response,” *Hydrological Processes*, 13(5), pp. 633–652 (cited on pp. 3, 20).
- Western, A. W., S.-L. Zhou, R. B. Grayson, T. A. McMahon, G. Blöschl, and D. J. Wilson (2004), “Spatial correlation of soil moisture in small catchments and its relationship to dominant spatial hydrological processes,” *Journal of Hydrology*, 286(1), pp. 113–134, DOI: 10.1016/j.jhydro1.2003.09.014 (cited on p. 20).

- Wetzel, P. J. and J. T. Chang (1987), "Concerning the relationship between evapotranspiration and soil moisture," *Journal of Climate and Applied Meteorology*, 26(1), pp. 18–27 (cited on pp. 3, 18).
- Wigneron, J.-P. and B. K. Hornbuckle (2006), "Modelling the effect of vegetation structure - evaluating the sensitivity of the vegetation model parameters to the canopy geometry and to the configuration parameters (frequency, polarisation and incidence angle)," in: *Thermal Microwave Radiation-Applications for Remote Sensing*, ed. by C. Mätzler, P. W. Rosenkranz, A. Battaglia, and J.-P. Wigneron, vol. 52, IEE Electromagnetic Waves Series, London, UK: The Institution of Engineering and Technology, pp. 324–333 (cited on p. 31).
- Wigneron, J.-P., A. Chanzy, J.-C. Calvet, and N. Bruguier (1995), "A simple algorithm to retrieve soil moisture and vegetation biomass using passive microwave measurements over crop fields," *Remote Sensing of Environment*, 51(3), pp. 331–341, DOI: 10.1016/0034-4257(94)00081-w (cited on pp. 8, 29, 32).
- Wigneron, J.-P., P. Waldteufel, A. Chanzy, J.-C. Calvet, and Y. H. Kerr (2000), "Two-dimensional microwave interferometer retrieval capabilities over land surfaces (SMOS Mission)," *Remote Sensing of Environment*, 73(3), 347GH Times Cited:75 Cited References Count:37, pp. 270–282, DOI: 10.1016/S0034-4257(00)00103-6 (cited on pp. 5, 29, 126).
- Wigneron, J.-P., J.-C. Calvet, T. Pellarin, A. A. Van de Griend, M. Berger, and P. Ferrazzoli (2003), "Retrieving near-surface soil moisture from microwave radiometric observations: current status and future plans," *Remote Sensing of Environment*, 85(4), pp. 489–506, DOI: 10.1016/S0034-4257(03)00051-8 (cited on pp. 6, 29).
- Wigneron, J.-P., J.-C. Calvet, P. de Rosnay, Y. H. Kerr, K. Saleh, M. J. Escorihuela, and P. Waldteufel (2004), "Soil Moisture Retrievals From Biangular L-Band Passive Microwave Observations," *IEEE Geoscience and Remote Sensing Letters*, 1(4), pp. 277–281, DOI: 10.1109/LGRS.2004.834594 (cited on p. 30).
- Wigneron, J.-P., Y. H. Kerr, P. Waldteufel, K. Saleh, M. J. Escorihuela, P. Richaume, P. Ferrazzoli, P. de Rosnay, R. J. Gurney, J.-C. Calvet, J. P. Grant, M. Guglielmetti, B. Hornbuckle, C. Mätzler, T. Pellarin, and M. Schwank (2007), "L-band Microwave

Emission of the Biosphere (L-MEB) Model: Description and calibration against experimental data sets over crop fields,” *Remote Sensing of Environment*, 107(4), pp. 639–655, DOI: 10.1016/j.rse.2006.10.014 (cited on pp. 27, 125, 126, 128).

## **Part II**

# **Analysis on airborne multi-incidence angle L-band data**

---

# 3

## Evaluation of L-MEB for vegetation and roughness effects [Paper 1]

**T**HIS chapter includes a research paper which has resulted from the studies undertaken for this degree and is published in a peer-reviewed journal. The IEEE copyrighted paper on “Wheat Canopy Structure and Surface Roughness Effects on Multiangle Observations at L-Band” will be reprinted in this thesis, with permission, from all authors (May, 2012).

S. Peischl et al. (2012b), “Wheat Canopy Structure and Surface Roughness Effects on Multiangle Observations at L-Band,” *IEEE Transactions on Geoscience and Remote Sensing*, 50(5), pp. 1498–1506, DOI: 10.1109/tgrs.2011.2174644 ©2012 IEEE.

**Declaration for Thesis Chapter 3**

In the case of Chapter 3, the nature and extent of my contribution to the work was the following:

Nature of contribution	Extent of contribution (%)
Review of literature, data processing and interpretation, and write up.	70 %

The following co-authors contributed to the work. Co-authors who are students at Monash University must also indicate the extent of their contribution in percentage terms: n/a

Name	Nature of contribution	Extent of contribution (%) for student co-authors only
Prof Jeffrey Walker	Ideas, interpretation and reviewing	n/a
Dr Dongryeol Ryu	Ideas and reviewing	n/a
Dr Yann Kerr	Ideas and reviewing	n/a
Dr Rocco Panciera	Data processing and reviewing	n/a
Dr Christoph Rüdiger	Interpretation and reviewing	n/a

Candidate's Signature	<i>Sandy Peisoli</i>	Date	<i>27/06/12</i>
-----------------------	----------------------	------	-----------------

**Declaration by co-authors**

The undersigned hereby certify that:

- (1) the above declaration correctly reflects the nature and extent of the candidate's contribution to this work, and the nature of the contribution of each of the co-authors.
- (2) they meet the criteria for authorship in that they have participated in the conception, execution, or interpretation, of at least that part of the publication in their field of expertise;
- (3) they take public responsibility for their part of the publication, except for the responsible author who accepts overall responsibility for the publication;
- (4) there are no other authors of the publication according to these criteria;
- (5) potential conflicts of interest have been disclosed to (a) granting bodies, (b) the editor or publisher of journals or other publications, and (c) the head of the responsible academic unit; and
- (6) the original data are stored at the following location(s) and will be held for at least five years from the date indicated below:

Location	Department of Civil Engineering, Monash University, Australia
----------	---

Signature 1	Prof Jeffrey Walker <i>JWalker</i>	Date	<i>4/7/12</i>
Signature 2	Dr Christoph Rüdiger <i>Christoph Ruediger</i>	Date	<i>27/6/2012</i>

.....

<b>Signature 4</b>	Dr Dongryeol Ryu 	<b>Date</b> 19-7-2012
<b>Signature 3</b>	Dr Yann Kerr 	1/12/2016
<b>Signature 5</b>	Dr Rocco Panciera 	19-7-2012

.....

### **3.1 Introduction**

---

This paper investigates the relationship between surface soil moisture and observed passive microwave emission at multiple incidence angles using L-band airborne data from two extensive field experiments in Australia.

First, a forward radio-brightness model is used to predict the brightness temperature response for a range of incidence angles given inputs of ground measured soil moisture, soil temperature and vegetation characteristics. These simulations are done across several locations mainly covered with mature wheat canopy and repeated for multiple dates and moisture conditions. Subsequently, the airborne L-band brightness temperature observations are compared against the forward-simulated response which is calculated using i) default sets of L-MEB parameters and ii) on-site calibrated retrieval parameters. Based on the derived model results the utility of multi-incidence angle soil moisture retrieval is assessed.

### **3.2 Wheat canopy structure and surface roughness effects on multi-angle observations at L-band**

---

# Wheat Canopy Structure and Surface Roughness Effects on Multiangle Observations at L-Band

Sandy Peischl, *Member, IEEE*, Jeffrey P. Walker, Dongryeol Ryu, *Member, IEEE*, Yann H. Kerr, *Senior Member, IEEE*, Rocco Panciera, and Christoph Rüdiger, *Member, IEEE*

**Abstract**—The multiangle observation capability of the Soil Moisture and Ocean Salinity mission is expected to significantly improve the inversion of soil microwave emissions for soil moisture, by enabling the simultaneous retrieval of the vegetation optical depth and other surface parameters. Consequently, this paper investigates the relationship between soil moisture and brightness temperature at multiple incidence angles using airborne L-band data from the National Airborne Field Experiment in Australia in 2005. A forward radio brightness model was used to predict the passive microwave response at a range of incidence angles, given the following inputs: 1) ground-measured soil and vegetation properties and 2) default model parameters for vegetation and roughness characterization. Simulations were made across various dates and locations with wheat cover and evaluated against the available airborne observations. The comparison showed a significant underestimation of the measured brightness temperatures by the model. This discrepancy subsequently led to soil moisture retrieval errors of up to  $0.3 \text{ m}^3/\text{m}^3$ . Further analysis found the following: 1) The roughness value  $H_R$  was too low, which was then adjusted as a function of the soil moisture, and 2) the vegetation structure parameters  $tt_h$  and  $tt_v$  required optimization, yielding new values of  $tt_h = 0.2$  and  $tt_v = 1.4$  from calibration to a single flight. Testing the optimized parameterization for different moisture conditions and locations found that the root-mean-square simulation error between the forward model predictions and the airborne observations was improved from 31.3 K (26.5 K) to 2.3 K (5.3 K) for wet (dry) soil moisture condition.

**Index Terms**—L-band Microwave Emission of the Biosphere (L-MEB), microwave radiometry, multiangle, National Airborne Field Experiment (NAFE), Soil Moisture and Ocean Salinity (SMOS).

## I. INTRODUCTION

THE POTENTIAL of passive microwave systems to monitor surface soil moisture has been extensively studied

Manuscript received April 14, 2011; revised July 26, 2011 and September 16, 2011; accepted September 24, 2011. Date of publication December 13, 2011; date of current version April 18, 2012. This work was supported by the Australian Research Council within the framework of the Moisture Map project under Grant DP0879212.

S. Peischl, J. P. Walker, and C. Rüdiger are with the Department of Civil Engineering, Faculty of Engineering, Monash University, Melbourne, Vic. 3800, Australia (e-mail: sandy.peischl@monash.edu; jeff.walker@monash.edu; chris.rudiger@monash.edu).

D. Ryu is with the Department of Infrastructure Engineering, Melbourne School of Engineering, The University of Melbourne, Melbourne, Vic. 3010, Australia (e-mail: dryu@unimelb.edu.au).

R. Panciera is with the Cooperative Research Centre for Spatial Information, Carlton, Vic. 3053, Australia (e-mail: panr@unimelb.edu.au).

Y. H. Kerr is with the Centre d'Etudes Spatiales de la Biosphère, 31401 Toulouse, France (e-mail: yann.kerr@cesbio.cnes.fr).

Color versions of one or more of the figures in this paper are available online at <http://ieeexplore.ieee.org>.

Digital Object Identifier 10.1109/TGRS.2011.2174644

during the past decades [1]–[7] and is considered as one of the most well-suited techniques. Microwave remote sensing is particularly suitable due to the following: 1) its high sensitivity to the dielectric properties of the soil–water medium, which can be directly related to the water content; 2) the reduced interference with the atmosphere and surface roughness; 3) the low attenuation effects of the vegetation layer; and 4) its all-weather capability. Moreover, at low frequencies, the sampling depth within the soil column is deeper compared to shorter wavelengths. Hence, the protected L-band ( $\sim 1$ – $2$  GHz) with a sampling depth of typically  $\sim 5$  cm and low sensitivity to canopy and surface roughness is preferred for the purpose of surface soil moisture remote sensing. Consequently, the strong scientific demand for large-scale L-band observations of surface soil moisture data, with a sufficient temporal resolution for application in hydrological, meteorological, and agronomical disciplines [8], has led to the first spaceborne mission specifically dedicated to the monitoring of surface soil moisture.

The Soil Moisture and Ocean Salinity (SMOS) satellite, launched in November 2009 by the European Space Agency, was designed to provide global maps of the surface soil moisture fields with an accuracy better than  $0.04 \text{ m}^3/\text{m}^3$  for the nominal case of bare or low-vegetated soils (nonnominal cases include mountainous and urban areas, frozen or very dry soils, ice, and significant snow-covered surfaces) [9], [10]. Importantly, the satellite's new antenna concept utilizes a 2-D interferometric L-band radiometer to overcome the constraints given by the proportional relationship between the antenna diameter and the resulting spatial resolution, achieving a pixel size of less than 50 km. Moreover, one of the innovative features of SMOS is its capability of multi-incidence-angle observations, which are obtained by the along-track movement of the satellite and the corresponding quasi-simultaneous acquisition of a series of brightness temperatures for a range of incidence angles over the same location on Earth. Previous studies [11]–[13] have shown that there are significant angular signatures on the measured radiometer signal associated with various land surface features and that, in some cases, it is difficult to separate the contribution of the vegetation from the actual soil emission based on single-angle measurements. Thus, by understanding these angular dependences, it has been suggested that model parameters such as vegetation attenuation and surface roughness may be simultaneously estimated, resulting in an enhanced and presumably more accurate surface soil moisture retrieval [14]. Due to the absence of comparable spaceborne observations regarding the novel SMOS configuration, retrieval algorithms such as L-band Microwave Emission of the Biosphere (L-MEB) [15] have been primarily developed and tested prelaunch using

synthetic simulations [16] and small-scale field experiments (e.g., Surface Monitoring Of the Soil Reservoir EXperiment (SMOSREX) [17], Mediterranean Ecosystem L-band characterisation EXperiment [18], and European campaign with the Salinity Temperature and Roughness Remote Scanner (EuroSTARRS) [19]), with the modeling of incidence angle relationships based on only a subset of the possible land cover types. Consequently, the derived relationships and the model interactions between land surface variables and observed brightness temperature response need to be verified at larger spatial scales and extended for a wider range of land surface conditions.

The objective of this paper is to compare multiangle L-band data from airborne observations with simulated brightness temperatures using the L-MEB model and ground truth data as input. Subsequently, the performance of the forward model parameterization is evaluated based on different surface soil moisture conditions and locations. Alternative parameterizations are also tested, including the following: 1) modifications of the modeled roughness and 2) vegetation structure characterization.

## II. EXPERIMENTAL DATA SET

The multi-incidence-angle airborne data used in this paper were acquired in November 2005 during the National Airborne Field Experiment (NAFE'05) in southeast Australia. The campaign was conducted over a period of four weeks including a combination of airborne observations and ground measurements. A complete description of the experiment and the data collection strategy is provided in [20], so only the pertinent details are summarized here.

### A. Study Area

The field experiment concentrated on the northern part of the Goulburn River catchment (32° S, 150° E) located in New South Wales, Australia. The 40 km × 40 km study region had been subdivided into two main focus areas: the Merriwa River and Krui River catchments. Across each of these two focus areas, several smaller sites had been selected for intensive airborne and ground operations at farm scale. The multi-incidence-angle flights, which are the emphasis of this study, covered only three out of a total of eight focus farms, being Midlothian, Merriwa Park, and Cullingral (Fig. 1). The observed terrain is fairly flat, with soil types ranging from clay loams to sandy soils [21]. The regional climate can be described as subhumid to temperate with an average annual rainfall of 700 mm and mean maximum annual temperatures of 30 °C in summer and 16 °C in winter. During the campaign period, the focus farms were dominated by grazing lands with native grass cover and cropping land use (mainly wheat, barley, and lucerne).

### B. Airborne Multiangle Data

The primary airborne instrument used in the NAFE'05 campaign was the Polarimetric L-band Multibeam Radiometer (PLMR), which operates at a frequency of 1.413 GHz with a bandwidth of 24 MHz. During the field experiment, the L-band radiometer was typically used to measure dual-

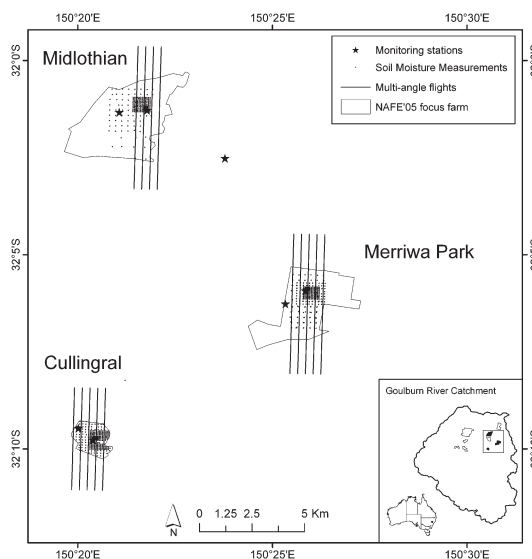


Fig. 1. Locations of the three focus farms covered by multiangle L-band observations in NAFE'05. Overlaid are the flight lines of the aircraft, the location of nearby monitoring stations, and the grid of HDAS surface soil moisture measurements. The high-resolution spatial sampling area of near-surface surface soil moisture (6.25–125 m) is displayed by a cluster of points in contrast to the coarser sampling scale (250–500 m), where each individual sampling location is marked. (Inset) Distribution of all NAFE'05 focus farms within the Goulburn River catchment, located in New South Wales, Australia.

polarized brightness temperatures in pushbroom mode at six across-track viewing angles ( $\pm 7^\circ$ ,  $\pm 21.5^\circ$ , and  $\pm 38.5^\circ$ ). However, for the multiangle data collection used in this study, PLMR was mounted on the aircraft in an along-track configuration, i.e., the instrument was rotated by  $90^\circ$  around its vertical axis, resulting in six along-track viewing angles, three PLMR beams pointing forward and three backward with respect to the flight direction of the aircraft. Consequently, as the aircraft moved along its flight path, this setup provided a minimum of six quasi-simultaneous multi-incidence-angle observations of the same location on Earth with an  $\sim 15^\circ$  (3-dB) antenna beamwidth. Due to an aircraft pitch of about  $4^\circ$ , the resulting angles of the six PLMR beams were approximately  $3^\circ$ ,  $11^\circ$ ,  $17^\circ$ ,  $26^\circ$ ,  $34^\circ$ , and  $43^\circ$  along track. The nominal flight altitude was about 750 m which corresponds to a spatial resolution of approximately 250 m. In general, an area of 1.5 km × 6 km was covered by four to five parallel south–north-oriented flight lines at each of the three farms. Dual-polarized multiangle data were acquired in the early afternoon between 12:00 P.M. and 3:00 P.M. on four days (once a week) at Merriwa Park and one day each for Midlothian and Cullingral. Additionally, specific dive flights (i.e., successive steep ascents/descents) were conducted immediately following the multiangle flights over the focus farms in order to provide observations with an even wider range of incidence angles ( $\sim 3^\circ$ – $60^\circ$ ).

Calibration of the PLMR instrument was carried out on a daily basis before and after the flight using both the sky (cold calibration) and a blackbody box (warm calibration) as target. Supplementary in-flight calibration checks were made through flights over a large water body that was continuously monitored

TABLE I  
CHARACTERISTICS OF SELECTED NAFE'05 FOCUS FARMS WITH MULTI-INCIDENCE-ANGLE OBSERVATIONS

SITE	OBSERVATIONS DAYS	LAND COVER	TOPOGRAPHY	SOIL TYPE	SAND CONTENT [%]	CLAY CONTENT [%]	VEGETATION WATER CONTENT <sup>a</sup> MIN-MAX [kg/m <sup>2</sup> ]	SOIL MOISTURE <sup>a</sup> MIN-MAX [m <sup>3</sup> /m <sup>3</sup> ]
Merriwa Park	4	Native grass + agriculture (wheat)	Gently sloping	Silty clay loam	21	30	0.70 - 3.00	0.10 - 0.50
Cullingral	1	Native grass + agriculture (wheat/barley)	Flat	Silty loam	36	26	0.14 - 0.47	0.03 - 0.09

<sup>a</sup>for area with wheat cover

in terms of surface water temperature and salinity. A detailed description of the complete calibration procedures can be found in [20]. Considering the range of brightness temperature measurements over land during the campaign (150–300 K), the PLMR accuracy was estimated in [20] to be higher than 0.7 K for H-polarization and 2 K for V-polarization. The calibrated radiometer observations have been further processed to provide local incidence angle and effective footprint size information, taking into account ground topography, aircraft position, and attitude. Finally, the data were filtered to eliminate large aircraft yaw and roll angles due to turbulence and strong crosswinds. As a result, sun glint effects in the external beams were also reduced.

### C. Ground Data

Extensive ground sampling activities were conducted coincident with the airborne observations, focusing on an area of approximately 1.5 km × 3.0 km at each farm (see Fig. 1). The measurements of near-surface soil moisture (0–5 cm) were made using the Hydraprobe Data Acquisition System (HDAS) [22], which consists of a Hydraprobe surface soil moisture sensor, a Global Positioning System, and a handheld pocket personal computer that has a geographic information system installed to provide a visual output of the sampling location and the corresponding surface soil moisture observation. The HDAS measurements were typically collected between 9:00 A.M. and 1:30 P.M. over a spatial sampling grid with varying spacing from 6.25 m to 2 km, as shown in Fig. 1. The high-resolution sampling (6.25–12.5 m) was mainly concentrated on an area of 150 m × 150 m within the cropping fields at Merriwa Park and Cullingral and within a large patch of native grass at Midlothian. The surrounding areas were sampled at coarser spatial scales. The Hydraprobe surface soil moisture output was calibrated against both laboratory data and gravimetric soil samples from the field, resulting in an estimated accuracy of ±0.033 m<sup>3</sup>/m<sup>3</sup> [22]. The gravimetric samples were further analyzed in terms of soil texture and soil properties (Table I). Supplementary data, including land use, surface roughness, rock cover fraction, rock temperature, dew amount, vegetation biomass, and vegetation water content (VWC), were also recorded at each farm site. Long-term surface soil moisture (0–5, 0–30, 30–60, and 60–90 cm), soil temperature (0–5 and 0–30 cm), and rainfall data were available through an existing *in situ* monitoring network [21]. During the campaign, a few stations were temporarily upgraded with additional instrumentation, including thermal infrared sensors, surface soil-temperature profiles (1, 2.5, and 4 cm), and leaf wetness sensors, to determine the presence of dew. Midlothian, Merriwa Park, and Cullingral were each equipped with one per-

manent and one temporary monitoring station. The latter was always located within the high-resolution surface soil moisture sampling area of the focus farm.

This paper focuses on the use of multi-incidence-angle airborne observations and ground data collected across the cropping fields at Merriwa Park and Cullingral. Both sites were covered by mature wheat, whereas Midlothian was predominantly characterized by native grass and some lucerne. Consequently, data collected across the Midlothian site were not considered in this study. The PLMR observations used herein were selected in such a way that the following holds: 1) they fell in the high-resolution surface soil moisture sampling area, and 2) the individual PLMR footprints were located entirely within the wheat crop. This ensured that homogeneous surface conditions (vegetation type, vegetation state, and topography) were mapped by the different PLMR beams. Table I summarizes the main features of the Merriwa Park and Cullingral study sites, showing an overall dynamic surface soil moisture range of about 0.05–0.55 m<sup>3</sup>/m<sup>3</sup> for Merriwa Park over the entire period. Moist soil conditions were generally observed at the start of the campaign in response to significant rainfall in the area, while toward the end of the field experiment, the topsoil showed substantial drying effects. However, the daily temporal near-surface surface soil moisture variability was found to be negligible within the time period of ground and airborne data acquisition. Cullingral was only covered once with multiangle flights and corresponding *in situ* surface soil moisture measurements during the campaign. The spatial surface soil moisture distribution across Cullingral ranged from 0.05 to 0.25 m<sup>3</sup>/m<sup>3</sup> on the observation day.

### III. RADIATIVE TRANSFER MODEL

The radiative transfer model used in this study is the L-MEB model [15], which is the core element of the operational surface soil moisture retrieval algorithm developed for SMOS [23]. A detailed description of the model structure and parameterization is presented in [15], so the following discussion concentrates only on the basic principles of L-MEB.

The presence of vegetation and the resulting interaction with the soil surface emission are described in terms of a simplified (zero-order) solution of the radiative transfer approach, also known as the tau-omega model. This algorithm assumes that the influence of the vegetation layer on the P-polarized soil reflectivity ( $r_{GP}$ ) is accounted for by vegetation attenuation ( $\gamma_P$ ) and scattering effects ( $\omega_P$ ), resulting in a composite brightness temperature ( $T_{BP}$ ) as follows:

$$T_{BP} = (1 - \omega_P)(1 - \gamma_P)(1 + \gamma_P r_{GP}) \cdot T_C + (1 - r_{GP}) \gamma_P \cdot T_G \quad (1)$$

TABLE II  
 PARAMETERIZATION OF THE FORWARD MODELS STUDIED

MODEL ID	ROUGHNESS			VEGETATION				COMMENT
	$H_R$	$N_{Rh}$	$N_{Rv}$	$tt_h$	$tt_v$	$\omega_h$	$\omega_v$	
M1_def	0.1	0	0	1	8	0	0	Model with default parameterization proposed by [15]
M2_HR	1.5-1.6-SM <sup>a</sup> 1.6-1.0-SM <sup>b</sup>	0	0	1	8	0	0	Model with $H_R=f(SM)$ parameterization as suggested by [26]
M3_opt	1.5-1.6-SM <sup>a</sup> 1.6-1.0-SM <sup>b</sup>	0	0	0.2	1.4	0	0	Model parameterization includes $H_R=f(SM)$ [26] and optimized vegetation structure values calibrated from multi-angle data from Merriwa Park 09/11/2005

SM: Soil Moisture;

<sup>a</sup>linear roughness function for Merriwa Park; <sup>b</sup>linear roughness function for Cullingral

where  $T_G$  and  $T_C$  correspond to the effective soil and vegetation temperatures (in kelvins), respectively. The reflectivity of the underlying soil surface is a function of the wave polarization, the observation frequency, and the incidence angle and can be quantified for nonsmooth surfaces by calculating the smooth surface Fresnel reflectivity ( $r_{GP}^*$ ) and adjusting it through the use of a set of soil roughness parameters (i.e.,  $H_R$  and  $N_{RP}$ )

$$r_{GP} = r_{GP}^* \cdot \exp[-H_R \cos \theta^{(N_{RP})}]. \quad (2)$$

Note that  $N_{RP}$  is introduced to parameterize the angular dependence of the surface roughness. The attenuation effect caused by the canopy, also referred to as transmissivity, is expressed as a function of the vegetation optical depth ( $\tau_P$ ) and the incidence angle ( $\theta$ )

$$\gamma_P = \exp[-\tau_P / \cos \theta]. \quad (3)$$

The optical depth given in (3) describes a modified optical depth which considers the canopy contribution in terms of  $\tau = \tau_{NAD} \times f(\theta, P)$ , with  $\tau_{NAD}$  being the nadir estimate of the overall optical depth ( $\theta = 0^\circ$ ), which is independent of both the incidence angle and the polarization. The parameter  $\tau_{NAD}$  can be computed as a linear function of the VWC and the empirical parameter  $b_P$ , which is mainly dependent on the sensor frequency, polarization, canopy type, and plant structure [24]

$$\tau_{NAD} = VWC \cdot b_P. \quad (4)$$

In order to correct for nonnadir views on the optical depth, particularly with regard to the vegetation structure, i.e., in our case, the dominantly vertical structure of the wheat canopy, two additional specific vegetation structure parameters  $tt_h$  and  $tt_v$  ( $h$  and  $v$  denoting horizontal and vertical polarizations, respectively) are introduced that account for the angular effect on the optical depth and, hence, on the vegetation transmissivity

$$\tau_P = \tau_{NAD} (\sin^2 \theta \cdot tt_P + \cos^2 \theta). \quad (5)$$

Considering a value of  $tt_P > 1$  or  $tt_P < 1$  results in either an increasing or decreasing trend of the optical depth, respectively, as a function of the incidence angle. The particular case of  $tt_v = tt_h = 1$  corresponds to the isotropic state, where the optical depth of the standing canopy is assumed to be independent of both polarization and incidence angle.

#### IV. MODELING APPROACH AND PARAMETERIZATION

The L-MEB forward model was used to generate dual-polarized brightness temperatures at a range of incidence angles and moisture conditions using the NAFE'05 data described in

Section II. The model setup was based on a combination of two types of input fields: 1) ground truth information collected at the focus farms and 2) default model parameters as a function of the land cover class. The available ground data included surface soil moisture, soil texture, bulk density, soil profile temperature, VWC, and vegetation temperature data. The input surface soil moisture was calculated by averaging all high-resolution near-surface ground measurements falling within the same PLMR footprint for each observation day. The total number of HDAS measurements was generally between  $\sim 250$  and 300 points per observation day and radiometer footprint. Further model input included a special set of parameters for surface roughness and vegetation characterization, i.e., variables  $H_R$  and  $N_{RP}$  for the soil layer and  $tt_P$ ,  $\omega_P$ , and  $b_P$  for the wheat canopy (see Table II). These values were sourced from the study in [15], in which the parameters had been calibrated from the PORTOS-93 experiment over wheat at the Avignon test site in France [25]. The parameterization proposed in [15] is hereafter referred to as the “default” parameter set (M1\_def). Using the ground data and the default parameterization, brightness temperature estimates were calculated for both H- and V-polarizations and incidence angles ranging from  $0^\circ$  to  $50^\circ$ . The forward simulations were undertaken for all available dates at Merriwa Park and Cullingral with the L-MEB results compared against the actual airborne multi-incidence-angle observations of the corresponding day and test site.

Further to the default model simulations described previously (M1\_def), two additional parameter sets were tested based on modifications of the initial model parameterization (Table II). In the second forward model approach (M2\_HR), the default parameterization was changed in terms of a single model parameter; the soil roughness value  $H_R$  given in [15] was replaced by the surface soil moisture-dependent roughness value proposed in [26] for the same study site. The basis for using a soil roughness value as a function of surface soil moisture is due to a phenomenon known as “dielectric roughness,” which contributes to volume scattering of the signal coming from deeper soil layers and is assumed to be caused by a variation of dielectric properties within the soil column due to a nonuniform distribution of the water particles at microscale [27], [28]. Thus, in addition to the spatial variations in the surface height (“geometric roughness”), it has been postulated that the “dielectric roughness” should also be accounted for in terms of an effective  $H_R$  parameter. The study in [26] was based on high-resolution (62.5 m) single-angle PLMR data from the NAFE'05 experiment and suggested that the default  $H_R$  value in L-MEB was too low for vegetation with dominantly vertical structure such as wheat and barley. Note that Saleh *et al.* [29] also had to increase the  $H_R$  parameter for their studies when using airborne L-band data acquired by the EMIRAD radiometer over

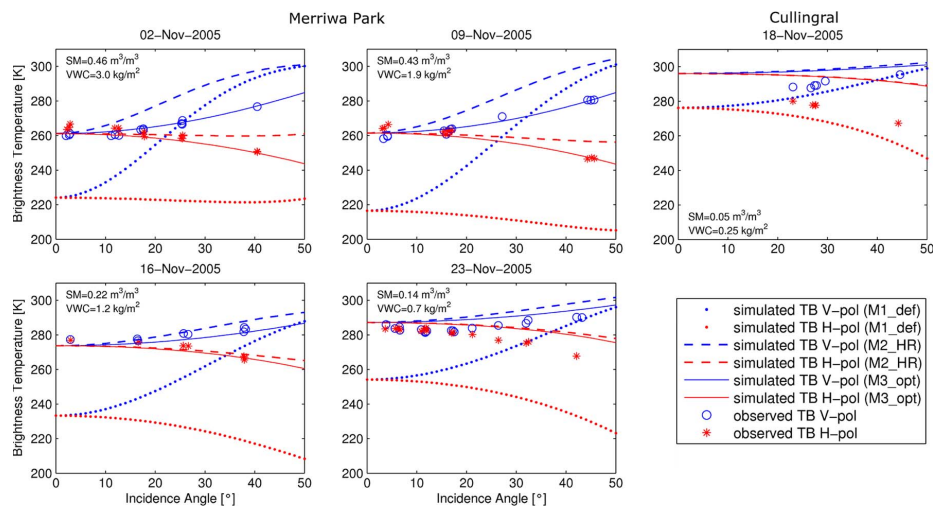


Fig. 2. Dual-polarized brightness temperature estimates plotted against incidence angle and compared to multiangle PLMR observations over wheat canopy for the Merriwa Park and Cullingral study sites. The measured soil moisture (SM) and the VWC are individually displayed for each observation day.

the same test site, suggesting that the higher roughness values were not related to an instrument-specific bias of the PLMR sensor itself. Moreover, Panciera *et al.* [26] found that the calibrated  $H_R$  value demonstrated a notable temporal variation which correlated with the observed moisture conditions during the field experiment. These results were consistent with those published in [30] over bare soil at the SMOSREX test site. Hence, Panciera *et al.* [26] developed a simple linear relationship between  $H_R$  and the surface soil moisture content for the NAFE'05 test sites, which estimated lower  $H_R$  values with increasing moisture content. Considering these results, the second parameterization had been set to include a roughness value specifically calculated for each observation date depending on the corresponding surface soil moisture information of that day. Note that, since this linear function is soil type specific, the defined relationship between roughness effects and surface soil moisture, based on earlier studies [26], is different for Merriwa Park and Cullingral, where the soil texture changes from silty clay loam to silty loam, respectively (see Table I). However, it should be pointed out that recent results in [31] revealed that the approach of an surface soil moisture-dependent roughness function  $H_R = f(SM)$  might simply be compensating for a difference in sampling depths of the L-band observations and the ground measurements. Using data from the SMOSREX experimental site in France in 2004 [17], they found that the radiometer response was generally related to a sampling depth of 0–2 cm, with a shallower sampling depth (0–1 cm) for moist conditions.

The current SMOS Level 2 surface soil moisture retrieval algorithms [23] include the sensitivity of surface roughness on surface soil moisture in terms of a simple function, such as that applied in this study. However, the roughness estimation is confined by the field capacity as an upper limit and a transition moisture point as the lower limit, with both parameters being a function of the soil texture (sand/clay content). Above and below these two points, the roughness value is a constant, and the minimum  $H_R$  value is expressed by  $H_{R\_MIN} = (2k\sigma)^2$  [32],

with  $k$  being the wavenumber and  $\sigma$  defined as the surface root-mean-square height. Note the following: 1) the corresponding minimum and maximum  $H_R$  values are dependent on the actual land cover type observed, and 2) the maximum  $H_{R\_MAX}$  parameter is retrieved from the individual SMOS scene.

The third parameter set (M3\_opt) included two modifications compared to the default L-MEB parameterization: 1)  $H_R$  calculated as a function of the actual surface soil moisture content (as in M2\_HR) and 2) calibrated vegetation structure variables  $tt_h = 0.2$  and  $tt_v = 1.4$  using the available multi-incidence-angle data for one of the four observation days. These new values for the vegetation parameters were estimated through an optimization routine which had been applied to a single flight day over Merriwa Park (November 9, 2005). The calibrated values for  $tt_h$  and  $tt_v$  corresponded to a decrease ( $tt_h < 1$ ) and an increase ( $tt_v > 1$ ), respectively, of the optical depth with the incidence angle at each polarization, which was expected due to the dominantly vertical structure of the wheat canopy. This parameterization was then applied to all remaining observation days at Merriwa Park to assess its performance. Subsequently, the calibrated model variables were further tested on airborne data from Cullingral in order to study their robustness and to verify the parameterization derived from the Merriwa Park study site. The assumption that the remaining vegetation values as proposed in [15] for 1) the vegetation parameter  $b$  and 2) the single scattering albedo  $\omega$  were representative was justified based on the following: 1) a site-specific calibration across the available observation dates that showed no significant variations from  $b = 0.08$  and  $\omega = 0$  and 2) the fact that the parameterization resulted from an extensive literature review in [15]. Further analysis of the three parameterizations (M1\_def, M2\_HR, and M3\_opt) included iterative inversion of the L-MEB model to solve an optimization problem for the retrieval of surface soil moisture given *a priori* ground truth information. The algorithm was based on a minimized cost function that calculated the quadratic difference between the measured and simulated brightness temperatures.

## V. RESULTS AND DISCUSSION

The comparison of the L-MEB predicted brightness temperature response with the airborne multiangle observations from Merriwa Park and Cullingral for incidence angles ranging from  $0^\circ$  to  $50^\circ$  showed significant discrepancies depending on the model parameterization chosen (Fig. 2). Using the default L-MEB parameterization (M1\_def), the forward model consistently underestimated the multiangle observations at H-polarization, whereas at V-polarization (particularly for large incidence angles and wet soil conditions), the simulated brightness temperatures were much higher than those observed. Furthermore, the incidence-angle-related trends of the dual-polarized observations were only partially captured by the simulation results. Hence, differences of up to  $\sim 40$  K in brightness temperatures were observed, particularly within the range of low incidence angles. While this difference decreased for the vertically polarized curve with larger incidence angles, the simulated horizontal brightness temperatures were always lower than the measured data. Note that, for wet conditions at Merriwa Park during the first two observation days, the simulated horizontally polarized curve is relatively flat due to the high VWC and the corresponding large value for the optical depth. The explanation behind this trend is that both the attenuation of the soil emission and the emission by the wheat canopy itself increased, causing the effective composite brightness temperature of both media to be closer to the effective temperature of the vegetation. Therefore, with larger incidence angles, the attenuation of the vegetation increased with respect to the  $1/\cos(\theta)$  relationship, as shown in (3). Setting a default value of one for  $tt_h$  further assumes that there are no significant angular dependencies across the observed wheat canopy at H-polarization. The comparison of the predicted and observed brightness temperatures across the four observation days at Merriwa Park produced a root-mean-square error (rmse) ranging from  $rmse_{def} = 38$  K to  $rmse_{def} = 26$  K for wet and dry conditions, respectively (Fig. 3), when using the default parameters.

The overall model performance was improved by introducing the surface soil moisture-dependent roughness value  $H_R$  (M2\_HR) from the site-specific calibration presented in [26]. Consequently, an upward translation of the modeled brightness temperature curves was achieved, resulting in a closer agreement with the observations. The corresponding rmse for the Merriwa Park site ranged from  $rmse_{HR} = 9.6$  K (wet) to  $rmse_{HR} = 2.9$  K (dry) and were thus significantly reduced compared to the default model parameterization output. However, the simulated angular behavior was still unable to capture the observed brightness temperature trend exhibited at large incidence angles ( $> 25^\circ$ ), which was particularly dominant for moist conditions at Merriwa Park at the start of the campaign. Moreover, for relatively low moisture contents ( $< 0.1$  m<sup>3</sup>/m<sup>3</sup>), the curve shift forced by the moisture-dependent adjusted roughness value toward higher brightness temperatures was too strong. Hence, the predicted emissions tended to overestimate the brightness temperature measurements, particularly for dry conditions.

A site-specific calibration of  $H_R$  based on the multiangle observations available for Merriwa Park (results not shown) demonstrated a nonlinear relationship between surface soil moisture and surface roughness. Specifically, the calibration

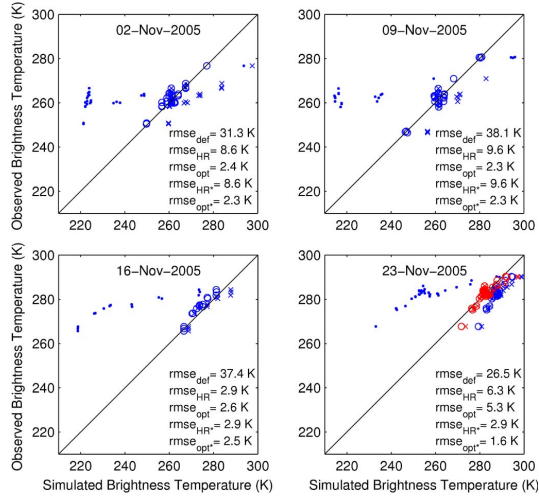


Fig. 3. Scatterplot of the L-MEB model simulations in comparison with independent ground data from Merriwa Park on different observation dates using (dots) the default model parameterization “M1\_def” [15], (crosses) the site-specific roughness parameterization “M2\_HR” [26], and (circles) the optimized model parameterization “M3\_opt.” Additionally, results based on a nonlinear daily-optimized  $H_R^* = f(SM)$  approach are shown in red for days where model predictions were improved by more than 0.1 K compared to “M2\_HR” and “M3\_opt” results. The rmse calculated between the observed and simulated brightness temperatures is given for all model approaches on all days.

showed the following: 1) a positive correlation between the surface roughness parameter  $H_R$  and surface soil moisture for dry conditions, resulting in small  $H_R$  values for dry soil, and 2) a negative trend for surface soil moisture values of  $\sim 0.20$  m<sup>3</sup>/m<sup>3</sup> or higher by decreasing the roughness effect with increasing moisture content. These findings also agreed with the results published in [33] which investigated the impact of surface soil moisture on surface roughness using single-angle NAFE’05 data. In that study, the decrease of the roughness effect for low surface soil moisture was associated with a reduced dielectric heterogeneity at microscale during the drying process of the clay loam soils that dominate the study area. That is, the microscale variability and, thus, the dielectric roughness peaked at intermediate surface soil moisture content and decreased toward very wet or very dry conditions. Applying a reduced roughness parameter optimized for dry conditions produced better results, as shown in red in Fig. 3 for November 23, 2005.

The L-MEB parameterization of the third model (M3\_opt) with optimized  $H_R$  and  $tt_P$  parameters showed the overall best agreement with the airborne data considering the following: 1) the linear  $H_R = f(SM)$  approach, i.e.,  $rmse_{opt} = 2.3$ – $5.3$  K, and 2) the nonlinear  $H_R = f(SM)$  approach, i.e.,  $rmse_{opt} = 1.6$ – $2.6$  K. Moreover, the angular trend of the predicted dual-polarization curves captured that of the measured data for both moist and dry surface soil moisture conditions. Compared to the default parameterization and the high  $tt_v$  value of eight obtained for the vertically dominated wheat canopy [15], the vegetation structure parameters calibrated and tested in this study were significantly lower and closer to unity ( $\sim 1$ ) (see Table II). However, it should be noted that an individual calibration of the  $tt_P$  parameters for each single day suggested

TABLE III  
COMPARISON OF GROUND-MEASURED SURFACE SOIL MOISTURE (STANDARD DEVIATION IN BRACKETS) WITH SURFACE SOIL MOISTURE VALUES RETRIEVED USING DIFFERENT SURFACE ROUGHNESSES AND VEGETATION STRUCTURE PARAMETERIZATIONS

Location	Date	HDAS SM (std) [m <sup>3</sup> /m <sup>3</sup> ]	Model M1_def SM retrieved [m <sup>3</sup> /m <sup>3</sup> ]	Model M2_HR SM retrieved [m <sup>3</sup> /m <sup>3</sup> ]	Model M3_opt SM retrieved [m <sup>3</sup> /m <sup>3</sup> ]
Merriwa Park	02-Nov-2005	0.46 (0.04)	0.18	0.55	0.44
Merriwa Park	09-Nov-2005	0.43 (0.06)	0.15	0.50	0.42
Merriwa Park	16-Nov-2005	0.22 (0.07)	0.05	0.21	0.19
Merriwa Park	23-Nov-2005	0.14 (0.05)	0.04	0.22 / 0.14*	0.20 / 0.14*
Cullingral	18-Nov-2005	0.05 (0.02)	0.03	0.30 / 0.05*	0.27 / 0.05*

SM: Soil Moisture

\*Soil moisture retrieved using a non-linear, daily-optimized  $H_R \rightarrow f(\text{SM})$  approach

a value of  $tt_v = 3$  in one case, but overall, only minor variations across the different dates were observed. Consequently, the calibrated vegetation structure parameters from November 9, 2005, were validated on different moisture conditions and locations (Cullingral), confirming the good results obtained using this particular parameterization. Note that further analysis (not shown) using the estimated  $tt_p$  values individually calibrated for each observation day, instead of the values retrieved from November 9, demonstrated only a minor improvement of the model rmse performance (0.3 K at most).

Overall, the results presented in this paper revealed that the adjustment of both angular correction parameters, based on the Merriwa Park November 9 data, had a more significant impact on the predicted brightness temperatures, when the ground-measured VWC was high ( $> 1.9 \text{ kg/m}^2$ ), and thus, the attenuation effects of the canopy and its own contribution to the composite brightness temperature were increased as well. Consequently, both structure parameters play a major role, particularly for large incidence angles ( $> 30^\circ$ ) where the path length of the emitted energy through the vegetation layer is longer.

Using the available ground information (soil texture, soil temperature, VWC, etc.), together with the individual model parameterization (M1–M3; see Table II), the inverse problem was solved for surface soil moisture and compared to the HDAS measurements (Table III). The surface soil moisture retrieval based on an iterative least squared algorithm resulted in a range of surface soil moisture values per observation day depending on the model parameterizations chosen (Fig. 4). The default parameterization (M1\_def) generally produced too low surface soil moisture values with a maximum difference of  $\sim 0.3 \text{ m}^3/\text{m}^3$ , when compared against the measured surface soil moisture at Merriwa Park. The overall best results for this site ( $\leq 0.06 \text{ m}^3/\text{m}^3$  difference from observations) to the observed moisture conditions were achieved using the optimized set of parameters, which included the surface soil moisture-dependent roughness value  $H_R$  and the calibrated vegetation structure values  $tt_p$  (M3\_opt). The results for Cullingral, where it was dry ( $0.05 \text{ m}^3/\text{m}^3$ ) on the day of observation, demonstrated that the default parameterization (M1\_def) works well for this condition. However, the surface soil moisture retrieval was further improved by optimizing the surface roughness parameter  $H_R$ . Due to the relatively low VWC  $\sim 0.25 \text{ kg/m}^2$  measured at the Cullingral site, the effect of the vegetation structure parameters was minor considering these extremely dry soil conditions.

## VI. CONCLUSION

This paper has presented simulations of brightness temperatures at a range of incidence angles and the subsequent com-

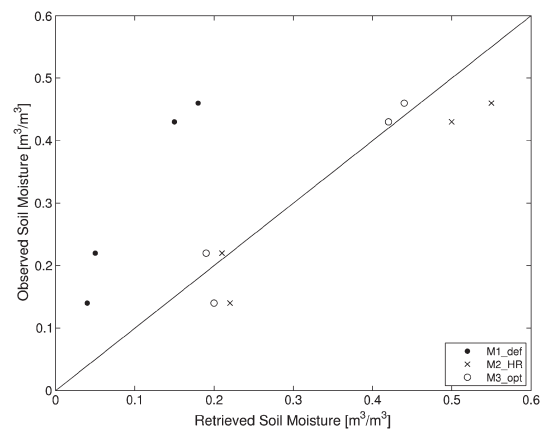


Fig. 4. Scatterplot showing the retrieved against measured surface soil moisture values at the Merriwa Park focus farm for the four available observation days. The inverse application of the L-MEB model was made for all model parameterizations discussed in Section IV.

parison with multi-incidence-angle airborne observations over two wheat canopy test sites in eastern Australia. The forward model used in this research was the L-MEB model which is one of the core elements of the SMOS surface soil moisture retrieval algorithm. Apart from the default model parameterization proposed in [15], two additional parameterizations were studied, including modifications of the surface roughness and vegetation structure characterization. The performance of the individual model approach was assessed based not only on changing moisture conditions but also on different locations in order to test its robustness. The agreement of the predicted and measured brightness temperature data from different forward model parameterizations varied significantly, with the observed discrepancy being much larger for wet conditions than for dry surface soil moisture values. However, compared to results using the default model parameterization, a stepwise improvement was achieved, first, by introducing a surface soil moisture-dependent roughness factor and, second, by retrieving new values for the vegetation structure parameters of wheat canopy ( $tt_h = 0.2$  and  $tt_v = 1.4$ ). Consequently, the dual-polarized brightness temperature predictions were improved by minimizing the rmse on November 2 from  $rmse_{def} = 38.1 \text{ K}$  to  $rmse_{opt} = 2.3 \text{ K}$  for wet soil conditions ( $\sim 0.46 \text{ m}^3/\text{m}^3$ ) and from  $rmse_{def} = 26.5 \text{ K}$  to  $rmse_{opt} = 5.3 \text{ K}$  for dry soils ( $\sim 0.14 \text{ m}^3/\text{m}^3$ ) on November 23.

This study confirms that neglecting the sensitivity of the surface roughness parameter  $H_R$  on surface soil moisture leads

to a significant underestimation of the soil emission at L-band, which would consequently affect the overall surface soil moisture retrieval accuracy. However, it should be noted that the use of an surface soil moisture-dependent roughness value might mask the issue of incorrect sampling depths for comparison with the L-band radiometer [31]. Furthermore, it was shown that the transmissivity of a dominantly vertical canopy structure and the angular dependence of the optical depth should not be neglected for VWCs of  $> 1.9 \text{ kg/m}^2$  and wet soil conditions ( $> 0.4 \text{ m}^3/\text{m}^3$ ); otherwise, the error introduced into the retrieved surface soil moisture product for the given data set could be up to  $0.3 \text{ m}^3/\text{m}^3$ . Considering the spatial resolution of SMOS observations and a footprint size of approximately 42 km, which captures a mixture of land cover types, the angular effect of the various vegetation types and structures might be intensified, particularly for conditions of high VWC, causing additional errors in the SMOS surface soil moisture retrieval if not accurately accounted for. However, this issue needs to be investigated in future research to understand the impact of the angular vegetation structure effects on the surface soil moisture retrieval at satellite scale. Based on the demonstrated results, the effect of dominantly vertically structured canopies should be assessed by comparing the single-angle and multiangle surface soil moisture retrieval performances using both passive microwave data from airborne observations and SMOS.

## ACKNOWLEDGMENT

The authors would like to thank the National Airborne Field Experiment 2005 team for collecting and providing the data set used in this study.

## REFERENCES

- [1] T. J. Schmugge, P. E. O'Neill, and J. R. Wang, "Passive microwave soil moisture research," *IEEE Trans. Geosci. Remote Sens.*, vol. GRE-24, no. 1, pp. 12–22, Jan. 1986.
- [2] J. C. Calvet, J. P. Wigneron, A. Chanzy, and D. Haboudane, "Retrieval of surface parameters from microwave radiometry over open canopies at high frequencies," *Remote Sens. Environ.*, vol. 53, no. 1, pp. 46–60, Jul. 1995.
- [3] T. J. Jackson, T. J. Schmugge, and E. T. Engman, "Remote sensing applications to hydrology: Soil moisture," *Hydrol. Sci. J.*, vol. 41, no. 4, pp. 517–530, Aug. 1996.
- [4] E. G. Njoku and D. Entekhabi, "Passive microwave remote sensing of soil moisture," *J. Hydrol.*, vol. 184, no. 1/2, pp. 101–129, 1996.
- [5] C. Pathe, W. Wagner, D. Sabel, M. Doubkova, and J. B. Basara, "Using ENVISAT ASAR global mode data for surface soil moisture retrieval over Oklahoma, USA," *IEEE Trans. Geosci. Remote Sens.*, vol. 47, no. 2, pp. 468–480, Feb. 2009.
- [6] C. Rüdiger, J.-C. Calvet, C. Gruhier, T. R. H. Holmes, R. A. M. de Jeu, and W. Wagner, "An intercomparison of ERS-Scat and AMSR-E soil moisture observations with model simulations over France," *J. Hydrometeorol.*, vol. 10, no. 2, pp. 431–447, Apr. 2009.
- [7] J. Wigneron, J. Calvet, T. Pellarin, A. Van de Griend, M. Berger, and P. Ferrazzoli, "Retrieving near-surface soil moisture from microwave radiometric observations: Current status and future plans," *Remote Sens. Environ.*, vol. 85, no. 4, pp. 489–506, 2003.
- [8] J. Leese, T. Jackson, A. Pitman, and P. Dirmeyer, "GEWEX/BAHC International workshop on soil moisture monitoring, analysis, and prediction for hydrometeorological and hydroclimatological applications," *Bull. Amer. Meteorol. Soc.*, vol. 82, no. 7, pp. 1423–1430, 2001.
- [9] Y. Kerr, P. Waldteufel, J. P. Wigneron, J. M. Martinuzzi, J. Font, and M. Berger, "Soil moisture retrieval from space: The Soil Moisture and Ocean Salinity (SMOS) mission," *IEEE Trans. Geosci. Remote Sens.*, vol. 39, no. 8, pp. 1729–1735, Aug. 2001.
- [10] Y. Kerr, P. Waldteufel, J. Wigneron, S. Delwart, F. Cabot, J. Boutin, M. Escorihuela, J. Font, N. Reul, and C. Gruhier, "The SMOS mission: New tool for monitoring key elements of the global water cycle," *Proc. IEEE*, vol. 98, no. 5, pp. 666–687, May 2010.
- [11] M. Pardé, J. P. Wigneron, A. Chanzy, P. Waldteufel, Y. Kerr, and S. Huet, "Retrieving surface soil moisture over a wheat field: Comparison of different methods," *Remote Sens. Environ.*, vol. 87, no. 2/3, pp. 334–344, Oct. 2003.
- [12] M. J. Sandells, I. J. Davenport, and R. J. Gurney, "Passive L-band microwave soil moisture retrieval error arising from topography in otherwise uniform scenes," *Adv. Water Resour.*, vol. 31, no. 11, pp. 1433–1443, Nov. 2008.
- [13] J. Wigneron, M. Parde, P. Waldteufel, A. Chanzy, Y. Kerr, S. Schmidl, and N. Skou, "Characterizing the dependence of vegetation model parameters on crop structure, incidence angle, and polarization at L-band," *IEEE Trans. Geosci. Remote Sens.*, vol. 42, no. 2, pp. 416–425, Feb. 2004.
- [14] J. Wigneron, P. Waldteufel, A. Chanzy, J. Calvet, and Y. Kerr, "Two-dimensional microwave interferometer retrieval capabilities over land surfaces (SMOS mission)," *Remote Sens. Environ.*, vol. 73, no. 3, pp. 270–282, Sep. 2000.
- [15] J. Wigneron, Y. Kerr, P. Waldteufel, K. Saleh, M. Escorihuela, P. Richaume, P. Ferrazzoli, P. de Rosnay, R. Gurney, and J. Calvet, "L-band Microwave Emission of the Biosphere (L-MEB) model: Description and calibration against experimental data sets over crop fields," *Remote Sens. Environ.*, vol. 107, no. 4, pp. 639–655, Apr. 2007.
- [16] I. Davenport, J. Fernandez-Galvez, and R. Gurney, "A sensitivity analysis of soil moisture retrieval from the  $\tau$ - $\omega$  microwave emission model," *IEEE Trans. Geosci. Remote Sens.*, vol. 43, no. 6, pp. 1304–1316, Jun. 2005.
- [17] P. de Rosnay, J. Calvet, Y. Kerr, J. Wigneron, F. Lemaître, M. Escorihuela, J. Sabater, K. Saleh, J. Barrié, and G. Bouhours, "SMOSREX: A long term field campaign experiment for soil moisture and land surface processes remote sensing," *Remote Sens. Environ.*, vol. 102, no. 3/4, pp. 377–389, Jun. 2006.
- [18] A. Cano, K. Saleh, J.-P. Wigneron, C. Antofin, J. E. Balling, Y. H. Kerr, A. Kruszwski, C. Millán-Scheiding, S. S. Søbjerg, N. Skou, and E. López-Baeza, "The SMOS Mediterranean Ecosystem L-Band characterisation EXperiment (MELBEX-I) over natural shrubs," *Remote Sens. Environ.*, vol. 114, no. 4, pp. 844–853, Apr. 2010.
- [19] K. Saleh, J. Wigneron, J. Calvet, E. Lopez-Baeza, P. Ferrazzoli, M. Berger, P. Wursteisen, L. Simmonds, and J. Miller, "The EuroSTARSS airborne campaign in support of the SMOS mission: First results over land surfaces," *Int. J. Remote Sens.*, vol. 25, no. 1, pp. 177–194, Jan. 2004.
- [20] R. Panciera, J. P. Walker, J. D. Kalma, E. J. Kim, J. M. Hacker, O. Merlin, M. Berger, and N. Skou, "The NAFE'05/CoSMOS data set: Toward SMOS soil moisture retrieval, downscaling, and assimilation," *IEEE Trans. Geosci. Remote Sens.*, vol. 46, no. 3, pp. 736–745, Mar. 2008.
- [21] C. Rüdiger, G. Hancock, H. M. Hemakumara, B. Jacobs, J. D. Kalma, C. Martinez, M. Thyer, J. P. Walker, T. Wells, and G. R. Willgoose, "Goulburn River experimental catchment data set," *Water Resour. Res.*, vol. 43, p. W10403, 2007.
- [22] O. Merlin, J. Walker, R. Panciera, R. Young, J. Kalma, and E. Kim, "Soil moisture measurement in heterogeneous terrain," in *Proc. MODSIM Soc. Australia New Zealand*, Christchurch, New Zealand, 2007, pp. 2604–2610.
- [23] Y. H. Kerr, P. Waldteufel, P. Richaume, J.-P. Wigneron, P. Ferrazzoli, and R. J. Gurney, SMOS level 2 processor for soil moisture—Algorithm Theoretical Based Document (ATBD), Sep. 12, 2010, Tech. Note, CBSA, SO-TN-ESL-SM-GS-0001, Issue 3.e, 121 pp. [Online]. Available: <http://www.cesbio.ups-tlse.fr/fr/indexsmos.html>
- [24] T. J. Jackson and T. J. Schmugge, "Vegetation effects on the microwave emission of soils," *Remote Sens. Environ.*, vol. 36, no. 3, pp. 203–212, Jun. 1991.
- [25] J. Wigneron, A. Chanzy, J. Calvet, and N. Bruguier, "A simple algorithm to retrieve soil moisture and vegetation biomass using passive microwave measurements over crop fields," *Remote Sens. Environ.*, vol. 51, no. 3, pp. 331–341, Aug. 1995.
- [26] R. Panciera, J. Walker, J. Kalma, E. Kim, K. Saleh, and J. Wigneron, "Evaluation of the SMOS L-MEB passive microwave soil moisture retrieval algorithm," *Remote Sens. Environ.*, vol. 113, no. 2, pp. 435–444, Feb. 2009.
- [27] J. Wigneron, L. Laguerre, and Y. Kerr, "A simple parameterization of the L-band microwave emission from rough agricultural soils," *IEEE Trans. Geosci. Remote Sens.*, vol. 39, no. 8, pp. 1697–1707, Aug. 2001.
- [28] T. Mo and T. Schmugge, "A parameterization of the effect of surface roughness on microwave emission," *IEEE Trans. Geosci. Remote Sens.*, vol. GRE-25, no. 8, pp. 47–54, Jan. 1987.

- [29] K. Saleh, Y. H. Kerr, P. Richaume, M. J. Escorihuela, R. Panciera, S. Delwart, G. Boulet, P. Maisongrande, J. P. Walker, and P. Wursteisen, "Soil moisture retrievals at L-band using a two-step inversion approach (COSMOS/NAFE'05 Experiment)," *Remote Sens. Environ.*, vol. 113, no. 6, pp. 1304–1312, Jun. 2009.
- [30] M. Escorihuela, Y. Kerr, P. de Rosnay, J. Wigneron, J. Calvet, and F. Lemaitre, "A simple model of the bare soil microwave emission at L-band," *IEEE Trans. Geosci. Remote Sens.*, vol. 45, no. 7, pp. 1978–1987, Jul. 2007.
- [31] M. Escorihuela, A. Chanzy, J.-P. Wigneron, and Y. H. Kerr, "Effective soil moisture sampling depth of L-band radiometry: A case study," *Remote Sens. Environ.*, vol. 114, pt. 1, no. 5, pp. 995–1001, May 2010. doi:10.1016/j.rse.2009.12.011.
- [32] B. Choudhury, T. J. Schmugge, A. Chang, and R. Newton, "Effect of surface roughness on the microwave emission from soils," *J. Geophys. Res.*, vol. 84, no. C9, pp. 5699–5706, 1979.
- [33] R. Panciera, J. Walker, and O. Merlin, "Improved understanding of soil surface roughness parameterization for L-band passive microwave soil moisture retrieval," *IEEE Geosci. Remote Sens. Lett.*, vol. 6, no. 4, pp. 625–629, Oct. 2009.



**Sandy Peischl** (M'10) received the M.S. degree in geocology from the Technische Universität Bergakademie Freiberg, Freiberg, Germany, in 2007. She is currently working toward the Ph.D. degree in the Department of Civil Engineering, Faculty of Engineering, Monash University, Melbourne, Australia.

Her research focuses on the retrieval of soil moisture using multi-incidence-angle L-band data acquired from airborne observations as well as from Soil Moisture and Ocean Salinity (SMOS). She has

extensive experience in the organization and planning of remote-sensing-related field campaigns, particularly experiments designed to benefit European Space Agency's validation activities for the land component of the SMOS mission.



**Jeffrey P. Walker** received the B.E. degree (with Honours 1 and University Medal) in civil engineering and the B. Surveying degree (with Honours 1 and University Medal) in 1995 and the Ph.D. degree in water resources engineering in 1999 from The University of Newcastle, Newcastle, Australia. His Ph.D. thesis was among the early pioneering research on estimation of root-zone soil moisture from remotely sensed surface soil moisture observations.

He then joined the NASA Goddard Space Flight Center, to implement his soil moisture work globally.

In 2001, he moved to the Department of Civil and Environmental Engineering, The University of Melbourne, Melbourne, Australia, as a Lecturer, where he continued his soil moisture work, including development of the only Australian airborne capability for simulating new satellite missions for soil moisture. Since 2010, he has been a Professor with the Department of Civil Engineering, Faculty of Engineering, Monash University, Melbourne, where he is continuing this research. He is contributing to soil moisture satellite missions at both NASA and the European Space Agency, as a Science Definition Team Member for the Soil Moisture Active Passive mission and a Calibration/Validation Team Member for the Soil Moisture and Ocean Salinity mission, respectively.



**Dongryeol Ryu** (M'05) received the B.S. and M.S. degrees in geology from Seoul National University, Seoul, Korea, in 1997 and 2000, respectively, and the Ph.D. degree in earth system science from the University of California, Irvine, in 2006.

He is currently a Senior Lecturer with the Department of Infrastructure Engineering, Melbourne School of Engineering, The University of Melbourne, Melbourne, Australia. His specialization is hydrology with particular emphases on remote sensing of land surface variables such as soil moisture and vegetation characteristics, their spatial and temporal variability, and hydrologic application of the remotely sensed land surface properties.

Dr. Ryu is a member of the IEEE Geoscience and Remote Sensing Society, the American Geophysical Union, and the Engineers Australia.



**Yann H. Kerr** (M'88–SM'01) received the B.E. degree from the Ecole Nationale Supérieure de l'Aéronautique et de l'Espace, Toulouse, France, the M.Sc. degree in electronics and electrical engineering from Glasgow University, Glasgow, U.K., and the Ph.D. degree from Université Paul Sabatier, Toulouse.

From 1980 to 1985, he was with Centre National d'Etudes Spatiales (CNES). In 1985, he joined the Laboratoire d'Etudes et de Recherches en Télé-détection Spatiale, for which he was the Director from 1993–1994. From 1987–1988, for 19 months, he was with the Jet Propulsion Laboratory, Pasadena, CA. Since 1995, he has been with Centre d'Etudes Spatiales de la Biosphère, Toulouse, where he was the Deputy Director and has been the Director since 2007. His fields of interest include the theory and techniques for microwave and thermal infrared remote sensing of the Earth, with emphasis on hydrology, water resources management, and vegetation monitoring. He has been involved with many space missions. He was also a Principal Investigator (PI) (interdisciplinary investigations) of the Earth Observing System and a PI and a precursor of the use of the SCAT over land. In 1989, he started to work on the interferometric concept applied to passive microwave Earth observation and was subsequently the Science Lead on the MIRAS project for the European Space Agency (ESA) with Maritime Management System and Operations Management Plan. He was also a Coinvestigator (CoI) on IRIS, OSIRIS, and HYDROS for the National Aeronautics and Space Administration. He was a Science Advisor for MIMR and a CoI on AMSR. He is a member of the Soil Moisture Active Passive Science Definition Team. In 1997, he first proposed the natural outcome of the previous MIRAS work with what was to become the Soil Moisture and Ocean Salinity (SMOS) mission to CNES, a proposal which was selected by ESA in 1999 with him as the Lead Investigator of the SMOS mission and the Chair of the Science Advisory Group. He is also in charge of the SMOS science activity coordination in France. He is currently involved in the exploitation of SMOS data, in the calibration/validation activities, and in related level 2 soil moisture and level 3 and 4 development. He is also working on the SMOS next concept.

Dr. Kerr has organized all the SMOS workshops and was a Guest Editor on three IEEE special issues.



**Rocco Panciera** received the M.S. degree in environmental engineering from the University of Trento, Trento, Italy, in 2003 and the Ph.D. degree in environmental engineering (remote sensing) from The University of Melbourne, Melbourne, Australia, in 2010.

In 2009–2010, he was a Research Fellow with The University of Melbourne, where he led the first two Soil Moisture Active Passive (SMAP) Experiments (SMAPEx-1 and SMAPEx-2) for algorithm development of the SMAP mission. He is currently a

Research Fellow with the Cooperative Research Centre for Spatial Information, Carlton, Australia, under an Australian Research Council Super Science Fellowship program, where he is working on soil moisture retrieval from synthetic aperture radar. His expertise resides in remote sensing of soil moisture using active and passive microwave techniques.



**Christoph Rüdiger** (M'10) received the B.E. degree in civil engineering from the University of Applied Sciences of Wiesbaden, Wiesbaden, Germany, in 2002 and the Ph.D. degree in environmental engineering from The University of Melbourne, Melbourne, Australia, in 2007. His undergraduate thesis covered the topic of groundwater and contaminant flow around future buildings. His Ph.D. thesis was on the potential to assimilate streamflow data into land surface models for soil moisture prediction.

He then joined the Centre National de Recherches Météorologiques, Météo, Toulouse, France, where he worked on the preparation of surface soil moisture and leaf area index data assimilation into the French land surface model ISBA. During this period, he also worked on the validation of different passive and active microwave satellite products over France, with a particular focus on Soil Moisture and Ocean Salinity (SMOS). Since his return to Australia in July 2008, he has coordinated and led a number of calibration/validation (cal/val) campaigns for the Australian land validation segment of European Space Agency's SMOS mission in the Australian arid zone and the Murrumbidgee River catchment. In addition to this, he continues to work on land surface data assimilation and also participates in the Australian cal/val campaigns for the Soil Moisture Active Passive and the Aquarius missions. He is currently with Monash University, Melbourne.

### 3.3 Summary

---

The agreement of the predicted and measured brightness temperature data from different forward model parameterizations varied significantly, with the observed discrepancy being much larger for wet conditions than for dry soil moisture values. Using the default L-MEB parameterization, the forward model consistently underestimated the multi-angle observations at h-polarization whereas at v-polarization (especially for large incidence angles and wet soil conditions) the simulated brightness temperatures were much higher than those observed. Furthermore, the incidence angle related trends of the dual-polarized observations were only partially captured by the simulation results. Hence, differences of up to 40 K in brightness temperatures were observed, particularly within the range of low incidence angles. However, a stepwise improvement was achieved by first introducing a soil moisture dependent roughness factor  $H_R$ , which caused an upward translation of the modelled brightness temperature curves resulting in a closer agreement with observations at small incidence angles, and second by retrieving new values for the vegetation structure parameters of wheat canopy ( $tt_h=0.2$ ,  $tt_v=1.4$ ). Consequently, the dual-polarized brightness temperature predictions were improved by minimizing the root mean square error (rmse) between simulated and observed brightness temperatures from  $rmse_{def}=38.1$  K to  $rmse_{opt}=2.3$  K for wet soil conditions ( $0.46 \text{ m}^3/\text{m}^3$ ) and from  $rmse_{def}=26.5$  K to  $rmse_{opt}=5.3$  K for dry soils ( $0.14 \text{ m}^3/\text{m}^3$ ).

This study confirms that an inaccurate parameterization of the surface roughness parameter  $H_R$  leads to a significant underestimation of the soil emission at L-band, which consequently would affect the overall soil moisture retrieval quality. However, the simulated angular behaviour was still unable to capture the observed brightness temperature trend exhibited at large incidence angles ( $>25^\circ$ ), which was especially dominant for moist conditions. Additionally, it should be noted that the use of a soil moisture dependent roughness value might mask the issue of different sampling depths between the L-band radiometer observations and the ground measurements (Escorihuela et al., 2010). Moreover, it was shown that the transmissivity of a dominantly

vertical canopy structure and the angular dependency of the optical depth should not be neglected for vegetation water contents of  $>1.9 \text{ kg/m}^2$  and wet soil conditions ( $>0.4 \text{ m}^3/\text{m}^3$ ), otherwise the error introduced into the retrieved soil moisture product for the given data set could be up to  $0.3 \text{ m}^3/\text{m}^3$ .



# 4

## Evaluation of L-MEB for angular retrieval preferences [Paper 2]

**T**HIS chapter includes a research paper which has resulted from the studies undertaken for this degree and is published in a peer-reviewed journal. The inclusion of co-authors reflects the fact that the work came from active collaboration between researchers from different institutes in Australia and France, and acknowledges input into team-based research.

S. Peischl et al. (2014), “Sensitivity of multi-parameter soil moisture retrievals to incidence angle configuration,” *Remote Sensing of Environment*, 143(0), pp. 64–72, DOI: <http://dx.doi.org/10.1016/j.rse.2013.11.019> ©2014 Elsevier Inc.

**Declaration for Thesis Chapter 4**

In the case of Chapter 4, the nature and extent of my contribution to the work was the following:

Nature of contribution	Extent of contribution (%)
Review of literature, data processing and interpretation, and write up.	65 %

The following co-authors contributed to the work. Co-authors who are students at Monash University must also indicate the extent of their contribution in percentage terms: n/a

Name	Nature of contribution	Extent of contribution (%) for student co-authors only
Prof Jeffrey Walker	Ideas, interpretation and reviewing	n/a
Nan Ye	Data processing and interpretation	10
Dr Dongryeol Ryu	Ideas and reviewing	n/a
Dr Yann Kerr	Ideas and reviewing	n/a

Candidate's Signature		Date	27/02/17
-----------------------	---	------	----------

**Declaration by co-authors**

The undersigned hereby certify that:

- (1) the above declaration correctly reflects the nature and extent of the candidate's contribution to this work, and the nature of the contribution of each of the co-authors.
- (2) they meet the criteria for authorship in that they have participated in the conception, execution, or interpretation, of at least that part of the publication in their field of expertise;
- (3) they take public responsibility for their part of the publication, except for the responsible author who accepts overall responsibility for the publication;
- (4) there are no other authors of the publication according to these criteria;
- (5) potential conflicts of interest have been disclosed to (a) granting bodies, (b) the editor or publisher of journals or other publications, and (c) the head of the responsible academic unit; and
- (6) the original data are stored at the following location(s) and will be held for at least five years from the date indicated below:
- (7)

Signature 1	Prof Jeffrey Walker Jeff Walker 	Date	22/2/17
Signature 2	Nan Ye 	Date	2017/02/20

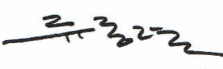
Location	Department of Civil Engineering, Monash University, Australia
----------	---

.....

**Signature 3** Dr Yann Kerr  **Date** 1/12/2016

**Location** Biospheric Processes, CESBIO, France

.....

**Signature 4** Dr Dongryeol Ryu  **Date** 27/02/2017

**Location** The University of Melbourne, Australia

.....

## **4.1 Introduction**

---

The retrieval of soil moisture from L-band microwave observations over vegetated areas is relatively complex compared to bare soil conditions, since the additional vegetation contribution on the emission signal needs to be accounted for within the model. Thus, with the increasing number of input parameters, even more ground information is needed to ensure accurate soil moisture estimates from remote sensing instruments. The ancillary data might be obtained from different ground and space borne instruments. However, issues due to spatial or temporal discrepancies between the different data sources arise. Consequently, previous studies have shown that using the multi-angle capability of sensors such as that deployed by SMOS may enhance the overall retrieval process, depending on the field of view, the moisture conditions, the vegetation type and growth state.

Hence, this paper analyses the multi-angular soil moisture retrieval quality over a wheat canopy site using airborne brightness temperature data collected at different ranges of incidence angles. The effect of i) changing moisture conditions and ii) the type and number of simultaneously retrieved parameters on the model performance are also investigated.

## **4.2 Sensitivity of multi-parameter soil moisture retrieval to incidence angle configuration**

---



## Sensitivity of multi-parameter soil moisture retrievals to incidence angle configuration



Sandy Peischl<sup>a</sup>, Jeffrey P. Walker<sup>a,\*</sup>, Nan Ye<sup>a</sup>, Dongryeol Ryu<sup>b</sup>, Yann Kerr<sup>c</sup>

<sup>a</sup> Department of Civil Engineering, Monash University, Australia

<sup>b</sup> Department of Infrastructure Engineering, The University of Melbourne, Australia

<sup>c</sup> Centre d'Etudes Spatiales de la Biosphère (CESBIO), Toulouse, France

### ARTICLE INFO

#### Article history:

Received 20 June 2012

Received in revised form 20 November 2013

Accepted 23 November 2013

Available online xxx

#### Keywords:

Multi-incidence angle

Passive microwave remote sensing

L-band

Soil moisture

Soil Moisture and Ocean Salinity (SMOS)

### ABSTRACT

This paper focuses on the sensitivity of L-band multi-parameter retrievals across the range of angular measurements available from the SMOS (Soil Moisture and Ocean Salinity) mission. The SMOS core algorithm was used to evaluate two-parameter retrieval scenarios including soil moisture and one of either i) vegetation water content, ii) surface roughness, iii) vegetation temperature, or iv) surface soil temperature. For all pairs a range of parameter value combinations were compiled to run the model in forward mode. Subsequently, the resulting angular brightness temperature simulations with two unknown parameters were compared against the brightness temperature response derived from reference simulations using data from the National Airborne Field Experiment 2005 (NAFE'05) in Australia. This paper showed that the two-parameter retrieval accuracy of soil moisture is strongly affected by the surface moisture conditions, the polarization of the brightness temperature data, and the choice of the secondary ancillary parameter to be retrieved. The synthetic analysis demonstrated a tendency for better retrievals from dual-polarized data at large incidence angles (40–50°). Validation with airborne brightness temperature observations at L-band did not demonstrate such a strong angular dependency, although it confirmed that the simultaneous retrieval of soil moisture and vegetation properties is not preferable as opposed to i) soil moisture and surface roughness or ii) soil moisture and surface soil temperature, especially under dry moisture conditions.

© 2014 Elsevier Inc. All rights reserved.

### 1. Introduction

Passive microwave observations have been proven as one of the most promising techniques for near-surface soil moisture measurement (Jackson, 1993; Njoku & Entekhabi, 1996; Schmugge, O'Neill, & Wang, 1986; Walker & Houser, 2004; Wigneron et al., 2003). The high sensitivity to moisture and the robustness of the sensor signal in response to surface roughness and vegetation canopy effects make brightness temperature measurements in the protected microwave range of 1–2 GHz (L-band) the spectrum window of choice. A range of retrieval algorithms have been developed and tested using data collected from a series of small-scale truck and tower-based experiments, and airborne radiometers to a more limited extent (e.g. de Rosnay et al., 2006; Jackson et al., 1999; Saleh et al., 2004; Schmugge, Wang, & Asrar, 1988; Schmugge, Jackson, Kustas, & Wang, 1992; Wigneron, Calvet, Kerr, Chanzy, & Lopes, 1993; Wigneron, Kerr, Chanzy, & Jin, 1993; Wigneron, Schmugge, Chanzy, Calvet, & Kerr, 1998). These results ultimately contributed to the design of the first spaceborne instrument dedicated to global soil moisture mapping: the Soil Moisture and

Ocean Salinity (SMOS) mission (Kerr, Font, Waldteufel, & Berger, 2000).

SMOS was launched by the European Space Agency (ESA) in November 2009 and operates in the 1.400–1.427 GHz L-band (McMullan et al., 2008). The satellite incorporates a novel interferometric synthesized antenna concept, utilizing over 69 small antenna patches distributed along the Y-shaped satellite arms and central hub (Kerr et al., 2010). This innovative satellite design yields multi-incidence angle brightness temperature observations ranging from 0° to 60° across a 900 km swath with an approximately 45 km spatial resolution and a 2–3 day recurrence interval at 6 A.M. and 6 P.M. local time. The sequence of snapshots obtained over the same pixel but at different incidence angles is intended to enhance the soil moisture retrieval to meet the target accuracy of 0.04 m<sup>3</sup> m<sup>-3</sup>, when the biomass density is lower than 4 kg m<sup>-2</sup> (Kerr et al., 2001).

The estimation of soil moisture from microwave observations becomes more complex with the presence of a vegetation layer above the surface compared to bare soil conditions. Although it is expected that at around 6 A.M. overpass time, conditions will be such that the vegetation and the soil surface will be close to thermal equilibrium, the additional interaction of the emitted energy with the vegetation canopy still needs to be accounted for. Consequently, a larger set of ancillary input parameters is required to accurately describe the ground

\* Corresponding author.

E-mail addresses: [spei2@student.monash.edu](mailto:spei2@student.monash.edu) (S. Peischl), [jeff.walker@monash.edu](mailto:jeff.walker@monash.edu) (J.P. Walker), [dryu@unimelb.edu.au](mailto:dryu@unimelb.edu.au) (D. Ryu), [yann.kerr@cesbio.cnes.fr](mailto:yann.kerr@cesbio.cnes.fr) (Y. Kerr).

**Table 1**  
Overview of the L-MEB input parameter values for the two experiment days.

Date	NAFE'05 ground measurements				Ancillary data					
	SM (std) [m <sup>3</sup> m <sup>-3</sup> ]	VWC [kg m <sup>-2</sup> ]	T <sub>veg</sub> [K]	T <sub>surf</sub> [K]	H <sub>r</sub> <sup>a</sup> [-]	N <sub>r</sub> <sup>b</sup> [-]	b <sup>a</sup> [-]	ω <sup>b</sup> [-]	t <sub>t1</sub> <sup>b</sup> [-]	t <sub>t2</sub> <sup>b</sup> [-]
09.Nov	0.43 (±0.06)	1.9	309	303	0.8	0	0.08	0	1	8
23.Nov	0.14 (±0.05)	0.7	309	303						

<sup>a</sup> Sourced from Peischl et al. (2012).

<sup>b</sup> Sourced from Wigneron et al. (2007).

state. While much of these ancillary data can be obtained from i) point measurements at monitoring sites, ii) other spaceborne sensors, and iii) data assimilation models, there are issues with spatial and/or temporal discrepancies due to the variety of data sources. Therefore Wigneron, Waldteufel, Chanzy, Calvet, and Kerr (2000) considered the use of dual-polarized microwave data, acquired at multiple incidence angles by the same instrument, as an approach to overcome the need for ancillary data from external sources. They demonstrated the potential for simultaneous retrieval of soil moisture together with ancillary data, described as multi-parameter retrieval. Multi-angle observations also provide a possibility to reduce the impact of noise, such as radio frequency interference as experienced by SMOS (e.g. Camps et al., 2010; Castro, Gutierrez, & Barbosa, 2012; Oliva et al., 2012) by being able to identify RFI sources through angular anomalies.

If compared to the SMOS configuration only a very narrow range of angular observations is available, or if the SMOS angular range is reduced for some reason, then the benefits of multi-angle soil moisture retrievals might be compromised. In this context, it is necessary to assess the multi-parameter retrieval capability under alternate angular ranges and subsets of angles, to see if equivalent retrieval results can be achieved. Since the main parameters of interest beside soil moisture “SM” are: i) the vegetation water content “VWC” (through the vegetation optical depth), ii) the surface roughness conditions “H<sub>r</sub>”, iii) the surface soil temperature “T<sub>surf</sub>”, and iv) the vegetation temperature “T<sub>veg</sub>” (in case of non-early morning brightness temperature measurements), these variables will be the focus of this study. Specifically, the questions addressed by this paper include:

1. What range of incidence angles for brightness temperature observations provides optimal multi-parameter results considering a maximum angular range for radiometric measurements of 0–50°?
2. Would a combination of brightness temperature observations from different angular groups yield better results compared to a specified range of incidence angles only?

A variety of land surface conditions are studied, including dry and wet soils under a mature wheat canopy with moderate and high vegetation water contents, to investigate these questions. This study differs from previous work on the sensitivity of multi-angle data measurements in so much that it includes a validation of findings from synthetic experiments using airborne L-band observations acquired at farm-scale resolution, while others have focused solely on ground-based observations (e.g. Calvet et al., 2011; Wigneron et al., 2000, 2004).

## 2. Radiative transfer model

The radiative transfer model used to simulate the wheat canopy emission at L-band, and to test the multi-parameter retrieval across varying ranges of incidence angles, is one of the core algorithms applied to SMOS data (Kerr et al., 2011, 2012). A detailed description of the L-band Microwave Emission for the Biosphere model (L-MEB) can be found in Wigneron et al. (2007), together with a parameter analysis for crop application and derived values for wheat canopy analysis. The inversion of the model allows the retrieval of soil moisture and ancillary data by minimizing the root mean square error between the simulated and reference brightness temperatures.

The interaction and individual contributions of the soil and vegetation media on the composite brightness temperature (TB) are accounted for in L-MEB using a radiative transfer approach, also called the tau-omega model (Mo, Choudhury, Schmugge, Wang, & Jackson, 1982):

$$TB_{(p,\theta)} = (1 - \omega_{(p)}) \cdot (1 - \gamma_{(p,\theta)}) \cdot (1 + \gamma_{(p,\theta)} \cdot r_{G(p,\theta)}) \cdot T_C + (1 - r_{G(p,\theta)}) \cdot \gamma_{(p,\theta)} \cdot T_G \quad (1)$$

with P representing the measured polarization (H for horizontal, and V for vertical, respectively),  $\theta$  the incidence angle, and  $T_C$  and  $T_G$  corresponding to the effective soil and vegetation temperature [K],

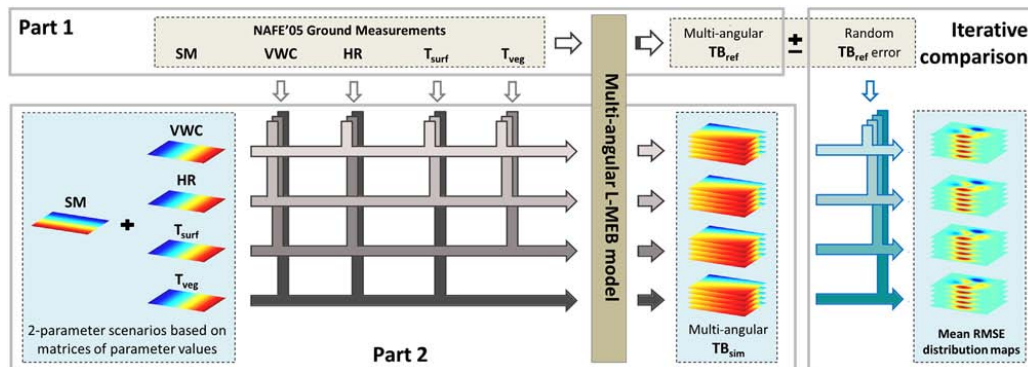


**Fig. 1.** Schematic of simulating synthetic multi-angular brightness temperature data (TB) using the forward model L-MEB. Part 1 illustrates the simulation of synthetic TB<sub>ref</sub> based on NAFE'05 ground measurements. Part 2 describes the simulation of synthetic TB<sub>sim</sub> based on NAFE'05 ground measurements and a matrix of two parameter value combinations depending on the scenario chosen (scenario: SM-VWC; SM-HR; SM-T<sub>surf</sub>; or SM-T<sub>veg</sub>). The final iterative comparison considers inclusion of a random TB error of maximum  $\pm 2$  K for TB<sub>ref</sub> and calculates the root mean square error between the varying TB<sub>ref</sub> and TB<sub>sim</sub> for each iteration step to arrive at a mean TB RMSE map.

**Table 2**  
Range of values (min-max) tested in multi-parameter retrieval combinations.

SM [m <sup>3</sup> m <sup>-3</sup> ]	VWC [kg m <sup>-2</sup> ]	H <sub>R</sub> [-]	T <sub>veg</sub> [K]	T <sub>surf</sub> [K]
0–0.6	0–3	0–1.5	278–340	278–340

respectively. The reflectivity of non-smooth soil surfaces  $r_{G(p,\theta)}$ , which is sensitive to the incidence angle and the polarization, can be quantified using a modification of the Fresnel equation by including a set of soil roughness parameters  $H_R$  and  $N_{R(p)}$ :

$$r_{G(p,\theta)} = r_{G(p,\theta)}^* \cdot \exp[-H_R \cdot \cos \theta^{(N_{R(p)})}]. \quad (2)$$

The Fresnel reflectivity  $r_{G(p,\theta)}^*$  from a smooth, ideally flat surface can be related in turn to soil moisture content through a dielectric mixing model, such as the one developed by Dobson, Ulaby, Hallikainen, and El-Rayes (1985) that was used in this study. The model variables characterizing the canopy are the single scattering albedo  $\omega_{(p)}$  and the vegetation transmissivity  $\gamma_{(p,\theta)}$ . The latter, also known as vegetation attenuation, is modeled as a function of the incidence angle and the optical depth at nadir  $\tau_{NAD}$ :

$$\gamma_{(p,\theta)} = \exp[-\tau_{NAD} \cdot (\sin^2 \theta \cdot tt_{(p)} + \cos^2 \theta) / \cos \theta] \quad (3)$$

with the vegetation structure parameters  $tt_H$  and  $tt_V$  correcting the optical depth for non-nadir viewing angles at each polarization. Hence, the optical depth increases with the amount of water on/in the canopy, which consequently reduces the transmission of the emitted soil energy within the vegetation medium. L-MEB assumes a linear relationship between the vegetation water content VWC and the nadir optical depth:

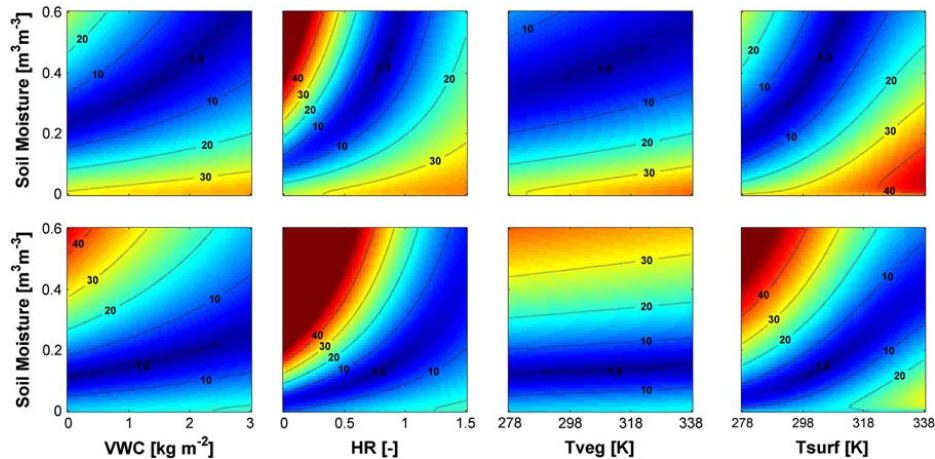
$$\tau_{NAD} = \text{VWC} \cdot b_{(p)}, \quad (4)$$

where the empirical vegetation parameter  $b_{(p)}$  is mainly dependent on the sensor frequency, polarization, canopy type and plant structure (Jackson & Schmugge, 1991).

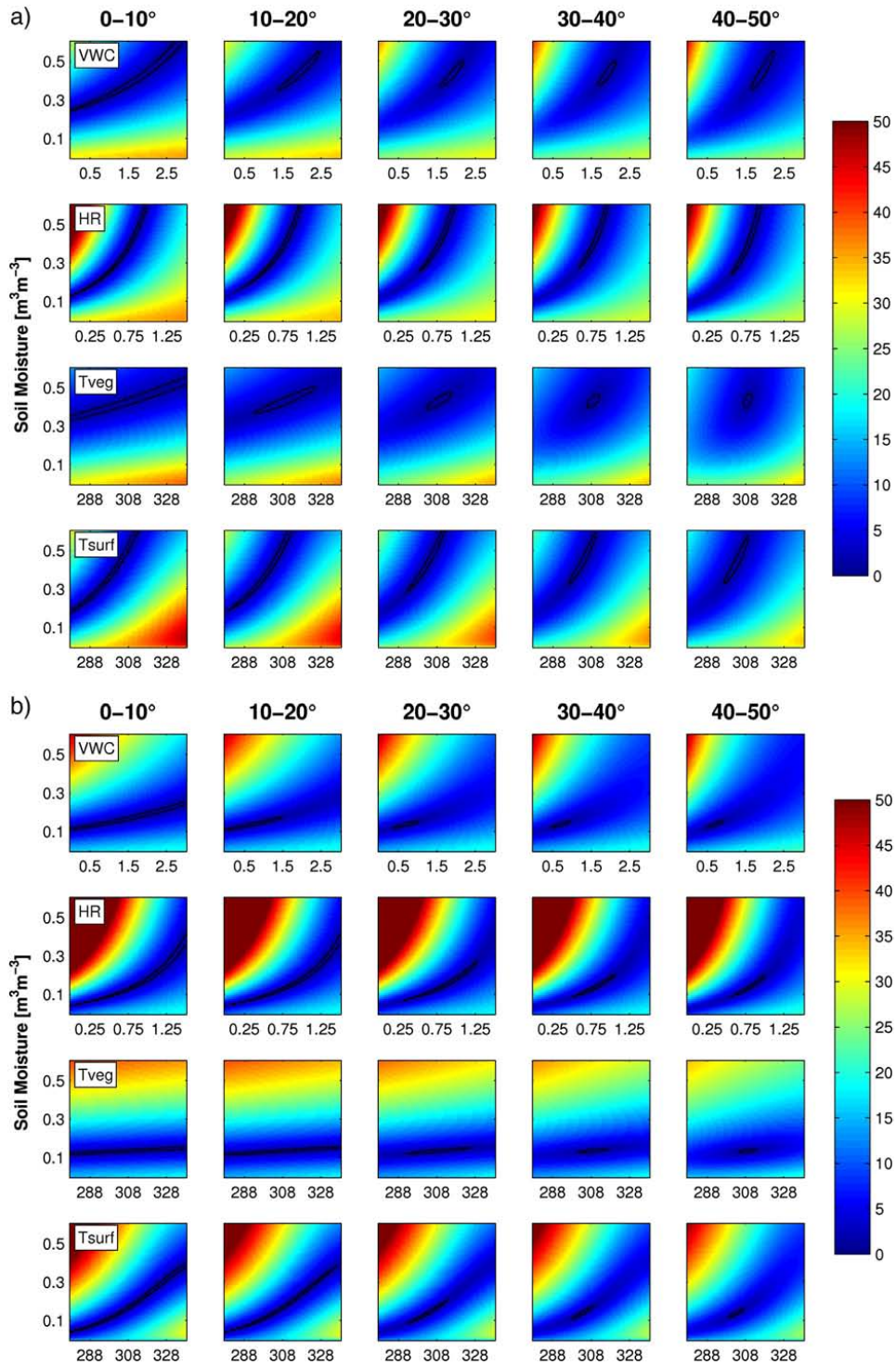
### 3. Experimental dataset and model setup

The present study is based on both simulated brightness temperatures and radiometric measurements acquired over a wheat field during the November 2005 National Airborne Field Experiment (NAFE'05) in south-eastern Australia (Panciera et al., 2008). The campaign was conducted across selected focus farms in the Goulburn River catchment (31°46'S to 32°51'S and 149°40'E to 150°36'E), where a combination of airborne as well as extensive ground monitoring was carried out. The primary sensor operated aboard the aircraft was the Polarimetric L-band Multi-beam Radiometer (PLMR), which used six pushbroom receivers at along track incidence angles of nominally  $\pm 7^\circ$ ,  $\pm 21.5^\circ$  and  $\pm 38.5^\circ$ , respectively, for the flights analyzed in this study. The multi-angle observation mode was achieved by rotating the radiometer by  $90^\circ$ , and thus allowing three beams measuring forward and three beams backward along the flight direction. Due to an aircraft pitch of about  $6^\circ$ , the actual angles of the six PLMR beams were approximately  $1^\circ$ ,  $13^\circ$ ,  $16^\circ$ ,  $28^\circ$ ,  $33^\circ$ , and  $45^\circ$  along track. The radiometer was calibrated daily using cold/warm targets, with a calibration accuracy determined as being 0.7 K and 2 K for H- and V-polarization, respectively (Panciera et al., 2008). The multi-angle flights of this study were undertaken at an altitude of approximately 750 m (AGL), providing a spatial resolution of  $\sim 250$  m.

Extensive ground monitoring was undertaken coincident with the airborne observations. High-resolution near-surface soil moisture measurements using the Hydraprobe Data Acquisition System (HDAS, Merlin et al., 2007) were taken across the focus farms (Panciera, Allahmoradi, Merlin, Young, & Walker, 2009). The Hydraprobe soil moisture sensor calibration was developed in the laboratory and from field samples, with a measurement accuracy of  $0.04 \text{ m}^3 \text{ m}^{-3}$ . The data used in this study were collected on four sampling days (once per week) within a cropping field of mature wheat canopy on silty clay loam soil, and capturing a dry down period within the observed time frame going from almost saturated soil surface ( $\sim 0.43 \text{ m}^3 \text{ m}^{-3}$ ) to moderate-dry soil conditions ( $\sim 0.14 \text{ m}^3 \text{ m}^{-3}$ ). The NAFE'05 in-situ soil moisture was averaged from  $\sim 250$  HDAS measurements and the respective standard deviation calculated for use in the data analysis. The vegetation water content demonstrated a similar decrease from approximately  $3 \text{ kg m}^{-2}$  to  $1 \text{ kg m}^{-2}$ . Additional ground information about soil texture, surface roughness, soil profile temperature and soil



**Fig. 2.** Plots of mean TB RMSE distribution [K] for four scenarios of two-parameter combinations (SM-VWC, SM-HR, SM-T<sub>veg</sub>, SM-T<sub>surf</sub>). The RMSE was calculated from the iterative difference in TB<sub>ref</sub> and TB<sub>sim</sub> considering all dual-polarized TB data within 0–50° incidence angle range. The contour lines indicate the level of RMSE in the parameter space. The top row represents wet conditions (SM =  $0.43 \text{ m}^3 \text{ m}^{-3}$ , VWC =  $1.9 \text{ kg m}^{-2}$ ) and the bottom row dry conditions ( $0.14 \text{ m}^3 \text{ m}^{-3}$ , VWC =  $0.7 \text{ kg m}^{-2}$ ).



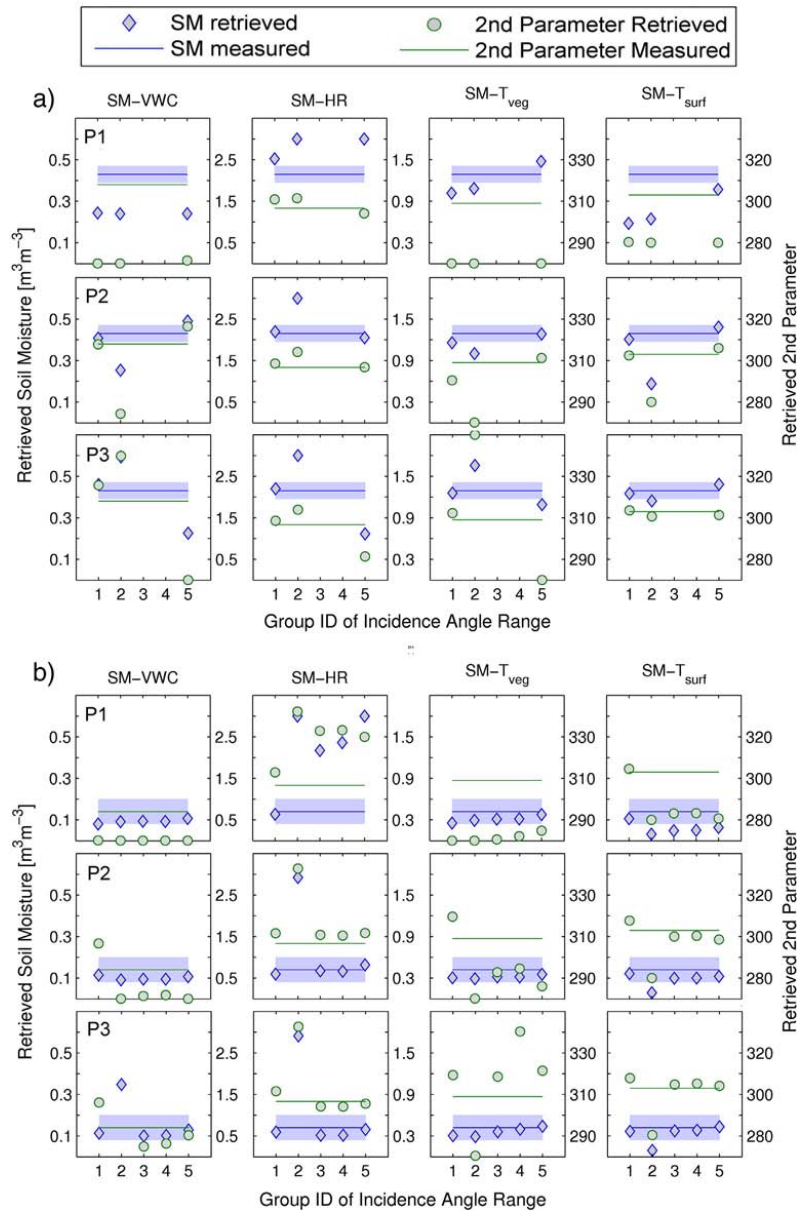


**Fig. 4.** Comparison of two-parameter retrieval results derived from the airborne dual-polarized NAFE'05 TB measurements, which were classified into five angular groups as shown on the x-axis (1: 0–10°; 2: 10–20°; 3: 20–30°; 4: 30–40°; 5: 40–50°). The shaded area depicts the standard deviation of the NAFE'05 ground measured soil moisture with the average value indicated by the blue line. Note that in each plot the left y-axis corresponds to the retrieved soil moisture and the right y-axis relates to the additionally retrieved parameter indicated at the top of each column: i) VWC [ $\text{kg m}^{-2}$ ], ii)  $H_R$  [–], iii)  $T_{\text{veg}}$  [K], and iv)  $T_{\text{surf}}$  [K]. Panel (a) illustrates wet conditions with  $SM = 0.43 \text{ m}^3 \text{ m}^{-3}$  and  $VWC = 1.9 \text{ kg m}^{-2}$ , while panel (b) illustrates dry moisture conditions with  $SM = 0.14 \text{ m}^3 \text{ m}^{-3}$  and  $VWC = 0.7 \text{ kg m}^{-2}$ , respectively. The index of each row relates to a different parameterization (P) used for the vegetation structure characterization in the retrieval model: i) P1:  $tt_{H1} = 1, tt_{V1} = 8$ ; ii) P2:  $tt_{H1} = 0.2, tt_{V1} = 1.4$ ; iii) P3:  $tt_{H1} = 1, tt_{V1} = 1$ . (For interpretation of the references to color in this figure legend, the reader is referred to the web version of this article.)

**Fig. 3.** Evolution of the mean dual-polarized TB RMSE distribution [K] across varying ranges of incidence angle for four scenarios of two-parameter combinations (rows 1 & 5: SM–VWC, rows 2 & 6: SM–HR, rows 3 & 7: SM– $T_{\text{veg}}$ , rows 4 & 8: SM– $T_{\text{surf}}$ ). The black contour line indicates an RMSE level of 1.5 K. Panel (a) illustrates moist conditions with  $SM = 0.43 \text{ m}^3 \text{ m}^{-3}$ ,  $VWC = 1.9 \text{ kg m}^{-2}$ , and panel (b) illustrates dry conditions with  $SM = 0.14 \text{ m}^3 \text{ m}^{-3}$  and  $VWC = 0.7 \text{ kg m}^{-2}$ .

**Table 3**  
Classification of angular groups according to incidence angle [°] and polarization (d – dual, h – horizontal, v – vertical).

ID	1		2		3		4		5		6	
Angular range	0–50d (all)		0–10d		10–20d		20–30d		30–40d		40–50d	
ID	7	8	9	10	11	12	13	14	15	16		
Angular range	0–10d, 10–20d	0–10d, 20–30d	0–10d, 30–40d	0–10d, 40–50d	10–20d, 20–30d	10–20d, 30–40d	10–20d, 40–50d	20–30d, 30–40d	20–30d, 40–50d	30–40d, 40–50d		
ID	17	18	19	20	21	22	23	24	25	26		
Angular range	0–10h, 10–20v	0–10h, 20–30v	0–10h, 30–40v	0–10h, 40–50v	10–20h, 20–30v	10–20h, 30–40v	10–20h, 40–50v	20–30h, 30–40v	20–30h, 40–50v	30–40h, 40–50v		
ID	27	28	29	30	31	32	33	34	35	36		
Angular range	0–10v, 10–20h	0–10v, 20–30h	0–10v, 30–40h	0–10v, 40–50h	10–20v, 20–30h	10–20v, 30–40h	10–20v, 40–50h	20–30v, 30–40h	20–30v, 40–50h	30–40v, 40–50h		

profile moisture were gathered from supplementary measurements made by the ground team and/or in-situ monitoring stations.

The synthetic analysis of this current study was based on simulated brightness temperature data that would represent the land surface conditions of the NAFE'05 test field using L-MEB. Table 1 presents an overview of the L-MEB parameter values used for the modeling. Processing of the synthetic brightness temperatures was divided into two parts, as indicated in Fig. 1. The first step focused on simulating a reference set of dual-polarized brightness temperatures ( $T_{Bref}$ ) across incidence angles of 0–50° (top part in Fig. 1). This was achieved by feeding the forward model with all available NAFE'05 ground truth

information and ancillary parameters (as given in Table 1). The resultant multi-angular  $T_{Bref}$  were subsequently perturbed, taking into account a random TB error of maximum  $\pm 2$  K, corresponding to the V-polarization calibration error of the PLMR instrument.

The second step of data processing involved the simulation of multiple sets of microwave responses ( $T_{Bsim}$ ) by varying input data according to a range of two-parameter scenarios. The scenarios considered were: i) soil moisture and vegetation water content (SM–VWC), ii) soil moisture and surface roughness (SM– $H_R$ ), iii) soil moisture and vegetation temperature (SM– $T_{veg}$ ), or iv) soil moisture and surface soil temperature (SM– $T_{surf}$ ). For instance, according to the SM–VWC scenario it

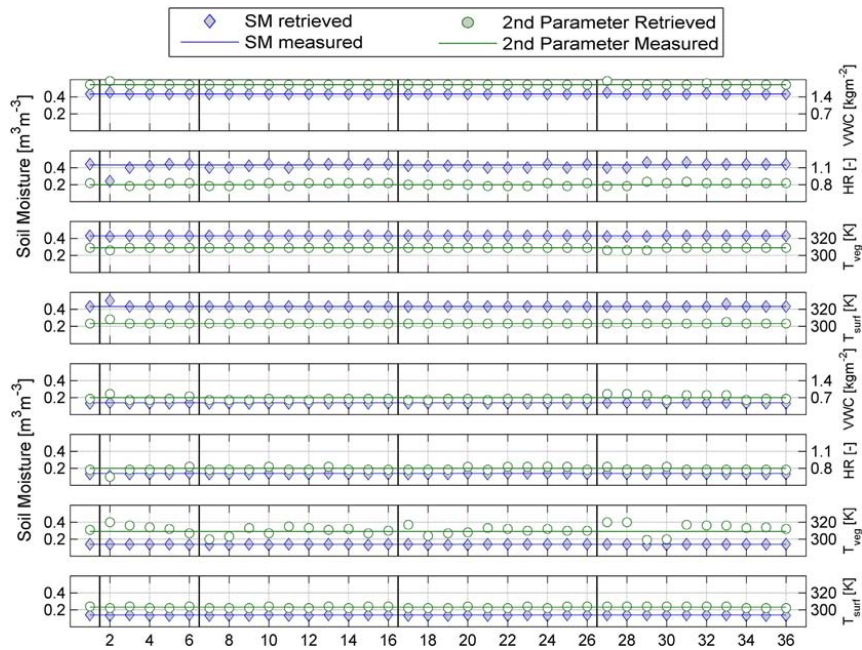


**Fig. 5.** Comparison of two-parameter retrieval results (blue diamond: SM, green circle: secondary parameter) against NAFE'05 ground measurements (blue line: measured SM; green line: second parameter ground truth) obtained from synthetic, dual-polarized TB data. Different angular group combinations (x-axis) were tested for the retrieval as given in Table 3. Note that in each plot the left y-axis corresponds to soil moisture and the right y-axis relates to the additionally retrieved parameter. The top four panels represent wet conditions and the bottom four panels illustrate dry conditions, respectively. (For interpretation of the references to color in this figure legend, the reader is referred to the web version of this article.)

was assumed that there were no NAFE'05 ground data available for these two parameters, and a feasible range of values was set for each individual parameter to simulate the multi-angular brightness temperature response. Table 2 presents the upper and lower limits used for each parameter. Consequently, soil moisture and one of either i) VWC, ii)  $H_R$ , iii)  $T_{veg}$ , or  $T_{surf}$  were varied – as opposed to the fixed parameter values used for  $T_{Bref}$  – to obtain the range of possible brightness temperature responses for each scenario pair.

Next, the root mean square error (RMSE) was calculated between the reference ( $T_{Bref}$ ) and the simulated ( $T_{Bsim}$ ) brightness temperatures (see right side of Fig. 1), and the value stored in a RMSE matrix referring to the respective combination of parameter values of the scenario pair (see Table 2). This process was repeated numerous times – considering the varying amplitude in random TB error for the  $T_{Bref}$  simulation – until the difference between the RMSE matrix of the current iteration and the mean RMSE matrix calculated from the previous iterations was lower than a certain threshold. Hence, the final RMSE matrix illustrates a mean RMSE distribution map, describing the general sensitivity of the retrieval model, when  $2\text{ K} > \text{TB error} > -2\text{ K}$  was considered. In order to examine the performance of multi-parameter retrievals from L-band data acquired at various incidence angles, the brightness temperature and RMSE model results were further classified into five angular groups of  $0\text{--}10^\circ$ ,  $10\text{--}20^\circ$ ,  $20\text{--}30^\circ$ ,  $30\text{--}40^\circ$ , and  $40\text{--}50^\circ$ . Consequently, each of these five angular bins contained a minimum of ten TB measurements per polarization.

For validation of the results obtained from the simulated TB datasets, the airborne L-band observations from the NAFE'05 experiment were used. The airborne measurements were processed under the same angular configurations as the synthetic TB. The inverse L-MEB model retrieval results for SM, VWC,  $H_R$ ,  $T_{veg}$  and  $T_{surf}$  were then compared to the NAFE'05 ground measurements and the possible angular preferences assessed.

#### 4. Retrieval sensitivity to incidence angle configuration

With respect to the four available NAFE'05 campaign days, simulations were performed for all stages of soil moisture and vegetation water conditions. However, only the two moisture extremes, the very wet case with  $SM = 0.43\text{ m}^3\text{ m}^{-3}/VWC = 1.9\text{ kg m}^{-2}$ , and the dry case with  $SM = 0.14\text{ m}^3\text{ m}^{-3}/VWC = 0.7\text{ kg m}^{-2}$  are presented here, since the analysis of the remaining dates showed overall similar results.

##### 4.1. Analysis of synthetic L-MEB simulated brightness temperatures

The iterative re-calculation of the mean RMSE between  $T_{Bsim}$  and  $T_{Bref}$  yielded a mean RMSE distribution map for each two-parameter scenario that was tested (Fig. 2). The sensitivity of the retrieval model was assessed by initially focusing on the pattern of the RMSE evolution within the studied parameter space (SM and one additional parameter of VWC,  $H_R$ ,  $T_{veg}$ , or  $T_{surf}$ ), when all incidence angles and dual-polarized TB were considered. Across all four scenarios the derived RMSE contour lines indicated a single global minimum as depicted by Fig. 2. This implied that the minimization algorithm, which is the core process in the retrieval, will most likely approach the “true” solution rather than a local minimum. Moreover, the outline of the illustrated minimum can be used to interpret the precision of the retrieval within the considered two-parameter space. For example, a long valley may result in a large error due to random noise in the TB observations, which hampers the system to reach a definite solution. In particular, the retrieval scenarios SM- $H_R$  and SM- $T_{surf}$  demonstrated a long elliptical valley covering a wide range of  $H_R$ - and  $T_{surf}$ -values, respectively. The dominantly vertical extent of the minimum denotes low retrieval sensitivity to soil moisture and higher sensitivity to the parameter on the x-axis, which is simultaneously derived with soil moisture. The two remaining scenarios SM- $T_{veg}$  and SM-VWC displayed better

defined mean RMSE minima outlined by a more circular shape. Notably, the position and shape of the global minima shifted for all parameter combinations under dry conditions, generally leading to high retrieval sensitivity to soil moisture as well as to the additionally retrieved parameter. Note, the mean TB RMSE maps represent the general sensitivity of the retrieval model, and the effect of random TB uncertainty (in our case the impact of 2 K error in TB) is indicated by the standard deviation of the TB maps. We tested different options with TB errors of  $\pm 4\text{ K}$  and found that the shape of the global minima varied slightly but kept the general pattern of the mean TB pattern shown in Fig. 2. Thus, we concluded that the mean TB RMSE distribution is likely to be independent of the TB uncertainty that is chosen.

Subsequent separation of the mean dual-polarized TB RMSE pattern into five angular groups of  $10^\circ$  bins each is shown in Fig. 3. In general, better defined global minima of small circular extent were observed for large incidence angles, independent of the tested parameter space. Conversely, the mean TB RMSE pattern derived from an angular range of  $0\text{--}10^\circ$  demonstrated dominantly vertically or diagonally elongated minima. This behavior suggested a range of equi-possible parameter combinations of SM and the respective ancillary parameter, making it more difficult to find the correct solution. For dry conditions, the sensitivity to soil moisture increased slightly with respect to the more horizontally positioned minima in all angular cases and parameter combination.

Comparison of the two-parameter retrieval results with NAFE'05 ground measurements indicated no clear preference for any of the angular groups for both moisture states. All angular groups performed well for the soil moisture modeling. Though in the case of dry conditions, especially for the retrieval of the secondary parameter, there was a slight tendency towards less accurate parameter estimates from TB obtained at small to mid-range angles. This effect was rather distinct in the case of the SM- $T_{veg}$  retrieval scenario.

Further analysis (not shown in this paper) of the retrieval model sensitivity, by separating the dual-polarized TB data into single-polarization, yielded a notably stronger scattering behavior of the retrieval results especially in the low- to mid-angular groups and for dry conditions – being most prominent for the  $T_{veg}$  retrieval. This implies that the vegetation structure and surface roughness effects on  $T_{BH}$  and  $T_{BV}$  differ substantially in those angular ranges and that the use of dual-polarization observations might smooth out the diverse contribution under such conditions. In contrast,  $T_{BH}$  and  $T_{BV}$  are almost equal when acquired at near-nadir views, so not much additional information is to be expected from dual-polarized TB.

##### 4.2. Analysis of NAFE'05 airborne brightness temperatures

In terms of validating the synthetic study results, an additional analysis was carried out using the passive microwave measurements obtained during the NAFE'05 campaign. The data set was processed according to the same angular settings chosen for the synthetic model simulations, focusing on five angular groups of TB data. However, due to the PLMR configuration with its six fixed beams and slight variations in aircraft pitch across the sampling dates, not all angular groups were represented on all sampling days. An overview of results from the two-parameter retrievals per angular group, as compared with the NAFE'05 ground measurements, is presented in Fig. 4.

Contrary to the synthetic findings, the parameters were not accurately retrieved across all angular groups. Large deviations from the NAFE'05 ground measurements were observed for soil moisture and the simultaneously retrieved ancillary parameters. With the lower moisture conditions there was a slight improvement for the retrieved soil moisture in the SM-VWC and SM- $T_{veg}$  scenarios, but the overall multi-angular model performance was still poor. Thus, two additional parameterizations were tested, which account differently for the non-nadir viewing impacts on the optical depth, through the vegetation structure parameters  $tt_H$  and  $tt_V$  (see Eq. (3)). The vegetation structure

plays an important role, especially for the wheat canopy of the NAFE'05 test site, as it is predominantly vertically structured in a mature state. As opposed to the initial configuration "P1" of  $tt_H = 1$  and  $tt_V = 8$  (Wigneron et al., 2007), alternate configurations "P2" with  $tt_H = 0.2$  and  $tt_V = 1.4$ , both computed from the same experimental dataset in an earlier study (Peischl et al., 2012), and "P3" with  $tt_H = 1$  and  $tt_V = 1$  (referring to an isotropic case with no dependence on polarization and incidence angle) were also tested. The P3 parameterization is often used in the case of grass and pasture land cover types.

With respect to the mean TB RMSE pattern, similar results to P1 as illustrated in Figs. 2 and 3 were found, but with mostly elongated global minima, suggesting less retrieval sensitivity for P2 and P3. However, comparison of the P2 and P3 retrieved parameter estimates with the NAFE'05 measurements demonstrated a significant improvement for both the soil moisture as well as the secondary retrieved parameters. The retrieved soil moisture values were overall within the range of standard deviation except for a few cases, predominantly from the 10–20° angular group. Regarding the simultaneously retrieved ancillary parameter, satisfying results were observed for  $H_R$  and  $T_{surf}$ . In the case of the vegetation water content (VWC) as well as the vegetation temperature ( $T_{veg}$ ), the model estimates were rather scattered with no specific trend for moist or dry conditions. In terms of an angular preference, results agreed with the synthetic findings from the dual-polarized retrieval, that there was no optimal result either when the soil was wet and the VWC high or when the soil moisture and the vegetation water content were low.

In summary out of the three model configurations studied, the initially tested parameterization P1 yielded unsatisfying results in contrary to its good performance in the synthetic analysis. Better retrieval estimates were obtained using the two alternate parameterizations, which considered either a minor or no angular dependence of the vegetation structure on the optical depth. Moreover, results from the airborne data suggested that a simultaneous retrieval of SM and  $H_R$  or  $T_{surf}$  was better posed than SM and either VWC or  $T_{veg}$ .

### 5. Cross-combination of multi-angular L-band data

Here the five previously assigned angular groups of synthetic TB data were merged into different combinations – mainly considering groups of opposite polarization – to investigate if particular combinations would lead to improved retrieval accuracy as opposed to focusing on a single-polarization and angular group. All tested cross-combinations are listed in Table 3 and the retrieval results are summarized in Fig. 5.

Qualitatively all retrieval results from the cross-combinations demonstrated mostly no or minor variations from the NAFE'05 ground measurements for soil moisture and its ancillary parameters. The particular angular groups which yielded peaks in the parameter estimations all had one aspect in common: that simulated TB data from small to mid-range angles (0–10° or 10–20°) was used for the retrieval. This feature was specifically prominent in the SM- $T_{veg}$  scenario for the retrieval of  $T_{veg}$ , and a bit less pronounced for VWC or  $H_R$  estimates. A stepwise improvement of the modeled parameters was clearly related to the use of TB data from larger incidence angles in combination with the small angular TB data. Best results were obtained when the 0–10° observations were combined with the angles >40°, partially confirming the ground-based studies by Wigneron et al. (2004), who found that best soil moisture estimates were derived at H-polarization when the difference in angle was >30° for biangular measurements. Conversely, when V-polarized TB data from small angles was combined with large H-polarized TB data no significant improvement was observed.

The scattering behavior of the retrieval results regarding different angular cross-combinations was especially dominant under dry conditions (low soil moisture and vegetation water content). These effects are likely to be caused by the increased contribution of soil emission to the overall brightness temperature response. The reduced relative vegetation contribution to the overall brightness temperature response

makes it more difficult to retrieve the desired vegetation properties. Moreover, the sensitivity to the effective surface soil roughness might change with moisture content since the soil emission originates from deeper layers of the soil column under dry conditions.

### 6. Conclusion

A two-step analysis of multi-parameter retrievals was conducted to investigate the sensitivity of the retrieval to the angular viewing configurations of an L-band radiometer. The analysis was based on synthetic and airborne multi-angle brightness temperature data acquired over a wheat canopy.

It was concluded from the angular synthetic data study that the circular global minima with small extent required for high retrieval sensitivity was generally achieved when dual-polarized brightness temperature measurements from large incidence angles (40–50°) were selected. The sensitivity of the retrieval model decreased when – in addition to the usage of TB data from small incidence angles – dry conditions in terms of low surface soil moisture and vegetation water content were observed. These circumstances also hampered the simultaneous retrieval of the ancillary data leading to stronger scattering of the model estimates across the tested angular groups. Combining microwave data acquired at different angles and polarization yielded the most significant retrieval enhancements, where TB data obtained jointly at angles between 0 and 10° (H-polarized) and 40–50° (V-polarized) were used.

The validation study confirmed the synthetic results in terms of a preference for dual-polarized over single-polarized microwave data for two-parameter retrievals. However, best retrieval results were often derived when the characterization of the vegetation structure parameters was adjusted from  $tt_H = 1$ ,  $tt_V = 8$  to  $tt_H = 0.2$ ,  $tt_V = 1.4$  (calibrated values for wheat) or even  $tt_H = 1$ ,  $tt_V = 1$  (implying little/no angular/polarization dependency). However, these parameter values also yielded more elongated global minima, suggesting lower retrieval accuracy. Moreover, the airborne retrieval did not confirm the synthetic findings based on the extent of the global minima that retrievals at small angles were generally less accurate than other angular groups.

Overall, both the synthetic and the airborne results showed that a simultaneous retrieval of SM-VWC or SM- $T_{veg}$  was less preferable to SM- $H_R$  or SM- $T_{surf}$  retrievals, based on the highly variable results that were obtained. Especially in the case of dry conditions when the relative vegetation contribution to the composite TB signal is decreasing, it was complicated to retrieve information about the canopy independent of the vegetation structure parameterization we applied.

### Acknowledgment

The authors would like to acknowledge the National Airborne Field Experiment 2005 team for collecting and providing the data set used in this study. The NAFE'05 campaign has been made possible through infrastructure (LE0453434 and LE0560930) and research (DP0557543 and DP0556941) funding from the Australian Research Council. This study was financially supported by Australian Research Council grant DP0879212 in the framework of the MoistureMap project. The authors appreciate the helpful feedback by the reviewers which improved the manuscript substantially.

### References

- Calvet, J.-C., Wigneron, J.-P., Walker, J. P., Karbou, F., Chanzy, A., & Albergel, C. (2011). Sensitivity of passive microwave observations to soil moisture and vegetation water content: L-band to W-band. *IEEE Transactions on Geoscience and Remote Sensing*, 49(4), 1190–1199. <http://dx.doi.org/10.1109/TGRS.2010.2050488>.
- Camps, A. J., Gourion, J., Tarongi, J. M., Gutierrez, A., Barbosa, J., & Castro, R. (2010, 25–30 July). RFI analysis in SMOS imagery. Paper presented at the *IEEE International Geoscience and Remote Sensing Symposium (IGARSS)*, Honolulu, Hawaii, USA, 2007–2010. <http://dx.doi.org/10.1109/IGARSS.2010.5654268>.

- Castro, R., Gutierrez, A., & Barbosa, J. (2012). A first set of techniques to detect radio frequency interferences and mitigate their impact on SMOS data. *IEEE Transactions on Geoscience and Remote Sensing*, 50(5), 1440–1447, <http://dx.doi.org/10.1109/tgrs.2011.2179304>.
- de Rosnay, P., Calvet, J. -C., Kerr, Y., Wigneron, J. -P., Lemaître, F., Escorihuela, M. J., et al. (2006). SMOSREX: A long term field campaign experiment for soil moisture and land surface processes remote sensing. *Remote Sensing of Environment*, 102(3–4), 377–389, <http://dx.doi.org/10.1016/j.rse.2006.02.021>.
- Dobson, M. C., Ulaby, F. T., Hallikainen, M. T., & El-Rayes, M. A. (1985). Microwave dielectric behavior of wet soil—Part II: Dielectric mixing models. *IEEE Transactions on Geoscience and Remote Sensing*, GE-23(1), 35–46, <http://dx.doi.org/10.1109/TGRS.1985.289498>.
- Jackson, T. J. (1993). III. Measuring surface soil moisture using passive microwave remote sensing. *Hydrological Processes*, 7(2), 139–152, <http://dx.doi.org/10.1002/hyp.3360070205>.
- Jackson, T. J., Le Vine, D. M., Hsu, A. Y., Oldak, A., Starks, P. J., Swift, C. T., et al. (1999). Soil moisture mapping at regional scales using microwave radiometry: The Southern Great Plains hydrology experiment. *IEEE Transactions on Geoscience and Remote Sensing*, 37(5), 2136–2151, <http://dx.doi.org/10.1109/36.789610>.
- Jackson, T. J., & Schmugge, T. J. (1991). Vegetation effects on the microwave emission of soils. *Remote Sensing of Environment*, 36(3), 203–212, [http://dx.doi.org/10.1016/0034-4257\(91\)90057-D](http://dx.doi.org/10.1016/0034-4257(91)90057-D).
- Kerr, Y. H., Font, J., Waldteufel, P., & Berger, M. (2000). The Soil Moisture and Ocean Salinity Mission—SMOS. *ESA Earth Observation Quarterly*(66), 18–26.
- Kerr, Y. H., Waldteufel, P., Richaume, P., Wigneron, J. -P., Ferrazzoli, P., & Gurney, R. J. (2011). SMOS level 2 processor for soil moisture – Algorithm Theoretical Based Document (ATBD). Report. CESA, SO-TN-ESI-SM-CS-0001. Issue 3.e, CESBIO, Toulouse, France, 24.01.2011.
- Kerr, Y. H., Waldteufel, P., Richaume, P., Wigneron, J. -P., Ferrazzoli, P., Mahmoodi, A., et al. (2012). The SMOS soil moisture retrieval algorithm. *IEEE Transactions on Geoscience and Remote Sensing*, 50(5), 1384–1403, <http://dx.doi.org/10.1109/tgrs.2012.2184548>.
- Kerr, Y. H., Waldteufel, P., Wigneron, J. -P., Delwart, S., Cabot, F., Boutin, J., et al. (2010). The SMOS mission: New tool for monitoring key elements of the global water cycle. *Proceedings of the IEEE*, 98(5), 666–687, <http://dx.doi.org/10.1109/JPROC.2010.2043032>.
- Kerr, Y. H., Waldteufel, P., Wigneron, J. -P., Martinuzzi, J. M., Font, J., & Berger, M. (2001). Soil moisture retrieval from space: The Soil Moisture and Ocean Salinity (SMOS) mission. *IEEE Transactions on Geoscience and Remote Sensing*, 39(8), 1729–1735, <http://dx.doi.org/10.1109/36.942551>.
- McMullan, K. D., Brown, M. A., Martin-Neira, M., Rits, W., Ekholm, S., Marti, J., et al. (2008). SMOS: The payload. *IEEE Transactions on Geoscience and Remote Sensing*, 46(3), 594–605, <http://dx.doi.org/10.1109/Tgrs.2007.914809>.
- Merlin, O., Walker, J. P., Panciera, R., Young, R., Kalma, J., & Kim, E. J. (2007, December). Soil moisture measurement in heterogeneous terrain. Paper presented at the 17th International Congress on Modelling and Simulation (MODSIM), New Zealand (pp. 2604–2610).
- Mo, T., Choudhury, B. J., Schmugge, T. J., Wang, J. R., & Jackson, T. (1982). A model for microwave emission from vegetation-covered fields. *Journal of Geophysical Research*, 87(C13), 11,229–211,237, <http://dx.doi.org/10.1029/JC087iC13p11229>.
- Njoku, E. G., & Entekhabi, D. (1996). Passive microwave remote sensing of soil moisture. *Journal of Hydrology*, 184(1–2), 101–129, [http://dx.doi.org/10.1016/0022-1694\(95\)02970-2](http://dx.doi.org/10.1016/0022-1694(95)02970-2).
- Oliva, R., Daganzo-Eusebio, E., Kerr, Y. H., Mecklenburg, S., Nieto, S., Richaume, P., et al. (2012). SMOS radio frequency interference scenario: Status and actions taken to improve the RFI environment in the 1400–1427-MHz passive band. *IEEE Transactions on Geoscience and Remote Sensing*, 50(5), 1427–1439.
- Panciera, R., Allahmoradi, M., Merlin, O., Young, R., & Walker, J. P. (2009, November). *The Hydraprobe Data Acquisition System (HDAS) V.5: User guide*. [V.1 created: September 2006]. Australia: University of Melbourne, Melbourne (5).
- Panciera, R., Walker, J. P., Kalma, J. D., Kim, E. J., Hacker, J., Merlin, O., et al. (2008). The NAFE05/CoSMOS data set: Toward SMOS soil moisture retrieval, downscaling, and assimilation. *IEEE Transactions on Geoscience and Remote Sensing*, 46(3), 736–745, <http://dx.doi.org/10.1109/Tgrs.2007.915403>.
- Peischl, S., Walker, J. P., Ryu, D., Kerr, Y. H., Panciera, R., & Rüdiger, C. (2012). Wheat canopy structure and surface roughness effects on multiangle observations at L-band. *IEEE Transactions on Geoscience and Remote Sensing*, 50(5), 1498–1506, <http://dx.doi.org/10.1109/tgrs.2011.2174644>.
- Saleh, K., Wigneron, J. -P., Calvet, J. -C., Lopez-Baeza, E., Ferrazzoli, P., Berger, M., et al. (2004). The EuroSTARRS airborne campaign in support of the SMOS mission: First results over land surfaces. *International Journal of Remote Sensing*, 25(1), 177–194, <http://dx.doi.org/10.1080/0143116031000116444>.
- Schmugge, T. J., Jackson, T., Kustas, W. P., & Wang, J. R. (1992). Passive microwave remote sensing of soil moisture: Results from HAPEX, FIFE and MONSOON 90. *ISPRS Journal of Photogrammetry and Remote Sensing*, 47(2–3), 127–143, [http://dx.doi.org/10.1016/0924-2716\(92\)90029-9](http://dx.doi.org/10.1016/0924-2716(92)90029-9).
- Schmugge, T. J., O'Neill, P., & Wang, J. R. (1986). Passive microwave soil moisture research. *IEEE Transactions on Geoscience and Remote Sensing*, GE-24(1), 12–22, <http://dx.doi.org/10.1109/TGRS.1986.289584>.
- Schmugge, T. J., Wang, J. R., & Asrar, G. (1988). Results from the push broom microwave radiometer flights over the Konza Prairie in 1985. *IEEE Transactions on Geoscience and Remote Sensing*, 26(5), 590–596.
- Walker, J. P., & Houser, P. R. (2004). Requirements of a global near-surface soil moisture satellite mission: Accuracy, repeat time, and spatial resolution. *Advances in Water Resources*, 27(8), 785–801, <http://dx.doi.org/10.1016/j.advwatres.2004.05.006>.
- Wigneron, J. -P., Calvet, J. -C., de Rosnay, P., Kerr, Y. H., Saleh, K., Escorihuela, M. J., et al. (2004). Soil moisture retrievals from biangular L-band passive microwave observations. [Abstract]. *IEEE Geoscience and Remote Sensing Letters*, 1(4), 277–281, <http://dx.doi.org/10.1109/LGRS.2004.834594>.
- Wigneron, J. -P., Calvet, J. -C., Kerr, Y. H., Chanzy, A., & Lopes, A. (1993). Microwave emission of vegetation: Sensitivity to leaf characteristics. *IEEE Transactions on Geoscience and Remote Sensing*, 31(3), 716–726, <http://dx.doi.org/10.1109/36.225537>.
- Wigneron, J. -P., Calvet, J. -C., Pellarin, T., Van de Griend, A. A., Berger, M., & Ferrazzoli, P. (2003). Retrieving near-surface soil moisture from microwave radiometric observations: Current status and future plans. *Remote Sensing of Environment*, 85(4), 489–506, [http://dx.doi.org/10.1016/S0034-4257\(03\)00051-8](http://dx.doi.org/10.1016/S0034-4257(03)00051-8).
- Wigneron, J. -P., Kerr, Y. H., Chanzy, A., & Jin, Y. -Q. (1993). Inversion of surface parameters from passive microwave measurements over a soybean field. *Remote Sensing of Environment*, 46(1), 61–72, [http://dx.doi.org/10.1016/0034-4257\(93\)90032-S](http://dx.doi.org/10.1016/0034-4257(93)90032-S).
- Wigneron, J. -P., Kerr, Y. H., Waldteufel, P., Saleh, K., Escorihuela, M. J., Richaume, P., et al. (2007). L-band Microwave Emission of the Biosphere (L-MEB) model: Description and calibration against experimental data sets over crop fields. *Remote Sensing of Environment*, 107(4), 639–655, <http://dx.doi.org/10.1016/j.rse.2006.10.014>.
- Wigneron, J. -P., Schmugge, T. J., Chanzy, A., Calvet, J. -C., & Kerr, Y. H. (1998). Use of passive microwave remote sensing to monitor soil moisture. *Agronomie*, 18(1), 27–43, <http://dx.doi.org/10.1051/agro:19980102>.
- Wigneron, J. -P., Waldteufel, P., Chanzy, A., Calvet, J. -C., & Kerr, Y. H. (2000). Two-dimensional microwave interferometer retrieval capabilities over land surfaces (SMOS Mission). *Remote Sensing of Environment*, 73(3), 270–282, [http://dx.doi.org/10.1016/S0034-4257\(00\)00103-6](http://dx.doi.org/10.1016/S0034-4257(00)00103-6).

### 4.3 Summary

---

In this research the L-MEB model was used to investigate the soil moisture retrieval results obtained when only specific ranges of multi-angle brightness temperature observations over wheat canopy were used. Moreover, the impact of varying moisture conditions and multi-parameter retrievals were studied to further assess the model performance and soil moisture accuracy. The results demonstrated overall good soil moisture estimates in relation to the ground measurements ( $SM=0-0.03 \text{ m}^3/\text{m}^3$ ), if i) soil moisture was retrieved solely and ii) all available brightness temperature data collected across  $0-50^\circ$  incidence angles were used. However when attempting the simultaneous retrieval of soil moisture together with ancillary data and focusing on specific angular ranges of observations, large variations in soil moisture estimates were observed. In particular, L-band data collected at incidence angles of  $10^\circ$  or higher seemed to be more strongly affected by the canopy, since vegetation effects of the dominant vertical wheat structure increased with larger incidence angles. Hence, L-band data measured at near-nadir views ( $0-10^\circ$ ) produced the soil moisture results closest to those measured - independently of the observed moisture conditions - when the optical depth and/or the surface roughness parameter were retrieved simultaneously with soil moisture.

# 5

## Evaluation of data acquisition time on angular observations [Paper 3]

**T**HIS chapter includes a research paper which has resulted from the studies undertaken for this degree and which is currently under review in a peer-reviewed journal. The inclusion of co-authors reflects the fact that the work came from active collaboration between researchers from different institutes in Australia and France, and acknowledges input into team-based research.

**Peischl, S., Walker, J. P., Ryu, D., and Kerr, Y. H. (2017):** Analysis on data acquisition time on soil moisture retrieval from L-Band observations, IEEE Transactions on Geoscience and Remote Sensing (TGRS), in press.

**Declaration for Thesis Chapter 5**

In the case of Chapter 5, the nature and extent of my contribution to the work was the following:

Nature of contribution	Extent of contribution (%)
Review of literature, data processing and interpretation, and write up.	80 %

The following co-authors contributed to the work. Co-authors who are students at Monash University must also indicate the extent of their contribution in percentage terms: n/a

Name	Nature of contribution	Extent of contribution (%) for student co-authors only
Prof Jeffrey Walker	Ideas, interpretation and reviewing	n/a
Dr Dongryeol Ryu	Ideas, interpretation and reviewing	n/a
Dr Yann Kerr	Ideas, interpretation and reviewing	n/a

Candidate's Signature	<i>Sandy Pearson</i>	Date	<i>08/02/17</i>
-----------------------	----------------------	------	-----------------

**Declaration by co-authors**

The undersigned hereby certify that:

- (1) the above declaration correctly reflects the nature and extent of the candidate's contribution to this work, and the nature of the contribution of each of the co-authors.
- (2) they meet the criteria for authorship in that they have participated in the conception, execution, or interpretation, of at least that part of the publication in their field of expertise;
- (3) they take public responsibility for their part of the publication, except for the responsible author who accepts overall responsibility for the publication;
- (4) there are no other authors of the publication according to these criteria;
- (5) potential conflicts of interest have been disclosed to (a) granting bodies, (b) the editor or publisher of journals or other publications, and (c) the head of the responsible academic unit; and
- (6) the original data are stored at the following location(s) and will be held for at least five years from the date indicated below:

Location	Department of Civil Engineering, Monash University, Australia
----------	---

Signature 1	Prof Jeffrey Walker <i>JWalker</i>	Date	<i>7/3/17</i>
-------------	------------------------------------	------	---------------

Location	Department of Infrastructure Engineering , The University of Melbourne, Australia
----------	---

Signature 2	Dr Dongryeol Ryu <i>[Signature]</i>	Date	<i>7/3/17</i>
-------------	-------------------------------------	------	---------------

Digitally signed by  
com.apple.idms.appleid.prd.77436a386971656456566336364234356b46  
746357513d3d  
DN:  
c=us,com.apple.idms.appleid.prd.77436a386971656456566336364234356  
b467d3357513d3d  
Date: 2017.03.07 12:59:51 +1000

**Location** Biospheric Processes, CESBIO, France

**Signature 3** 

Dr Yann Kerr 	<b>Date</b> February 14 <sup>th</sup> 2017
--	---



## 5.1 Introduction

---

To test the robustness of the adopted multi-angle retrieval algorithm, it needs to be applied to an area different to the calibration conditions. Therefore, in the following study we worked extensively on the NAFE'06 data set collected across the Murrumbidgee catchment in South-East Australia. This study region represents a totally different environment with areas especially used for pasture and cropping. One special feature of the data set includes the multi-angle L-band observations which are to be analyzed for the first time in this study. The airborne flights were conducted at 6 am and 6 pm which is also coincident with SMOS overpass times. Simulations comparing morning against evening retrieval results will investigate the time effect and eventual (dis-)advantages of each observation type. Furthermore, the multi-angle information is used to derive information on the vegetation cover which is an essential part for the parameterization of the ancillary data in the retrieval model.

## 5.2 Analysis of data acquisition time on soil moisture retrieval from L-Band observations

---

# Analysis of data acquisition time on soil moisture retrieval from multi-angle L-Band observations

Sandy Peischl, *Member, IEEE*, Jeffrey P. Walker *Senior Member, IEEE*, Dongryeol Ryu, *Member, IEEE* and Yann H. Kerr, *Senior Member, IEEE*

**Abstract**— This study investigated the sensitivity of passive microwave L-band soil moisture retrieval from multi-angle airborne brightness temperature data obtained under morning and afternoon conditions from the National Airborne Field Experiment (NAFE) conducted in south-east Australia in 2006. Ground measurements at a dryland focus farm including soil texture, soil temperature and vegetation water content were used as ancillary data to drive the retrieval model. The derived soil moisture was then in turn evaluated with the ground measured near-surface soil moisture patterns. Results of this study show that the SMOS target accuracy of  $0.04 \text{ m}^3\text{m}^{-3}$  for single soil moisture retrievals is achievable irrespective of the 6 A.M. morning and 6 P.M. afternoon overpass acquisition time for moisture conditions  $\leq 0.15 \text{ m}^3\text{m}^{-3}$ . Additional tests on the use of the air temperature as proxy for the vegetation temperature also showed no preference for the acquisition time. The performance of multi-parameter retrievals of soil moisture and an additional parameter proved to be satisfactory for soil moisture modelling - independent of the acquisition time - with root mean square errors less than  $0.06 \text{ m}^3\text{m}^{-3}$  for the focus farm.

**Index Terms**— multi-incidence angle, passive microwave remote sensing, L-band, soil moisture, acquisition time, Soil Moisture and Ocean Salinity (SMOS)

## I. INTRODUCTION

ONE of the main motivations for earth observing satellite missions is the enhancement of meteorological and climatic model predictions. Amongst others the global soil moisture is considered as a significant input parameter to

enhance model forecasts of climate and weather evolution. After decades of intensive research in near-surface soil moisture remote sensing, the application of passive microwave observations has been proven as one of the most promising [1-4]. The 2009 launched L-band (1.4 GHz) passive microwave satellite by the European Space Agency (ESA) has not only heralded the first dedicated mission for global Soil Moisture and Ocean Salinity (SMOS) mapping [5, 6], but its novel design also provides a unique opportunity to utilise multi-angle observations of the same area on the ground to derive the ancillary information required in the soil moisture retrieval more reliably. Moreover, the SMOS mission has a 2-3 day revisit cycle, designed around a polar sun-synchronous orbit with a 6 A.M. local solar time ascending node and 6 P.M. descending node; the emphasis being on the 6 A.M. overpass time for soil moisture retrieval [7].

The basis of soil moisture measurement from SMOS is the relationship between a measured brightness temperature and the dielectric constant of the near-surface soil, which is in turn related to its moisture content. With this soil moisture relationship being affected by a range of factors, including surface roughness and vegetation cover (e.g. type, vegetation water content, growth state, litter presence), the SMOS mission uses the multi-incidence angle observations to derive some of the ancillary parameters (e.g. vegetation optical depth and surface roughness) and hence facilitate the retrieval algorithm. However, the emphasis to date has been on the morning SMOS overpass, as the ideal conditions for soil moisture retrieval at L-band are generally assumed to be around dawn when the Faraday rotation occurring in the ionosphere is at its minimum [8, 9] and the top soil column is in close thermal equilibrium with the overlying canopy. The latter simplifies the model by assuming an effective temperature that represents both the near-surface soil and canopy temperature, implying that there is no temperature gradient in the vegetation or soil profile. However, the afternoon SMOS observations might also hold valuable soil moisture information, and indeed yield better soil moisture retrievals in places like Europe where the ascending SMOS data is often corrupted due to radio frequency interference (RFI) [10, 11], requiring filtering or in severe case even complete masking. These findings were supported by the study presented by Al-Yaari et al. [12] who compared the

Manuscript received March 12, 2017; revised July 19, 2017; revised August 26, 2017; accepted XX 2017. Date of publication XX. The authors would like to acknowledge the National Airborne Field Experiment 2006 team for collecting and providing the data set used in this study. Financial support for this campaign was received from the Australian Research Council (ARC) through infrastructure (LE0453434 and LE0560930) and research (DP0557543) grants. The initial setup and maintenance of the Murrumbidgee catchment monitoring system was funded by the CRC for Catchment Hydrology and the ARC (DP0343778, DP0557543).

S. Peischl and J. P. Walker are with the Department of Civil Engineering, Faculty of Engineering, Monash University, Melbourne, Vic. 3800, Australia (e-mail: jeff.walker@monash.edu).

D. Ryu is with the Department of Infrastructure Engineering, Melbourne School of Engineering, The University of Melbourne, Melbourne, Vic. 3010, Australia (e-mail: dryu@unimelb.edu.au).

Y. H. Kerr is with the Centre d'Etudes Spatiales de la Biosphère, 31401 Toulouse, France (e-mail: yann.kerr@cesbio.cnes.fr).

&gt; TGRS-2017-0031 &lt;

2

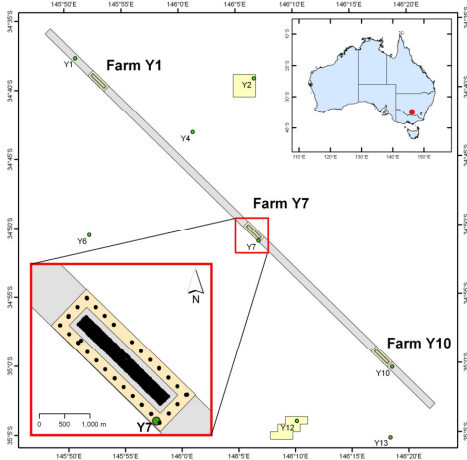


Fig. 1. Top: Location of the NAFE'06 focus farms Y1, Y7 and Y10 and the OzNet monitoring network (green dots) within the Yanco study area. Bottom inset: Y7 focus farm which was covered by multi-angle transect flights (grey), location of the corresponding monitoring station Y7 and distribution of the intensive soil moisture sampling grid (black points).

SMOS L3 soil moisture products from ascending and descending overpasses against reference surface soil moisture products derived from the AMSR-E satellite and a land data assimilation product provided by the European Centre for Medium Range Weather Forecasts (ECMWF). Further varying patterns in the accuracy of retrieval products obtained from active and passive microwave satellite sensors at different acquisition times were also demonstrated by Lei et al. [13].

## II. RADIATIVE TRANSFER MODEL

The model used for simulating the grass canopy emission at L-band in this paper is one of the core algorithms applied to SMOS data [7]. A detailed description of the L-band Microwave Emission for the Biosphere model (L-MEB) can be found in Wigneron et al. [14], so only the pertinent details are given here. In brief, inversion of the model allows the retrieval of near-surface soil moisture and additional model parameters by minimizing the root mean square error between observed and simulated brightness temperatures using initial ancillary input and soil moisture assumptions.

In L-MEB, the individual contributions of the soil and vegetation media and their interaction on the composite brightness temperature TB are accounted for using a radiative transfer approach called the tau-omega model [15, 16]:

$$TB(P, \theta) = (1 - \omega(P)) \cdot (1 - \gamma(P, \theta)) \cdot (1 + \gamma(P, \theta) \cdot rG(P, \theta)) \cdot TC + (1 - rG(P, \theta)) \cdot \gamma(P, \theta) \cdot TG, \quad (1)$$

with P representing the polarization (H: horizontal, and V: vertical),  $\theta$  the incidence angle, and TG and TC corresponding to the effective soil and vegetation temperature [K], respectively. The reflectivity of non-smooth soil surfaces rGP, which is sensitive to the incidence angle and the polarization,

can be quantified using a modification of the Fresnel equation by including soil roughness parameters HR and NR(P):

$$G(P, \theta) = r * G(P, \theta) \cdot \exp[-HR \cdot \cos \theta (NR(P))]. \quad (2)$$

The Fresnel reflectivity from a smooth, ideally flat surface  $r * G(P, \theta)$  can in turn be related to soil moisture content through a dielectric mixing model such as that developed by Dobson et al. [17] or Mironov et al. [18]. The latter was used in this study. The model variables characterizing the canopy are the single scattering albedo  $\omega(P)$  and the vegetation transmissivity  $\gamma(P)$ , also known as vegetation attenuation, is modelled as a function of the incidence angle and the optical depth at nadir  $\tau_{NAD}$ :

$$\gamma(P, \theta) = \exp[-\tau_{NAD} \cdot (\sin 2\theta \cdot tt(P)) + (\cos 2\theta) / \cos \theta], \quad (3)$$

with the vegetation structure parameters  $tt(P)$  correcting the optical depth for non-nadir views at each polarization. Hence, the optical depth increases with the amount of water on/in the canopy, which consequently reduces the transmission of the emitted soil energy within the vegetation medium. L-MEB uses the commonly assumed linear relationship between the vegetation water content and the nadir optical depth:

$$\tau_{NAD} = VWC \cdot b(P), \quad (4)$$

where the empirical vegetation parameter  $b(P)$  is mainly dependent on the sensor frequency, polarization, canopy type and plant structure [19].

## III. EXPERIMENTAL DATASET

This study is based on airborne measured L-band brightness temperatures acquired during the National Airborne Field Experiment (NAFE) in Australia, which is described extensively in Merlin et al. [20]. The NAFE campaign was conducted for a three-week period in November 2006 in the central region of the Murrumbidgee River catchment, New South Wales. The primary instrument aboard the aircraft was the Polarimetric L-band Multibeam Radiometer (PLMR), which operates at a frequency of 1.413 GHz with a 24 MHz bandwidth. Dual-polarized measurements are acquired through polarization switching, with an accuracy of 3 K and 2 K for V- and H-polarization, respectively [21]. The PLMR is a patch-array antenna capable of scanning the surface depending on pitch of the aircraft with three viewing angles ( $\pm 7^\circ$ ,  $\pm 21.5^\circ$  and  $\pm 38.5^\circ$ ) in forward and backward direction of the flight axis, when used in along-track configuration.

The NAFE'06 multi-angle flights were undertaken along a 75 km long transect line in the Yanco region of the Murrumbidgee River Catchment, with a triple repetition per flight and spatial resolution of about 500 m (Fig. 1). For comparison with SMOS characteristics, these pre-launch of SMOS flights were centered around both 6 A.M. and 6 P.M.

&gt; TGRS-2017-0031 &lt;

3

TABLE I  
DAILY VARIABLE L-MEB INPUT PARAMETERS FOR FARM Y7

Date [DD/MM/YYYY]	SM (std) [m <sup>3</sup> m <sup>-3</sup> ]	VWC [kg m <sup>-2</sup> ]	Tsurf [K]	Tdeep [K]
01/11/2006	0.02 (0.02)	0.03	293	297
03/11/2006	0.12 (0.02)	0.17	306	297
08/11/2006	0.05 (0.02)	0.03	292	296
10/11/2006	0.04 (0.02)	0.03	309	303
15/11/2006	0.13 (0.04)	0.17	288	295
17/11/2006	0.10 (0.03)	0.10	304	300

local solar time, coinciding with the ascending and descending SMOS overpasses. A total of six flight days with three morning and three afternoon flights were available for this study, which is the first to utilize this multi-angle aspect of the NAFE'06 data set [20].

The airborne observations were supported by ground measurements at three focus areas located along the flight transect. These so-called focus farms were of approximately 1 km × 3 km in size, and chosen to be co-located with the permanent OzNet monitoring stations [22]. The long-term OzNet stations mainly provide time-series of profile soil moisture, profile soil temperature and rainfall observations. Additionally, monitoring at the focus farms was supplemented with temporary NAFE stations, which provided profile soil moisture and soil temperature, as well as rainfall and thermal infrared data of either the soil surface in the case of bare soil or the canopy layer in the case of vegetation cover. Supplementary data were collected by assigned ground teams focusing on i) near-surface soil moisture measurements (SM) using the Hydraprobe Data Acquisition System (HDAS) [23], ii) biomass characterization including vegetation water content (VWC), surface reflectance and leaf area index (LAI), and iii) surface roughness measurements across each individual farm using a pin-profiler. The three focus farms that were covered by the transect flight included two dry land farms (Y7, Y10) with pasture as dominant land use and one irrigated farm (Y1) with different types of crops such as wheat, barley and maize. This study focused on data collected across farm Y7 (see Figure 1) which demonstrated a natural variability in soil moisture from 0.03-0.12 m<sup>3</sup>m<sup>-3</sup> in response to a few small rainfall events throughout the campaign. Biomass samples obtained across the dry land focus farms demonstrated rather low vegetation water content of ~ 0.08 kg m<sup>-2</sup>, whereas for vegetation samples obtained at the irrigated cropping site Y1 a range of 0.3-1.8 kg m<sup>-2</sup> in VWC was measured.

#### IV. MULTI-ANGLE SOIL MOISTURE RETRIEVAL

The multi-angle retrieval was performed using the L-MEB retrieval algorithm developed for processing SMOS data [24]. The parameterization of soil texture, soil profile temperature and bulk density was based on the available ground measurements taken at or nearby focus farm Y7 (Table 2). Supplementary information for the characterization of grass cover and surface roughness in the model was sourced from Saleh et al. [25] and Wigneron et al. [26]. Table 2 presents the main model parameterization applied to all observation days. The design of the focus farm and the spatial resolution of

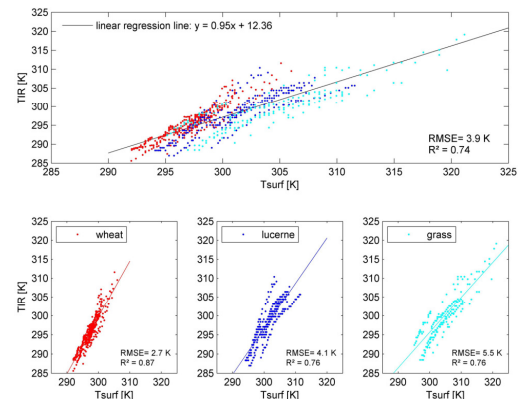


Fig. 2. Linear regression applied to ground measured thermal infrared (TIR) and surface soil temperature (Tsurf) from 1cm depth measurements considering three types of vegetation cover.

PLMR yielded a total of five independent PLMR pixels co-located at the farm with a size of approximately 500 m × 500 m each. Within each of these pixels, all angular brightness temperature measurements from the triple flight repetitions were gathered and applied to L-MEB so as to facilitate the multi-angle soil moisture retrieval per pixel. A total of four retrieval scenarios for each of the morning and afternoon data sets were studied including i) 1P single-parameter retrieval of soil moisture, ii) 2P retrieval of soil moisture and vegetation water content (SM-VWC), iii) 2P retrieval of soil moisture and surface roughness (SM-HR), and iv) 2P retrieval of soil moisture and vegetation temperature (SM-Tveg).

Regarding the afternoon retrieval two different approaches with respect to the vegetation temperature information, which is essential to run the L-MEB model, were tested. First, the vegetation temperature was set equal to the air temperature, as per the morning overpasses, where it is commonly assumed that the vegetation temperature is expected to be close to the air temperature at dawn. Second, the afternoon vegetation

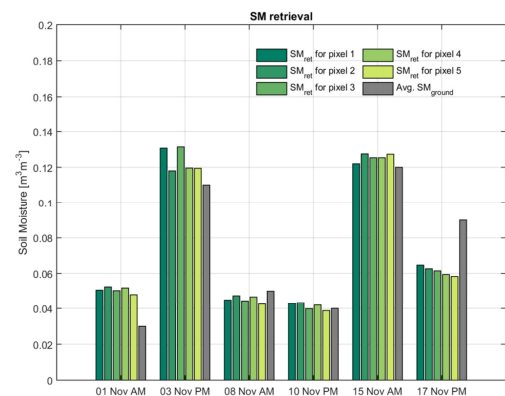


Fig. 3. Comparison of 1P retrieved soil moisture values (SMret) across the focus farm Y7 per PLMR pixel (green shades) with the farm-averaged ground measured HDAS (Avg. SMground in grey) observations per sampling day. AM: morning flight; PM: afternoon flight.

TABLE II  
FIXED L-MEB INPUT PARAMETERS FOR FARM Y7

Soil texture [%]		Bulk density [g m <sup>-3</sup> ]	Roughness [-]			Vegetation [-]			
Sand	Clay		HR	Q	NR(P)	b	ω(V)	ω(H)	tt(P)
39	25	1.3	0.5	0	0	0.15	0.05	0	1

temperature was estimated from a linear regression derived between surface soil temperature  $T_{surf}$  at 1 cm depth and thermal infrared temperature (TIR) measurements of the overlying canopy (see Fig. 2). The relationship was determined for specific types of vegetation as well as for a mixed vegetation cover. Note, only the duration of the afternoon overpass between 4:30-7:00 P.M. local solar time was considered when establishing the relationship. Both options, either using  $T_{air}$  or the TIR- $T_{surf}$  derived vegetation temperature, were tested as input to run the L-MEB model. Even though the difference between the observed temperature  $T_{air}$  and the TIR- $T_{surf}$  derived vegetation temperature for the afternoon overpass was up to 12 K for the different dates, the forward modelling yielded no significant improvement ( $< 0.03$  K) when the TB predictions were compared to the observed brightness temperature responses across the various dates and angular range measured. The authors would like to point out that the soil moisture and vegetation conditions captured during the field campaign showed limited range across the test dates, so the impact of higher moisture conditions with respect to the afternoon vegetation temperature and the subsequent effect on the soil moisture retrieval algorithm could not be fully tested with this dataset. The AACES field campaigns, which covered the whole Murrumbidgee catchment including the NAFE'06 test sites, will offer a wider range of soil moisture conditions for further analysis [27].

A. Spatial soil moisture pattern at farm scale

The single-parameter retrieval of soil moisture conditions for all five PLMR pixels at focus farm Y7 were compared against the ground measured near-surface soil moisture content in Figure 3. Across the five pixels, and hence within the entire focus farm, there were only minor variations in soil moisture observed per day with the standard deviation of HDAS measurements ranging between 0.02-0.04 m<sup>3</sup>m<sup>-3</sup>. Similar variations were achieved across the five PLMR pixels from L-MEB retrievals. Direct comparison with the averaged ground measured soil moisture per farm and observation day

TABLE III  
RMSE OF THE RETRIEVAL RESULTS FOR SOIL MOISTURE COMPARED TO MEASUREMENTS AT FARM Y7

Date [DD/MM/YYYY]	1P retrieval	2P retrieval		
	SM [m <sup>3</sup> m <sup>-3</sup> ]	SM-HR [m <sup>3</sup> m <sup>-3</sup> ]	SM-VWC [m <sup>3</sup> m <sup>-3</sup> ]	SM-Tveg [m <sup>3</sup> m <sup>-3</sup> ]
01/11/2006	0.02	0.04	0.02	0.02
03/11/2006	0.02	0.02	0.01	0.02
08/11/2006	0.01	0.01	0.00	0.00
10/11/2006	0.00	0.05	0.01	0.00
15/11/2006	0.01	0.06	0.00	0.00
17/11/2006	0.03	0.02	0.02	0.03
RMSE max	0.03	0.06	0.02	0.03
RMSE average	0.01	0.03	0.01	0.01

demonstrated a good agreement with the model predictions with RMSE values of  $\leq 0.03$  m<sup>3</sup>m<sup>-3</sup>. The model results captured the variabilities and the magnitude of soil moisture across the test dates caused by two precedent rain events, on the 2nd of November with 5mm rainfall and the 13th of November with 10.4 mm of rainfall.

By introducing a second unknown parameter and running a 2P retrieval model the modelled soil moisture yielded similar RMSE values of less than 0.03 m<sup>3</sup>m<sup>-3</sup> when soil moisture was derived simultaneously with either vegetation water content or vegetation temperature (Table 3). In case of the SM-HR retrieval scenario the corresponding RMSE was on average 0.03 m<sup>3</sup>m<sup>-3</sup> with a peak of 0.06 m<sup>3</sup>m<sup>-3</sup> for one test date.

B. Comparison of acquisition time

In order to study the effect of acquisition time on the soil moisture retrieval performance using brightness temperature data acquired at various incidence angles, the model results for all retrieval scenarios (single- and multi-parameter retrievals) were classified into morning and afternoon. Consequently, the model retrieved soil moisture values were compared against the ground measured near-surface soil moisture conditions across the field campaign and quantified in terms of the root mean square error (see Fig. 4).

Across the range of moisture conditions captured during the NAFE'06 campaign, only minor variations were observed between the model predictions and the in-situ measurements. In general, the difference was between 0.01-0.04 m<sup>3</sup>m<sup>-3</sup> for morning overpasses and 0.02-0.03 m<sup>3</sup>m<sup>-3</sup> for evening overpasses – all results being well within the desired SMOS target accuracy. Comparison of the three morning and three afternoon flights did not exhibit any significant difference or preference in acquisition time for soil moisture retrieval modelling. Thus, providing rather low soil moisture conditions, no degradation of soil moisture quality is expected

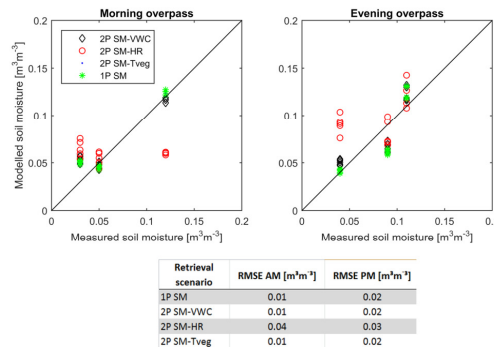


Fig. 4. Comparison of retrieved soil moisture values across the focus farm Y7 per PLMR pixel with the ground measured HDAS information classified into morning (6 A.M.) and afternoon (6 P.M.) observations.

&gt; TGRS-2017-0031 &lt;

5

when using the descending overpass L-band data from SMOS. Moreover, there may even be an improved accuracy in places like Europe where descending SMOS data is less affected by RFI than ascending data [8, 9].

#### V. POLARIZATION INDEX ANALYSIS

Further analysis of the NAFE'06 data set focussed on calculation of the polarization ratio PR (difference between the horizontal and the vertical brightness observations divided by the sum). The index is a normalized quantity which describes the decreasing deviation from horizontal and vertical emissivity correspondingly to the increase of LAI. Since the contribution of the vegetation layer to the emission is unpolarised and tends to be rather independent of the polarization, the PR is often used to gather information on the vegetation canopy, its density and evolution. Moreover, the index demonstrates a strong dependence on soil moisture content and varies from approximately 0.04-0.22 within the range of soil moisture encountered.

The NAFE'06 brightness temperature data were classified in five assigned angular groups and the individual polarization ratio per incidence angle determined for each sampling day (Fig. 5). Generally there was a higher polarization ratio for incidence angles  $>30^\circ$  than for the smaller incidence angles, resulting in two groups of polarization ratios for all six sampling days tested. As described in [28] for view angles  $>30^\circ$  there is a distinct difference in PR for bare soils due to TBH being significantly larger than TBV. With increasing vegetation presence the signal becomes progressively depolarized, ultimately resulting in  $TBH \approx TBV$  for dense vegetation. Consequently, with regard to the previous analysis of the air temperature  $T_{air}$  versus the TIR-Tsurf derived vegetation temperature as a proxy for model parameterization in terms of the canopy and surface temperature in the afternoon, the demonstrated PR behaviour supports the earlier findings. The noticeable contrast between the low and high angular groups and the related PR implies a rather sparse vegetation cover which in turn allows a strong emission from the soil without major scattering effects due to overlying vegetation. Thus the usage of the TIR-Tsurf derived vegetation temperature might not be able to demonstrate its full potential for the given surface conditions.

Visual inspection of all polarization ratios against the observed soil moisture certainly presented a trend with respect to the moisture conditions across all angular groups tested. There was an overall increase in the polarization ratio with an increase in soil moisture, as expected due to the higher polarization impacts on the soil emission with higher water content. Moreover, the slope varied across the groups, being higher for the large angular observations compared to the small angular measurements.

#### VI. CONCLUSION

This paper studied the soil moisture retrieval performance from airborne L-band observations in Australia for different times of data acquisition. The multi-angle radiometer data

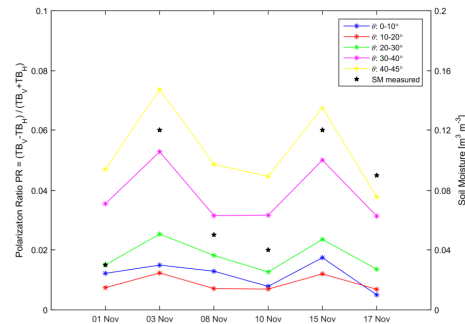


Fig. 5. Comparison of polarization ratios between the vertical and horizontal brightness temperature observations measured during the course of the NAFE'06 field campaign. Overlain is the HDAS soil moisture information averaged from all samples taken across focus farm Y7.

were available for three morning flights around 6 A.M. local solar time and three afternoon flights around 6 P.M. local solar time, closely matching the ascending and descending overpass times of SMOS. For soil moisture retrieval over this pastured study site, the L-MEB model was parameterized using ground measurements in combination with empirical variables sourced from literature. Results showed providing a sparse dryland vegetation cover and rather low soil moisture conditions for afternoon retrievals, the canopy and surface soil temperature information might be used as for early morning measurements, by assuming air temperature values for both. It was not possible to check the effect of higher soil moisture and dense vegetation presence on this assumption.

The comparison of the soil moisture retrieval performance under morning and afternoon acquisition times yielded similar results, with all being less than or equal to the SMOS target accuracy of  $0.04 \text{ m}^3\text{m}^{-3}$  for the SMOS L2 soil moisture product. These findings were consistent throughout the numerous retrieval scenarios that were tested in this study, including single- as well as multi-parameter retrievals.

#### REFERENCES

- [1] T. J. Jackson, "III. Measuring surface soil moisture using passive microwave remote sensing," *Hydrol. Processes*, vol. 7, pp. 139-152, 1993.
- [2] E. G. Njoku and D. Entekhabi, "Passive microwave remote sensing of soil moisture," *J. Hydrol.*, vol. 184, pp. 101-129, Oct 1996.
- [3] J. P. Walker and P. R. Houser, "Requirements of a global near-surface soil moisture satellite mission: accuracy, repeat time, and spatial resolution," *Adv. Water Resour.*, vol. 27, pp. 785-801, Jul 2004.
- [4] T. J. Schmugge, P. O'Neill, and J. R. Wang, "Passive microwave soil moisture research," *IEEE Trans. Geosc. Remote Sens.*, vol. GE-24, pp. 12-22, 1986.
- [5] Y. H. Kerr, P. Waldteufel, J.-P. Wigneron, S. Delwart, F. Cabot, J. Boutin, M.-J. Escorihuela, J. Font, N. Reul, C. Gruhier, S. E. Juglea, M. R. Drinkwater, A. Hahne, M. Martin-Neira, and S. Mecklenburg, "The SMOS Mission: New Tool for Monitoring Key Elements of the Global Water Cycle," *Proc. IEEE*, vol. 98, pp. 666-687, 2010.
- [6] Y. H. Kerr, P. Waldteufel, J.-P. Wigneron, J. M. Martinuzzi, J. Font, and M. Berger, "Soil moisture retrieval from space: The Soil Moisture and Ocean Salinity (SMOS) mission," *IEEE Trans. Geosc. Remote Sens.*, vol. 39, pp. 1729-1735, Aug 2001.
- [7] Y. H. Kerr, P. Waldteufel, P. Richaume, J.-P. Wigneron, P. Ferrazzoli, and R. J. Gurney, "SMOS level 2 processor for soil moisture - Algorithm Theoretical Based Document (ATBD)," CESBIO, Toulouse, France, Report ESA No.: SO-TN-ESL-SM-GS-0001, 24.01.2011 2011.

- [8] S. H. Yueh, "Estimates of Faraday rotation with passive microwave polarimetry for microwave remote sensing of Earth surfaces," *IEEE Trans. Geosc. Remote Sens.*, vol. 38, pp. 2434-2438, 2000.
- [9] R. ITU-R, "P. 531-6: Ionospheric propagation data and prediction methods required for the design of satellite services and systems," ed: Geneva, 2001.
- [10] A. J. Camps, J. Gourrion, J. M. Tarongi, A. Gutierrez, J. Barbosa, and R. Castro, "RFI analysis in SMOS imagery," in *IEEE International Geoscience and Remote Sensing Symposium (IGARSS)*, Honolulu, Hawaii, USA, 2010, pp. 2007-2010.
- [11] R. Oliva, E. Daganzo-Eusebio, Y. H. Kerr, S. Mecklenburg, S. Nieto, P. Richaume, and C. Gruhier, "SMOS radio frequency interference scenario: status and actions taken to improve the RFI environment in the 1400-1427-MHz passive band," *IEEE Trans. Geosc. Remote Sens.*, vol. 50, pp. 1427-1439, May 2012.
- [12] A. Al-Yaari, J.-P. Wigneron, A. Ducharme, Y. Kerr, P. De Rosnay, R. De Jeu, A. Govind, A. Al Bitar, C. Albergel, and J. Munoz-Sabater, "Global-scale evaluation of two satellite-based passive microwave soil moisture datasets (SMOS and AMSR-E) with respect to Land Data Assimilation System estimates," *Remote Sens. Environ.*, vol. 149, pp. 181-195, 2014.
- [13] F. Lei, W. T. Crow, H. Shen, R. M. Parinussa, and T. R. Holmes, "The impact of local acquisition time on the accuracy of microwave surface soil moisture retrievals over the contiguous United States," *Remote Sensing*, vol. 7, pp. 13448-13465, 2015.
- [14] J.-P. Wigneron, Y. H. Kerr, P. Waldteufel, K. Saleh, M. J. Escorihuela, P. Richaume, P. Ferrazzoli, P. de Rosnay, R. J. Gurney, J.-C. Calvet, J. P. Grant, M. Guglielmetti, B. Hornbuckle, C. Mätzler, T. Pellarin, and M. Schwank, "L-band Microwave Emission of the Biosphere (L-MEB) Model: Description and calibration against experimental data sets over crop fields," *Remote Sens. Environ.*, vol. 107, pp. 639-655, Apr 2007.
- [15] Y. H. Kerr and E. G. Njoku, "A semiempirical model for interpreting microwave emission from semiarid land surfaces as seen from space," *IEEE Trans. Geosc. Remote Sens.*, vol. 28, pp. 384-393, 1990.
- [16] T. Mo, B. J. Choudhury, T. J. Schmugge, J. R. Wang, and T. Jackson, "A model for microwave emission from vegetation-covered fields," *J. Geophys. Res.*, vol. 87, pp. 11,229-11,237, Dec 1982.
- [17] M. Dobson, F. Ulaby, M. Hallikainen, and M. El-royes, "Microwave Dielectric Behavior of Wet Soil-Part II: Dielectric Mixing Models," *IEEE Trans. Geosc. Remote Sens.*, vol. GE-23, pp. 35-46, Jan 1985.
- [18] V. L. Mironov, M. C. Dobson, V. H. Kaupp, S. A. Komarov, and V. N. Kleshchenko, "Generalized refractive mixing dielectric model for moist soils," *IEEE Trans. Geosc. Remote Sens.*, vol. 42, pp. 773-785, 2004.
- [19] T. J. Jackson and T. J. Schmugge, "Vegetation effects on the microwave emission of soils," *Remote Sens. Environ.*, vol. 36, pp. 203-212, 1991.
- [20] O. Merlin, J. P. Walker, J. D. Kalma, E. J. Kim, J. Hacker, R. Panciera, R. Young, G. Summerell, J. Hornbuckle, M. Hafeez, and T. Jackson, "The NAFE'06 data set: Towards soil moisture retrieval at intermediate resolution," *Adv. Water Resour.*, vol. 31, pp. 1444-1455, 2008.
- [21] R. Panciera, J. P. Walker, J. D. Kalma, E. J. Kim, J. Hacker, O. Merlin, M. Berger, and N. Skou, "The NAFE'05/CoSMOS Data Set: Toward SMOS Soil Moisture Retrieval, Downscaling, and Assimilation," *IEEE Trans. Geosc. Remote Sens.*, vol. 46, pp. 736-745, Mar 2008.
- [22] A. B. Smith, J. P. Walker, A. W. Western, R. I. Young, K. M. Ellett, R. C. Pipunic, R. B. Grayson, L. Sriwardena, F. H. S. Chiew, and H. Richter, "The Murrumbidgee soil moisture monitoring network data set," *Water Resour. Res.*, vol. 48, pp. n/a-n/a, Jul 2012.
- [23] R. Panciera, M. Allahmoradi, O. Merlin, R. Young, and J. P. Walker, "The Hydraprobe Data Acquisition System (HDAS) V.5: User Guide," University of Melbourne, Melbourne, Australia November 2009 2009.
- [24] Y. H. Kerr, P. Waldteufel, P. Richaume, J. P. Wigneron, P. Ferrazzoli, A. Mahmoodi, A. Al Bitar, F. Cabot, C. Gruhier, S. E. Juglea, D. Leroux, A. Mialon, and S. Delwart, "The SMOS Soil Moisture Retrieval Algorithm," *IEEE Trans. Geosc. Remote Sens.*, vol. 50, pp. 1384-1403, May 2012.
- [25] K. Saleh, Y. H. Kerr, G. Boulet, P. Maisongrande, P. de Rosnay, D. Floricioiu, M. J. Escorihuela, J.-P. Wigneron, A. Cano, E. Lopez-Baeza, J. P. Grant, J. E. Balling, N. Skou, M. Berger, S. Delwart, P. Wursteisen, R. Panciera, and J. P. Walker, "The CoSMOS L-band experiment in Southeast Australia," in *IEEE International Geoscience and Remote Sensing Symposium (IGARSS)* Barcelona, Spain, 2007, pp. 3948-3951.
- [26] J.-P. Wigneron, M. Pardé, P. Waldteufel, A. Chanzy, Y. H. Kerr, S. Schmidl, and N. Skou, "Characterizing the dependence of vegetation

model parameters on crop structure, incidence angle, and polarization at L-band," *IEEE Trans. Geosc. Remote Sens.*, vol. 42, pp. 416-425, 2004.

- [27] S. Peischl, J. P. Walker, C. Rüdiger, N. Ye, Y. H. Kerr, E. J. Kim, R. Bandara, and M. Allahmoradi, "The AACES field experiments: SMOS calibration and validation across the Murrumbidgee River catchment," *Hydrol. Earth Syst. Sci.*, vol. 16, pp. 1697-1708, Jun 2012.
- [28] J.-P. Wigneron, J.-C. Calvet, T. Pellarin, A. A. Van de Griend, M. Berger, and P. Ferrazzoli, "Retrieving near-surface soil moisture from microwave radiometric observations: current status and future plans," *Remote Sens. Environ.*, vol. 85, pp. 489-506, 2003.



**Sandy Peischl** (M'10) received the M.S. degree in geocology from the Technische Universität Bergakademie Freiberg, Freiberg, Germany, in 2007. She is currently working toward the Ph.D. degree in the Department of Civil Engineering, Faculty of Engineering, Monash University, Melbourne, Australia. Her research focuses on the retrieval of soil moisture using multi-incidence-angle L-band data acquired from airborne observations as well as from Soil Moisture and Ocean Salinity (SMOS).



**Jeffrey P. Walker** received the B.E. degree (with Honours 1 and University Medal) in civil engineering and the B. Surveying degree (with Honours 1 and University Medal) in 1995 and the Ph.D. degree in water resources engineering in 1999 from The University of Newcastle, Newcastle, Australia. His Ph.D. thesis was among the early pioneering research on estimation of root-zone soil moisture from remotely sensed surface soil moisture observations. Since 2010, he has been a Professor with the Department of Civil Engineering, Faculty of Engineering, Monash University, Melbourne. He is contributing to soil moisture satellite missions at both NASA and the European Space Agency, as a Science Definition Team Member for the Soil Moisture Active Passive mission and a Calibration/Validation Team Member for the Soil Moisture and Ocean Salinity mission, respectively.



**Dongryeol Ryu** (M'05) received the B.S. and M.S. degrees in geology from Seoul National University, Seoul, Korea, in 1997 and 2000, respectively, and the Ph.D. degree in earth system science from the University of California, Irvine, in 2006. He is currently a Senior Lecturer with the Department of Infrastructure Engineering, Melbourne School of Engineering, The University of Melbourne, Melbourne, Australia. His specialization is hydrology with particular emphases on remote sensing of land surface variables such as soil moisture and vegetation characteristics, their spatial and temporal variability, and hydrologic application of the remotely sensed land surface properties.



**Yann H. Kerr** (M'88-SM'01) received the B.E. degree from the Ecole Nationale Supérieure de l'Aéronautique et de l'Espace, Toulouse, France, the M.Sc. degree in electronics and electrical engineering from Glasgow University, Glasgow, U.K., and the Ph.D. degree from Université Paul Sabatier, Toulouse. From 1980 to 1985, he was with Centre National d'Etudes Spatiales (CNES). In 1985, he joined the Laboratoire d'Etudes et de Recherches en Télé-détection Spatiale, for which he was the Director from 1993-1994. From 1987-1988, for 19 months, he was with the Jet Propulsion Laboratory, Pasadena, CA. Since 1995, he has been with Centre d'Etudes Spatiales de la Biosphère, Toulouse, where he was the Deputy Director and has been the Director since 2007. In 1989, he started to work on the interferometric concept applied to passive microwave Earth observation and was subsequently the Science Lead on the MIRAS project for the European Space Agency (ESA) with Maritime Management System and Operations Management Plan. In 1997, he first proposed the natural outcome of the previous MIRAS work with what was to become the Soil Moisture and Ocean Salinity (SMOS) mission to CNES, a proposal which was selected by ESA in 1999 with him as the Lead Investigator of the SMOS mission and the Chair of the Science Advisory Group. He is also in charge of the SMOS science activity coordination in France. He is currently involved in the exploitation of SMOS data, in the calibration/validation activities, and in related level 2 soil moisture and level 3 and 4 development. He is also working on the SMOS next concept.

### 5.3 Summary

---

Considering the polar sun-synchronous orbit of SMOS with a 6 A.M. local solar time ascending node and 6 P.M. descending node, the potential of the different acquisition time for the soil moisture retrieval was studied. Airborne multi-angle radiometer data were available for three morning and three afternoon flights over a pasture test site. Model parameterization results showed that under the tested vegetation and soil moisture conditions the canopy and surface soil temperature information might be used in the afternoon as for morning measurements, by assuming air temperature values for both. Consequently, the comparison of the soil moisture retrieval performance under morning and afternoon acquisition times yielded similar results, with all being less than or equal to the SMOS target accuracy of  $0.04 \text{ m}^3/\text{m}^3$  for the SMOS L2 soil moisture product. Numerous retrieval scenarios including single- as well as multi-parameter retrievals were tested in this study, with consistent results across all scenarios. No preference for any of the acquisition times was proven.



## **Part III**

# **Analysis on spaceborne multi-incidence angle L-band data**

---

# 6

## Australian Airborne Cal/val Experiments for SMOS (AACES) [Paper 4]

**T**HIS chapter includes a research paper which has resulted from the studies undertaken for this degree and is published in a peer-reviewed journal. The inclusion of co-authors reflects the fact that the work came from active collaboration between researchers from Australia, France and the USA, and acknowledges input into team-based research.

**Peischl, S.**, Walker, J. P., Rüdiger, C., Ye, N., Kerr, Y. H., Kim, E., Bandara, R., and Allahmoradi, M.: The AACES field experiments: SMOS calibration and validation across the Murrumbidgee River catchment, *Hydrology and Earth System Sciences*, 16, 1697-1708, doi:10.5194/hess-16-1697-2012, 2012.

**Declaration for Thesis Chapter 6**

In the case of Chapter 6, the nature and extent of my contribution to the work was the following:

Nature of contribution	Extent of contribution (%)
Experimental design, data collection, data processing and interpretation, and write up.	60 %

The following co-authors contributed to the work. Co-authors who are students at Monash University must also indicate the extent of their contribution in percentage terms:

Name	Nature of contribution	Extent of contribution (%) for student co-authors only
Prof Jeffrey Walker	Ideas, interpretation and reviewing	n/a
Dr Christoph Rüdiger	Ideas and reviewing	n/a
Nan Ye	Data processing	10
Dr Yann Kerr	Ideas and reviewing	n/a
Dr Ed Kim	Ideas and reviewing	n/a
Ranmalee Bandara	Data processing	5
Mahdi Allamoradhi	Data processing	n/a

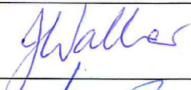
Candidate's Signature Sandy Peironi Date 27/06/12

**Declaration by co-authors**

The undersigned hereby certify that:

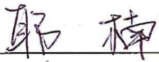
- (1) the above declaration correctly reflects the nature and extent of the candidate's contribution to this work, and the nature of the contribution of each of the co-authors.
- (2) they meet the criteria for authorship in that they have participated in the conception, execution, or interpretation, of at least that part of the publication in their field of expertise;
- (3) they take public responsibility for their part of the publication, except for the responsible author who accepts overall responsibility for the publication;
- (4) there are no other authors of the publication according to these criteria;
- (5) potential conflicts of interest have been disclosed to (a) granting bodies, (b) the editor or publisher of journals or other publications, and (c) the head of the responsible academic unit; and
- (6) the original data are stored at the following location(s) and will be held for at least five years from the date indicated below:

Location Department of Civil Engineering, Monash University, Australia

Signature 1 Prof Jeffrey Walker  Date 4/7/12

Signature 2 Dr Christoph Rüdiger  Date 27/6/2012

---

Signature 3	Nan Ye 	Date 20/07/2012
Signature 4	Dr Yann Kerr 	1/12/2016
Signature 5	Dr Edward Kim 	18/07/2012
Signature 6	Ranmalee Bandara 	20/07/2012
Signature 7	Mahdi Allamoradhi 	19/07/2012

---

## 6.1 Introduction

---

The validation approach chosen for SMOS land products relies on extensive usage of ground and aircraft data, that are intended to capture a broad range of topography, climate, land cover and vegetation types. Consequently, several locations distributed across the world have been selected as test sites (Delwart et al., 2008; Mecklenburg et al., 2009). In Australia the Murrumbidgee River catchment was chosen as focus area for two extensive field campaigns in order to provide validation data sets for SMOS.

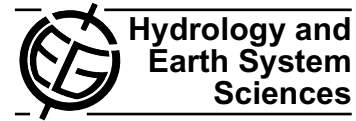
This paper describes the general objectives of the Australian Airborne Cal/val Experiment for SMOS (AACES), and the airborne and ground data collected across the Murrumbidgee River catchment during both AACES-1 and AACES-2 campaigns. A brief overview of the study area, the reasoning of the experimental strategy and a summary of the data sets is presented.

## 6.2 The AACES field experiments: SMOS calibration and validation across the Murrumbidgee River catchment

---

Hydrol. Earth Syst. Sci., 16, 1697–1708, 2012  
 www.hydrol-earth-syst-sci.net/16/1697/2012/  
 doi:10.5194/hess-16-1697-2012

© Author(s) 2012. CC Attribution 3.0 License.



## The AACES field experiments: SMOS calibration and validation across the Murrumbidgee River catchment

S. Peischl<sup>1,\*</sup>, J. P. Walker<sup>1,\*</sup>, C. Rüdiger<sup>1,\*</sup>, N. Ye<sup>1,\*</sup>, Y. H. Kerr<sup>2</sup>, E. Kim<sup>3</sup>, R. Bandara<sup>1,\*</sup>, and M. Allahmoradi<sup>4</sup>

<sup>1</sup>Monash University, Department of Civil Engineering, Melbourne, Australia

<sup>2</sup>Centre d'Etudes Spatiales de la Biosphère (CESBIO), Toulouse, France

<sup>3</sup>Goddard Space Flight Center, NASA, Hydrospheric and Biospheric Sciences Laboratory, Greenbelt, USA

<sup>4</sup>The University of Melbourne, Department of Infrastructure Engineering, Melbourne, Australia

\*formerly at: The University of Melbourne, Department of Infrastructure Engineering, Melbourne, Australia

Correspondence to: S. Peischl (sandy.peischl@monash.edu)

Received: 17 February 2012 – Published in Hydrol. Earth Syst. Sci. Discuss.: 2 March 2012

Revised: 18 May 2012 – Accepted: 23 May 2012 – Published: 22 June 2012

**Abstract.** Following the launch of the European Space Agency's Soil Moisture and Ocean Salinity (SMOS) mission on 2 November 2009, SMOS soil moisture products need to be rigorously validated at the satellite's approximately 45 km scale and disaggregation techniques for producing maps with finer resolutions tested. The Australian Airborne Cal/val Experiments for SMOS (AACES) provide the basis for one of the most comprehensive assessments of SMOS data worldwide by covering a range of topographic, climatic and land surface variability within an approximately  $500 \times 100 \text{ km}^2$  study area, located in South-East Australia. The AACES calibration and validation activities consisted of two extensive field experiments which were undertaken across the Murrumbidgee River catchment during the Australian summer and winter season of 2010, respectively. The datasets include airborne L-band brightness temperature, thermal infrared and multi-spectral observations at 1 km resolution, as well as extensive ground measurements of near-surface soil moisture and ancillary data, such as soil temperature, soil texture, surface roughness, vegetation water content, dew amount, leaf area index and spectral characteristics of the vegetation. This paper explains the design and data collection strategy of the airborne and ground component of the two AACES campaigns and presents a preliminary analysis of the field measurements including the application and performance of the SMOS core retrieval model on the diverse land surface conditions captured by the experiments. The data described in this paper are publicly available from the website: <http://www.moisturemap.monash.edu.au/aaces>.

### 1 Introduction

In May 1999, the Soil Moisture and Ocean Salinity (SMOS) concept was selected as the second Earth Explorer Opportunity mission by the European Space Agency (ESA), with SMOS aiming at dedicated space borne observations of two crucial environmental variables: soil moisture and sea surface salinity (Kerr et al., 2001). Ten years later on 2 November 2009, the SMOS satellite was launched successfully into a heliosynchronous orbit (758 km altitude) with a mean local solar time overpass of 06:00 a.m. at the ascending node (Barré et al., 2008). The single SMOS payload is the Microwave Imaging Radiometer with Aperture Synthesis (MIRAS) operating in the protected L-band at 1.400–1.427 GHz. The SMOS mission targets for soil moisture observations are (i) a product accuracy of  $0.04 \text{ m}^3 \text{ m}^{-3}$  or better over bare soil and low vegetated areas, defined as biomass having an integrated vegetation water content of less than  $5 \text{ kg m}^{-2}$ , (ii) a revisit time of at least every three days at approximately 06:00 a.m. LST (local solar time), and (iii) a spatial resolution of preferably less than 45 km, with the latter being addressed by simulating a large antenna size using interferometric aperture synthesis (Kerr et al., 2010).

This innovative two-dimensional Y-shaped radiometer and the novel interferometric antenna concept represent a new generation technology, which requires comprehensive testing for both the SMOS brightness temperature measurements and the retrieved soil moisture products. The validation approach chosen for the land component of SMOS relies on

Published by Copernicus Publications on behalf of the European Geosciences Union.

the extensive usage of ground and aircraft data, that preferably capture a broad range of topography, climate, land cover and vegetation types. Consequently, numerous locations distributed across the world have been selected for that purpose: for instance the Antarctic plateau DOME C, the French Mauzac site near Toulouse, and ESA's two core validation sites: (i) the Valencia Anchor Station located in the East of Spain and (ii) the Upper Danube Catchment in Southern Germany (Delwart et al., 2008; Mecklenburg et al., 2009). Moreover, permanent soil moisture measurements obtained from long-term monitoring stations provide an additional basis for world-wide validation activities. The International Soil Moisture Network (ISMN) has been established to serve as a platform making station data available (Dorigo et al., 2011). Given the large 45 km SMOS footprint and the inherent heterogeneity in topography and land cover, a representative in situ sampling strategy needs to be considered for a sophisticated analysis of the SMOS models and products.

The focus of the European experimental sites is limited to a single SMOS pixel and/or a single airborne transect through several SMOS pixels, with repeat flights over a given time period: e.g., SMOSREX (de Rosnay et al., 2006), MEL-BEX (Cano et al., 2008, 2010), and EuroSTARRS (Saleh et al., 2004). In contrast, the field campaigns described in this paper, named Australian Airborne Cal/val Experiments for SMOS (AACES), were designed to provide an extensive validation dataset by completely covering a minimum of 20 independent ( $\approx 40$  overlapping) SMOS pixels, which correspond to a study area of approximately 50 000 km<sup>2</sup> (Fig. 1). The range of topographic, climatic and land cover conditions captured within the AACES study area is not only typical of Australia, but also across the world, thus, making it an excellent validation site for the soil moisture component of the SMOS satellite mission. Moreover, the existing long-term soil moisture network together with the variability in natural features across the study area means this experimental site has also been the focus of several other extensive campaigns: (i) the National Airborne Field Experiment (NAFE) in 2006, that monitored and sampled a single SMOS pixel over three weeks (Merlin et al., 2008) and (ii) the Soil Moisture Active and Passive Experiments (SMAPex) (Panciera et al., 2012), conducted in support of the planned Soil Moisture Active-Passive (SMAP) mission led by the National Aeronautics and Space Administration (NASA), that will combine an active and passive microwave system to provide a 10 km soil moisture product.

The AACES experiment comprises a set of two separate field campaigns which each combined extensive airborne and ground based data collection across the Murrumbidgee River catchment in 2010. While AACES-1 took place from 18 January to 21 February 2010 (5 weeks), capturing the Australian summer conditions, AACES-2 was performed during the Australian winter from 8–26 September 2010 (3 weeks). This paper describes the general objectives of the AACES field experiments, along with the airborne and ground data

collected during both AACES-1 and AACES-2 campaigns. A brief overview of the study area, the reasoning of the experimental strategy and a summary together with a preliminary analysis of the datasets are presented. The detailed sampling protocols for all airborne and ground activities are given in the respective field experiment plan of each AACES campaign (see Walker et al., 2010a,b).

## 2 Study area description

The AACES field experiments were undertaken across an approximate 500 × 100 km<sup>2</sup> study area within the Murrumbidgee River catchment ( $-33^\circ$  to  $-37^\circ$  S and  $143^\circ$  to  $150^\circ$  E), which forms the southern part of the Murray Darling Basin in south-eastern Australia (Fig. 1). The Murrumbidgee River catchment comprises of about 82 000 km<sup>2</sup>, ranging from elevations as low as 50 m in the West to around 2000 m in the East (Geoscience Australia, 2008), as presented in Fig. 2. Together with the broad variation in topography, the climate conditions change from semi-arid climate in the flat, clay-loam dominated western plains, to alpine conditions in the mountainous areas with coarse-textured sandy soils (McKenzie et al., 2000). The average annual rainfall varies from 300 mm in the West to 1900 mm in the high elevated ranges (Australian Bureau of Rural Science, 2001). However, in the eastern alpine region only half of the precipitated water is evapotranspired, whereas in the dry flat western areas of the catchment the actual evaporation rate is similar to the total amount of rain received. During the Southern Hemisphere winter season the eastern areas with elevations above 1200 m typically experience precipitation in the form of snow, with a temporary snow cover of up to a few weeks for regions above 1400 m. Areas above 1800 m are usually covered by snow for four months or more (Whetton et al., 1996). Due to the natural conditions, land use in the Murrumbidgee River catchment is primarily characterised by agriculture and livestock farming (Fig. 2). Extensive grazing areas dominate the wide western plains, whereas broad-acre cropping and agriculture with irrigation districts is more common in the central region. The (very) eastern regions mainly consist of conservation areas and state forests (Australian Bureau of Rural Science, 2006). Note that while there was no snow cover in the study area during AACES-1 and AACES-2, there was snow in the alpine region. Consequently, an additional flight was undertaken during AACES-2 coincident with ground sampling activities, to provide an opportunity to also assess the impact of snow on SMOS.

## 3 Airborne data description

The AACES-1 summer campaign in January 2010 focused on the entire 50 000 km<sup>2</sup> transect outlined in Fig. 1. The subsequent AACES-2 winter campaign in September 2010 was reduced in terms of spatial coverage and ground sampling

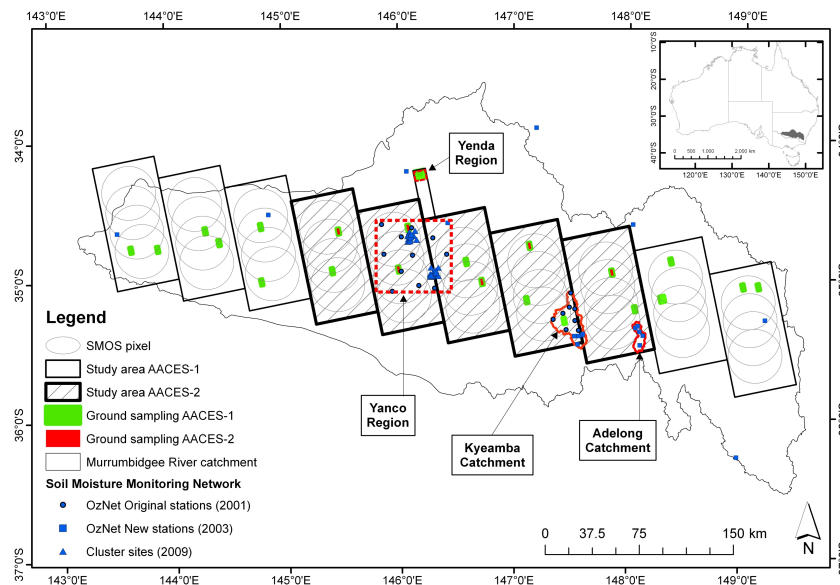


**Fig. 1.** Overview of the Murrumbidgee River catchment in Australia (inset), with AACES-1 covering all ten flight patches and AACES-2 focusing on the central half of the study area. SMOS footprints within each flight patch and the location of ground sampling activities as well as the existing long-term soil moisture network sites (OzNet) are indicated on the map.

activities representing a subset of the original transect that covered the central half (approximately  $250 \times 100 \text{ km}^2$ ). Data from the AACES-1 campaign had shown that this area was scientifically the most interesting, having a representative range of soil and vegetation conditions for the entire catchment. The airborne data acquisition started in the West of the Murrumbidgee River catchment and moved towards the East during each campaign. The AACES study area had been divided into ten flight patches of  $50 \times 100 \text{ km}^2$ , each corresponding to a single flight day and aligned with the SMOS level 1C fixed ISEA (Icosahedral Snyder Equal Area projection) grid. Consequently, each patch contained a minimum of two independent (four overlapping) SMOS pixels of approximately 45 km size in their entirety.

The airborne measurements were conducted using a single-engine fixed-wing aircraft, which can carry a typical science payload of up to 250 kg in addition to a scientist and pilot. The typical cruising speed is about  $150\text{--}270 \text{ km h}^{-1}$  with a range of 9 h reserve (5 h for maximum payload). The aircraft ceiling is 3000 m or up to 6000 m with oxygen supply. The scientific equipment carried during experiments is installed in an underbelly pod and in the wingtips. The aircraft navigation and flight lines for the experiments, as well as instrument statuses are displayed via a computer screen in front of the scientist/co-pilot.

### 3.1 Airborne instrumentation

The airborne instruments operated in both AACES campaigns were the Polarimetric L-band Multi-beam Radiometer (PLMR), six thermal infrared sensors, and two sets of six multi-spectral sensors with four bands in the visible/near-infrared and four bands in the shortwave infrared wavelength region (Table 1). The PLMR instrument consists of a flat-array antenna resulting in six beams which allow the land surface to be observed at three incidence angles ( $\pm 7^\circ$ ,  $\pm 21.5^\circ$ , and  $\pm 38.5^\circ$ ). During each campaign the radiometer was mounted in the across-track or push-broom configuration, thus, scanning the earth surface at three angles to each side of the aircraft. The resulting 3 dB beam width of each beam corresponds to about  $14^\circ$ , producing a 6 km wide swath from a 3000 m a.g.l. flying height. The L-band radiometer operates at a frequency of 1.413 GHz with a bandwidth of 24 MHz and achieves a 40 m along-track ground sampling rate at approximately  $72 \text{ m s}^{-1}$  flight speed. Using a polarization switch, the PLMR is capable of dual-polarized measurements with an accuracy of higher than 2 K and 3 K for H- and V-polarization, respectively (Panciera et al., 2008). Moreover, the radiometer was removed from the aircraft and calibrated on a daily basis before and after each flight, using the sky as cold target and a blackbody box as warm target. The collected PLMR data were geolocated, with the local

1700

S. Peischl et al.: The AACES field experiments

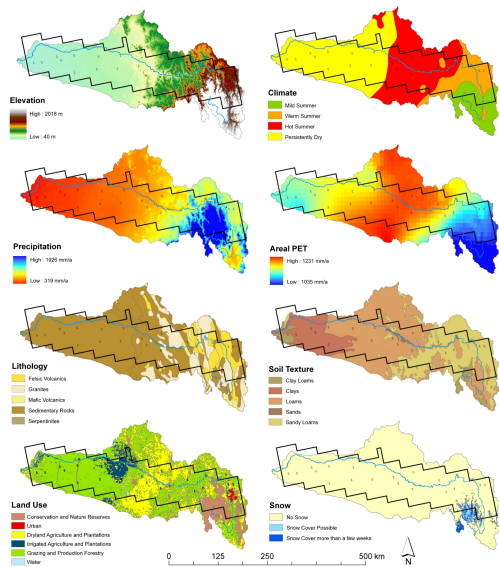


**Fig. 2.** Overview of the Murrumbidgee River catchment and its climatic, topographic and soil diversity. Overlain is the outline of the AACES study area with the course of the Murrumbidgee River and the location of the 20 focus farms, where the ground sampling activities took place. The spatial dataset is publicly available through Australian Bureau of Rural Science (2001, 2006) and Geoscience Australia (2008).

incidence angles and beam location calculated, taking into account ground topography, aircraft position and attitude information, which was all provided with each set of observations. The thermal infrared and multi-spectral sensors with a  $15^\circ$  field of view were aligned with the PLMR beams, in order to have the same incidence angles and footprint sizes as the microwave radiometer.

### 3.2 SMOS validation flights

The airborne observations were classified into two flight types: (i) patch flights (P) with each patch being mapped on a single day when full SMOS coverage was ensured for the specific patch, and (ii) transect flights (T) across the study area when the AACES study site was covered by SMOS in its entirety (Fig. 3). While the patch flights were only done once per patch and campaign, transect flights were flown several times during each campaign. The reasoning for this schedule was that the patch flights allowed the mapping of the whole AACES study area and hence the spatial variability in soil moisture across it, whereas the transect flights captured the temporal variation of the surface conditions throughout each field experiment.

**Table 1.** Multispectral and thermal infrared instrument characteristics.

Sensor	MODIS band	Wavelength [nm]
VIS/NIR (SKR 1850A)		
Channel 1	1	620–670
Channel 2	2	841–876
Channel 3	3	459–479
Channel 4	4	545–565
SWIR (SKR 1870A)		
Channel 1	6	1628–1652
Channel 2	–	2026–2036
Channel 3	7	2105–2155
Channel 4	–	2206–2216
Everest InterScience 3800ZL		8000–14000

The aircraft was based at a centrally located airport with the average flight time for a sampling day including the ferry and calibration flight segments being about 7 h. A total of 85 mission hours were conducted during the first campaign and about 45 mission hours during the AACES-2 campaign. The nominal flight altitude was 3000 m a.g.l. – with the exception of alpine terrain, where the altitude was capped at 3400 m a.g.l. – in order to provide airborne data at a nominal 1 km spatial resolution. All flights were centred around 06:00 a.m. LST (20:00 UTC) to ensure aircraft observations were nearly coincident with SMOS overpasses. The typical time of the airborne mapping was between 04:30–09:30 a.m. LST (17:30–22:30 UTC), excluding ferry flights to and from the airport. The availability of VIS/NIR/SWIR data is, therefore, limited by the illumination conditions of the earth, with a large portion of the patch flight completed before sunrise.

The airborne coverage of each patch flight was designed to include a 6 km overlap with the adjacent patch by repeating part of the last flight line of the previous sampling day. This guaranteed full coverage of the SMOS pixels while also providing continuity between the different flight days. Furthermore, changes in brightness temperature data compared to the previous flight day allowed an assessment of soil moisture and/or effective temperature variations. The individual flight lines within a single patch were 5 km apart from each other, achieving a 1 km overlap of the outer beams of two adjacent flight lines on both sides of the aircraft. This ensured as best as possible the complete coverage of the patch considering the possible impact of strong cross winds on attitude and heading of the aircraft.

In addition to the patch flights, there were at least two transect flights across the AACES domain when SMOS covered the entire study area (start and end of each campaign – plus one in the middle of AACES-1). These flights were designed in such a way that they would cover as many permanent monitoring stations and focus farms as practical. Thus, they

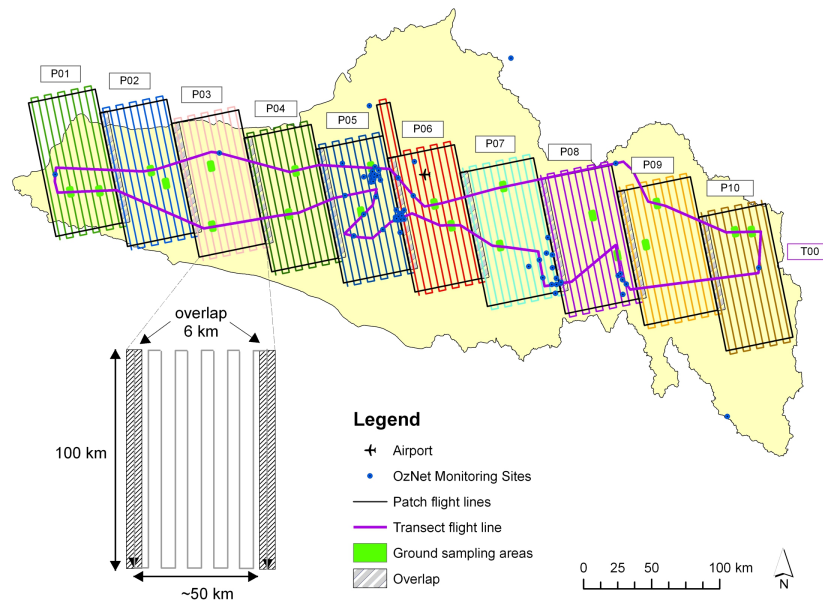


**Fig. 3.** Schematic of the airborne sampling strategy showing the flight lines for each individual patch flight (P) and the transect flight (T) across the AACES study area, with the latter designed to include as many ground sampling farms and OzNet monitoring sites as practical.

provided a snapshot of the soil moisture conditions across the entire AACES study area and allowed (i) an assessment of the temporal variability over the period of each individual campaign and (ii) a comparison with the European validation strategies. Furthermore, all transect and patch flights included a repeat of the first  $\approx 12$  km of the first flight line in order to assess temporal changes during the flight.

### 3.3 Additional flight segments

The ferry flights to and from the airport included at least one permanent monitoring station, and if practical, additional ground sampling farms located outside the target patch. Moreover, at the end of each flight period the aircraft flew at low level over Lake Wyangan, near Griffith, to calibrate the airborne L-band radiometer. The lake was continuously monitored for near-surface temperature and salinity throughout the campaigns. In addition, periodical in situ transect measurements of both parameters were undertaken in order to check for spatial gradients across the lake. Together with the airborne observations these data were used for the purpose of in-flight sensor calibration and data evaluation. Due to the early sampling and minimum altitude requirements for night flights, all calibration flights over the water storage target were conducted on the return flight only.

## 4 Ground data description

The ground monitoring was specifically designed to validate the aircraft observations at 1 km resolution and subsequently enable evaluation of the large scale SMOS products. Consequently, the ground team activities followed the aircraft across the study area from West to East during each campaign. The in situ data acquisition consisted of three components: (i) a permanent soil moisture profile monitoring network, (ii) temporarily installed monitoring stations, and (iii) intensive high resolution surface soil moisture and vegetation measurements. The ground sampling was concentrated on areas representative of the land use conditions within the respective airborne observed flight patch. Overall, these so-called focus farms captured the major climatic, topographic and soil texture variability across the entire AACES study area.

### 4.1 Soil moisture monitoring network

The OzNet hydrological monitoring network ([www.oznet.org.au](http://www.oznet.org.au); Smith et al., 2012) has been operational since 2001 and comprises a total of 62 stations throughout the entire Murrumbidgee River catchment (see Fig. 1). The network was upgraded in 2003 by adding additional monitoring sites and in 2006 by including near-surface soil moisture sensors

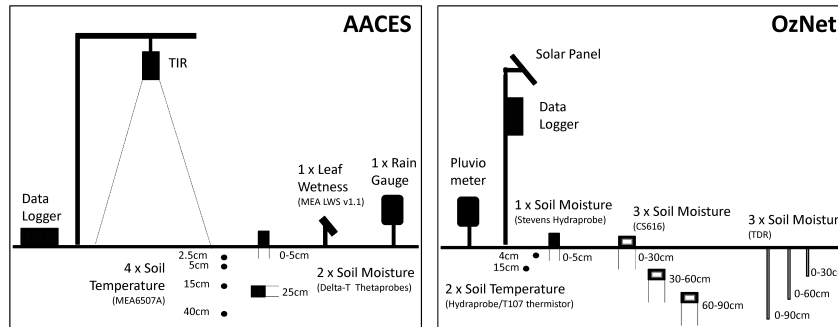


**Fig. 4.** Schematic of the temporary monitoring station instrumentation during the AACES field campaigns (left panel) and the permanent instrumentation at the new OzNet monitoring sites in the Murrumbidgee River catchment (right panel).

at all stations. In 2009, it was further augmented with two clusters of 12 supplementary stations within a  $60 \times 60 \text{ km}^2$  area focusing on the Yanco region in the western plains of the catchment. The network provides area-wide surface soil moisture measurements at 0–5 cm (or 0–7 cm for the older sites), using CS616 (CS615) water reflectometers, with the majority of stations additionally collecting soil moisture profile data across three depths (0–30 cm, 30–60 cm, and 60–90 cm). Supplementary parameters including (i) rainfall using a tipping bucket rain gauge, (ii) soil temperature (2.5 cm and 15 cm) and (iii) soil suction are also recorded (Fig. 4).

#### 4.2 Focus farm ground sampling

The ground observations for AACES-1 (AACES-2) were concentrated on a total of 20 focus farms (6 focus farms), with two farms (one farm) per patch, distributed across the study area. The locations of the sampling farms were selected based on (i) the available background information including topography, land use, soil texture and (ii) logistics, including the accessibility and travel time from the ground team base. The focus farms were chosen to be fairly homogeneous and represent the locally dominant soil and vegetation type, while capturing the naturally existing variability within each patch. The  $2 \times 5 \text{ km}^2$  sized ground sampling farms were aligned along the aircraft flight lines and centred underneath the two inner PLMR beams in order to (i) guarantee aircraft coverage and (ii) allow ground truth data for a minimum of four independent PLMR pixels per farm.

In addition to the existing long-term soil moisture network operating across the Murrumbidgee River catchment, each focus farm was instrumented with two almost identical temporary monitoring stations. Due to limited equipment, these supplementary stations were moved across the study area according to the aircraft and ground sampling locations. The temporary stations were equipped with two soil moisture probes (0–6 cm and 23–29 cm), four soil temperature sensors

(2.5 cm, 5 cm, 15 cm, and 40 cm), one tipping rain gauge and one leaf wetness sensor to determine the presence of dew observed during the satellite overpass (Fig. 4). Furthermore, one station per farm made thermal infrared measurements using a Raytek Thermalert TX (LT/LTP) to record the skin temperature of the (i) soil surface in the case of bare soil or (ii) canopy layer in the presence of vegetation. The TIR sensor used has a temperature range of  $-18^\circ\text{C}$  to  $500^\circ\text{C}$  and a spectral range from  $8\mu\text{m}$  to  $14\mu\text{m}$ . The rationale for setting up supplementary short-term stations on the focus farms was to verify three assumptions: (i) the effective temperature was relatively constant during the aircraft observations, (ii) the vegetation and soil temperature were in equilibrium around 06:00 a.m. LT (local time), and (iii) the soil moisture content within the top 5 cm did not change significantly throughout the course of the ground sampling. The temporary monitoring stations were ideally installed at least two days before the scheduled airborne sampling and spatial soil moisture measurements took place, as part of the focus farm reconnaissance activities. This ensured sufficient time for the soil temperature and soil moisture sensors to equilibrate within the partly disturbed soil column.

The focus farms were mapped with near-surface soil moisture measurements along six parallel lines of 5 km in length and 330 m spacing between them (Fig. 5). Along each of these transect lines a minimum of three soil moisture measurements (within a radius of 1 m) of the top 5 cm were made every 50 m using the Hydraprobe Data Acquisition System (HDAS). By taking replicate measurements at each sampling point the effect of random errors at local scale was sought to be minimized. The HDAS system comprises a Global Positioning System (GPS), a hydraprobe soil moisture sensor and a Geographic Information System (GIS) that combines the information about location and soil moisture in a visual output (Panciera et al., 2009). The accuracy of the Stevens Water hydraprobe sensor implemented in the HDAS system has been determined to be  $\pm 0.039 \text{ m}^3 \text{ m}^{-3}$  on the

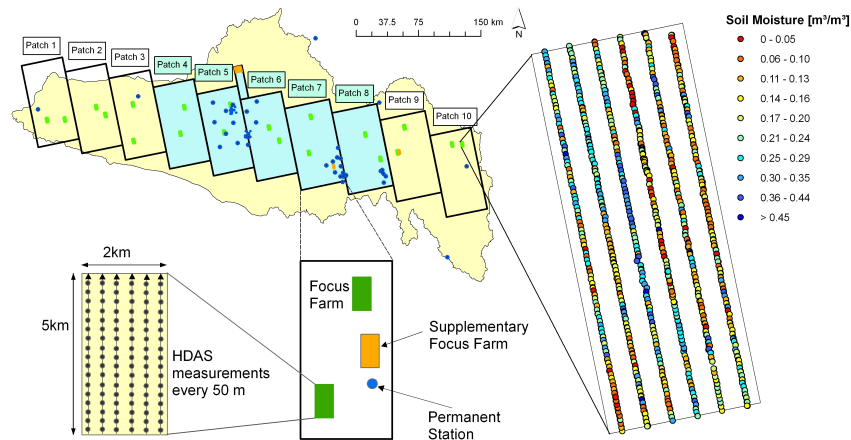


**Fig. 5.** Left panel: schematic of the ground sampling strategy concentrating on two focus farms per patch. Each focus farm was instrumented with two temporary monitoring stations and covered by six soil moisture sampling lines. Right panel: example of ground sampled, near-surface soil moisture data using the HDAS system.

basis of 155 gravimetric soil samples collected across the Murrumbidgee River catchment during AACES. The estimated error is consistent with results from an earlier study (Merlin et al., 2008) that used a combined calibration approach with laboratory and field measurements. The archived gravimetric soil samples from the AACES campaigns have been further analysed for soil texture particle distribution to determine silt, sand and clay content (Table 2). Ancillary data including vegetation type and height, a visual estimate of rock cover fraction, dew presence and dew characteristics were also recorded for each HDAS sampling location and stored within the system. In the case of visible dew, leaf wetness samples were taken using pre-weighed paper towels to determine the actual amount of dew on the plant leaves (Kabela et al., 2009). All soil moisture and dew measurements were made as early in the morning as practical, while aiming for coincident data with the aircraft flights and SMOS overpasses at around 06:00 a.m. LT. The dew sampling, however, was limited to the time period of 05:30–07:00 a.m. LST to focus the investigation on likely effects of dew on the L-band observations of SMOS and the airborne PLMR instrument. The 5 km soil moisture transects were generally completed between 05:30–10:00 a.m. (06:00 a.m.–12:00 p.m.) for AACES-1 and (AACES-2) on a sampling day. Note, the longer sampling time during the AACES-2 winter campaign was due to (i) the moist soil conditions, which increased the cleaning time of the HDAS probe pins after each measurement, and (ii) the relatively dense canopy layer which significantly slowed down the pace of the sampler – especially when walking through mature canola crops.

On each focus farm, specific vegetation data including biomass and spectral surface samples were collected at multiple locations (Table 2). Vegetation water content (VWC) information is crucial in the soil moisture retrieval process and together with the spectral properties of the canopy has been shown to provide relationships for estimating the VWC and other vegetation variables. In general, all canopy measurements were undertaken for all the major vegetation types present on each focus farm within a 1 km<sup>2</sup> box, which corresponded to one PLMR pixel. Across that box approximately five equally distributed sampling locations per vegetation type were chosen to characterise the dominant land cover. The actual vegetation data recorded at each focus farm included (i) leaf area index (LAI) using a LI-COR LAI-2000, (ii) hyper-spectral properties of the vegetation using a FieldSpec 3 instrument developed by ASD Inc., and (iii) destructive biomass samples from sampling locations previously observed with the LI-COR and ASD instruments. At each of the five sampling locations 3–5 individual LAI measurements were conducted within an approximate 10 m radius. Each LAI measurement consisted of five individual LAI readings: one above the canopy as a clear sky reference and four beneath the canopy (where possible half-way and near-soil). The final LAI measurement recorded was the average calculated from the combination of those readings.

The reflectance data were collected across a 5 × 5 m<sup>2</sup> area with a minimum of 25 ASD measurements on a regular grid of 1 m spacing, with a white reference measurement each 3–4 ASD measurements. In the case of rapid changing sky conditions white reference measurements were conducted before each individual ASD reading. The 5 × 5 m<sup>2</sup>

**Table 2.** Characteristics of all focus farms sampled during AACES-1 and AACES-2 (shaded rows).

Patch	Farm	Soil <sup>a</sup>		Vegetation <sup>b</sup>		Roughness <sup>c</sup>		Soil Moisture <sup>d</sup>			
		Class	Sand [%]	Clay [%]	Type	Dry Biomass [kg m <sup>-2</sup> ] min-max	VWC [kg m <sup>-2</sup> ] min-max	RMS height [mm]	Corr. length [cm]	Mean [m <sup>3</sup> m <sup>-3</sup> ]	Std [m <sup>3</sup> m <sup>-3</sup> ]
1	1	LS	73	6	grass	0.12–0.37	0.12–0.55	5.36	11.23	0.05	0.02
1	2	SL	52	14	grass	0.01–0.22	0.01–0.20	4.87	11.32	0.05	0.03
2	3	SL	35	21	grass	0.14–0.35	0.01–0.25	3.10	7.23	0.04	0.02
2	4	SL	38	24	grass	0.28–0.59	0.10–0.19	3.55	13.11	0.04	0.02
3	5	SL	66	10	grass	0.17–0.68	0.12–0.32	2.77	8.18	0.04	0.02
3	6	SCL	35	31	grass	0.22–0.51	0.03–0.10	4.72	12.88	0.04	0.02
4	7	SL	63	11	grass	0.07–0.84	0.04–1.01	2.86	11.91	0.03	0.02
4	7	–	–	–	grass	0.20–0.45	0.83–3.16	2.73	13.20	0.36	0.11
4	8	SCL	42	31	grass	0.13–0.23	0.02–0.13	2.37	9.95	0.03	0.02
5	9	SL	40	20	grass	0.01–0.26	0.01–0.06	3.48	10.34	0.09	0.07
5	9	–	–	–	grass	0.11–0.29	0.21–1.12	3.06	11.52	0.28	0.10
5	10	LS	68	9	grass/crop	0.20–0.57	0.01–0.19	4.15	11.76	0.08	0.06
5	10	–	–	–	crop/grass	0.37–0.66	1.48–3.55	6.65	13.55	0.38	0.09
6	11	LS	82	5	grass/crop	–	–	–	–	0.11	0.04
6	12	LS	85	4	grass/crop	–	–	–	–	0.15	0.04
6	12	–	–	–	crop	0.41–0.96	2.30–5.46	4.05	11.05	0.33	0.06
7	13	SL	55	9	grass	0.02–0.16	0.05–0.15	7.06	12.45	0.11	0.05
7	13	–	–	–	crop/grass	0.38–0.74	1.11–2.22	6.22	13.77	0.30	0.08
7	14	SL	67	24	crop/grass	0.10–0.36	0.01–0.21	7.64	9.14	0.11	0.04
8	15	LS	74	7	grass	0.05–0.50	0.07–0.38	6.07	11.47	0.29	0.05
8	15	–	–	–	crop	0.26–0.58	0.87–2.91	3.74	11.21	0.26	0.06
8	16	LS	92	1	grass	–	–	4.86	10.01	0.33	0.07
9	17	LS	77	5	grass	0.18–0.35	0.20–0.92	5.73	16.21	0.21	0.06
9	18	LS	74	4	grass	0.12–0.49	0.28–1.24	7.18	15.64	0.25	0.06
10	19	LS	89	2	grass	0.21–0.35	0.30–1.07	5.77	15.97	0.25	0.08
10	20	LS	80	3	grass	0.08–0.09	0.03–0.05	9.29	15.99	0.19	0.10

<sup>a</sup>Class: LS=loamy sand, SL=silty loam, SCL=silt clay loam (based on the Australian soil texture classification standard); <sup>b</sup>type: in case of two major land cover types, the dominant vegetation is named first (VWC: Vegetation Water Content); <sup>c</sup>average of slope corrected roughness profiles (RMS height: root mean square height; Corr. length: correlation length); <sup>d</sup>average soil moisture and standard deviation (Std) measured with the HDAS system.

destructive sampling area was always located at the centre point of the grid. To assist with the data analysis, supplementary information including vegetation type and height, row spacing and direction, and photographs of the sky/cloud conditions as well as of the actual sample were taken for each sampling point. To ensure optimal spectral sampling conditions, the ASD vegetation measurements were made between 10:00 a.m.–02:00 p.m. LST. The LAI data were collected earlier at about 07:00–09:30 a.m. to reduce the effect of direct sunlight on the sensor. The destructive vegetation sampling took place by removing all organic matter within the sampling area and subsequently monitoring the weight loss through oven drying at 40 °C until a constant weight was achieved. In addition to the vegetation sampling, the ground teams recorded at least three surface roughness profiles of 2 m length in North-South and East-West direction across each focus farm (Table 2). At each location a pin-profiler was positioned and levelled, and subsequently the height of each pin recorded manually as well as in a photograph. An overview of the total amount of ground data sampled during both AACES campaigns is given in Table 3.

**Table 3.** Overview of total ground data collected during the AACES field campaigns.

Measurement	AACES-1	AACES-2
HDAS near-surface soil moisture	36 800	10 800
2 m surface roughness profile (NS, EW)	48	16
Gravimetric soil sample	126	29
LAI sample	497	158
Dew sample	38	26
ASD sample	1575	175
Destructive vegetation sample	81	31

In addition to the 20 AACES focus farms, three supplementary focus farms were included in the campaign dataset. These were operated by the CSIRO Griffith and the NSW Department of Environment and Climate Change in Wagga Wagga. While the ground sampling strategy was not identical to the general AACES experiment, similar measurements in terms of soil moisture, vegetation and gravimetric soil samples were collected and details are included in the online data archive.

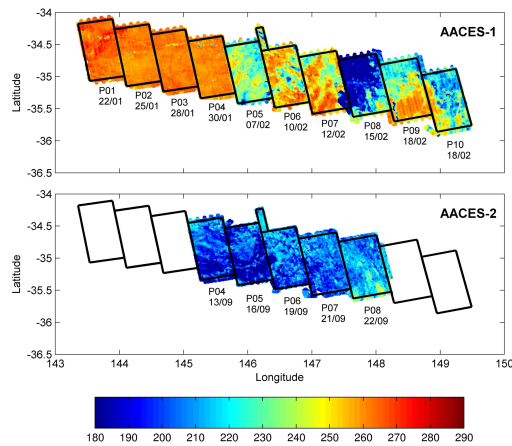


**Fig. 6.** Example of airborne L-band data collected at H-polarization during the summer (AACES-1) and winter (AACES-2) field campaigns with the brightness temperatures given in Kelvin. Note, each flight patch represents a single flight day.

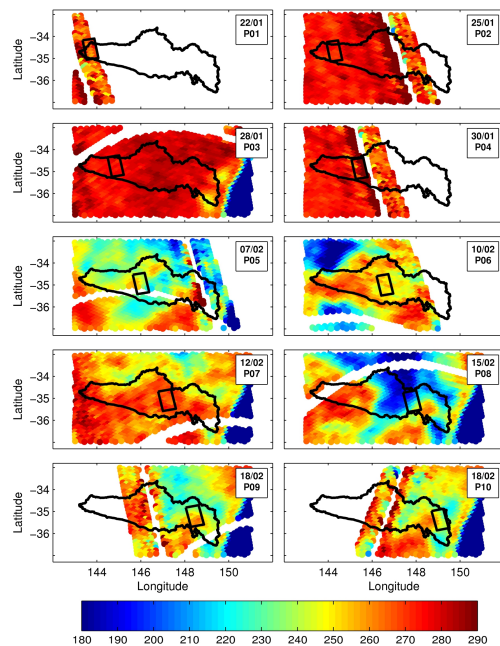


**Fig. 7.** Temporal and spatial patterns of H-polarized SMOS L1C brightness temperature data [K] collected during the summer field campaign (AACES-1). Overlain are the Murrumbidgee catchment boundary and the individual flight patch of that particular day, where airborne L-band data is available.

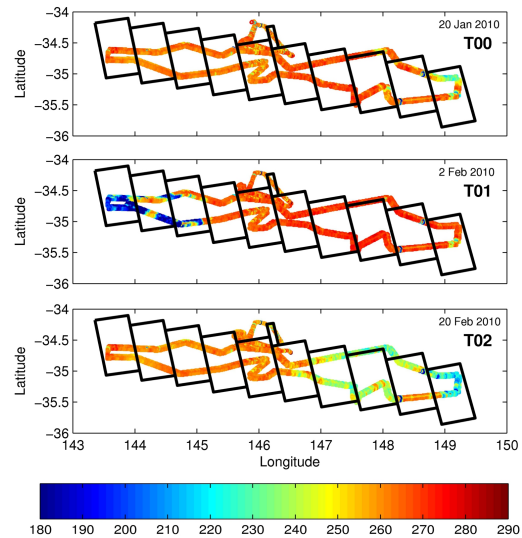


**Fig. 8.** Example of airborne L-band data collected at H-polarization during the AACES-1 campaign in transect flight mode (brightness temperatures given in Kelvin).

### 5 Towards SMOS data validation

During the AACES field experiments, significant changes in soil moisture conditions and land cover were observed (see Table 2). The AACES-1 campaign in summer 2010 commenced with daytime air temperatures above 30 °C and very dry surface soil moisture conditions of approximately 0.05–0.10 m<sup>3</sup> m<sup>-3</sup>. However, this changed to relatively moist (0.25–0.35 m<sup>3</sup> m<sup>-3</sup>) and cool conditions due to a few significant rain events during the middle and towards the end of the campaign, with up to 140 mm rainfall on a single day. Moreover, the vegetation was relatively sparse (vegetation water content 0.1–0.6 kg m<sup>-2</sup>) and dominated by salt bushes in the western grazing areas, while the central and eastern parts of the study area were mainly characterised by low-vegetated pastures and mostly fallow or fresh ploughed farmland in cropping areas. In contrast, the AACES-2 campaign, undertaken during the Southern Hemisphere winter, provided relatively dense vegetation conditions (vegetation water content 0.1–5.2 kg m<sup>-2</sup>) with long pasture and mature crops (mainly wheat, barley, canola and lucerne) under moderate to wet surface soil moisture conditions (0.2–0.4 m<sup>3</sup> m<sup>-3</sup>). Average air temperatures were 15 °C throughout the campaign, with two days of rain having 10–20 mm each.

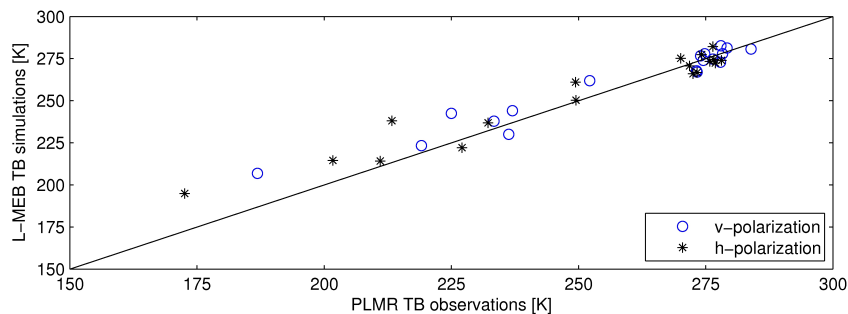


Fig. 9. Comparison of 1 km PLMR observations with L-MEB simulated brightness temperature data for AACES-1.

### 5.1 Evaluation of L-Band brightness temperature patterns

Figure 6 shows an example of the 1 km H-polarized PLMR observations collected during both AACES campaigns and normalized to  $38^\circ$  incidence angle. For AACES-1, the intensive rain events that occurred during the middle (6–7 February) and end of the campaign (13–15 February) caused a significant drop in brightness temperatures (TB) in response to the sudden rise in soil moisture. Note that the course of the Murrumbidgee River can be clearly distinguished in the upper part of patches P01–P04, displaying low L-band observations for the river in comparison to the high brightness temperatures emitted by the surrounding dry soil surface. During the AACES-2 winter campaign with predominantly wet and cool conditions, the brightness temperatures mapped across the study area showed overall small variations. The comparison with the SMOS L1C brightness temperature data acquired during the AACES-1 campaign demonstrated that both temporal and spatial patterns of near-surface soil moisture are similar to those obtained by the airborne radiometer (Fig. 7). The evolution of the initially dry conditions present across the entire Murrumbidgee River catchment to wet conditions in the central and eastern parts of the study area is clearly depicted in the satellite data over the assigned flight patches. A detailed quantitative assessment of the SMOS L1C brightness temperature data with respect to the AACES dataset is the subject of a separate paper by Rüdiger et al. (2011).

Figure 8 presents the temporal patterns observed by the L-band sensor, when compared between the individual transect flights conducted during the AACES-1 summer campaign. The initial dry soil conditions across the study area (T00) for the western patches (P01–P03) showed a change in response to a local storm, causing lower brightness temperature measurements for those three patches on the second transect flight (T01). Conversely for the far eastern patch (P10) there was a dry down observed between T00 and T01. The transect

flight at the end of the campaign (T02) captured (i) the moist soil conditions of the eastern study area after a few intense rainfall events, but also (ii) the dry down of the surface soil compared to the patch flight flown earlier over the precipitated area of P01–P03.

### 5.2 Analysis of L-MEB performance

The core algorithm in the SMOS soil moisture retrieval is the L-band Microwave Emission of the Biosphere (L-MEB) model (Kerr et al., 2011; Wigneron et al., 2007). A preliminary analysis of the AACES dataset has included tests of the L-MEB model performance for the range of topographic, land cover and soil moisture conditions observed during the field experiments. Based on the collected in situ ground data from all 20 focus farms, brightness temperature signals were simulated and subsequently compared against the airborne L-band measurements (Fig. 9). These results showed that for the range of brightness temperatures measured in AACES-1 (170–290 K), the L-MEB predictions with default parameters were close to the PLMR observations for dry conditions, such as those encountered during the beginning of the summer campaign with relatively high brightness temperature responses. However, with increasing soil moisture and correspondingly lower brightness temperatures, the L-MEB algorithm tended to overestimate the emission, leading to significantly higher values of up to 25 K difference to that measured by the PLMR instrument. It is believed that this trend might be induced by the presence of water on the vegetation due to extensive rainfall events at those times. Consequently, for moderate-wet soil conditions, soil moisture estimates modeled by the L-MEB algorithm might be outside the SMOS target accuracy, if the source for such an offset is not considered. Further analysis of the AACES dataset will support a better understanding of the retrieval capabilities of SMOS, both in terms of the L1C brightness temperature as well as the derived L2 soil moisture product.

## 6 Summary

The two AACES field experiments and associated datasets collected across the Murrumbidgee River catchment in Australia have been described. The study area, comprising more than 20 independent SMOS pixels in entirety, was extensively monitored under two seasonal conditions, summer (AACES-1) and winter (AACES-2) in 2010. The campaign sampling strategy included a combination of airborne L-band observations and extensive ground sampling activities coincident with SMOS overpasses. As the preliminary results in this paper and ongoing studies show, the AACES dataset is being used in various ways, such as validating (i) SMOS brightness temperature observations (level 1C product) (Rüdiger et al., 2011), (ii) SMOS derived soil moisture products (level 2), (iii) SMOS downscaled soil moisture products to 1 km resolution (Merlin et al., 2012) and (iv) the representativeness of the in situ monitoring network for soil moisture monitoring at 1 km and 45 km scale. Issues due to the low spatial resolution and the mixed land cover within a SMOS pixel can also be addressed by including the 1 km PLMR measurements and the ground data collected at the focus farms. Moreover, the AACES data allow a validation of the joint retrieval of ancillary parameters and soil moisture according to the SMOS approach using dual-polarized multi-angle brightness temperature data. The much larger spatial and temporal scale of the AACES experiment compared to equivalent studies in Europe further enhances the ability to assess potential error sources that might be introduced by partial and/or transect sampling of SMOS pixels for validation purposes.

## 7 Data availability

The AACES dataset presented in this paper is available online at <http://www.moisturemap.monash.edu.au/aaces>. The website includes a detailed description of the two field campaigns (AACES-1 and AACES-2) and provides all the information required for data interpretation. A general overview of the Murrumbidgee River catchment, photographs, sampling techniques, as well as a copy of both field experiment plans and addenda are also given. Due acknowledgment in any publication or presentation arising from use of these data is required.

*Acknowledgements.* The authors would like to acknowledge all the farmers and landholders involved in the field experiments for their helpful cooperation and permission to access their properties. We further thank the Yanco Agricultural Research Institute (YAI) for providing accommodation, research and laboratory facilities. The AACES field experiments were a result of numerous collaborative efforts including Australian, Chinese, European and North American institutions. We wish to thank all participants that helped us to conduct these two very successful AACES campaigns (Channah Betgen, Simone Bircher, Tao Che,

Andrew French, Claire Gruhier, Xujun Han, Jon Johanson, Catherine Jolly, Olaf Klimczak, Jane Lai, Delphine Leroux, Xin Li, Mateusz Lukowski, Arnaud Mialon, Robert Pipunic, Ulrike Port, Dongryeol Ryu, Roosanne Schrooten, Sandra Slowinska, Mariette Vreugdenhill, Jun Wen, Anna Wojciga and Rodger Young), the student's supervisors (Richard de Jeu, Alexander Loew and Wojciech Marczewski), and the contributions made through additional ground sampling at the supplementary focus farms by the teams led by John Hornbuckle, Victor Shoemark and Gregory Summerell.

The AACES campaigns were funded through the Australian Research Council (DP0879212) as part of the MoistureMap project. The initial setup and maintenance of the Murrumbidgee monitoring network was funded by two ARC grants (DP0343778, DP0557543) and the CRC for Catchment Hydrology. The airborne instrumentation has been developed through ARC infrastructure grants (LE0453434, LE0560930). Further financial support for travel expenses was provided by ESA for the European participants and by the Australian Academy of Science for the Chinese visiting scientists.

Edited by: F. Pappenberger

## References

- Australian Bureau of Rural Science: Gridded rainfall data, based on the standard rainfall climatology (1961–1990), available at: <http://www.bom.gov.au/climate/how/newproducts/IDCraintempgrids.shtml> (last access: August 2009), 2001.
- Australian Bureau of Rural Science: Land Use of Australia, version 3 – 2001/2002, available at: <http://adl.brs.gov.au/mapserv/landuse> (last access: August 2009), 2006.
- Barré, H. M., Duesmann, B., and Kerr, Y. H.: SMOS: The mission and the system, *IEEE T. Geosci. Remote*, 46, 587–593, doi:10.1109/TGRS.2008.916264, 2008.
- Cano, A., Millán-Scheiding, C., Wigneron, J., Antolín, C., Balling, J. E., Kruszcwski, A., Saleh, K., Søbjaerg, S. S., Skou, N., and Lopez-Baeza, E.: The Mediterranean Ecosystem L-Band EXperiment over vineyards (Melbex-2), in: 10th Specialist Meeting on Microwave Radiometry and Remote Sensing for the Environment (MicroRad), 2008.
- Cano, A., Saleh, K., Wigneron, J., Antolín, C., Balling, J. E., Kerr, Y. H., Kruszcwski, A., Millán-Scheiding, C., Søbjaerg, S. S., Skou, N., and López-Baeza, E.: The SMOS Mediterranean Ecosystem L-Band characterisation EXperiment (MELBEX-I) over natural shrubs, *Remote Sens. Environ.*, 114, 844–853, doi:10.1016/j.rse.2009.11.019, 2010.
- de Rosnay, P., Calvet, J., Kerr, Y., Wigneron, J., Lemaître, F., Escorihuela, M. J., Sabater, J. M. N., Saleh, K., Barrié, J., Bouhours, G., Coret, L., Cherel, G., Dedieu, G., Durbe, R., Fritz, N. E. D., Froissard, F., Hoedjes, J., Kruszcwski, A., Lavenu, F., Suquia, D., and Waldteufel, P.: SMOSREX: A long term field campaign experiment for soil moisture and land surface processes remote sensing, *Remote Sens. Environ.*, 102, 377–389, doi:10.1016/j.rse.2006.02.021, 2006.
- Delwart, S., Bouzinac, C., Wursteisen, P., Berger, M., Drinkwater, M., Martin-Neira, M., and Kerr, Y. H.: SMOS Validation and the COSMOS Campaigns, *IEEE T. Geosci. Remote*, 46, 695–704, doi:10.1109/tgrs.2007.914811, 2008.

- Dorigo, W. A., Wagner, W., Hohensinn, R., Hahn, S., Paulik, C., Xaver, A., Gruber, A., Drusch, M., Mecklenburg, S., van Oevelen, P., Robock, A., and Jackson, T.: The International Soil Moisture Network: a data hosting facility for global in situ soil moisture measurements, *Hydrol. Earth Syst. Sci.*, 15, 1675–1698, doi:10.5194/hess-15-1675-2011, 2011.
- Geoscience Australia: GEODATA 9 second DEM and D8: Digital Elevation Model version 3 and Flow Direction Grid 2008, available at: <http://www.ga.gov.au/topographic-mapping/digital-elevation-models/index.jsp> (last access: August 2009), 2008.
- Kabela, E. D., Hornbuckle, B. K., Cosh, M. H., Anderson, M. C., and Gleason, M. L.: Dew frequency, duration, amount, and distribution in corn and soybean during SMEX05, *Agr. Forest Meteorol.*, 149, 11–24, doi:10.1016/j.agrformet.2008.07.002, 2009.
- Kerr, Y. H., Waldteufel, P., Wigneron, J., Martinuzzi, J. M., Font, J., and Berger, M.: Soil moisture retrieval from space: The Soil Moisture and Ocean Salinity (SMOS) mission, *IEEE T. Geosci. Remote.*, 39, 1729–1735, doi:10.1109/36.942551, 2001.
- Kerr, Y. H., Waldteufel, P., Wigneron, J., Delwart, S., Cabot, F., Boutin, J., Escorihuela, M. J., Font, J., Reul, N., and Gruhier, C.: The SMOS Mission: New Tool for Monitoring Key Elements of the Global Water Cycle, *Proc. IEEE*, 98, 666–687, doi:10.1109/JPROC.2010.2043032, 2010.
- Kerr, Y. H., Waldteufel, P., Richaume, P., Wigneron, J.-P., Ferrazzoli, P., and Gurney, R. J.: SMOS level 2 processor for soil moisture – Algorithm Theoretical Based Document (ATBD), Tech. Rep. ESA No.: SO-TN-ESL-SM-GS-0001, Issue 3.4, CESBIO, Toulouse, France, available at: [http://www.cesbio.ups-tlse.fr/fr/smos/smos\\_atbd.html](http://www.cesbio.ups-tlse.fr/fr/smos/smos_atbd.html) (last access: 20 June 2012), 2011.
- McKenzie, N., Jacquier, D., Ashton, L., and Cresswell, H.: Estimation of soil properties using the Atlas of Australian Soils, Tech. Rep. 11/00, CSIRO Land and Water, 2000.
- Mecklenburg, S., Bouzinac, C., and Delwart, S.: Overview on calibration and validation activities for ESA's soil moisture and ocean salinity mission, in: *IEEE International Geoscience and Remote Sensing Symposium (IGARSS)*, Vol. 3, The Institute of Electrical and Electronics Engineers, Inc. (IEEE), 3, III-85–III-88, doi:10.1109/IGARSS.2009.5418111, 2009.
- Merlin, O., Walker, J. P., Kalma, J. D., Kim, E. J., Hacker, J., Panciera, R., Young, R., Summerell, G., Hornbuckle, J., Hafeez, M., and Jackson, T. J.: The NAFE'06 dataset: Towards soil moisture retrieval at intermediate resolution, *Adv. Water Resour.*, 31, 1444–1455, doi:10.1016/j.advwatres.2008.01.018, 2008.
- Merlin, O., Rüdiger, C., Al Bitar, A., Richaume, P., Walker, J. P., and Kerr, Y. H.: Disaggregation of SMOS soil moisture over the AACES area with DisPATCH, *IEEE T. Geosci. Remote.*, 50, 1556–1571, doi:10.1109/TGRS.2011.2175000, 2012.
- Panciera, R., Walker, J. P., Kalma, J. D., Kim, E. J., Hacker, J., Merlin, O., Berger, M., and Skou, N.: The NAFE'05/CoSMOS Data Set: Toward SMOS Soil Moisture Retrieval, Downscaling, and Assimilation, *IEEE T. Geosci. Remote.*, 46, 736–745, doi:10.1109/Tgrs.2007.915403, 2008.
- Panciera, R., Allahmoradi, M., Merlin, O., Young, R., and Walker, J. P.: The Hydraprobe Data Acquisition System (HDAS) V.5: User Guide, Tech. rep., The University of Melbourne, 2009.
- Panciera, R., Walker, J. P., Jackson, T., Ryu, D., Gray, D., Moneris, A., Yardley, H., Tanase, M., Rüdiger, C., Wu, X., Gao, Y., and Hacker, J.: The Soil Moisture Active Passive Experiments (SMAPEX): Towards Soil Moisture Retrieval from the SMAP Mission, submitted to *IEEE T. Geosci. Remote.*, 2012.
- Rüdiger, C., Walker, J. P., and Kerr, Y. H.: On the Airborne Spatial Coverage Requirement for Microwave Satellite Validation, *IEEE Geosci. Remote S.*, 8, 824–828, doi:10.1109/LGRS.2011.2116766, 2011.
- Saleh, K., Wigneron, J., Calvet, J., Lopez-Baeza, E., Ferrazzoli, P., Berger, M., Wursteisen, P., Simmonds, L. P., and Miller, J.: The EuroSTARRS airborne campaign in support of the SMOS mission: first results over land surfaces, *Int. J. Remote Sens.*, 25, 177–194, doi:10.1080/0143116031000116444, 2004.
- Smith, A., Walker, J. P., Western, A. W., Young, R., Ellett, K. M., Pipunic, R. C., Grayson, R. B., Siriwidena, L., Chiew, F. H. S., and Richter, H.: The Murrumbidgee Soil Moisture Monitoring Network Data Set, *Water Resour. Res.*, online first: doi:10.1029/2011WR011749, 2012.
- Walker, J. P., Rüdiger, C., Peischl, S., Ye, N., Bandara, R., Allahmoradi, M., Kerr, Y. H., Kim, E. J., Gurney, R. J., Barrett, D., and LeMarshall, J.: Australian Airborne Cal/val Experiments for SMOS (AACES) – Winter Campaign: Experiment Plan, Tech. rep., Monash University, available at: <http://www.moisturemap.monash.edu.au/aaces/> (last access: 20 June 2012), 2010a.
- Walker, J. P., Rüdiger, C., Peischl, S., Ye, N., Bandara, R., Allahmoradi, M., Ryu, D., Kerr, Y. H., Kim, E. J., Gurney, R. J., Barrett, D., and LeMarshall, J.: Australian Airborne Cal/val Experiments for SMOS (AACES): Experiment Plan, Tech. rep., The University of Melbourne, available at: <http://www.moisturemap.monash.edu.au/aaces/> (last access: 20 June 2012), 2010b.
- Whetton, P. H., Haylock, M. R., and Galloway, R.: Climate change and snow-cover duration in the Australian Alps, *Climatic Change*, 32, 447–479, doi:10.1007/BF00140356, 1996.
- Wigneron, J., Kerr, Y. H., Waldteufel, P., Saleh, K., Escorihuela, M. J., Richaume, P., Ferrazzoli, P., de Rosnay, P., Gurney, R. J., Calvet, J., Grant, J. P., Guglielmetti, M., Hornbuckle, B., Mätzler, C., Pellarin, T., and Schwank, M.: L-band Microwave Emission of the Biosphere (L-MEB) Model: Description and calibration against experimental datasets over crop fields, *Remote Sens. Environ.*, 107, 639–655, doi:10.1016/j.rse.2006.10.014, 2007.

### 6.3 Summary

---

Given the large  $\approx 50$  km SMOS pixel size and the inherited heterogeneity in topography and land cover conditions, a representative in-situ sampling strategy needs to be considered for a sophisticated analysis of the SMOS models and products. The focus of the European experimental sites is limited to a subset of a single SMOS pixel and/or airborne transects through several SMOS pixels with repeat flights over a given time period (i.e. SMOSREX (Rosnay et al., 2006), MELBEX (Cano et al., 2008) and EuroSTARRS (Saleh et al., 2004).

In contrast, the field campaigns described in this paper, named Australian Airborne Cal/val Experiment for SMOS (AACES), were designed to provide an extensive validation data set by completely covering a minimum of 20 independent (40 overlapping) SMOS pixels. The AACES study area, which is located in south-eastern Australia, comprises approximately  $\approx 50000$  km<sup>2</sup> and represents about two-third of the entire Murrumbidgee River catchment. The range of topographic, climatic and land cover conditions captured within that confined region is typical of Australia but also across the world, and therefore makes the AACES study area an excellent validation site for the land component of the SMOS satellite mission. Moreover, having the benefit of an existing long-term soil moisture network operating in the Murrumbidgee River catchment together with the given variability in natural features across the study area, the experimental site has already been the focus of several extensive campaigns in the past.

# References for Chapter 6

- Cano, A., C. Millán-Scheiding, J.-P. Wigneron, C. Antolín, J. E. Balling, A. Kruszewski, K. Saleh, S. S. Sobjaerg, N. Skou, and E. Lopez-Baeza (2008), “The Mediterranean Ecosystem L-Band EXperiment over vineyards (Melbex-2),” in: *10th Specialist Meeting on Microwave Radiometry and Remote Sensing for the Environment (MicroRad)* (cited on p. 103).
- Delwart, S., C. Bouzinac, P. Wursteisen, M. Berger, M. Drinkwater, M. Martin-Neira, and Y. H. Kerr (2008), “SMOS Validation and the COSMOS Campaigns,” *IEEE Transactions on Geoscience and Remote Sensing*, 46(3), pp. 695–704, DOI: 10.1109/tgrs.2007.914811 (cited on p. 90).
- Mecklenburg, S., C. Bouzinac, and S. Delwart (2009), “Overview on calibration and validation activities for ESA’s soil moisture and ocean salinity mission,” in: *IEEE International Geoscience and Remote Sensing Symposium (IGARSS)*, vol. 3, The Institute of Electrical and Electronics Engineers, Inc. (IEEE), pp. III–85–III–88, DOI: 10.1109/IGARSS.2009.5418111 (cited on p. 90).
- Rosnay, P. de, J.-C. Calvet, Y. Kerr, J.-P. Wigneron, F. Lemaître, M. J. Escorihuela, J. M. n. Sabater, K. Saleh, J. Barrié, G. Bouhours, L. Coret, G. Cherel, G. Dedieu, R. Durbe, N. E. D. Fritz, F. Froissard, J. Hoedjes, A. Kruszewski, F. Lavenu, D. Suquia, and P. Waldteufel (2006), “SMOSREX: A long term field campaign experiment for soil moisture and land surface processes remote sensing,” *Remote Sensing of Environment*, 102(3), pp. 377–389, DOI: 10.1016/j.rse.2006.02.021 (cited on p. 103).
- Saleh, K., J.-P. Wigneron, J.-C. Calvet, E. Lopez-Baeza, P. Ferrazzoli, M. Berger, P. Wursteisen, L. P. Simmonds, and J. Miller (2004), “The EuroSTARRS airborne campaign in support of the SMOS mission: first results over land surfaces,”

*International Journal of Remote Sensing*, 25(1), pp. 177–194, DOI: 10 . 1080 / 0143116031000116444 (cited on p. 103).



# 7

## Evaluation of SMOS data products for the Australian validation site

**T**HE extensive datasets available from the AACES field campaigns provide a vital source, not only for the assessment of spatial soil moisture patterns and their temporal evolution, but also for evaluation of the various SMOS data products that are available over land.

### 7.1 Overview of SMOS L0 to L3 products

---

For the SMOS mission there are different data products available to the science community. In general, these products are classified into several data groups, including the raw SMOS observations and the processed data describing a “level” of quality (Table 7.1). Level 0 to level 2 products are under the mandate of ESA, whereas the level 3 and 4 products are produced by the Centre Aval de Traitement des Données SMOS (CATDS)/Centre de Production des Données du CATDS (CPDC) and the Barcelona Expert Center (SMOS-BEC).

Level 0 (L0) data are consolidated raw data (i.e. sorted and grouped by half orbit) comprising the radiometer observation data and telemetry information of the system.

**Table 7.1:** Overview of SMOS data products

Level	Description	Provider	Reference*
L0	SMOS payload data in so-called Source Packets with added Earth Explorer product headers	ESA	L0 Data Processing Model Document
L1A	Reformatted and calibrated observations and housekeeping data in engineering units	ESA	L1A Data Processing Model Document
L1B	Output of the image reconstruction with Fourier components of brightness temperatures in the antenna polarisation reference frame.	ESA	L1B Data Processing Model Document
L1C	Multi-incidence angle brightness temperatures at the top of the atmosphere, geolocated in an equal-area grid system	ESA	L1C Data Processing Model Document
L2	Contain the retrieved swath-based soil moisture, vegetation optical depth and other ancillary data derived during processing (surface temperature, roughness parameter, dielectric constant and brightness temperature retrieved at top of atmosphere and at surface) with their corresponding uncertainties	ESA	L2SM ATBD
L3	Soil moisture, vegetation optical depth and other land data products: daily, 3-day, 10-day and monthly products on 25 km (EASE grid)	CATDS-CPDC	CATDS SMOS L3SM ATBD
L3	Soil moisture, vegetation optical depth and other land data products: daily, 3-days average, 9-days average, monthly and annual maps	SMOS-BEC	SMOS-BEC Ocean and Land Products Description

---

\*for more information see reference section for this chapter

The level 1 data are generated by the L1OP processor for use of different scientific applications and are subdivided into three individual products: level L1A, L1B and L1C. All records from the spacecraft are converted into engineering units by calibrating the visibilities between the individual antenna receivers to radiance and are specified as L1A data product. The level L1B products are reconstructed into brightness temperature Fourier components before being processed to L1C data which is brightness temperatures sorted by the ISEA grid. The L1C product is differentiated between one product for land and for sea and separate datasets for each one of them are available.

For level 2 (L2) the processors compute either soil moisture(L2SM) or sea surface salinity (L2OS) by deriving geophysical quantities using an iterative scheme with the multi-incidence angle data. I.e. fully simulated SMOS measurements in the antenna reference frame are implemented and certain geophysical parameters are continuously adjusted until the cost function reaches a minimum. The final refinement of (L2SM) and (L2OS) to provide global temporal synthesis maps of soil moisture as well as retrieve enhanced soil moisture from SMOS brightness temperatures by using improved geophysical variables is done by Level 3 processors. The Level 3TB data are a daily global polarised brightness temperature product, arranged by incidence angle values, in full polarisation. Ascending and descending orbits are processed separately since the overpasses and the corresponding different viewing configuration of the sensor induce different values of the retrieved parameters that may not be always comparable. The level 3 products are presented in the NetCDF format on the EASE (Equal Area Scalable Earth) grid version 2 with a 25 km cylindrical projection.

## **7.2 Comparison of SMOS brightness temperature data products**

---

The AACES sampling strategy was designed to provide a range of conditions with the maximum overlap in space and time between the spaceborne, airborne and in-situ ground measurements. Consequently, the aircraft schedule and flight coverage were planned to be coincident with the SMOS overpass for the individual AACES patches throughout the entire field campaign. This unique setting allowed both radiometers, airborne and spaceborne, to map quasi-simultaneously the same area on the surface but at different spatial resolution. The resulting surface observations were expected to capture similar patterns in terms of the prevailing soil moisture conditions.

### **7.2.1 SMOS L1C data**

As described in section 7.1, one category of available SMOS products is the L1C brightness temperature data processed and provided by ESA. For the subsequent analysis of the SMOS and PLMR data during the AACES field campaigns, both datasets

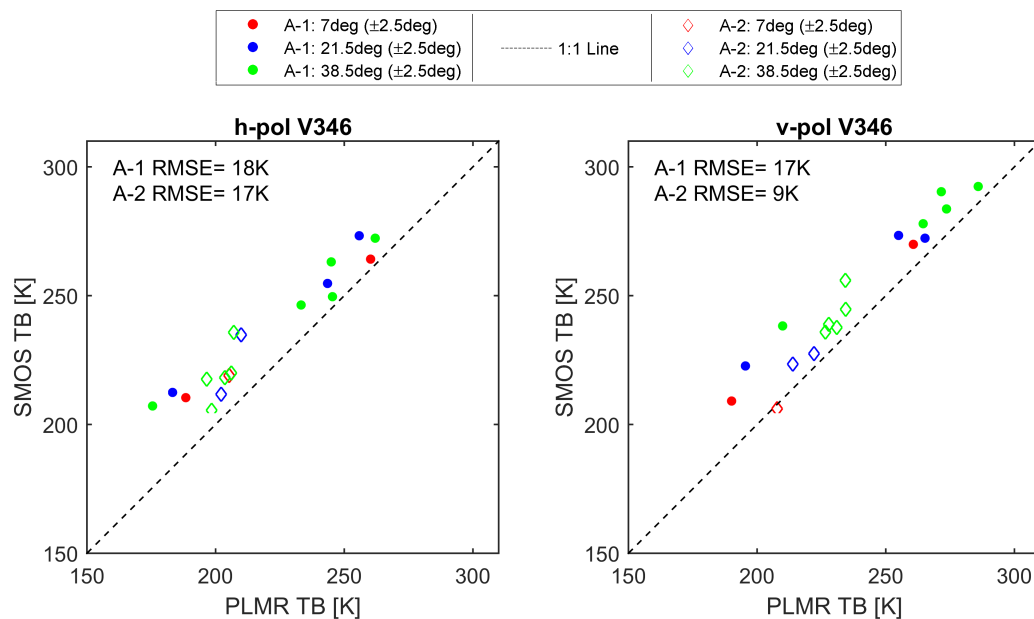


**Figure 7.1:** Comparison of SMOS L1C (V346) and airborne brightness temperature (TB) observations at three groups of incidence angles extracted for all AACES patches (A-1: AACES-1, A-2: AACES-2)

have been pre-processed to facilitate the comparison between them. The airborne as well as the SMOS L1C brightness temperature data (V346) were grouped according to the angular setting determined by the six radiometer beams from the airborne instrument. That is, the airborne brightness temperature values were classified in three separate ranges of  $4.5^{\circ}$ - $9.5^{\circ}$  (group 1),  $19^{\circ}$ - $24^{\circ}$  (group 2), and  $36^{\circ}$ - $41^{\circ}$  (group 3), for all available SMOS data within the Murrumbidgee study area. Figure 7.1 shows the comparison of the SMOS and airborne observations, grouped into the angular classes, and separated for brightness temperature measurements at horizontal and vertical polarization. Overall there is a noticeable bias towards higher brightness temperature measurements made by SMOS. Between the three angular groups there is no distinct trend notable for the particular range of angular observations tested here. Furthermore, for the first (summer) campaign similar overestimations were noted with a root mean square error of 18 K/17 K for h- and v-polarization, respectively. During the winter campaign a clearly more narrow range of brightness temperatures was captured though the rmse values were 17 K and 9 K.

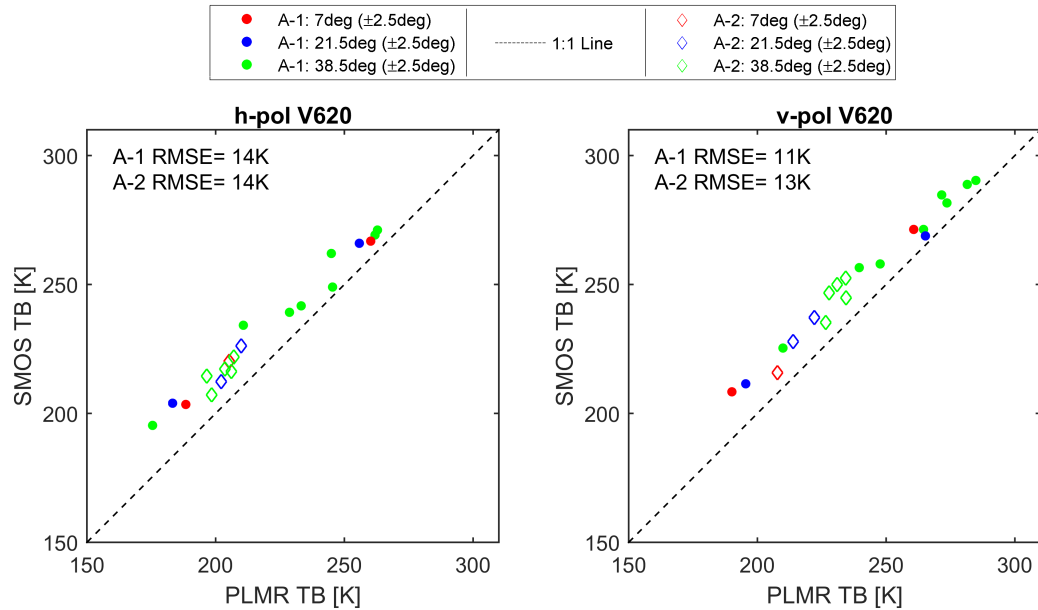


**Figure 7.2:** Comparison of SMOS L1C (V620) and airborne brightness temperature (TB) observations at three groups of incidence angles extracted for all AACES patches (A-1: AACES-1, A-2: AACES-2).

As mentioned earlier the SMOS L1C data product is under the mandate of ESA which is constantly working on the product quality. Since May 2015 the SMOS Level 1 products have been generated by the Level 1 Operational Processor (L1OP) and by the Near Real Time (NRT) Processor, both version 620. According to a release note by the SMOS Calibration team and Expert Support Laboratory Level 1 (2015) the main improvements of the new version were related to four main areas: i) the stability of measurements, ii) the reduction of spatial biases after enhancements in the calibration and image reconstruction techniques, iii) the quality of the third and fourth Stokes parameters, and iv) the RFI flagging. Additionally, an overview of the most significant changes is given by the CESBIO SMOS-Team (2015–04). Therefore, all data prior to May 2015 have been reprocessed with the new 620 version aiming at improved quality of these data.

Based on this development the comparison of the SMOS L1C and AACES PLMR data has been re-done accordingly for a new assessment of the two datasets. Both data have been grouped again into the three angular classes corresponding to the airborne L-band instrument configuration. The resulting plot is shown in Figure 7.2. With the

SMOS L1C (V620) data the comparison against PLMR brightness temperatures still confirms a distinct bias in terms of higher TB data for SMOS with respect to the PLMR observations with no specific angular trend for any of the three groups is noticeable. The rmse slightly improved with 11-14K compared to the previous SMOS L1C data

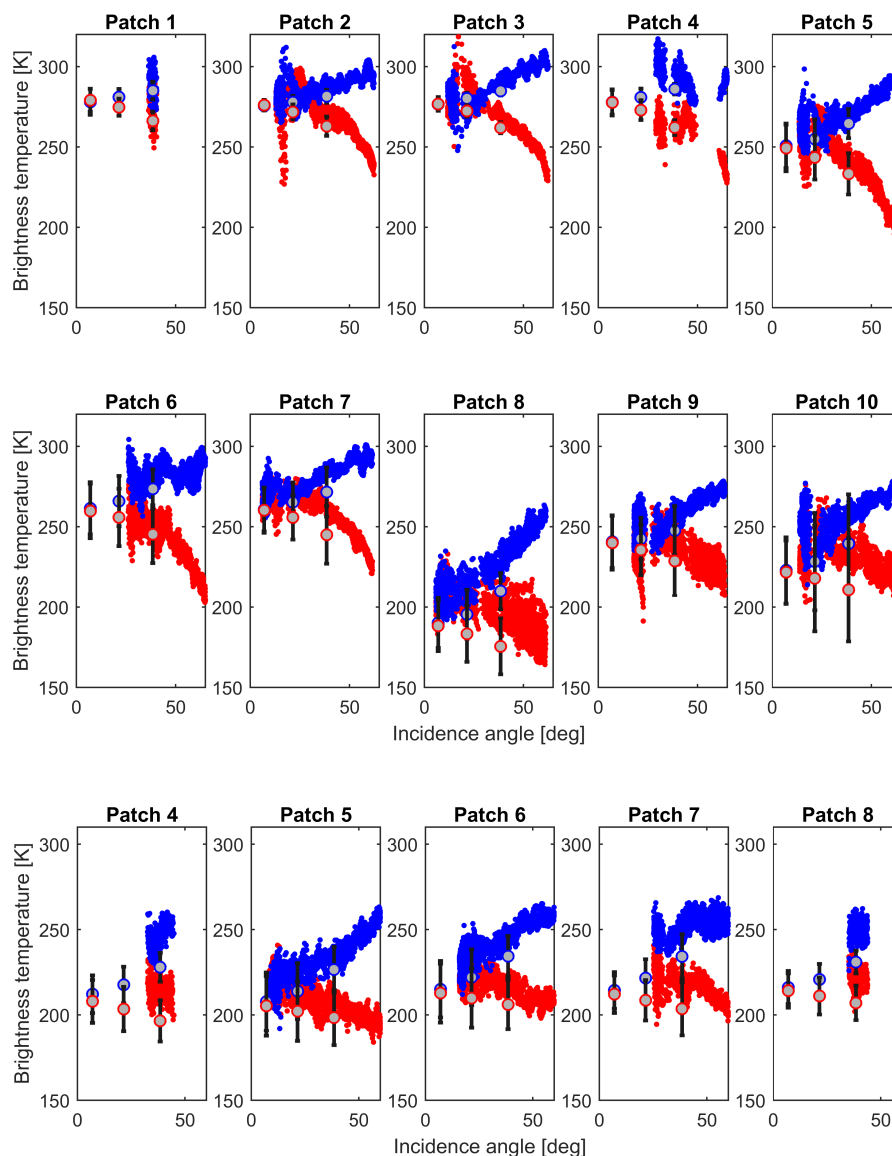


**Figure 7.3:** Comparison of SMOS L1C (V620) and PLMR TB observations for all AACES patches with v-polarization in blue and h-polarization in red, respectively. PLMR TB data are given by three correspondingly coloured angular focus points with its standard deviation indicated by black error bars. Top two rows: AACES-1; bottom row: AACES-2.

(V346). However, there is less data in the mid to low angular range. Mainly data from group 3 containing brightness temperature data taken at angles between  $36^{\circ}$ - $41^{\circ}$

are present in the comparison. In order to investigate this behaviour in a bit more detail, the SMOS-PLMR comparison was analysed in a slightly different perspective by evaluating all available brightness temperature data from both radiometers across the whole range of angles for the two field campaigns.

The plots in Figure 7.3 reveal the relation between the SMOS L1C and PLMR brightness temperature data. Across all the shown AACES patches there is a pronounced correlation between the two radiometers and the angular brightness response measured for the different instances in space and time. TB signatures in both dual-polarizations capture the soil moisture evolution during the field campaign. Especially, the large drop in the overall brightness temperature for patch 8, which was due to a series of extreme precipitation events with close to 200 mm of cumulative precipitation prior to the sampling of that particular patch. In terms of the available angular range of data, Figure 7.3 supports the previous findings depicting numerous instances where SMOS L1C data at small incidence angles have been flagged with the new processing scheme (620V) so that these data are not available anymore.

### **7.2.2 SMOS L3TB data**

As mentioned in section 7.1 there is a higher-level brightness temperature product available from SMOS data provided by CATDS-CPDC. The SMOS L3TB data product aims at producing a synthesis of daily global maps of enhanced soil moisture. A preliminary analysis of the L3TB data covering the time period of the AACES field campaigns is presented in this section. The comparison between SMOS L3TB and PLMR TB was done according to the previous SMOS L1C analysis, apart from the fact that the descending SMOS L3TB product was included in the analysis as well. Both datasets were grouped into three classes,  $4.5^{\circ}$ - $9.5^{\circ}$  (group 1),  $19^{\circ}$ - $24^{\circ}$  (group 2) and  $36^{\circ}$ - $41^{\circ}$  (group 3), for a comparison including the entire AACES study area.

First, both data sources were compared against each other per AACES patch covered during the field experiments (Figure 7.4 for AACES-1 and Figure 7.5 for AACES-2). The plots for AACES- 1 show strong scattering behaviour for both overpass L3TB

products yielding large rmse values of 25-32 K. However the overall trend between SMOS TB and PLMR TB, which was previously noticed in the L1C comparison, still holds here with SMOS L3TB data being higher on average with respect to PLMR measurements. Regarding the multi-angular data there is no distinct trend apparent between small, mid-range and data taken at large incidence angles. In terms of the ascending and descending dataset the scattering is slightly stronger for the latter with larger rmse values. This was expected due to the fact that PLMR observations were timed to be coincident with SMOS morning overpass (ascending). Hence the offset in time between PLMR TB measurements and the SMOS afternoon overpass might likely introduce an additional error source.

The comparison of the AACES-2 field experiment shows a narrow range of brightness temperatures, which conforms with the rather uniform moisture conditions that were observed on the ground. Consequently the rmse values are slightly improved compared to AACES-1 with 12-13 K (ascending), which is similar to the L1C data, and 17-19 K for descending data. Moreover, between the two polarizations there is a small shift with h-polarized data being usually lower than v-polarized data which becomes especially clear for the large incidence angles.

In order to analyse the data further, the comparison between L3TB and PLMR TB was shifted to the multi-angular focus by plotting all the available L3TB data per patch together with the PLMR measurements versus the incidence angle (Figure 7.6 and 7.7). Across the AACES study site and the PLMR TB observations the angular signature of the L3TB data varies drastically. For some patches there is obviously a strong agreement with the airborne measurements, whereas for some other patches such as patch 8 there is a large offset. Interestingly for this particular patch is, that the L1C data showed a similar response as the PLMR data with the drop in the overall brightness temperatures due to the heavy precipitation events ( $\geq 200$  mm/day) before the sampling day. The L3TB data however exhibit no distinct change in the angular behaviour. Overall the L3TB angular signatures are at a similar level of brightness temperature across the sampling dates even though the background climatic conditions

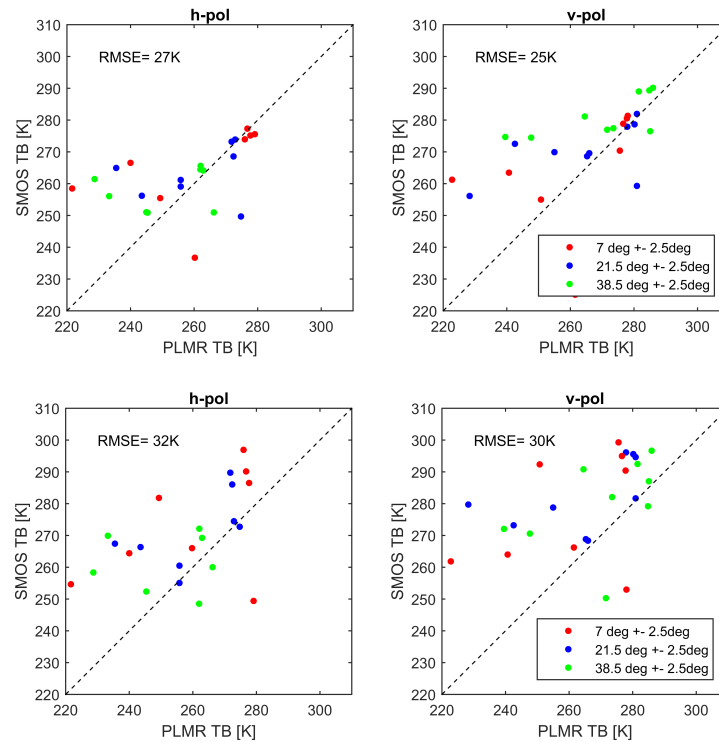


**Figure 7.4:** Comparison of SMOS L3TB data and PLMR TB observations at three groups of incidence angles extracted for the AACES-1 study area. Top: L3TB ascending data, bottom: L3TB descending data.

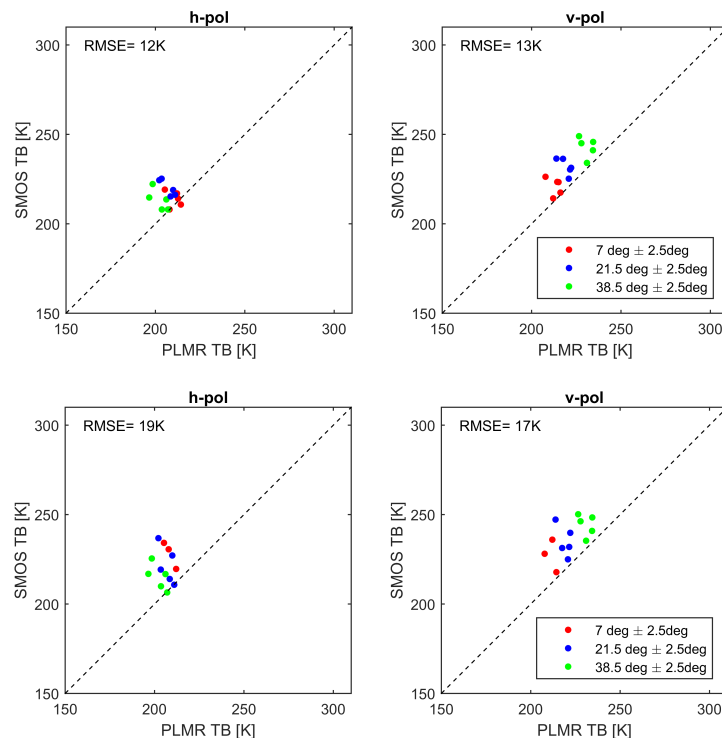


**Figure 7.5:** Comparison of SMOS L3TB data and PLMR TB observations at three groups of incidence angles extracted for the AACES-2 study area. Top: L3TB ascending data, bottom: L3TB descending data.

varied significantly. Best matches with PLMR TB data are observed for the very dry study regions patch 2-4 with exception of patch 1.

Similar results were obtained for the descending L3TB data. The scattering of the L3TB angular signatures seems slightly stronger than for the ascending data. In detail the data variability was especially prominent for the low- to mid-angular range from patch 6 and onwards. The previously mentioned good match for the dry patches demonstrates in this case a distinct offset. This behaviour actually might likely represent the natural moisture conditions since the topsoil surface moisture might indeed be drier in the afternoon (with SMOS descending overpass) due to the intense evaporation processes during the hot summer days.

During the AACES-2 winter campaign the moisture conditions for the five sampled patches were relatively similar. The brightness temperatures from PLMR and SMOS L3TB confirm that as well. The L3TB for the second campaign captured the dual-polarized trend however with a slight positive offset towards higher brightness temperatures. This is valid for all patches except for the last (patch 8). This behaviour is similar for ascending as well as descending SMOS data. The overall scattering as seen in the AACES-1 L3TB data is less pronounced for the second campaign.

In general, the SMOS L3TB data demonstrates its potential with regard to the AACES study site to capture the dominant soil moisture patterns. However, it seems that there are some aspects that need more attention (such as strong angular scattering, drop in soil moisture patch 8) in order to improve the quality of the L3TB SMOS product and thus provide good estimates and reliable maps of global soil moisture.

With respect to this it should be pointed out, that the AACES validation campaigns took place at an early stage after SMOS was launched and the system was still in test mode (e.g. switching between dual- and full-polarization). Thus, the original SMOS data quality from that time might have its drawback compared to SMOS data acquired at later stages in time.

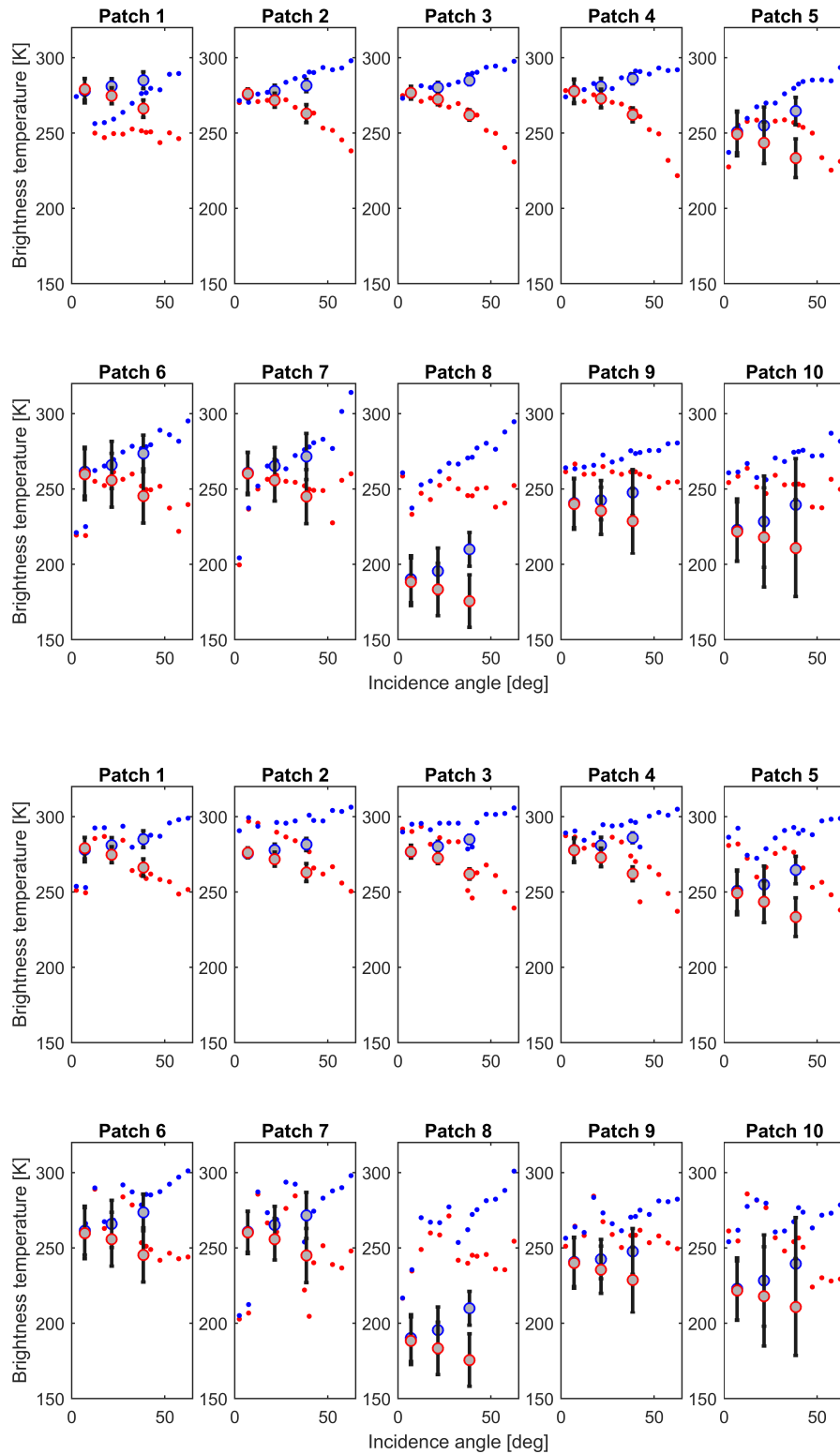


**Figure 7.6:** Comparison of SMOS L3TB and PLMR TB observations for all patches covered by AACES-1. PLMR TB data are given by three angular focus points with the standard deviation for each indicated by error bars. Underlain are the SMOS L3TB data as red (h-polarization) and blue dots (v-polarization). Top rows: SMOS L3TB ascending data. Bottom row: SMOS L3TB descending data.

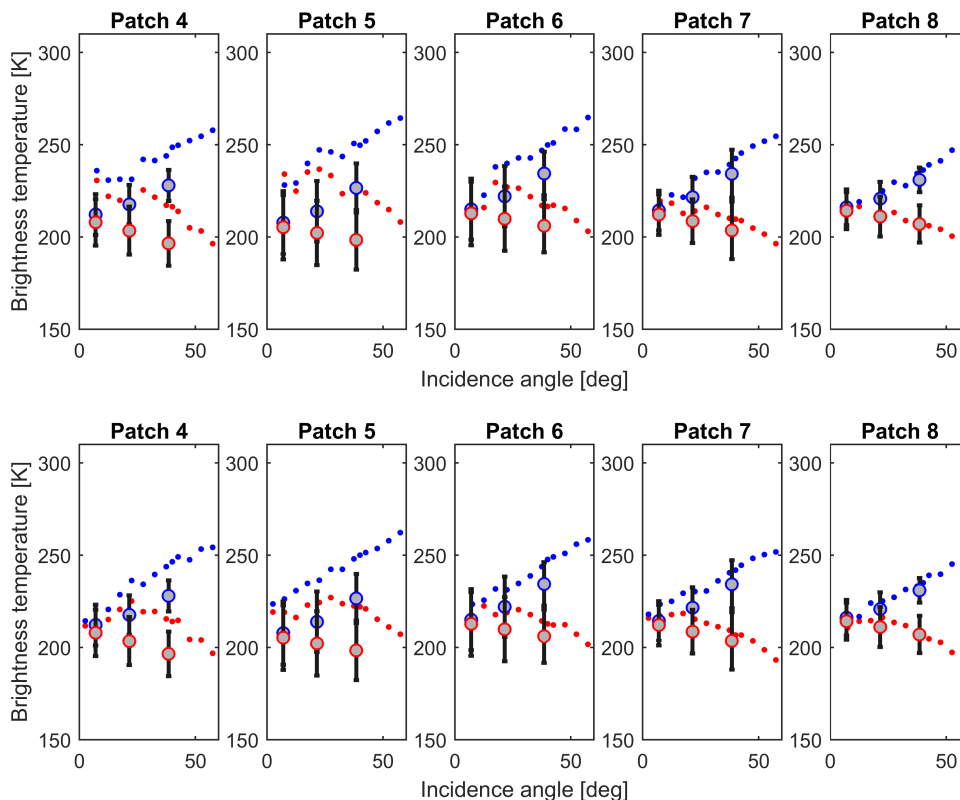


**Figure 7.7:** Comparison of SMOS L3TB and PLMR TB observations for all patches covered by AACES-2. PLMR TB data are given by three angular focus points with the standard deviation for each indicated by error bars. Underlain are the SMOS L3TB data as red (h-polarization) and blue dots (v-polarization). Top rows: SMOS L3TB ascending data. Bottom row: SMOS L3TB descending data.

### 7.3 Summary

The AACES campaigns were designed in such a way that the airborne (PLMR) and spaceborne (SMOS) observations were obtained quasi-simultaneously for the study site. The comparison of radiometer measurements for the individual AACES patches demonstrated a good agreement in terms of the captured moisture dynamics during the field experiments. Overall there was a distinct positive offset of the SMOS L1C data compared to the PLMR observation, which was consistent across all dates and both seasonal campaigns. There was no distinct trend for any of the tested angular classes. The rmse of 17-18 K was similar for both polarizations for the AACES-1 summer campaign, which was conducted roughly two months after SMOS launch. The data obtained during the following winter campaign demonstrated a more narrow range

in moisture conditions with a pronounced difference in rmse between h- (17 K) and v-polarization (9 K), respectively. Although the vegetation layer distinctively changed throughout the course of the field experiments from sparse dryland sites and juvenile crop canopy in summer to mature pastures and dense lush agricultural sites during the winter campaign, the observed rmse shift between the two polarizations was unexpected.

The available SMOS L1C brightness temperature data were sourced from two different versions V346 and V620. The latter was released in May 2015 after the level 1 processors were enhanced in order to improve the stability of the measurements, reduce the spatial biases after calibration and image reconstruction, and revise the RFI flagging. The re-analysis of the resulting SMOS L1C V620 data still demonstrated the positive offset in comparison with the dual-polarized PLMR data from both campaigns. Though the absolute rmse values decreased to 11-14 K with no distinct deviation between the polarizations, the total number of SMOS observations was significantly reduced after the reprocessing, resulting in a narrow range of angular measurements, mainly limited to angles between 36° and 41°. This significant limitation of the angular information of SMOS might have masked features such as described above with the rmse shift between the two polarizations, but might also help to detect outliers due to RFI or errors in the image reconstruction that would lead to a misinterpretation of the retrieval results.

Further analysis using the same PLMR data but in comparison with the SMOS L3TB product available for the time of the field campaign demonstrated a slightly different output. The L3TB product takes the temporal dynamics in terms of the climatic conditions into account to ultimately produce temporal averages of soil moisture. Hence the ascending and descending overpasses are treated separately. In terms of the direct evaluation of the PLMR measurements and the computed L3TB the rmse showed a large error of 25-27 K for the summer campaign and 12-13 K for the winter campaign. The scattering was rather strong for the wide range of moisture and vegetation conditions captured during the first campaign, with no significant trend towards any of the angular groups tested. In contrast, the results for the winter

campaign were relatively clustered within the angular ranges and confirmed the L1C results. One assumption might be that the strong scattering and the resulting high rmse for the first campaign might be due to the timing of the AACES-1 field experiment. As mentioned previously AACES-1 was conducted just two months after SMOS was launched. Due to the novel design of the satellite and changing polarization configurations between dual- and full-polarization mode during the initial operating phase of SMOS there might be some general issues with the SMOS data from that early phase.

# References for Chapter 7

- Barbosa, J. and A. Gutierrez (2014), *SMOS L1 Processor L0 to L1a Data Processing Model*, Report No.: SO-DS-DME-L1OP-0007, DEIMOS Engenharia, p. 186.
- CESBIO SMOS-Team (2015–04), *Brief history of changes to L2SM processor: SML2PP*, letter, CESBIO, p. 4 (cited on p. 111).
- Gutierrez, A., R. Castro, and N. Catarino (2014a), *SMOS L1 Processor L1a to L1b Data Processing Model*, Report No.: SO-DS-DME-L1OP-0008, DEIMOS Engenharia, p. 96.
- Gutierrez, A., R. Castro, and P. Vieira (2014b), *SMOS L1 Processor L1c Data Processing Model*, Report No.: SO-DS-DME-L1OP-0009, DEIMOS Engenharia, p. 80.
- Kerr, Y., E. Jacquette, A. Al Bitar, F. Cabot, A. Mialon, P. Richaume, A. Quesney, L. Berthon, and J. Wigneron (2013), *CATDS SMOS L3 soil moisture retrieval processor, Algorithm Theoretical Baseline Documentt (ATBD)*, Report No.: SO-TN-CBSA-GN-0029, CESBIO, p. 73.
- Kerr, Y. H., P. Waldteufel, P. Richaume, J.-P. Wigneron, P. Ferrazzoli, and R. J. Gurney (2011), *SMOS level 2 processor for soil moisture - Algorithm Theoretical Based Document (ATBD)*, Report ESA No.: SO-TN-ESL-SM-GS-0001, CESBIO, p. 121 (cited on p. 32).
- SMOS-BEC Team (2016), *SMOS-BEC Ocean and Land Products Description*, Report No.: BEC-SMOS-0001-PD. version 15, SMOS Barcelona Expert Centre, p. 24.
- SMOS Calibration team and Expert Support Laboratory Level 1 (2015), *Read-me-first note for the release of the SMOS Level 1 data products*, letter, ESA, p. 12 (cited on p. 111).



# 8

## Evaluation of multi-incidence angle soil moisture retrieval using AACES

**T**HE range of soil moisture and land surface conditions which were covered by the AACES field campaigns provide a wealth of data for intensive soil moisture research. In the previous studies on multi-incidence angle soil moisture retrieval (chapter 3, 4 and 5) multi-incidence angle data from field campaigns prior to the SMOS launch in 2009 was used. With the available AACES summer and winter datasets there is an additional data source to test and validate our recent findings from the NAFE datasets.

### **8.1 Analysis of canopy structure effects with respect to paper 1**

---

In chapter 3 the performance of L-MEB and the subsequent multi-incidence angle soil moisture retrieval over a NAFE'05 test site having extensive agricultural land use was investigated. The focus farm, named Merriwa Park, was characterized by mature wheat as dominant land cover. With respect to the prevalent vertical structure of the wheat stems a new set of vegetation structure parameters  $tt_p$  was determined with further analysis proving the new parameterization to ultimately enhance the L-MEB performance.

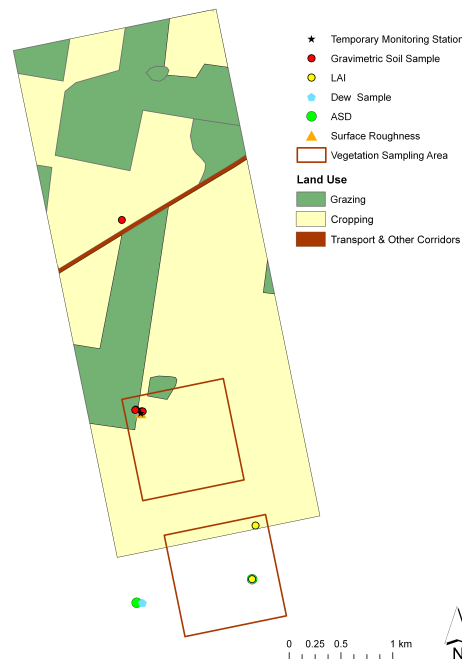


**Figure 8.1:** Overview of the land surface conditions and sampling strategy of patch 06 farm 12.

In order to test the key findings from chapter 3, AACES focus farm 12 in patch 6 (P06F12) with similar conditions and dominant agricultural land use was chosen for subsequent analysis (Figure 8.1). The farm was intensively monitored regarding soil moisture, vegetation and land surface conditions during the field experiment. A temporary monitoring station equipped with soil moisture and soil temperature sensors at different depth, a thermal infrared sensor, a leaf wetness sensor and a rain gauge provided time series data for the sampling period. Additional in-situ vegetation and gravimetric samples were taken to be analyzed in the lab. Coincident with the SMOS overpass the complete focus farm of 2 km x 5 km was mapped i) by the ground team using the HDAS system (Panciera et al., 2009) to obtain direct information on the soil moisture patterns across the farm, and ii) by the aircraft carrying the PLMR instrument to measure the L-band brightness temperatures for the test site.

With respect to the subsequent analysis the available multi-angle L-band measurements together with the ancillary data sampled at farm P06F12 were used to drive the L-MEB model to derive soil moisture. As described in chapter 3 two different sets of the vegetation structure parameterization were tested: a)  $tt_h=1$  and  $tt_v=8$  as suggested

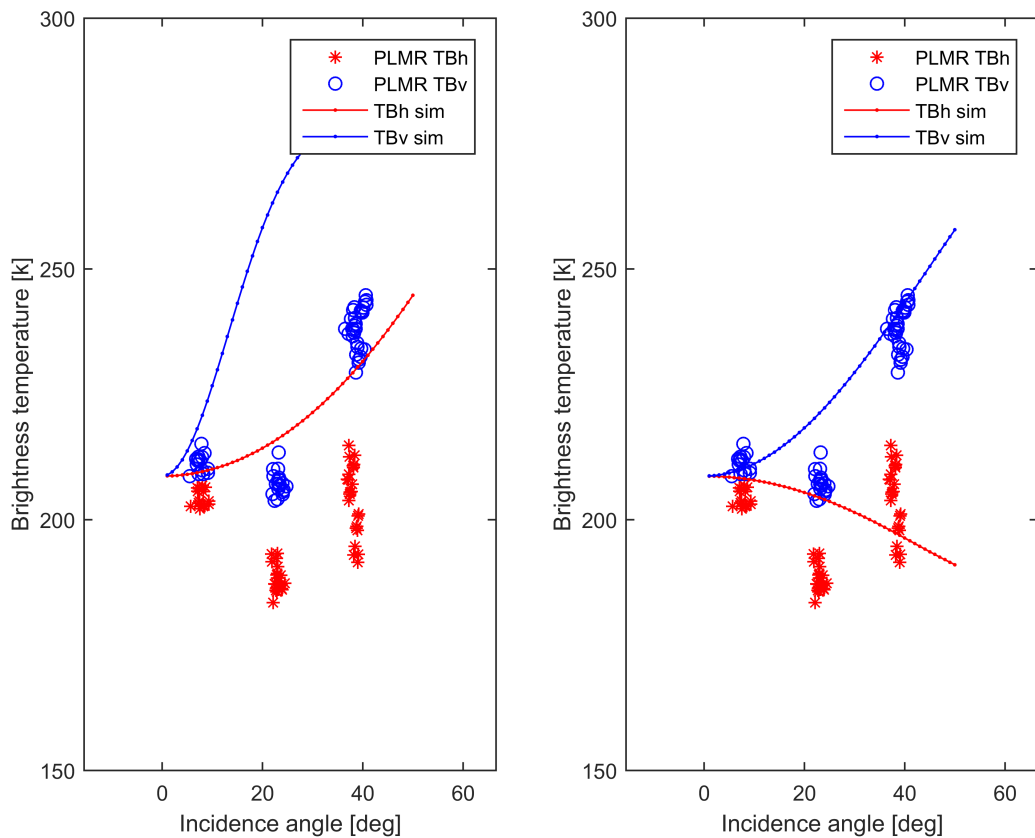


**Figure 8.2:** Comparison of PLMR TB for P06F12 with simulated brightness temperatures using vegetation structure parameters with  $tt_h=1$  and  $tt_v=8$  by Wigneron et al. (2007) (left) or vegetation structure parameterization as given in chapter 3 (right).

by Wigneron et al. (2007), and b) with  $tt_h=0.2$  and  $tt_v=1.4$ ; both accounting for the angular dependence of the optical depth and the transmissivity of a dominantly vertical canopy structure at different magnitude. Furthermore, after the successful retrieval the modelled soil moisture information was used to predict the angular brightness temperature response which then in turn was compared to the PLMR observations (Figure 8.2).

The simulated brightness temperatures do capture the observed angular trend given by the PLMR dataset. However, even though the retrieval model predicted the same soil moisture independently of the vegetation structure parameterization initially set to drive L-MEB, the simulated brightness temperatures differ. For the model assuming a strong angular dependency of the optical depth, as suggested by

Wigneron et al. (2007), the predicted TB response demonstrates a large discrepancy to the PLMR observations with an increasing TB trend with increasing incidence angle for both polarization curves. In contrast the forward model with a slightly reduced focus on the vertical vegetation structure and its impact on the transmissivity of the signal produces results closer to the PLMR observations with varying angular trends for h- and v-polarization. These findings are consistent with the results from chapter 3 where the modelled brightness temperature signatures using in-situ soil moisture data were significantly improved when the new set of vegetation structure parameters was used. In terms of the retrieved soil moisture the solution of the inverse algorithm yielded for both parameterizations a moisture content equivalent to what was determined by the ground team. The reasoning for this will further be addressed in the following section.

## **8.2 Analysis of angular moisture retrieval with respect to paper 2**

---

The potential of dual-polarized multi-incidence angle L-band data to facilitate the soil moisture retrieval while also reducing noise, such as radio frequency interference (RFI), has been demonstrated in numerous studies (Castro et al., 2012; Oliva et al., 2012; Wigneron et al., 2000). The wealth of data due to the quasi-simultaneous observations at different incidence angles available for the same spot on the earth surface is a preferable asset for the soil moisture retrieval. However, due to the diversity of L-band sensors, the instrument configurations, potential error sources, interferences and so on the range of available multi-angle data can sometimes be limited to only a narrow range of angles. The sensitivity of L-band soil moisture retrievals under these conditions of confined angular ranges was one of the core points of chapter 4. Thus, the subsequent analysis has focussed on the retrieval accuracy of the AACES airborne L-band data at different incidence angles. The dataset described in the previous section was used for this assessment.

With regard to a limited angular soil moisture retrieval, all available PLMR brightness temperature data were grouped according to the angular setting determined by the six radiometer beams from the airborne instrument. Hence, three groups of

**Table 8.1:** Results of angular soil moisture retrieval P06F12. Ground measured soil moisture: SM=0.34 [m<sup>3</sup>/m<sup>3</sup>]

Initial SM [m <sup>3</sup> /m <sup>3</sup> ]	Group 1 (4.5°-9.5°) SM retrieved [m <sup>3</sup> /m <sup>3</sup> ]	Group 2 (19°-24°) SM retrieved [m <sup>3</sup> /m <sup>3</sup> ]	Group 3 (36°-41°) SM retrieved [m <sup>3</sup> /m <sup>3</sup> ]
0.05	0.54	0.57	0.02
0.10	0.44	0.45	0.02
0.15	0.46	0.58	0.02
0.20	0.47	0.44	0.02
0.25	0.48	0.58	0.02
0.30	0.30	0.30	0.30
0.35	0.35	0.35	0.35
0.40	0.40	0.40	0.40
0.45	0.45	0.45	0.45
0.50	0.50	0.50	0.50

TB data including all observations between incidence angles of 4.5°-9.5° (group 1), 19°-24° (group 2) and 36°-41° (group 3), were used to drive the L-MEB model. The initial parameterization corresponded to the setting used in section 8.1.

As per Table 8.1, results show that the angular retrieval yielded different results for the modelled soil moisture depending on the angular input range chosen, but also depending on the initial soil moisture value - set in the model as first guess. Especially for the large angles together with an underestimation of the initial soil moisture value as input, a large discrepancy between model output and measured in-situ moisture was observed. The best performance of the three angular groups was demonstrated by the observations from very low incidence angles. This might be linked to the dominant wheat canopy at the test site with its distinct vertical vegetation structure, less signal interference between the soil and the vegetation layer are expected for near-nadir views. These results support the findings of the validation study in chapter 4.

### 8.3 Summary

---

The recent findings considering the multi-angular retrieval of airborne L-band observations from the NAFE dataset were tested and validated with the airborne L-band measurements obtained during the AACES campaign. The analysis first focussed on the angular dependency of the optical depth utilizing data from a test site with agricultural land use and vegetation canopy with a dominant vertical structure. As described in chapter 3 the parameterization of the L-MEB model was undertaken for two different sets. The first set used the vegetation structure parameterization applied by Wigneron et al. (2007) while the second included the parameters found in chapter 3. The following retrieval model yielded similar results of soil moisture for both parameterizations. However, further brightness temperature simulations based on the retrieved soil moisture demonstrated a significant difference in terms of comparison with i) the airborne observations over the test site and ii) the dual-polarized brightness temperature signatures across the available incidence angles.

The parameterization suggested by Wigneron et al. (2007) assumes a strong angular dependency of the optical depth. Consequently, the angular microwave signatures displayed a distinct increase of brightness temperatures with increasing incidence angle for both h- and v-polarization. Compared to the actual airborne observations the simulated brightness temperatures were overestimated by up to 50 K. In contrast, the parameterization determined in chapter 3, which also considers the vegetation structure effects on the optical depth but at a lower magnitude, led to brightness temperatures capturing the angular trend very close to the measurements. Recent studies have supported these findings (Yan et al., 2015), with Schwank et al. (2012) and Fernandez-Moran et al. (2015) additionally demonstrating small seasonal variations of the vegetation structure parameterization.

Even though the parameterizations of the vegetation structure and the resulting dependence of the optical depth on the polarization and incidence angles has been confirmed by several studies using airborne or tower-based microwave data, the impact at SMOS footprint scale is hypothesised to be minimal (Owe et al., 2001). Consequently,

the vegetation structure effects are currently neglected in the soil moisture retrieval processing of SMOS (Wigneron et al., 2017). More detailed research on this scale issue is needed.

Further analysis on the sensitivity of multi-parameter soil moisture retrieval to the incidence angle configuration was conducted as presented in chapter 4. Thus, the AACES test site data chosen for the vegetation structure analysis were also used here. The brightness temperature observations were classified according to their corresponding incidence angle information. The resulting three angular groups of 4.5°-9.5° (group 1), 19°-24° (group 2) and 36°-41° (group 3) were subsequently used to retrieve soil moisture, and in some cases, additional parameters of the L-MEB model.

The results confirmed the previous findings of best retrieval results for observations taken at small incidence angles. This is likely linked to the dominant vertical structure of the test site canopy. A recent study by Wang et al. (2016) found similar results regarding the sensitivity of various model parameters at near-nadir views. Using an extended Fourier amplitude sensitivity test they suggested that future calibration procedures need to take into account incidence angle sensitivities of model parameters such as vegetation structure, optical depth and surface roughness.

## References for Chapter 8

- Castro, R., A. Gutierrez, and J. Barbosa (2012), “A First Set of Techniques to Detect Radio Frequency Interferences and Mitigate Their Impact on SMOS Data,” *IEEE Transactions on Geoscience and Remote Sensing*, 50(5), pp. 1440–1447, DOI: 10.1109/tgrs.2011.2179304 (cited on p. 126).
- Fernandez-Moran, R., J.-P. Wigneron, E. Lopez-Baeza, A. Al-Yaari, A. Coll-Pajaron, A. Mialon, M. Miernecki, M. Parrens, P. Salgado-Hernanz, M. Schwank, et al. (2015), “Roughness and vegetation parameterizations at L-band for soil moisture retrievals over a vineyard field,” *Remote Sensing of Environment*, 170, pp. 269–279 (cited on p. 128).
- Oliva, R., E. Daganzo-Eusebio, Y. H. Kerr, S. Mecklenburg, S. Nieto, P. Richaume, and C. Gruhier (2012), “SMOS radio frequency interference scenario: status and actions taken to improve the RFI environment in the 1400-1427-MHz passive band,” *IEEE Transactions on Geoscience and Remote Sensing*, 50(5), pp. 1427–1439 (cited on p. 126).
- Owe, M., R. A. M. de Jeu, and J. P. Walker (2001), “A methodology for surface soil moisture and vegetation opticaldepth retrieval using the microwave polarization difference index,” *IEEE Transactions on Geoscience and Remote Sensing*, 39(8), pp. 1643–1654, DOI: 10.1109/36.942542 (cited on pp. 8, 128).
- Panciera, R., M. Allahmoradi, O. Merlin, R. Young, and J. P. Walker (2009), *The Hydraprobe Data Acquisition System (HDAS) V.5: User Guide*, University of Melbourne, p. 30 (cited on p. 124).
- Peischl, S., J. P. Walker, D. Ryu, Y. H. Kerr, R. Panciera, and C. Rüdiger (2012b), “Wheat Canopy Structure and Surface Roughness Effects on Multiangle Observations at L-Band,” *IEEE Transactions on Geoscience and Remote Sensing*, 50(5), pp. 1498–1506, DOI: 10.1109/tgrs.2011.2174644 (cited on p. 43).

- Peischl, S., J. P. Walker, N. Ye, D. Ryu, and Y. Kerr (2014), “Sensitivity of multi-parameter soil moisture retrievals to incidence angle configuration,” *Remote Sensing of Environment*, 143(0), pp. 64–72, DOI: <http://dx.doi.org/10.1016/j.rse.2013.11.019> (cited on p. 59).
- Schwank, M., J. P. Wigneron, E. Lopez-Baeza, I. Volksch, C. Matzler, and Y. H. Kerr (2012), “L-Band Radiative Properties of Vine Vegetation at the MELBEX III SMOS Cal/Val Site,” *Geoscience and Remote Sensing, IEEE Transactions on*, 50(5), pp. 1587–1601, DOI: 10.1109/tgrs.2012.2184126 (cited on p. 128).
- Wang, Z., T. Che, and Y.-A. Liou (2016), “Global sensitivity analysis of the L-MEB model for retrieving soil moisture,” *IEEE Transactions on Geoscience and Remote Sensing*, 54(5), pp. 2949–2962 (cited on p. 129).
- Wigneron, J.-P., T. Jackson, P. O’neill, G. De Lannoy, P. De Rosnay, J. Walker, P. Ferrazzoli, V. Mironov, S. Bircher, J. Grant, et al. (2017), “Modelling the passive microwave signature from land surfaces: A review of recent results and application to the L-band SMOS & SMAP soil moisture retrieval algorithms,” *Remote Sensing of Environment*, 192, pp. 238–262 (cited on p. 129).
- Wigneron, J.-P., P. Waldteufel, A. Chanzy, J.-C. Calvet, and Y. H. Kerr (2000), “Two-dimensional microwave interferometer retrieval capabilities over land surfaces (SMOS Mission),” *Remote Sensing of Environment*, 73(3), 347GH Times Cited:75 Cited References Count:37, pp. 270–282, DOI: 10.1016/S0034-4257(00)00103-6 (cited on pp. 5, 29, 126).
- Wigneron, J.-P., Y. H. Kerr, P. Waldteufel, K. Saleh, M. J. Escorihuela, P. Richaume, P. Ferrazzoli, P. de Rosnay, R. J. Gurney, J.-C. Calvet, J. P. Grant, M. Guglielmetti, B. Hornbuckle, C. Mätzler, T. Pellarin, and M. Schwank (2007), “L-band Microwave Emission of the Biosphere (L-MEB) Model: Description and calibration against experimental data sets over crop fields,” *Remote Sensing of Environment*, 107(4), pp. 639–655, DOI: 10.1016/j.rse.2006.10.014 (cited on pp. 27, 125, 126, 128).
- Yan, S., L. Jiang, L. Chai, J. Yang, and X. Kou (2015), “Calibration of the L-MEB model for croplands in HiWATER using PLMR observation,” *Remote Sensing*, 7(8), pp. 10878–10897 (cited on p. 128).



## **Part IV**

# **Resume and Perspective**

---

# 9

## Conclusion

**T**HIS thesis used the L-MEB retrieval algorithm, which is part of a set of mathematical models of ESA's L2SM processor, to investigate the utility of multi-incidence angle retrieval of soil moisture at L-band. Additionally, an extensive airborne validation campaign called AACES was designed, and conducted shortly after the launch of SMOS, for testing of the multi-incidence angle capability it provided. The validation strategy of the field experiment was based on intensive use of direct ground measurements for a comprehensive characterization of the vast study area, together with airborne L-band measurements, covering a minimum of 20 independent SMOS pixel. Consequently, this thesis ultimately aims at supporting a better understanding and utilization of multi-incidence angle observations for the purpose of large scale soil moisture mapping.

### 9.1 L-MEB related key findings

---

Initial work focussed on application of the L-MEB retrieval model on two available datasets from the NAFE field campaigns in Australia. After adapting the L-MEB algorithm to multi-incidence angle data the work included a study on wheat canopy structure and soil roughness effects on L-band multi-angle observations.

The study results presented in chapter 3 proposed a modification of the L-MEB model parameterization for wheat canopy. These recommendations focussed especially on the vegetation structure settings, described by the two vegetation structure parameters  $tt_h$  and  $tt_v$ , that account for the angular dependency of the vegetation optical depth. The default parameterization of  $tt_h=1$  and  $tt_v=8$  yielded an rmse of 31 K for wet and 26 K for dry conditions compared to airborne observations. Moreover, it was shown that the default fixed surface roughness factor  $H_R$  might not be the best choice for the surface conditions tested in this research. After the modification of the vegetation structure parameterization ( $tt_h=0.2$ ,  $tt_v=1.4$ ) and calibrated roughness the rmse was reduced to 2 K and 5 K, for wet and dry conditions respectively. Without considering these parameter updates, soil moisture retrieval errors of up to  $0.3 \text{ m}^3/\text{m}^3$  could be expected, which exceeds the SMOS target accuracy for the soil moisture product of  $0.04 \text{ m}^3/\text{m}^3$ .

Subsequently in chapter 4 a two-step analysis of different multi-parameter retrievals was conducted in order to investigate the sensitivity of the retrieval to the angular viewing configurations of an L-band radiometer. It was demonstrated that best retrieval results were obtained when the complete range of SMOS angles from  $0-50^\circ$  were used, instead of limiting the brightness temperature measurements to a specific range of incidence angles. This was particularly important for multi-parameter retrieval being ancillary data such as vegetation water content or soil temperature derived simultaneously with soil moisture. It was found that a sufficient representation of the brightness temperature trend across the angle range is required to ensure high quality parameter estimates. However, if the multi-angle observations are confined to a limited range of angles, the utilization of the near-nadir observations should be preferred over the mid-range angle measurements - especially when a mature wheat canopy cover is present.

The analysis in chapter 5 explored the single- and multi-parameter retrieval of multi-angle observations at different acquisition times using aircraft data. The multi-angle L-band measurements were taken around dawn 6 A.M. and around dusk 6 P.M., to simulate the ascending and descending overpass times of SMOS. The study focussed on

a pasture dryland site and tested the quality of different retrieval scenarios for both time frames. Results suggested that the retrieval accuracy was independent of acquisition time considering the retrieved soil moisture as well as the ancillary parameter derived from the model. Moreover, the usage of the multi-angle measurements to calculate the polarization index helped for a better understanding of the vegetation conditions due to a noticeable contrast between the low and high angular groups implying a rather sparse vegetation cover.

## **9.2 AACES related key findings**

---

The launch of SMOS in November 2009 introduced a new innovative concept of L-band observations from space for global soil moisture and ocean salinity maps. Previous research was mainly based on synthetic studies and small-scale field experiments to develop mathematical models which might be applied to the anticipated spaceborne SMOS data. Consequently, for calibration and validation campaigns all over the world were needed, providing a vital source for the assessment of SMOS products.

In chapter 6 we described the design, objectives and realisation of two extensive field campaigns, AACES-1 and AACES-2, which were specifically targeted to meet the validation requirements of SMOS. The study site chosen comprised the entire Murrumbidgee River catchment in South-East Australia. With an approximate 500 km x 100 km extent, which equates to a minimum of 20 independent and 40 overlapping SMOS pixels, the AACES validation site included an interesting range of soil and vegetation characteristics. The two campaigns were set to take place in summer and winter to capture an even wider range of moisture, vegetation and climatic conditions. Both campaigns included multi-angle L-band airborne measurements of 50 km x 100 km (called patch) per sampling day which were conducted coincident with the ascending SMOS overpass over the area. Additionally ground measurements of soil moisture, soil temperature, surface roughness, vegetation water content, LAI and dew were collected at representative focus farms of 2 km x 5 km.

An initial analysis of the multi-incidence angle L-band PLMR brightness temperatures compared to the SMOS L1C TB product was presented including two different versions of the L1C TB data. The SMOS L1C (V346) product had been processed with the prototype algorithm baseline as available at the end of the commissioning phase, whereas the L1C (V620) corresponds to the SMOS brightness temperature data product generated by the current-state-of-the-art processor. The comparison demonstrated for both versions of L1C data a distinct offset of SMOS TB with maximum of 18 K rmse with respect to the PLMR TB measurements. This positive offset was consistent for the two polarization, across the different angles and field campaigns. The usage of L1C (V620) data slightly reduced the offset but also had a reduced number of available measurements (especially low and mid-range angles), which were potentially flagged by the processor and hence removed from the dataset. A preliminary analysis on the latest L3TB brightness temperature product provided by CATDS showed rather different results with a lot of scattering in the data compared to PLMR. For some AACES patches there was a very good agreement between the multi-angular PLMR measurements and the SMOS L3TB product, while for others the L3TB data did not represent the actual conditions, e.g. there was no indication of a drop in brightness temperatures even though the PLMR and L1C data showed that particular rainfall event. Overall a distinct feature stood out in the direct comparison that suggested i) either a tendency of SMOS observations towards higher brightness temperatures, which in turn could lead to lower soil moisture estimates than recorded by in-situ monitoring networks, or ii) a tendency of PLMR towards lower brightness temperatures causing the opposite on the soil moisture estimates. This aspect together with the application of the proposed modification of the L-MEB parameterization will be subject to ongoing research.

# 10

## Future Work

**T**HE applicability of using multi-incidence angle L-band observations to facilitate near-surface soil moisture retrieval has been demonstrated at different instances in this thesis, through synthetic studies and use of airborne L-band data from numerous field campaigns. Moreover the benefit of field experiments for the validation of SMOS data products has been presented. The following section will discuss further research options, expanding the current stage of this study.

### **1. Evaluation of the vegetation structure parameterization**

Analysis on the L-MEB performance over a wheat covered test site resulted a new parameterization of the vegetation structure characterization in the model. However, a broader application on different agricultural land cover with similar characteristics as wheat (such as barley or maize) would provide a more general validation for the findings. Additionally, the study focussed on the spatial scale determined by the PLMR measurements and the available ground data from the field experiments. An interesting step would be analysis of the suggested new parameterization at a different spatial scales comparable to that of the SMOS L1C data product which is available at approximately 40 km spatial resolution. Due to the coarser resolution of SMOS the vegetation structure effect might not even be noticed, as the impact of the structure on the composite brightness temperature might dilute across the likely heterogeneous land cover grid pixel.

## **2. Evaluation of the angular single- and multi-parameter retrieval**

The present thesis work demonstrated a comprehensive synthetic study on the sensitivity of the single- but also multi-parameter retrieval from multi-angular L-band data, which was subsequently tested on a dataset from the NAFE field campaign. Further research on the retrieval sensitivity using SMOS brightness temperature data, limited to different angular ranges, for varying multi-parameter retrievals is suggested.

## **3. Evaluation of the SMOS L2SM data product using AACES**

An extensive dataset specifically designed for validation of SMOS was collected. A preliminary analysis of comparing PLMR TB against the SMOS brightness temperature products L1C as well as L3TB for the available angular ranges was shown. It suggested that both radiometers continuously measured similar patterns across the study area and a time series of SMOS overpasses for approximately 2 months. The cause of the offset could not be exactly determined in this study, so further tests with support of the available ground data should be done, taking into account the issue of representativeness when SMOS is compared to the AACES patch data. Additionally, ongoing research in terms of other SMOS products could include an inter-comparison of the SMOS L2SM soil moisture data product against PLMR retrieved soil moisture, which in turn might be validated using the ground measured soil moisture data from the HDAS system together with the monitoring station data.

## **Part V**

# **Appendix**

---



## Conference Proceeding I

**T**HIS appendix includes a research paper which has resulted from the studies undertaken for this degree and is published in a peer-reviewed conference proceeding.

**Peischl, S.**, Allahmoradi, M., Barrett, D., Gurney, R. J., Kerr, Y. H., Kim, E. J., LeMarshall, J., Rüdiger, C., Ryu, D., and Ye, N.: Towards validation of SMOS using airborne and ground data over the Murrumbidgee Catchment, 18<sup>th</sup> International Congress on Modelling and Simulation (MODSIM), Cairns, Australia, 13-17 July 2009, ISI:000290045003111, pp.3733-3739, 2009.

18<sup>th</sup> World IMACS / MODSIM Congress, Cairns, Australia 13-17 July 2009  
<http://mssanz.org.au/modsim09>

## Towards validation of SMOS using airborne and ground data over the Murrumbidgee Catchment

S. Peischl<sup>1</sup>, J.P. Walker<sup>1</sup>, M. Allahmoradi<sup>1</sup>, D. Barrett<sup>2</sup>, R. Gurney<sup>3</sup>, Y. Kerr<sup>4</sup>, E. Kim<sup>5</sup>, J. LeMarshall<sup>6</sup>, C. Rüdiger<sup>1</sup>, D. Ryu<sup>1</sup> and N. Ye<sup>1</sup>

<sup>1</sup>Department of Civil and Environmental Engineering, The University of Melbourne, Australia

<sup>2</sup>Sustainable Minerals Institute, The University of Queensland, Brisbane, Australia

<sup>3</sup>NERC Environmental Systems Science Centre, University of Reading, United Kingdom

<sup>4</sup>Biospheric Processes, CESBIO, France

<sup>5</sup>Hydrospheric and Biospheric Sciences Laboratory, NASA Goddard Space Flight Center, United States

<sup>6</sup>The Centre for Australian Weather and Climate Research, Bureau of Meteorology, Australia

Email: [s.peischl@pgrad.unimelb.edu.au](mailto:s.peischl@pgrad.unimelb.edu.au)

**Abstract:** With the launch of the European Space Agency's Soil Moisture and Ocean Salinity (SMOS) satellite scheduled for mid 2009, the first long-term space-borne passive microwave observations at L-band (~ 1.4 GHz) will soon be available. Consequently, SMOS will be the first mission dedicated to global mapping of near-real-time surface soil moisture information. Though space-borne microwave instruments have measured global data at high frequencies (e.g. C- and X-band) for the last 20 years, this innovative L-band radiometer will use a new synthetic aperture concept that will provide observations at multiple incidence angles. Consequently, the observed brightness temperature data and derived soil moisture product must be validated. To achieve this, intensive field campaigns are being planned world-wide to support the satellite mission with reliable data from i) passive microwave airborne observations at L-band, ii) detailed ground measurements of surface soil moisture content and associated environmental parameters, and iii) long-term soil moisture monitoring network data from anchor sites (e.g. Murrumbidgee in Australia, Valencia in Spain, Upper Danube in Germany etc.). With the SMOS launch likely to take place in the later part of 2009, Australia is particularly well positioned for conducting the first intensive SMOS validation campaign during its spring.

The Australian Airborne Cal/val Experiment for SMOS (AACES) will provide one of the most comprehensive assessments world-wide, due to its combined airborne and in-situ data collection strategy across an extensive transect of the Murrumbidgee catchment in south-eastern Australia. This area is unique as it comprises a distinct variety of topographic, climatic and land cover characteristics, and therefore represents an excellent validation site for the land component of this satellite mission. Moreover, a large database of previous campaign measurements, continuous soil moisture monitoring stations, and meteorological data over the past seven years is available for this region.

A total of four airborne campaigns are planned to cover a 100 km x 500 km (more than 20 SMOS pixels) transect of the Murrumbidgee catchment in its entirety at 1 km resolution using an L-band radiometer. The primary airborne instruments will include the Polarimetric L-band Multibeam Radiometer (PLMR) and thermal infrared sensors, supported by surface soil moisture content, soil temperature and rainfall data from the Murrumbidgee monitoring network. This will be further complemented by intensive soil moisture observations with the Hydraprobe Data Acquisition System (HDAS), short-term soil moisture and temperature monitoring stations with additional leaf wetness and thermal infrared measurements, and extensive vegetation characterisation. The four separate month-long campaigns are planned to extend across a two year timeframe, enabling the effects of seasonal variation in vegetation condition and land cover change to be assessed in addition to soil moisture. Consequently, issues related to snow cover, litter, vegetation dynamics etc. will be assessed in relation to soil moisture retrieval. This paper outlines the airborne campaigns and related ground monitoring for the first SMOS validation campaign, together with some of the major science questions to be addressed. Persons interested in participating in these campaigns are encouraged to contact the authors.

**Keywords:** SMOS, AACES, soil moisture, remote sensing, Murrumbidgee, airborne, passive microwave

Peischl *et al.*, Towards Validation of SMOS Using Airborne and Ground Data

## 1. INTRODUCTION

Soil moisture is a key variable in the water, carbon, and energy cycle. It controls not only the interactions at the soil-atmosphere interface by regulating the partitioning of rainfall into infiltration and runoff, but also the evapotranspiration and photosynthetic activity of plants (Western *et al.*, 1999). Amongst available remote sensing techniques, including visible, thermal infrared and microwave, which have each been tested for measuring spatial and temporal variations of soil moisture, passive microwave remote sensing has proven to be the most promising, because of its all-weather capability, the direct relationship with soil moisture through the soil's dielectric constant, and the reduced sensitivity to land surface roughness and vegetation cover (Njoku *et al.*, 2002). Though microwave data suffers from low resolution and attenuation effects of dense vegetation, microwave observations at L-band (~1.4 GHz) are preferred for near-surface soil moisture monitoring, since they are least affected by the vegetation and atmosphere when compared to shorter wavelengths (Wigneron *et al.*, 2003).

The first passive microwave satellite dedicated to soil moisture observation will be the Soil Moisture and Ocean Salinity (SMOS) mission, scheduled for launch by the European Space Agency (ESA) in the second half of 2009. The baseline SMOS payload is an L-band two dimensional interferometric radiometer that aims to provide global maps of soil moisture with accuracy better than 4 %  $\text{m}^3/\text{m}^3$  for vegetation water content less than 4  $\text{kg}/\text{m}^2$ , with a temporal repeat at least once every 3 days, and with a spatial resolution better than 50 km (Kerr *et al.*, 2001). Due to its new design and measurement technique, which uses aperture synthesis technology to simulate the large antenna size required for space-borne measurement at L-band, the SMOS brightness temperature values need to be calibrated and validated on different test sites. Moreover, because of the land surface heterogeneity that exists at 50 km scale in terms of topography, land cover type, and vegetation condition, the derived soil moisture products must also be validated globally. Experimental sites in Europe are limited to areas not larger than a single SMOS pixel and/or based on single aircraft transects through several SMOS pixels. Consequently the Australian Airborne Cal/val Experiment for SMOS (AACES) is expected to provide the most extensive validation of this new sensor. AACES plans to cover an entire 100 km x 500 km area of the Murrumbidgee Catchment in south-eastern Australia with 1 km resolution passive microwave L-band and supporting data, corresponding to about 20 independent SMOS pixels that are representative of a range of land surface conditions. This well-monitored catchment was also the focus of the very successful National Airborne Field Experiment (NAFE) in 2006, where a single SMOS pixel was monitored for a three week period (Merlin *et al.*, 2008).

With the SMOS launch likely to take place in the later part of 2009, Australia is particularly well positioned for conducting the first intensive SMOS validation campaign during its spring. Data collected from the AACES field campaigns are expected to not only validate the SMOS brightness temperature data (level 1C product), but also validate (and improve) the SMOS derived soil moisture (level 2 product), by addressing several important research issues. First, the low spatial resolution of SMOS means that individual pixels will always consist of a range of surface types that contribute differently to the overall microwave response. Such characteristics have been shown to significantly affect the soil moisture retrieval, leading to errors greater than the SMOS target accuracy if not properly accounted for (R. Panciera, "Effect of Land Surface Heterogeneity on Satellite Near-Surface Soil Moisture Observations", PhD Thesis, Submitted, Department of Civil and Environmental Engineering, University of Melbourne). Second, the soil moisture retrieval from SMOS requires ancillary information on soil properties, vegetation transmissivity, soil effective temperature, and surface roughness, to name a few. While the dual polarised (and multi-angle) information from SMOS will allow joint retrieval of some ancillary parameters, several assumptions are still required, and the current approach of SMOS is to use soil temperature information from numerical weather prediction, which is known to be inaccurate. Consequently, SMOS assumptions and derived ancillary information need to be tested.

A series of four AACES campaigns are planned for the next two years, with one in each of the four seasons. The first of these campaigns is planned for the southern hemisphere spring of 2009, extending across the month of November. This will be followed by a summer campaign in February 2010, a winter campaign in August 2010 and finally an autumn campaign in April 2011. Each campaign will extend for between three to four weeks in duration, dependent upon the actual SMOS orbit coverage, being the length of time required to cover the Murrumbidgee transect (13 flights) once with flights that coincide with SMOS overpasses. Consequently, the huge amount of airborne and ground data collected across the catchment will characterise a range of vegetation and soil moisture conditions in response to seasonal variability and land cover types.

In short, the planned campaigns include: i) time series of soil moisture and temperature profiles, leaf wetness, and thermal infrared data from long-term and/or temporary monitoring stations; ii) point-based surface soil moisture and temperature observations, gravimetric soil and vegetation samples, and surface roughness

Peischl *et al.*, Towards Validation of SMOS Using Airborne and Ground Data

profiles collected by ground teams; iii) airborne brightness temperature observations as well as thermal infrared data; and iv) spaceborne brightness temperature and soil moisture products from SMOS, complemented by high frequency microwave, thermal infrared, shortwave infrared and visible data from complementary satellites (e.g. WindSAT, MTSAT and MODIS). The details of the AACES campaigns are described in this paper.

## 2. STUDY AREA

The four AACES field campaigns will take place across the Murrumbidgee River Catchment ( $-33^{\circ}$  to  $-37^{\circ}$  S,  $143^{\circ}$  to  $150^{\circ}$  E), which is a sub-catchment of the Murray Darling Basin located in south-eastern Australia (Figure 1). The entire Murrumbidgee catchment covers a total area of approximately  $82,000 \text{ km}^2$ . Due to its distinctive topography with elevations ranging from 50 m in the west to 2000 m in the east, there exists a significant spatial variability in its climate (alpine to semi-arid), soil type, vegetation and land use (Figure 2).

The annual cumulative precipitation ranges from 300 mm in the west to 1900 mm towards the east (Australian Bureau of Meteorology, 1998). Accordingly, due to the drier climatic conditions in the west almost the same amount of water evaporates as rain falls, whereas in the higher elevated eastern parts of the catchment the actual evaporation rate represents only approximately half of the regional precipitation (Australian Bureau of Meteorology, 1998).

During the winter period, precipitation above about 1200 m typically falls as snow, with regions above 1400 m usually covered by snow for a few weeks of the year. Moreover, above 1800 m the snow cover can last for 4 months or more (Whetton *et al.*, 1996; see Figure 2).

In general, there is a range of sand to clay soil types present, with the western plains areas dominated by fine textured soils which become coarser towards the east (McKenzie *et al.*, 2000). Considering these aspects, the catchment is mainly used for agricultural purposes, including irrigation areas in the mid to lower Murrumbidgee, broad-acre cropping, and extensive grazing (Australian Bureau of Rural Science, 2006). The steeper parts in the east are predominantly characterized by a mixture of native eucalypt and exotic forestry plantations.

Overall the Murrumbidgee catchment offers a range of geographic diversity within a relatively confined area. This makes it an ideal validation site for the land component of the SMOS mission. Nevertheless, considering the size of the satellite footprint, there are still regions that are relatively homogeneous (especially the western part of the catchment) in regards to climate, soil type and vegetation when compared to other study sites in Europe and the United States.

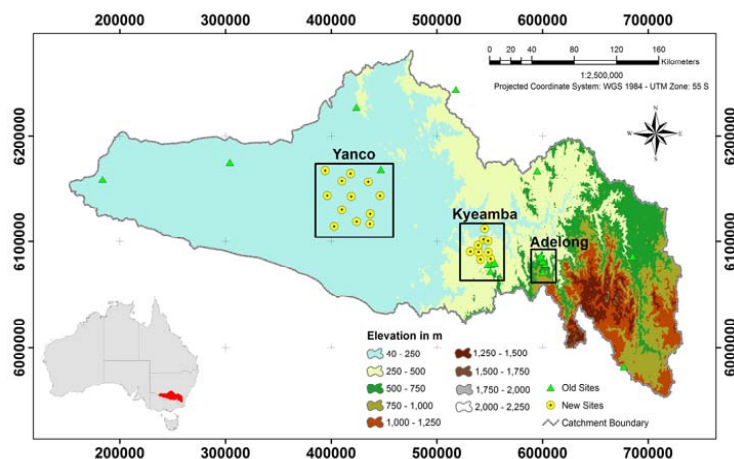


**Figure 1.** Murrumbidgee River catchment showing elevation and soil moisture monitoring network, together with names of areas having intensive monitoring. Note also that elevations above 1200 m are subject to periodic snow cover.

Peischl *et al.*, Towards Validation of SMOS Using Airborne and Ground Data

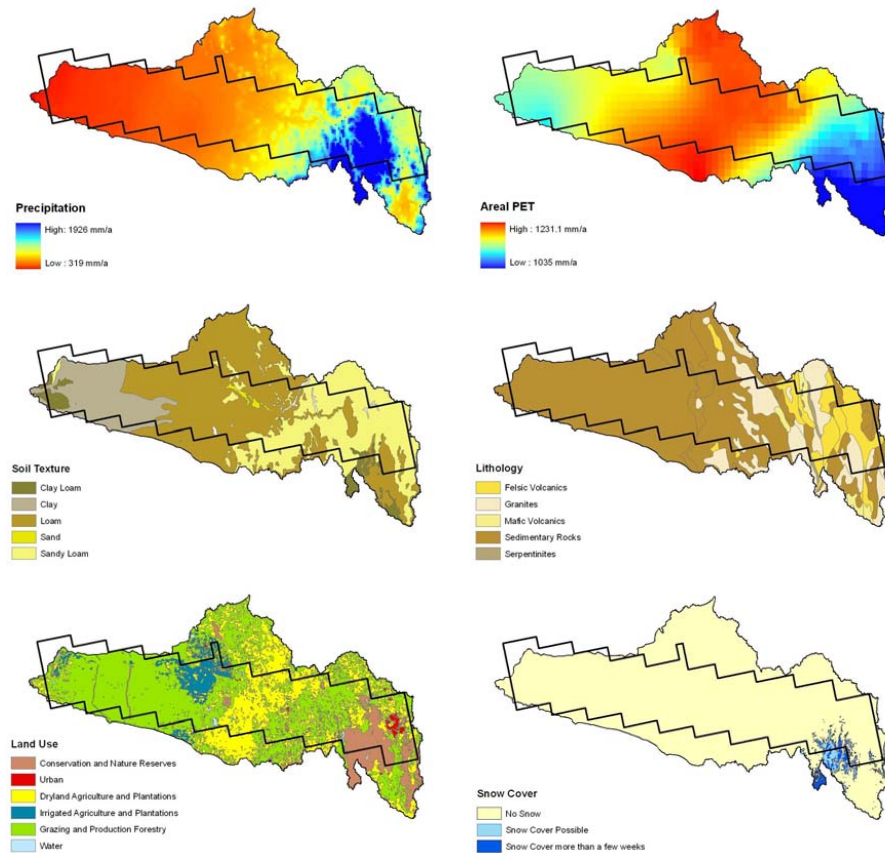


**Figure 2.** Topographic, climatic, soil and land use diversity across the Murrumbidgee catchment. Overlain is the proposed transect to be monitored by the AACES campaigns.

### 3. INSTRUMENTATION AND SAMPLING STRATEGY

The AACES campaigns are planned to cover a large area of the Murrumbidgee River catchment in entirety four times (one within each season). Compared to European validation test sites, which will comprise a single SMOS pixel or transects through a few SMOS pixels with a number of repeat flights over a few months, the Australian campaigns will focus on accurately mapping the spatial variability across an area comprising about 20 independent SMOS pixels, with temporal variability assessed according to season. Thus, features such as climatic, topographic and seasonal changes will be mapped on a much larger spatial and temporal scale than the equivalent campaigns elsewhere. Consequently, these experiments will contribute to comprehensive validation of SMOS brightness temperature and soil moisture, and are highly complementary to the planned activities in other countries.

#### 3.1. Airborne Measurements

The AACES campaigns will map an area of 100 km x 500 km across the Murrumbidgee river catchment at 1 km resolution using an L-band radiometer, repeated in each of the four seasons. Given the approximately 50 km sized SMOS pixels, the study transect has been aligned with the SMOS fixed grid and subdivided into ten patches approximately 100 km x 50 km in size, of which each will be mapped within a single day (Figure 3). The flight coverage's have been designed to include a minimum of 5 km overlap between each patch, thus ensuring continuity between the different flights and full coverage of the SMOS pixels. Moreover, it also allows an assessment of any brightness temperature change from the previous flight to be undertaken.

Peischl *et al.*, Towards Validation of SMOS Using Airborne and Ground Data

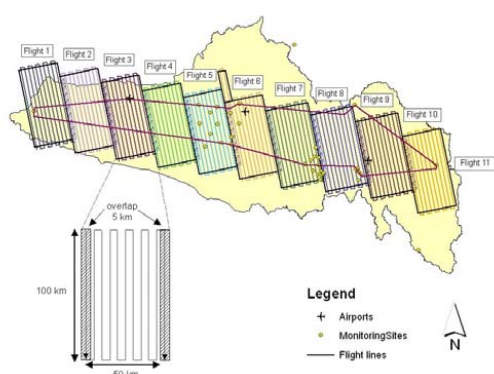


**Figure 3.** Schematic of the airborne sampling strategy showing flight patterns for each patch and a circuit flight throughout the transect.

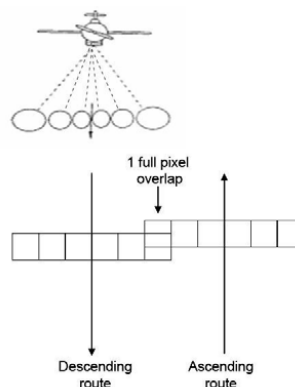


**Figure 4.** The pushbroom concept showing the 6 PLMR beams with a 1 beam overlap between flight lines (Walker and Panciera, 2005).

There will also be three repeated circuit flights throughout the study transect (flight 11); one each at the start, middle, and end of the campaign. This will capture temporal variability within the experimental site and allow comparison with the European validation strategies.

Scheduling of exact flight dates will depend on the actual SMOS coverage of the study transect, which is dependent on the actual launch date. However, preliminary flight planning analysis has shown that between 3 and 4 weeks will be required to map the study transect once with coincident SMOS coverage. Moreover, approximately 4 hours of flight time is required to cover each patch once, including a repeat pass of the first flight line. Consequently, all flights will be conducted such that they are centred on the 6am overpass time of SMOS.

The airborne observations will be undertaken at approximately 3000 m (AGL) altitude to provide passive microwave data with a 1 km spatial resolution. The aircraft will be equipped with the Polarimetric L-Band Multibeam Radiometer (PLMR) and thermal infrared sensors (TIR). The PLMR instrument will be used in across-track configuration (pushbroom, see figure 4) to scan the surface with three viewing angles ( $\pm 7^\circ$ ,  $\pm 21.5^\circ$  and  $\pm 38.5^\circ$ ) to each side of the flight direction, achieving a swath width of about 6 km. The PLMR operates with a frequency of 1.413 GHz and a bandwidth of 24 MHz in both V- and H-polarisations.

During the campaign, pre- and post-flight calibration of PLMR will be undertaken using a blackbody chamber as a warm target and the sky as cold target. Results of these calibrations will be used to compute daily adjustment coefficients to correct the raw brightness temperature data from PLMR. Moreover, PLMR will be flown over a large water body as an additional in-flight calibration check, using temperature and salinity measurements of the water body to model the water emission.

### 3.2. Ground Measurements

A well instrumented monitoring network with stations throughout the entire Murrumbidgee catchment has been operational since 2001. The network was upgraded in 2003 and 2006 to now provide a total of 38 monitoring stations with surface soil moisture measurements. This monitoring network provides an ideal basis for the validation of both space- and airborne soil moisture observations, with the majority of stations located within three focus areas: Yanco, Kyeamba and Adelong (Figure 1).

All monitoring stations make the following measurements: i) rainfall using a tipping bucket rain gauge; ii) soil moisture profiles using three vertically installed Campbell Scientific water content reflectometers (a mix of CS615 and CS616 sensors) across three different depths (0-30 cm, 30-60 cm and 60-90 cm), with a supplementary Hydraprobe for 0-5 cm ('03 sites) or CS615 installed at an angle for 0-7 cm ('01 sites); and iii) soil temperature at 2.5 cm and 15 cm depth (Smith *et al.*, The Murrumbidgee soil moisture monitoring network data set. Submitted to Water Resources Research, 2009). Additionally, several stations collect information on deeper soil temperature, soil suction and groundwater. Consequently, this monitoring network

Peischl *et al.*, Towards Validation of SMOS Using Airborne and Ground Data

provides an ideal basis for long term validation of SMOS and is an excellent source of data for planning the field campaign timing.

In order to validate the aircraft soil moisture retrievals at 1km resolution, account for soil moisture variability and the representativeness of single (or groups of) station measurements (see Azcurra and Walker, 2009), intensive ground based monitoring of soil moisture and related variables are planned as an essential part of the AACES campaigns. Consequently, a minimum of two focus farms have been identified for each patch of the Murrumbidgee transect (Figure 5). In this way the ground teams will follow the aircraft across the study transect once during each campaign.

Focus farms have been identified on the basis of background information including climate, topography, soil, vegetation and accessibility. Consequently, these focus farms represent locally the dominant soil and vegetation type and are within themselves fairly homogeneous, yet capture the variability that exists across the patch. A total of 20 focus farms have been identified across the entire campaign transect. Within each of these focus farms a 1.5 km by up to 5 km transect (oriented along the direction of flight lines) will be established and subdivided by six ground sampling lines, each a minimum of 3 km in length and 250 m apart (Figure 5). Ground teams will make three surface soil moisture measurements (within a radius of 1 m) every 50 m along these transects using the HDAS system. Concurrently, additional information about vegetation type and height, dew presence, land use and rock fraction will be visually observed and recorded. To facilitate comparisons between SMOS, airborne observations, and the detailed ground measurements, ground soil moisture sampling will take place as early in the morning as practical. Specifically, quantitative dew measurements will be made at the 6 am SMOS overpass time.

To maximise the efficiency of limited personnel currently involved in ground sampling, vegetation sampling is scheduled for the days when there are no coincident SMOS and aircraft flights (approximately every alternate day). Vegetation sampling is expected to include destructive samples of vegetation water content (VWC) and dry biomass together with leaf area index (LAI) and spectral measurements.

For calibration purposes, a minimum of five gravimetric surface soil samples will be collected at each focus farm. Moreover, at least two surface roughness profiles in north-south and east-west directions of 2 m length will be conducted at each focus farm.

Permanent monitoring stations will also be supplemented by temporary monitoring stations at each farm. Due to limited equipment, these stations will be moved across the study transect, with stations set up at least one day before airborne observations of the focus farm. These short-term monitoring stations will be instrumented with a raingauge, thermal infrared sensor, leaf wetness sensor, surface soil moisture thetprobe (0-5 cm) and two soil temperature sensors (2.5 cm and 50 cm depth) in order to provide time series data during the sampling period (Figure 6). Such measurements will be useful for identifying the presence or absence of dew, and verifying the assumptions that i) effective temperature has not changed throughout the course of the aircraft measurements; ii) vegetation and soil temperature are in equilibrium; and iii) soil moisture has not changed significantly during ground sampling.

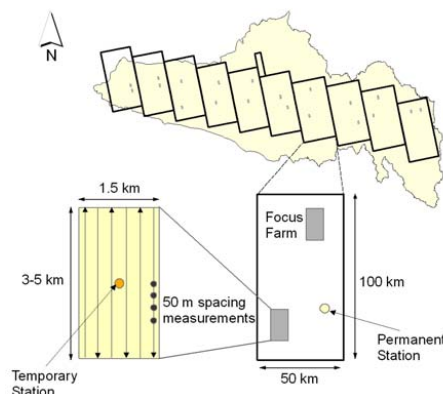


**Figure 5.** Schematic of the ground sampling strategy within the identified focus farms of each patch.

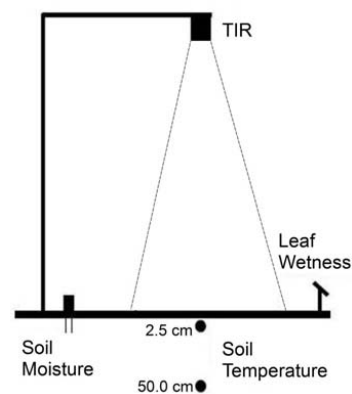


**Figure 6.** Schematic of the temporary monitoring station.

Peischl *et al.*, Towards Validation of SMOS Using Airborne and Ground Data

#### 4. SUMMARY

This paper has presented an overview of the Australian Airborne Cal/val Experiment for SMOS (AACES) scheduled to start in the spring of 2009. Against the background of the upcoming launch of the SMOS satellite, and the inevitable need for brightness temperature and derived soil moisture validation, these campaigns will provide one of the most comprehensive datasets. In addition to validating approximately 20 independent SMOS pixels in their entirety with validated 1 km airborne passive microwave observations at L-Band and derived soil moisture, the data will cover a range of topographic, climatic and geomorphologic characteristics, as well as varying soil texture, vegetation condition, vegetation type, and land use.

Interested parties are invited to participate in these planned field campaigns and benefit from collaborating in such an important validation activity. In particular, people with a focus on remote sensing of soil moisture, vegetation, evapotranspiration and precipitation or related areas of environmental remote sensing that can contribute to the data set, and utilise the collected ground and airborne data, are invited to join our team.

#### ACKNOWLEDGEMENTS

The AACES campaigns are funded by an Australian Research Council Discovery Project grant (DP0879212) as part of the MoistureMap project. Initial setup and maintenance of the Murrumbidgee monitoring network was funded by the Australian Research Council (DP0343778, DP0557543) and by the CRC for Catchment Hydrology. Airborne sensors were also funded by Australian Research Council through infrastructure grants (LE0453434 and LE0560930). Furthermore, this project leverages the very successful National Airborne Field Experiments also made possible through funding from the Australian Research Council grants indicated above.

#### REFERENCES

- Australian Bureau of Meteorology (1998), Gridded rainfall data, based on the standard rainfall climatology (1961-1990). National Climate Centre, Bureau of Meteorology, Melbourne.
- Australian Bureau of Rural Sciences - Department of Agriculture, Fisheries and Forestry, "Land Use of Australia, Version 3 - 2001/2002", Resource publication on 2006-09-21, accessed 18 February 2009, from <<http://adl.brs.gov.au/mapserv/landuse/>>.
- Azurra, C. and J.P. Walker (2009), Towards SMOS validation in south-eastern Australia. 18th World IMACS / MODSIM Congress, Cairns, Australia 13-17 July 2009.
- Kerr, Y.H., P. Waldteufel, J.P. Wigneron, J.M. Martinuzzi, J.M. Font and M. Berger (2001), Soil moisture retrieval from space: The Soil Moisture and Ocean Salinity (SMOS) mission. *IEEE Transactions on Geoscience and Remote Sensing*, 39(8): 1729–1735.
- McKenzie, N.J., D.W. Jacquier, L.J. Ashton and H.P. Cresswell (2000), Estimations of soil properties using the Atlas of Australian Soils. CSIRO Land and Water Technical Report 11/00.
- Merlin, O., Walker, J.P., Kalma, J.D., Kim, E., Hacker, J., Panciera, R., Young, R., Summerell, G., Hornbuckle, J., Hafeez, M., and Jackson, T. (2008), The NAFE'06 Data Set: Towards Soil Moisture Retrieval at Intermediate Resolution. *Advances in Water Resources*, In Press. doi:10.1016/j.advwatres.01.018.
- Njoku, E.G., W.J. Wilson, S.H. Yueh, S.J. Dinardo, F.K. Li, T.J. Jackson, V. Lakshmi and J. Bolten (2002), Observations of soil moisture using a passive and active low-frequency microwave airborne sensor during SGP99. *IEEE Transactions on Geoscience and Remote Sensing*, 40(12): 2659-2673.
- Walker, J. P. and R. Panciera (2005), National Airborne Field Experiment 2005: Experiment Plan. Department of Civil and Environmental Engineering, The University of Melbourne.
- Western A., Grayson R., and Green T., (1999), The Tarrawarra project: High resolution spatial measurement, modelling and analysis of soil moisture and hydrological response. *Hydrological Processes*: 13(5), 633–652.
- Whetton, P.H., M.R. Haylock and R. Galloway (1996), Climate change and snow-cover duration in the Australian Alps. *Climatic Change*, 32(4): 447-479.
- Wigneron, J.P., J. Calvet, T. Pellarin, A. Van de Griend, M. Berger and P. Ferrazzoli (2003), Retrieving near-surface soil moisture from microwave radiometric observations: current status and future plans. *Remote Sensing of Environment* 85, 489-506.

# B

## Conference Proceeding II

**T**HIS chapter includes a research paper which has resulted from the studies undertaken for this degree and is published as an invited paper in a peer-reviewed conference proceeding.

**Peischl, S.,** Ye, N., Walker, J. P., Ryu, D., and Kerr, Y. H.: Soil moisture retrieval from multi-incidence angle observations at L-band, 19<sup>th</sup> International Congress on Modelling and Simulation (MODSIM), Perth, Australia, 12-16 December 2011, 1987-1993, 2011.

19th International Congress on Modelling and Simulation, Perth, Australia, 12–16 December 2011  
http://mssanz.org.au/modsim2011

## Soil moisture retrieval from multi-incidence angle observations at L-band

S. Peischl<sup>a</sup>, N. Ye<sup>a</sup>, J.P. Walker<sup>a</sup>, D. Ryu<sup>b</sup> and Y.H. Kerr<sup>c</sup>

<sup>a</sup>Department of Civil Engineering, Monash University, Australia

<sup>2</sup>Department of Infrastructure Engineering, The University of Melbourne, Australia

<sup>c</sup>Centre d'Etudes Spatiales de la Biosphère (CESBIO), Toulouse, France

(E-mail: sandy.peischl@monash.edu)

**Abstract:** Soil moisture is an important environmental variable in regulating energy fluxes and water infiltration near the soil surface. This makes it a significant parameter in meteorological and climate modelling applications. While ground measurement of soil moisture at a large spatial scale is cumbersome and time-consuming, remote sensing offers the advantage of frequent observations in time and space. The most promising remote sensing technique for soil moisture observations is microwave radiometry at L-band, which is highly sensitive to moisture and less affected by roughness and canopy attenuation than compared to shorter wavelengths in the microwave range. Consequently, the first dedicated mission for global Soil Moisture and Ocean Salinity mapping (SMOS), launched in November 2009, has a passive microwave radiometer at L-band (1.4 GHz) that uses a two-dimensional interferometric Y-shaped antenna.

The novel design of this satellite, yielding multi-incidence angle observations, provides a unique opportunity to acquire accurate information on near surface soil moisture. However, the newly developed algorithms for this mission need to be thoroughly tested on a wide range of land surface conditions and spatial resolutions, since their parameterization has been mostly limited to small scale field studies that focused on data from tower radiometers and simulation experiments. The SMOS mission is based on the relationship between the measured brightness temperature and the dielectric constant of the soil, which is related to its moisture content. Since this relationship is affected by a range of factors, including surface roughness and vegetation cover, the SMOS mission is relying on the multi-incidence angle observations to estimate some of the ancillary parameters required by the retrieval algorithm.

In order to assess the performance of the core algorithm used by SMOS, multi-angle airborne data at L-band were studied from an Australian field campaign in 2005 (NAFE - National Airborne Field Experiment). The flights were conducted across three focus areas capturing a range of vegetation and soil moisture conditions on several observation days. The airborne instrument operated was the Polarimetric L-band Multi-beam Radiometer (PLMR) which provided dual-polarized brightness temperature measurements at six different incidence angles. The multi-angle observations were obtained by deploying a push-broom sensor rotated such that all beams were looking along the flight track, three forward and three backward, respectively. Corresponding ground sampling activities at specific focus farms included near surface-soil moisture, profile soil temperature, vegetation temperature, vegetation water content and biomass measurements. Additional rainfall, soil moisture profile and soil temperature data were collected at permanent monitoring sites nearby.

In this research the L-MEB model was used to investigate the soil moisture retrieval results obtained when only specific ranges of multi-angle brightness temperature observations over wheat canopy were used. Moreover, the impact of varying moisture conditions and multi-parameter retrievals were studied to further assess the model performance and soil moisture accuracy. The results demonstrated overall good soil moisture estimates in relation to the ground measurements ( $\Delta SM = 0-0.03 \text{ m}^3/\text{m}^3$ ), if i) soil moisture was retrieved solely and ii) all available brightness temperature data collected across 0-50° incidence angles were used. However when attempting the simultaneous retrieval of soil moisture together with ancillary data and focusing on specific angular ranges of observations, large variations in soil moisture estimates were observed. In particular, L-band data collected at incidence angles of 10° or higher seemed to be more strongly affected by the canopy, since vegetation effects of the dominant vertical wheat structure increased with larger incidence angles. Hence, L-band data measured at near-nadir views (0-10°) produced the soil moisture results closest to those measured - independently of the observed moisture conditions - when the optical depth and/or the surface roughness parameter were retrieved simultaneously with soil moisture.

**Keywords:** L-MEB, microwave radiometry, multi-incidence angle, NAFE, remote sensing, SMOS

Peischl *et al.*, Soil moisture retrieval from multi-incidence angle observations at L-band

## 1 INTRODUCTION

The retrieval of soil moisture from L-band microwave observations over vegetated areas is relatively complex compared to bare soil conditions, since the additional vegetation contribution on the emission signal needs to be accounted for within the model. Thus, with the increasing number of input parameters, even more ground information is needed to ensure accurate soil moisture estimates from remote sensing instruments, such as the recently launched Soil Moisture and Ocean Salinity (SMOS) satellite (Kerr *et al.*, 2010a). The ancillary data might be obtained from different ground and space borne instruments. However, issues due to spatial or temporal discrepancies between the different data sources arise. Consequently, previous work has studied the use of dual-polarized multi-incidence angle L-band data to retrieve soil moisture simultaneously with some of the ancillary data needed as model input (Wigneron *et al.*, 2000). It was shown that these so-called multi-parameter retrievals using the multi-angle capability of sensors such as that deployed by SMOS may enhance the overall retrieval process, depending on the field of view, the moisture conditions, the vegetation type and growth state. However, if a radiometer instrument is only capable of brightness temperature acquisition at a very narrow range of incidence angles compared to SMOS ( $\sim 0\text{--}60^\circ$ ), the accuracy of soil moisture estimated from multi-parameter retrieval might change depending on the angular range chosen for multi-angle observations; e.g. the near nadir measurements of SMOS are strongly affected by the low antenna gain in that particular area of the field of view. Hence, this paper analyses the multi-angular soil moisture retrieval quality over a wheat canopy site using airborne brightness temperature data collected at different ranges of incidence angles. The effect of i) changing moisture conditions and ii) the type and number of simultaneously retrieved parameters on the model performance are also investigated.

## 2 EXPERIMENTAL DATA

The data used in this paper was sourced from the National Airborne Field Experiment (NAFE'05), conducted during October–November 2005 in South-East Australia (Panciera *et al.*, 2008). The campaign focused on the northern part of the Goulburn River catchment ( $32^\circ$  S,  $150^\circ$  E) located in New South Wales (Figure 1). Within the main study region of  $40\times 40$  km, several smaller focus areas were selected for intensive airborne and ground operations at farm scale. The experimental data set comprised among others, airborne multi-incidence angle L-band measurements together with ground information from extensive in-situ sampling and monitoring stations. The Merriwa Park farm (Figure 1), which was the focus of this paper, had a gently sloping topography and was characterized by a mixture of wheat and grass land use on a silty clay loam soil.

### 2.1. Airborne Data

The airborne microwave radiometer used in the NAFE'05 campaign was the Polarimetric L-band Multi-beam Radiometer (PLMR), which is capable of dual-polarized brightness temperature measurements (TB) at a frequency of 1.413 GHz and bandwidth of 24 MHz. The instrument is equipped with six receiving beams, with fixed look angles of  $\pm 7^\circ$ ,  $\pm 21.5^\circ$  and  $\pm 38.5^\circ$ . For the multi-angle flights, PLMR was mounted in along-track configuration on the aircraft. This provided three beams pointing forward and three beams backward with respect to the flight direction of the aircraft. Considering an aircraft pitch of approximately  $4^\circ$ , the resulting look angles of the six PLMR beams were typically  $3^\circ$ ,  $11^\circ$ ,  $17^\circ$ ,  $26^\circ$ ,  $34^\circ$  and  $43^\circ$  in along-track mode. Consequently, as the aircraft moved along its flight path at a nominal altitude of 750 m, quasi-simultaneous multi-angle measurements at approximately 250 m spatial resolution were made for the same location on earth. The multi-angle data were acquired in the early afternoon between 12:00 pm and 3:00 pm on a total of four observation days (2-Nov, 9-Nov, 16-Nov and 23-Nov). The PLMR instrument was calibrated before and after each flight using cold (sky) and warm (blackbody box) calibration targets. Additional in-flight calibration checks were conducted through low-altitude flights across a large water body, which was monitored for surface water temperature and salinity. The instrument accuracy is given as 0.7 K for H- and 2 K for V-polarization (Panciera *et al.*, 2008). Further processing of the multi-angle data included

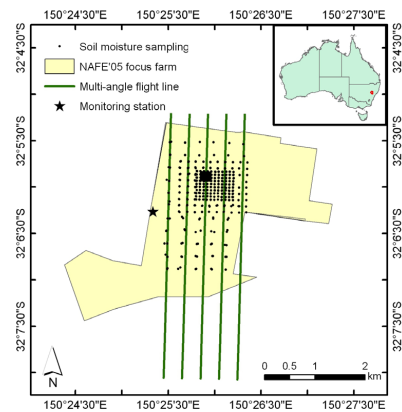


**Figure 1.** Outline of the Merriwa Park focus farm with the aircraft flight lines, the ground soil moisture sampling grid (6.25 m – 2 km) and the location of monitoring stations overlain. Inset: Location of the NAFE'05 test site in Australia.

Peischl *et al.*, Soil moisture retrieval from multi-incidence angle observations at L-band

calculation of the effective footprint size and the local incidence angle, taking into account the surface topography, aircraft position and attitude. Moreover, some of the PLMR data with large yaw and/or roll angles caused by strong cross-wind and turbulence were filtered.

## 2.2. Ground Data

Extensive ground sampling was conducted at the focus farm within an area of  $1.5 \times 3.0 \text{ km}^2$ , concurrent to the airborne observations. The near-surface (0-5 cm) soil moisture measurements (SM) were made with the Hydraprobe Data Acquisition System (HDAS), which includes a Hydraprobe soil moisture sensor, a Global Positioning System (GPS) and a handheld pocket PC (Merlin *et al.*, 2007). The calibration of the Hydraprobe standard soil moisture product was based on gravimetric soil samples and laboratory data. Considering the correction of temperature effects, the estimated accuracy of the HDAS system is  $\pm 0.033 \text{ m}^3/\text{m}^3$  (Merlin *et al.*, 2007). During the campaign, surface moisture contents were measured between 9:00 am to 1:30 pm on a regular grid with varying resolution. The spacing between the individual sampling points ranged from 6.25 m to 2 km and was designed in such a way that the high-resolution sampling zone was located within the cropping area of the Merriwa Park focus farm (Figure 1). Supplementary data including surface roughness, vegetation type, dew amount, vegetation water content and biomass were also collected by the ground teams. Long-term profile soil moisture (0-5 cm, 0-30 cm, 30-60 cm and 60-90 cm), soil temperature (0-5 cm and 0-30 cm) and rainfall records were available from an existing in-situ monitoring network (Rüdiger *et al.*, 2007). Moreover, temporary monitoring stations were set up during the period of the campaign and equipped with thermal infrared sensors (TIR), surface soil temperature instrumentation (1 cm, 2.5 cm and 4 cm) and leaf wetness sensors. The overall dynamic range of surface soil moisture measured was between  $0.14\text{-}0.46 \text{ m}^3/\text{m}^3$  at Merriwa Park. In response to a significant rainfall event before the start of the campaign, substantial drying effects of the topsoil were observed throughout the field experiment.

## 3 RADIOMETRIC MODEL

The core component of the operational soil moisture retrieval algorithm for SMOS is the L-band Microwave Emission of the Biosphere model (L-MEB), explained in detail in Wigneron *et al.* (2007) and implemented into the Community Microwave Emission Modelling Platform (CMEM) (Drusch *et al.*, 2009). This radiative transfer model is a simplified (zero-order) solution to describe the  $p$ -polarized ground emission ( $e_{GP}$ ) taking into account the presence of an overlying vegetation layer (with  $p=H$  for horizontal and  $p=V$  for vertical polarization). The contribution of the canopy to the soil reflectivity ( $r_{GP} = 1 - e_{GP}$ ) is modelled in terms of the vegetation attenuation ( $\gamma_p$ ) and scattering effects ( $\omega_p$ ), which together result in a composite brightness temperature ( $T_{Bp}$ ) [K]. Considering the soil and vegetation components and the effective temperature [K] of both media, i.e. soil  $T_C$  and vegetation  $T_C$ , the so-called tau-omega model is given as (Mo *et al.*, 1982)

$$T_{Bp} = (1 - \omega_p)(1 - \gamma_p)(1 + \gamma_p r_{GP}) \cdot T_C + (1 - r_{GP}) \gamma_p \cdot T_G. \quad (1)$$

The reflectivity of the soil surface can be estimated by the Fresnel reflectivity ( $r_{GP}^*$ ) and adjusted for non-smooth surfaces through the use of additional parameters, such as  $H_R$  and  $N_{RP}$  (Wang and Choudhury, 1981):

$$r_{GP} = r_{GP}^* \cdot \exp[-H_R \cos \theta^{N_{RP}}]. \quad (2)$$

The  $H_R$  parameter is included as a semi-empirical effective surface roughness parameter and  $N_{RP}$  for the dependency of the surface roughness on the incidence angle ( $\theta$ ). When modelling of the canopy attenuation, further referred to as transmissivity, the angular effect on the signal needs also to be taken into account through the optical depth ( $\tau_p$ ) by

$$\gamma_p = \exp[-\tau_p / \cos \theta]. \quad (3)$$

The optical depth as shown in (3) is strictly valid for nadir-views only and can be approximated using a linear function of the vegetation water content ( $VWC$ ) [ $\text{kg}/\text{m}^2$ ] and the empirical parameter  $b_p$ . The latter is mainly dependent on sensor frequency, polarization, canopy type and plant structure (Jackson and Schmugge, 1991):

$$\tau_{NAD} = VWC \cdot b_p. \quad (4)$$

Consequently, to correct for non-nadir observations two additional vegetation structure parameters  $tt_p$  are introduced, that account for an increasing ( $tt_p > 1$ ) or decreasing ( $tt_p < 1$ ) trend in the optical depth and hence in the vegetation transmissivity as a function of the incidence angle. For the particular case of  $tt_p = 1$ , the  $\tau_p$  of the standing canopy is independent of polarization and incidence angle, which is defined as isotropic state.

$$\tau_p = \tau_{NAD} (\sin^2 \theta \cdot tt_p + \cos^2 \theta). \quad (5)$$

Peischl *et al.*, Soil moisture retrieval from multi-incidence angle observations at L-band

For the purpose of this study, the L-MEB model was used to solve an optimization problem between the airborne dual-polarized brightness temperatures and the forward simulated brightness temperatures by iteratively minimizing a cost-function through least-square to retrieve soil moisture and ancillary data. Consequently, the number of parameters that were retrieved simultaneously depended on the number of available brightness temperature measurements for the same location on earth.

#### 4 MULTI-INCIDENCE ANGLE SOIL MOISTURE RETRIEVAL

In order to investigate how a specific angular range of brightness temperature measurements performs for soil moisture retrieval, all available L-band data within a designated PLMR pixel over the Merriwa Park wheat area were categorized according to their incidence angle information (Table 1). Note that due to the configuration of the PLMR instrument, there were a few cases where groups classified at a finer angular scale did not contain any data, but have been included for the sake of completeness. The total number of  $TB_p$  studied (collected across incidence angles of 0-50°) depended on the individual observation day, but ranged from 15 observations on the 16<sup>th</sup> November 2005 to 27-32 observations for the three remaining days. The corresponding HDAS measurements for the particular day/pixel comprised about ~250-300 points, which were averaged and the spatial variability estimated from the standard deviation.

The soil moisture retrieval was classified into single-parameter retrieval (soil moisture) and multi-parameter retrieval, considering - apart from soil moisture (SM) - additional model parameters as unknown. These ancillary parameters included the surface roughness  $H_R$  and the vegetation water content  $VWC$ . The vegetation water content was calculated from the retrieved optical depth information using Equation 4. The semi-empirical roughness parameter  $H_R$  was set as either dependent on the retrieved soil moisture  $H_R=f(SM)$  or independent within the retrieval process. The concept of a soil moisture dependent  $H_R$  parameter is also applied in the processing of SMOS data (Kerr *et al.*, 2010b), since work by Escorihuela *et al.* (2007) indicated better retrieval results when taking into account the topsoil moisture content for determining  $H_R$ . With regard to the NAFE'05 data set, similar results were found for the study site and the different moisture conditions observed (Peischl *et al.*, 2011; Panciera *et al.*, 2009a; 2009b). Recent findings suggest that the soil water contribution in  $H_R$  might alternatively result from a difference in sampling depth between the L-band radiometer observations and the ground measurements (Escorihuela *et al.*, 2010). The remaining L-MEB model parameters including soil texture, soil temperature, vegetation temperature, vegetation scattering albedo and further surface roughness characterization were taken mostly from literature (Wigneron *et al.*, 2007) or available in-situ measurements. The parameterization used in this study had been previously confirmed and tested for the same test site (Peischl *et al.*, 2011), demonstrating maximum root mean square errors of 2-5 K. The soil moisture retrievals were performed i) on all four multi-angle flight days over the Merriwa Park cropping area and ii) for each individual group of angular brightness temperature measurements across the different scenarios (Table 1).

##### 4.1. Single-parameter Retrieval

The single-parameter retrieval (1-P) focused solely on retrieving soil moisture and assumed all remaining L-MEB model input data as known. The resulting soil moisture estimates for each group of brightness temperatures (Table 1) are displayed in Figure 2. Generally, using all available angular brightness temperature observations for the 1-P soil moisture retrieval produced values close to the ground measurements for all observation days ( $\Delta SM=0-0.03 \text{ m}^3/\text{m}^3$ ). However by focusing on brightness temperatures collected at specific incidence angle ranges, the simulation accuracy varied. In particular,  $TB_p$  associated with very large incidence angles ( $>40^\circ$ ) tended to slightly overestimate soil moisture for very wet and very dry conditions. In addition, for soil moisture conditions less than  $0.22 \text{ m}^3/\text{m}^3$ , consistently lower values compared to the ground information were retrieved when only  $TB_p$  data at small incidence angles were used ( $<15^\circ$ ). Overall, all grouped soil moisture retrievals were still within the range of the standard deviation of the ground measurements independent of the varying moisture conditions observed.

Table 1. Overview of grouping criteria for PLMR brightness temperature measurements according to their corresponding incidence angle information.

Scenario	Group Identifier for Incidence Angle Ranges [°]								
	1	2	3	4	5	6	7	8	9
A	0-50								
B	0-25	25-50							
C	0-15	15-30	30-50						
D	0-14	14-22	22-35	35-50					
E	0-10	10-20	20-30	30-40	40-50				
F	0-8	8-16	16-24	24-32	32-40	40-50			
G	0-7	7-14	14-21	21-28	28-35	35-42	42-50		
H	0-5	5-10	10-15	15-20	20-25	25-30	30-35	35-40	40-50

Peischl *et al.*, Soil moisture retrieval from multi-incidence angle observations at L-band

#### 4.2. Multi-parameter Retrieval

The multi-parameter retrieval included three different combinations: i) simultaneous retrieval of soil moisture and vegetation water content; ii) simultaneous retrieval of soil moisture and the surface roughness parameter, and iii) simultaneous retrieval of soil moisture, vegetation water content and surface roughness. All model results are displayed in Figure 2 with the individual retrieval methods differentiated by symbol types. The 2-Parameter (2-P) retrieval of soil moisture and  $VWC$  showed for most observation days a reasonable agreement between measured and simulated soil moisture, when all available  $TB_p$  data were used ( $\Delta SM=0.02-0.08 \text{ m}^3/\text{m}^3$ ). However, focusing on data collected at mid-range and in particular at high incidence angles decreased the soil moisture accuracy significantly ( $\Delta SM=0.06-0.38 \text{ m}^3/\text{m}^3$ ). In contrast, very good retrieval results were obtained from  $TB_p$  observations at very small angles close to nadir-view ( $0-5^\circ$ ), implicating less impact by the vegetation due to i) shorter path lengths through the canopy and ii) the effective composite temperature being closer to that of the soil. Further, for very dry soils and a canopy with low vegetation water content ( $<1 \text{ kg}/\text{m}^2$ ) the vegetation contribution seemed to be less pronounced, enabling soil moisture estimates close to the ground measurements even for brightness temperature observations at angles of  $\leq 25^\circ$ .

The 2-P retrieval of soil moisture and  $H_R$  independently demonstrated a consistent improvement compared to the 1-P approach across all angular ranges, except for the case of low moisture content. The retrieved values followed exactly the angular behaviour of 1-P, which exhibited minor variations and corresponded well to the measurements in wet conditions. The soil moisture estimates for the last observation day, where the measured moisture was approximately  $0.14 \text{ m}^3/\text{m}^3$ , demonstrated a notable angular trend with increasing discrepancies between model and ground data, the larger the incidence angles of the brightness temperature

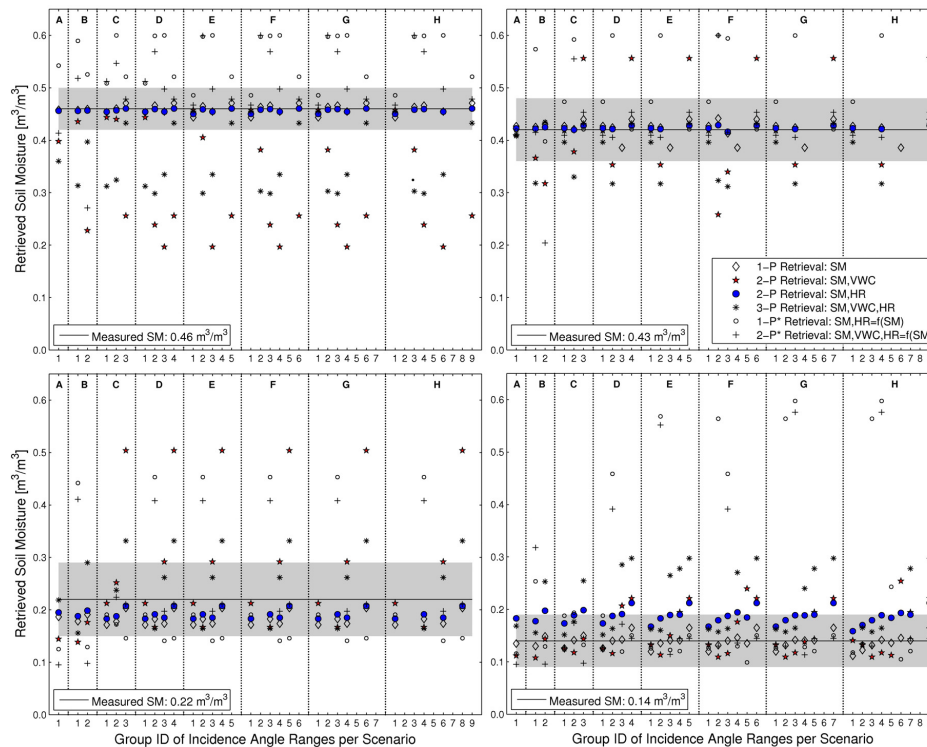


**Figure 2.** Comparison of modelled moisture values retrieved from airborne brightness temperature data at different incidence angles with measured ground soil moisture given as black line and its standard deviation indicated in grey. Refer to Table 1 for the angular information corresponding to each group and scenario displayed (scenarios are separated by vertical lines). The classification into n-parameter retrievals was based on both the number and type of parameters that were simultaneously derived with soil moisture (\* in the legend indicates  $H_R$  retrieved as a function of SM).

Peischl *et al.*, Soil moisture retrieval from multi-incidence angle observations at L-band

observations were. This phenomenon might be induced by the increased angular dependency of the optical depth with larger angles causing the model to overcompensate for soil moisture by  $\sim 0.05 \text{ m}^3/\text{m}^3$ . With respect to the soil moisture retrieval together with  $H_R$ , but constraining the surface roughness value as dependent on the retrieved soil moisture value, a linear relationship proposed by Panciera *et al.* (2009a) was implemented into the L-MEB model. Hence, the retrieval was not regarded as an independent 2-P retrieval and instead rather considered as a 1-parameter retrieval (1-P\*). The modelled soil moisture data were quite different to that estimated by the independent SM- $H_R$  approach, and did not follow the angular variations of the 1-P retrieval at all. One feature was particularly evident: that soil moisture values retrieved for the incidence angle range of 15-20° were far higher than observed ( $\Delta\text{SM}=0.14\text{-}0.46 \text{ m}^3/\text{m}^3$ ) across all observations days.

For the simultaneous 3-P retrieval of soil moisture,  $VWC$  and  $H_R$  was characterized by a strong variability of soil moisture estimates across the angles and observation days (Figure 2). In general, best soil moisture retrieval results were obtained from brightness temperature data measured at very small incidence angles (0-5°). This supports the earlier hypothesis of reduced signal interference by the canopy layer for near-nadir views. Besides, according to the observed ground conditions, the retrieved soil moisture values tended to underestimate the wet conditions and overestimate the dry conditions, with most of the results being outside the range of the standard deviation given per day. In contrast, the simultaneous 2-P\* retrieval of soil moisture,  $VWC$  and the soil moisture dependent  $H_R$ , mainly yielded soil moisture values within the range of the standard deviation, which varied slightly across the angular ranges. In comparison with all other retrieval approaches, the minor angular variations were similar to that of the 1-P retrieval of soil moisture with no significant changes for varying moisture conditions.

In order to further assess the performance of the different retrieval approaches across the various incidence angles, the root mean square error (RMSE) between the observed and simulated brightness temperatures were compared for scenario H (Figure 3). Generally, the RMSE tended to decrease with increasing incidence angles for wet conditions, whereas for dry conditions there was little variation across the angles. Moreover, the RMSE calculated for the different n-parameter retrievals applied per observation day were very similar and did not demonstrate any of the discrepancies observed when the actual soil moisture estimates were compared (as shown in Figure 2). This aspect emphasises that the RMSE should not be used as a single criterion for the evaluation of the soil moisture retrieval approach.

## 5 CONCLUSION

This study investigated the impact of using airborne L-band brightness temperature measurements collected at specific ranges of incidence angles on the accuracy of predicted soil moisture estimates at farm scale. Moreover, multi-parameter retrievals and varying moisture conditions were assessed to find the most suitable angular range of observations for soil moisture retrieval over wheat canopy. In general, the best soil moisture estimates in comparison to ground data were modelled from brightness temperature data collected at incidence-angles between 0-5° among the overall multi-incidence angle range tested (0-50°). This might be related to the dominant vertical structure of the wheat canopy, which affected the soil emission and brightness temperature measurements at near-nadir view to a lesser extent than at large incidence angles, where longer path lengths of the emission through the vegetation layer are more likely to lead to stronger attenuation effects. Additionally, in the case of multi-parameter retrievals model predictions degraded where ancillary data about the vegetation ( $VWC$ ) was unknown. In contrast, good results with only minor angular variations were observed when soil moisture and surface roughness were retrieved simultaneously. The changing moisture conditions did not show significant impact on the retrieval, except for very dry conditions where the contribution of the vegetation was reduced and instead the surface roughness component (and possibly an increased sampling depth) gained more weight

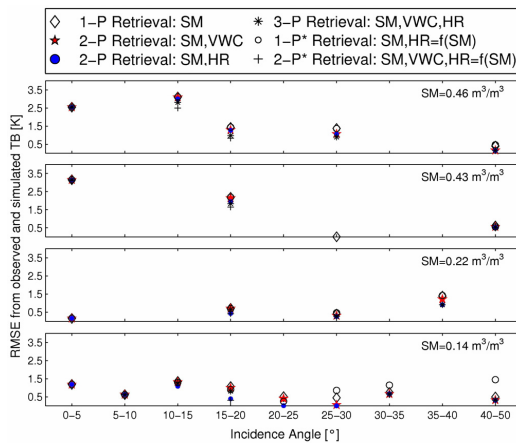


**Figure 3.** Calculated root mean square error (RMSE) between measured and simulated brightness temperatures (TB) derived for scenario H (Table 1) and n-parameter retrievals considering varying soil moisture conditions.

Peischl *et al.*, Soil moisture retrieval from multi-incidence angle observations at L-band

in the retrieval algorithm. Since the angular retrieval seemed to be closely linked to the vegetation structure, future work should extend the analysis to a wider range of land use types at varying spatial scales and consider combinations of different angular ranges. Moreover, the retrieval of further ancillary L-MEB parameters, such as the soil or vegetation temperature, should be investigated in particular with regard to SMOS data and the usage of descending orbits, where the vegetation temperature is most likely different to the effective temperature of the soil media.

#### ACKNOWLEDGMENTS

The authors would like to thank the NAFE'05 team for providing the data set used in this study and the anonymous reviewers for their helpful comments. This work was supported by the Australian Research Council (DP0879212) as part of the Moisture Map project.

#### REFERENCES

- Drusch, M., T.R.H. Holmes, P. de Rosnay and G. Balsamo (2009). Comparing ERA-40-based L-band brightness temperatures with Skylab observations: A calibration/validation study using the community microwave emission model. *Journal of Hydrometeorology*, 10(1), 213-226.
- Escorihuela, M.J., Y.H. Kerr, P. de Rosnay, J.-P. Wigneron, J.-C. Calvet and F. Lemaitre (2007). A Simple Model of the Bare Soil Microwave Emission at L-Band. *IEEE Transactions on Geoscience and Remote Sensing*, 45(7 Part 1), 1978-1987.
- Escorihuela, M.J., A. Chanzy, J.-P. Wigneron and Y.H. Kerr (2010). Effective soil moisture sampling depth of L-band radiometry: A case study. *Remote Sensing of Environment*, 114(5), 995-1001.
- Jackson, T.J. and T.J. Schmugge (1991). Vegetation effects on the microwave emission of soils. *Remote Sensing of Environment*, 36(3), 203-212.
- Kerr, Y.H., P. Waldteufel, J.-P. Wigneron, S. Delwart, F. Cabot, J. Boutin, M.J. Escorihuela, J. Font, N. Reul and C. Gruhier (2010a). The SMOS Mission: New Tool for Monitoring Key Elements of the Global Water Cycle. *IEEE Transactions on Geoscience and Remote Sensing*, 98(5), 666-687.
- Kerr, Y.H., P. Waldteufel, P. Richaume, J.-P. Wigneron, P. Ferrazzoli and R.J. Gurney (2010b). SMOS level 2 processor for soil moisture - Algorithm Theoretical Based Document (ATBD), Issue 3.e, pp.121.
- Merlin, O., J.P. Walker, R. Panciera, R. Young, J. Kalma and E.J. Kim (2007). Soil moisture measurement in heterogeneous terrain. International Congress on Modelling and Simulation (MODSIM), Modelling and Simulation Society of Australia and New Zealand, New Zealand, December 2007, 2604-2610.
- Mo, T., B.J. Choudhury, T.J. Schmugge, J.R. Wang and T.J. Jackson (1982). A model for microwave emission from vegetation-covered fields. *Journal of Geophysical Research*, 87, 11229-11237.
- Panciera, R., J.P. Walker, J.D. Kalma, E.J. Kim, J.M. Hacker, O. Merlin, M. Berger and N. Skou (2008). The NAFE'05/CoSMOS Data Set: Toward SMOS Soil Moisture Retrieval, Downscaling, and Assimilation. *IEEE Transactions on Geoscience and Remote Sensing*, 46(3), 736-745.
- Panciera, R., J.P. Walker, J. Kalma, E.J. Kim, K. Saleh and J.-P. Wigneron (2009a). Evaluation of the SMOS L-MEB passive microwave soil moisture retrieval algorithm. *Remote Sensing of Environment*, 113(2), 435-444.
- Panciera, R., J.P. Walker and O. Merlin (2009b). Improved Understanding of Soil Surface Roughness Parameterization for L-Band Passive Microwave Soil Moisture Retrieval. *IEEE Transactions on Geoscience and Remote Sensing*, 6(4), 625-629.
- Peischl, S., J.P. Walker, D. Ryu, Y.H. Kerr, R. Panciera and C. Rüdiger (2011). Wheat canopy structure and surface roughness effects on multi-angle observations at L-band. *IEEE Transactions on Geoscience and Remote Sensing*, accepted.
- Rüdiger, C., G. Hancock, H.M. Hemakumara, B. Jacobs, J.D. Kalma, C. Martinez, M. Thyer, J.P. Walker, T. Wells and G.R. Willgoose (2007). Goulburn River experimental catchment data set. *Water Resources Research*, 43(10), W10403.
- Wang, J.R. and B.J. Choudhury (1981). Remote Sensing of Soil Moisture Content Over Bare Field at 1.4 GHz Frequency. *Journal of Geophysical Research*, 86(C6), 5277-5282.
- Wigneron, J.-P., P. Waldteufel, A. Chanzy, J.-C. Calvet and Y.H. Kerr (2000). Two-dimensional microwave interferometer retrieval capabilities over land surfaces (SMOS Mission). *Remote Sensing of Environment*, 73(3), 270-282.
- Wigneron, J.-P., Y.H. Kerr, P. Waldteufel, K. Saleh, M.J. Escorihuela, P. Richaume, P. Ferrazzoli, P. de Rosnay, R.J. Gurney, J.-C. Calvet, J.P. Grant, M. Guglielmetti, B. Hornbuckle, C. Mätzler, T. Pellarin and M. Schwank (2007). L-band Microwave Emission of the Biosphere (L-MEB) Model: Description and calibration against experimental data sets over crop fields. *Remote Sensing of Environment*, 107(4), 639-655.



## Conference Proceeding III

**T**HIS chapter includes a research paper which has resulted from the studies undertaken for this degree and is published as an invited paper in a peer-reviewed conference proceeding.

Rüdiger, C., J.P Walker, M. Allahmoradi, D. Barrett, J. Costelloe, R. Gurney, J. Hacker, Y.H. Kerr, E. Kim, J. Le Marshall, W. Lieff, A. Marks, **S. Peischl**, D. Ryu , and N. Ye: Identification of Spaceborne Microwave Radiometer Calibration Sites for Satellite Missions, 19<sup>th</sup> International Congress on Modelling and Simulation (MODSIM), Perth, Australia, 12-16 December 2011, 1987-1993, 2011.

18<sup>th</sup> World IMACS / MODSIM Congress, Cairns, Australia 13-17 July 2009  
<http://mssanz.org.au/modsim09>

## Identification of Spaceborne Microwave Radiometer Calibration Sites for Satellite Missions

**Rüdiger, C.<sup>1</sup>, J.P. Walker<sup>1</sup>, M. Allahmoradi<sup>1</sup>, D. Barrett<sup>2</sup>, J. Costelloe<sup>1</sup>, R. Gurney<sup>3</sup>, J. Hacker<sup>4</sup>, Y.H. Kerr<sup>5</sup>, E. Kim<sup>6</sup>, J. Le Marshall<sup>7</sup>, W. Loeff<sup>4</sup>, A. Marks<sup>8</sup>, S. Peischl<sup>1</sup>, D. Ryu<sup>1</sup>, and N. Ye<sup>1</sup>**

<sup>1</sup> *Department of Civil and Environmental Engineering, The University of Melbourne, Parkville, Australia*

<sup>2</sup> *Sustainable Minerals Institute, The University of Queensland, Brisbane, Australia*

<sup>3</sup> *NERC Environmental Systems Science Center, University of Reading, Reading, United Kingdom*

<sup>4</sup> *Airborne Research Australia, Flinders University, Adelaide, Australia*

<sup>5</sup> *Biospheric Processes, CESBIO, Toulouse, France*

<sup>6</sup> *Hydrospheric and Biospheric Sciences Laboratory, NASA Goddard Space Flight Center, Greenbelt, United States*

<sup>7</sup> *Bureau of Meteorology Research Center, Bureau of Meteorology, Melbourne, Australia*

<sup>8</sup> *Environmental Observation and Landscape Science, CSIRO Land and Water, Canberra, Australia*

Email: [crudiger@unimelb.edu.au](mailto:crudiger@unimelb.edu.au)

**Abstract:** The first dedicated soil moisture satellite mission will be the European Space Agency's Soil Moisture and Ocean Salinity (SMOS) mission. This satellite, scheduled for launch in the second half of 2009, has a new type of satellite design that is based on the radio-astronomy technique of simulating a large antenna from a number of smaller ones placed some distance apart. Because of its unique design and the fact it is sensing in a currently unutilized frequency range makes it critical that on-orbit calibration targets be included in the calibration strategy. Consequently, targets such as the Antarctic, cold oceans, tropical forests and deserts are being considered. However, the large footprint size of passive microwave observations means that large scale homogeneous regions must be identified for calibration purposes. Moreover, these sites must also be either stable through time or the temporal variation easily described by models. In order to satisfy the calibration accuracy required by SMOS for soil moisture retrieval, such sites should be characterized with a brightness temperature uncertainty of less than 4K.

A field experiment has been undertaken in November 2008 in the Australian Arid Zone to explore the suitability of three potential on-orbit calibration targets for SMOS. These sites were chosen for their assumed spatial homogeneity in terms of surface conditions (soil moisture and temperature, vegetation, soil type etc.), and consequently their expected microwave response. Each site covers an area of approximately 50km x 50km, being the approximate size of a satellite footprint. These sites include i) Wurringula Hills, a station to the north-east of Coober Pedy that is characterized by a dense cover of gibber; ii) Lake Eyre, characterized by a predominantly moist material under a layer of salt crust; and iii) Simpson Desert, characterized by sand dunes orientated in a north-south direction.

The data collected during this field campaign consists of both airborne and ground-based measurements. The airborne data includes passive microwave emissions obtained with an L-band airborne radiometer, thermal infrared observations, and optical data. The ground data collection consisted of surface soil moisture measurements at targeted locations along sections of the high-resolution flight tracks, and station measurements of soil moisture and temperature profiles to a depth of 40cm. Additionally, there were soil core samples to a depth of 2m, surface characterization and surface roughness measurements. The airborne data were collected at two different resolutions, 1km and 50m.

This paper presents the results from airborne observations made during this campaign, and discusses their significance in relation to the calibration of SMOS. Of the three study sites assessed, Wurringula Hills appears to be the most promising, having a spatial variability in brightness temperatures of less than 4K at H polarisation. In comparison, the Simpson Desert had a spatial variability of about 10K, and the moist region of Lake Eyre had a spatial variability of about 13K. Moreover, Lake Eyre was found to also have considerable spatial heterogeneity, making it unsuitable for calibration at the spatial resolution of SMOS.

**Keywords:** *Soil Moisture, Remote Sensing, Microwave Radiometry, SMOS, Field Campaign*

Rüdiger *et al.*, Identification of Spaceborne Microwave Radiometer Calibration Sites

## 1 INTRODUCTION

The European Space Agency (ESA) has scheduled the launch of its Soil Moisture and Ocean Salinity (SMOS; Kerr *et al.*, 2001) mission for the second half of 2009; the first soil moisture dedicated mission at L-band. This satellite will provide global brightness temperature observations at better than 40km resolution with a repeat overpass approximately every three days at the equator. However, SMOS consists of a new type of satellite design, which uses synthetic aperture techniques similar to those used in radio-astronomy, to simulate the large antenna size required at L-band. One additional feature of this technique is that it also yields data at a range of incidence angles for each pixel in the swath. As each new satellite has its own individual technical specifications and retrieval algorithms, a post-launch commissioning phase of several months is required for validation and calibration purposes.

Because of the unique design of SMOS, it is especially important that this satellite be carefully calibrated using a range of techniques and targets. To demonstrate this point, the Advanced Microwave Scanning Radiometer for the Earth Observing system (AMSR-E), which used a traditional microwave sensing technique for frequencies higher than C-band, experienced a post-launch data release delay of several months due to a poor calibration accuracy. Initially, it was intended to perform on-board calibrations of AMSR-E with a two-point on-board calibration system, by providing a hot and cold load reference to the system. While the cold load involved looks at the deep space background temperature, the hot load was provided by an onboard reference target. However, this target experienced significant temperature gradients due to influences by the sun (Wentz *et al.*, 2003). The problem was overcome by using thermal information from other radiometers in orbit at the time, but not without a significant delay.

As a consequence of the AMSR-E experience, a large number of studies have been undertaken to find ways to provide a suitable warm load target that is not on the spacecraft. Such targets include tropical forests (Ferrazzoli *et al.*, 2002) Antarctica (Macelloni *et al.*, 2006 & 2007), arid regions and various parts of the ocean (Burrage *et al.*, 2008). Consequently, to avoid post-launch calibration problems with SMOS a more cautious approach is being pursued, by using a range of on-orbit calibration targets from cold to hot. Vicarious calibrations of the satellite instruments will take place over targets with presumed homogeneous and known surface emissions. For instance, the emissions from Dome-C in the Antarctic have been shown to be constant at about 190K (Macelloni *et al.*, 2006). Moreover, emissions from the Amazonian forest appear to have only little variation at C-band and higher frequencies and are therefore relatively constant at 290K (Brown and Ruf, 2005), which may suggest that they could be used as calibration targets at L-band. Other calibration targets include the ice-free sea surfaces, as the salinity effect is minimal and their physical temperature is well known and very stable with low or well known winds, and possibly the Taklamakan Desert in China. Additionally, SMOS will make a deep space observation for one orbit every two weeks (to be confirmed after the commissioning phase). More detailed discussions of the SMOS calibration and validation can be found in Brown *et al.* (2008) and Delwart *et al.* (2008).

Currently a number of experiments and campaigns are being planned and/or undertaken in order to identify further appropriate sites, such as deserts and salt lakes, particularly in Central Australia, Bolivia and China. In November 2008, a field experiment took place in the Australian Arid Zone (Lake Eyre and Simpson Desert regions; Fig. 1) in order to identify potential SMOS calibration sites in a predominantly dry environment. The study sites of this campaign were chosen for homogeneous surface conditions (Fig. 2) and their hypothesized spatial homogeneity in their microwave response. Similarly, if a temporal variation exists, it needs to be easily characterized through in-situ observations. Airborne observations collected during this experiment include brightness temperatures in the same microwave spectrum as SMOS, thermal infrared measurements, and high-resolution photographs. The ground data acquisition provided roaming surface soil moisture and thermal infrared measurements, profile soil temperature and moisture at base stations located within the focus areas, and finally soil and rock samples. In this paper, only the brightness temperature observations are presented.

The three field sites chosen for this experiment represent regions of large homogenous extent:

- a) Lake Eyre: a large flat salt lake, assumed to have homogeneously saturated soil moisture conditions immediately beneath its surface, based on previous visits to accessible parts of the lake;
- b) Simpson Desert: a sandy desert, with only little vegetation and few precipitation events per year, assumed to have homogeneously dry surface soil moisture conditions, based on our previous soil moisture measurements in the area;
- c) Wirrangula Hills: a rocky (gibber) desert with rock surface coverage of up to 90% and almost no vegetation, assumed to have a microwave response that is dominated by the rock cover emission.

Rüdiger *et al.*, Identification of Spaceborne Microwave Radiometer Calibration Sites

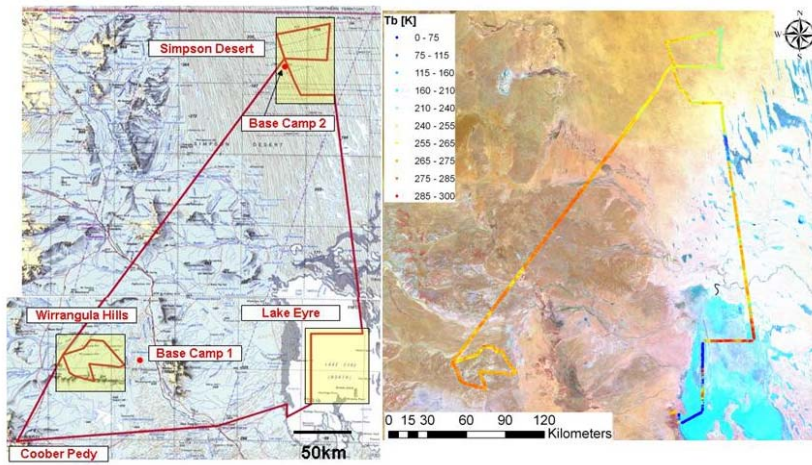


**Figure 1.** Overview of the three focus sites: Wirrangula Hills (gibber), Lake Eyre (salt lake), and the Simpson Desert (sandy desert) along with the corresponding LandSat false colour image. The red line on the left hand image shows the high-resolution and reconnaissance flights (50m), while the yellow boxes represent the low-resolution (1km) coverage. The data shown superimposed over the LandSat image (composite image of 2002) are the brightness temperature observations collected during the reconnaissance flight

Topographic effects across the sites should have only little impact on the hydrology and microwave response, as the areas of Wirrangula Hills and Lake Eyre are relatively flat (Fig. 2). The influence of the regular structure of dunes on the microwave signal may be studied with the high-resolution data set.

## 2. DATA

### 2.1. Airborne Data

The instruments carried onboard the aircraft during the campaign were the Polarimetric L-band Multibeam Radiometer (PLMR), six thermal infrared (TIR) sensors, a thermal imager, and a high resolution (21 MegaPixel) optical camera. The PLMR consists of six beams, each with a field of view of approximately  $15^\circ$ . The instrument was flown in the push-broom configuration, such that brightness temperature observations were made across the flight track at incidence angles of approximately  $\pm 7^\circ$ ,  $\pm 21^\circ$ , and  $\pm 38^\circ$  from nadir. The configuration of the six TIR sensors was such that the instruments field of view observed the same ground area as the six PLMR beams.



**Figure 2.** Surface conditions at Wirrangula Hills (left), Lake Eyre (centre) and Simpson Desert (right).

Rüdiger *et al.*, Identification of Spaceborne Microwave Radiometer Calibration Sites

**Table 1.** Overview of the four flights showing the areas flown and the data collected with the airborne instruments and on the ground. The statistics are standard deviations of the brightness temperatures observed over the areas at high (50m) and low (1km) resolution. For the Simpson Desert and Lake Eyre, those are presented separately for the “wet” and “dry” sections of the focus areas.

Site	Surface Type	Measurements airborne / in-situ	Date	Tb std. dev.
Reconnaissance (all three sites)	salt lake (LE) gibber (WH) sandy desert (SD)	PLMR, thermal IR / thermal IR, profile soil moisture and temperature	09 November 2008	only high-res.: 12.6 / 10.4 (LE – wet/dry) 5.2 (WH) 10.1 (SD)
Lake Eyre	salt lake	PLMR, thermal IR / profile soil temperature, surface soil moisture	10 November 2008	high-res. (wet/dry): 16.1 / 15.6 low-res. (wet/dry): 13.2 / 19.6
Wirrangula Hills	gibber	PLMR, thermal IR, photography / thermal IR, profile soil moisture and temperature, surface soil moisture, deep core samples	12 November 2008	high-res.: 4.1 low-res.: 3.3
Simpson Desert	sandy desert		14/15 November 2008	high-res. (wet/dry): 8.6 / 9.8 low-res. (wet/dry): 9.5 / 8.7

The airborne data were collected at both high- and low-resolution. The low-resolution flight covered a full SMOS pixel (i.e., ~50km x 50km) at 1km resolution, while the high-resolution flights covered local areas along pre-defined flight paths at 50m resolution. A general overview of the flight dates and observations collected is presented in Table 1. The regional flights were timed such that they would be centred on the 6am SMOS overpass time (e.g. 4am to 8am). An exception was the reconnaissance flight, which took place in the afternoon. This reconnaissance flight covered the high-resolution area across the three focus sites (Fig. 1). The data collected during the reconnaissance flight were used to identify areas of interest for the ground data collection, which was to be undertaken coincident with over-flights on the following flight days.

The brightness temperature data presented in this paper have been corrected to a reference time of 6am and reference incidence angle of 38deg, and filtered for data with an aircraft roll of more than 2.5°. The data were temporally corrected for diurnal changes in the effective soil temperature using the 6am temperature observed at 2.5cm at the base station as a reference (assuming its representativeness for the whole area – assumption to be verified during a second field experiment), and the ratio between the temperature at 6am to that measured at any other time (in Kelvin) as a scaling factor. The angular correction was performed by assuming that the ratio between the brightness temperature means of the different beams was spatially constant. Consequently, multiplying the observation at any one location with this ratio transfers the brightness temperature of the original beam to the reference beam. The data were finally binned onto a regular grid with a resolution of 1km, averaging all available observations within each pixel.

## 2.2. Ground-based Data

Ground data were collected for forward modelling (not presented here) and understanding of spatial variability in observed brightness temperature. Moreover, the forward modelling will serve as validation of the radiative transfer model and demonstrate the ability to predict the temporal response of the calibration site. The results from this analysis will be the topic of a future study, however, the ground data collected are briefly described here for completeness.

The ground-based measurements included base stations with temperature sensors installed at depths of 2.5, 5, 15, 25, and 40cm, soil moisture sensors at the surface (0-6 cm) and at 25cm depth, and a thermal infrared sensor for the skin surface temperatures. Additionally, surface soil moisture measurements were made for target transects of ~1km in length and 300m in width, using the Hydraprobe Data Acquisition System. Moreover, gravimetric soil moisture samples were taken for probe calibration, rock fraction samples and

Rüdiger *et al.*, Identification of Spaceborne Microwave Radiometer Calibration Sites

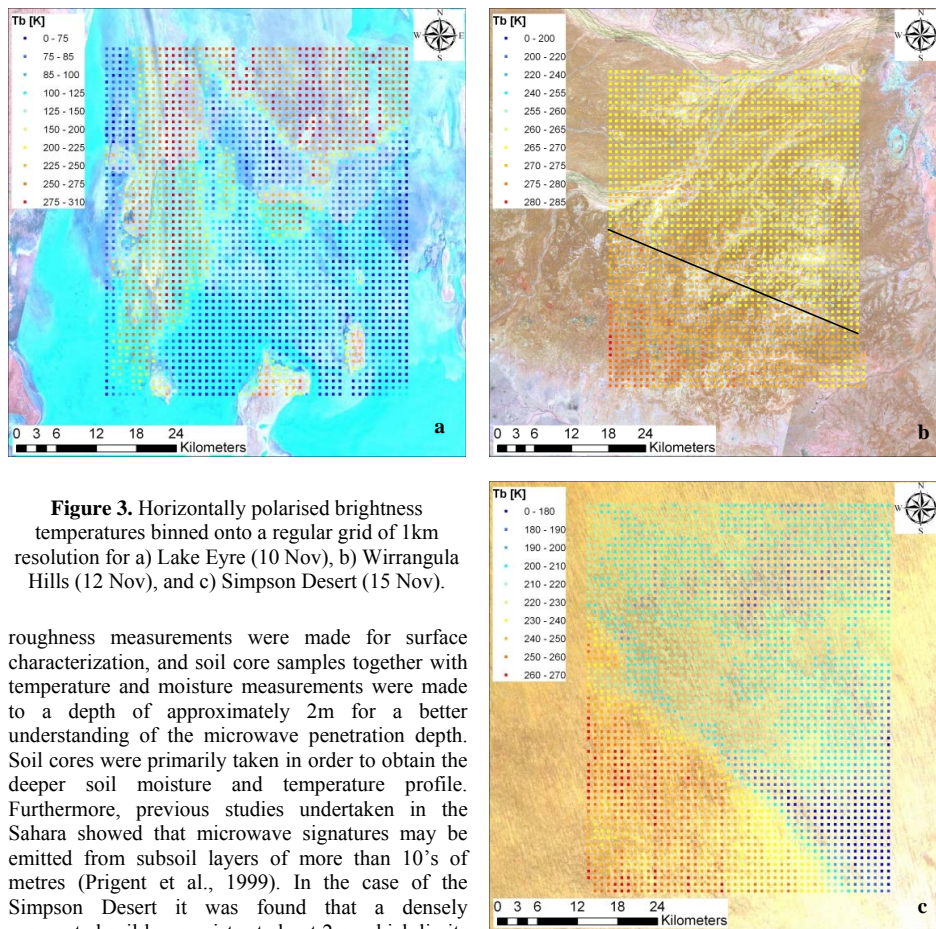


**Figure 3.** Horizontally polarised brightness temperatures binned onto a regular grid of 1 km resolution for a) Lake Eyre (10 Nov), b) Warrangula Hills (12 Nov), and c) Simpson Desert (15 Nov).

roughness measurements were made for surface characterization, and soil core samples together with temperature and moisture measurements were made to a depth of approximately 2m for a better understanding of the microwave penetration depth. Soil cores were primarily taken in order to obtain the deeper soil moisture and temperature profile. Furthermore, previous studies undertaken in the Sahara showed that microwave signatures may be emitted from subsoil layers of more than 10's of metres (Prigent *et al.*, 1999). In the case of the Simpson Desert it was found that a densely compacted soil layer exists at about 2m, which limits the observation depth to the profile above this layer. The surface roughness was determined, with a roughness board across 2m long transects oriented in north-south and east-west directions.

### 3. RESULTS AND DISCUSSIONS

Lake Eyre was hypothesized to represent a smooth and wet target having a homogeneous microwave response at mid-range brightness temperature, with the northern part of the Lake Eyre peninsula included to provide a land contrast. While the roughness measurements supported the smooth surface assumption (root mean square roughness of 1.35mm), the brightness temperature data showed unexpected results. The data suggest that the surface conditions of Lake Eyre are characterized according to two main types of response, brightness temperatures similar to those over land and a low brightness temperature response similar to that hypothesised (Fig. 3a). However, even the low brightness temperature response was lower than expected (mean value around 80K at H polarization), most likely due to the hyper-saline conditions that exist in the lake soil water. Moreover, the variability of brightness temperature across this low brightness temperature area is about 13K. The reason for this bi-modal response is not entirely clear, as access to Lake Eyre is very restricted without using a helicopter. However, the high brightness temperatures in the western and northern parts of the study region coincide with the areas receiving flood water from the Warburton and Cooper Creeks and the Diamantina River. The warm "tongue" in the north and west is the Warburton Groove, which receives the first flood water. As the flood waters enter Lake Eyre, sediments carried with the floods are deposited in this area. This apparently leads to a contrast in surface conditions, with potentially dry silt deposits in the north and moist hyper-saline conditions with a salt crust in the south. The only possible access

Rüdiger *et al.*, Identification of Spaceborne Microwave Radiometer Calibration Sites

to Lake Eyre from the west is via the Anna Creek Public Access Road (see Fig. 1), where it was found that the ground water level is immediately below the lake's surface, explaining the low brightness temperatures for this area.

The brightness temperature data obtained over the gibber areas of Wirrangula Hills showed a low variability in their brightness temperature response (3.3K; Fig. 3b and Fig. 4). This variability is within the requirements for a SMOS Cal/Val site (which is equivalent to the radiometric noise of the instrument of 2-4K; Kerr and Waldteufel, 2003). Moreover, the small brightness temperature gradient from the north-east to the south-west is possibly explained by the occurrence of a precipitation event that passed through the northern part of the focus area five days prior to the flight. The spatial variability in the brightness temperature observations is further reduced when separating the Wirrangula Hills observations into "wet" and "dry" (or radiometrically cool and warm) conditions. In this case, the variability of the brightness temperature to the north of the black line on Fig. 3b is 2.0K and to the south of the black line is 2.8K. Additionally, the high-resolution flight yielded a variability of 4.1K (5.2K during the reconnaissance flight).

The final flight was over the Simpson Desert (Fig. 3c). Unfortunately a significant precipitation event occurred over the north-eastern part of the focus area during the night of the 14<sup>th</sup> November, and continued throughout the flight on the morning of the 15<sup>th</sup> November. Due to the extreme remote location of this site and the distance from the operations airport, the aircrew was not aware of this unlikely rain event until arriving in the study area. Consequently, the brightness temperature response is bi-modal (Fig. 5). For the purpose of testing the hypothesis of a spatially homogenous brightness temperature response under dry conditions, it was assumed that no rainfall occurred in the south western part of the study site. However, the variability in brightness temperature for this area was 9.5K, which is still higher than that obtained for Wirrangula Hills, and well beyond the SMOS target requirement of 4K. To check the possibility that these results were affected by small amounts of rainfall across the south-western part, the brightness temperature variability was compared with that from the initial reconnaissance flight, which had a variability of 10.1K.

#### 4. CONCLUSIONS

This study has shown that the Wirrangula Hills area represents a possible warm on-orbit calibration target for SMOS, with an observed spatial variability of less than 4K. This value represents the SMOS requirement for sensor calibration accuracy. Such a warm calibration target will complement the proposed on-orbit calibration targets for colder temperatures, such as Dome-C in Antarctica and the Atlantic Ocean off New Foundland.

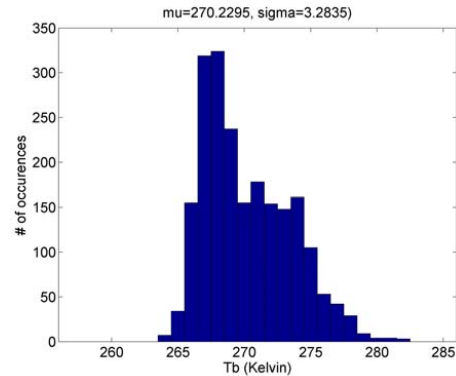


**Figure 4.** Frequency histogram of the gridded low-resolution brightness temperature data at Wirrangula Hill (12 November). The mean ( $\mu$ ) and standard deviation ( $\sigma$ ) are also given.

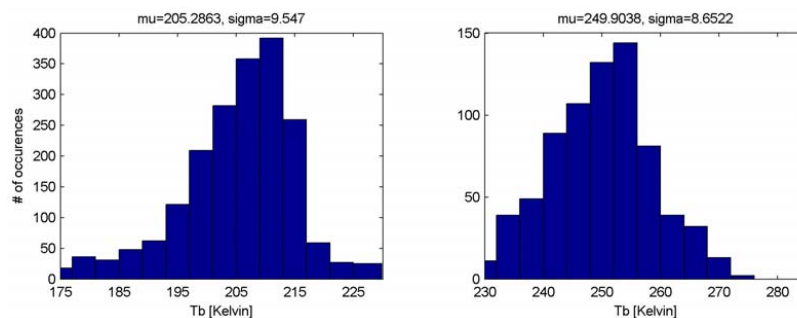


**Figure 5.** Frequency histogram of the gridded low-resolution brightness temperature data observed over the Simpson Desert (15 November). The mean ( $\mu$ ) and standard deviation ( $\sigma$ ) are also given.

Rüdiger *et al.*, Identification of Spaceborne Microwave Radiometer Calibration Sites

Lake Eyre is not a suitable target, due to its extreme bi-modal response at the spatial scale of a SMOS pixel. Moreover, even the hypothesized response from the moist salty areas of the lake had a brightness temperature variability of approximately 13K, which is more than three times that of the Wirrangula Hills site. Likewise the dry conditions of the Simpson Desert had a spatial brightness temperature variability of approximately 10K, being more than twice that of the Wirringula Hills site. Nevertheless, if the spatial variability were consistent and its mean constant throughout the seasons, the Simpson Desert may still be useful for warm target calibrations.

In order to confirm the spatial homogeneity of the Wirringula Hills site and the assumptions in relation to rainfall across the Simpson Desert, it is proposed that flights across these two regions be repeated during the winter of 2009, which is also likely to coincide with the post-launch calibration of SMOS. Consequently, these flights would be timed to coincide with SMOS overpasses. Moreover, to understand the temporal variation of these sites, in-situ soil moisture and temperature stations will be installed across the Wirringula Hills site in May. The proposed in-situ stations will provide the forward model input variables required to simulate the brightness temperature emissions from the surface. These modelled brightness temperatures can then be used for comparison with and subsequent calibration of the brightness temperatures observed by SMOS during its overpass of the site.

#### ACKNOWLEDGMENTS

This study was funded by the Australian Research Council (DP 0879212). Permission for data collection in the Simpson Desert National Park and the Lake Eyre Regional Reserve was granted through a South Australian Research Permit. Access and accommodation at Wirrangula Hills was provided by Trevor Williams. The authors also wish to thank Susan Hayes, Vjeko Matic, Peter Richards and Graeme Tomlinson for their participation in the field campaign, and Opal Air for providing hangar space at Coober Pedy airport.

#### REFERENCES

- Brown, S.T., and C.S. Ruf (2005), Determination of an amazon hot reference target for the on-orbit calibration of microwave radiometers. *Journal of Atmospheric and Ocean Technologies*, 22(9), 1340-1352.
- Brown, M.A., F. Torres, I. Corbella, and A. Colliander (2008), SMOS calibration. *IEEE Transactions on Geoscience and Remote Sensing*, 46(3), 645–658.
- Burrage, D., J. Wesson, and J. Miller (2008), Deriving sea surface salinity and density variations from satellite and aircraft microwave radiometer measurements. *IEEE Transactions on Geoscience and Remote Sensing*, 46(3), 765–785.
- Delwart, S., C. Bouzinac, P. Wursteisen, M. Berger, M. Drinkwater, M. Martin-Neira, and Y.H. Kerr (2008), SMOS validation and the COSMOS campaigns. *IEEE Transactions on Geoscience and Remote Sensing*, 46(3), 695–704.
- Ferrazzoli, P., L. Guerriero, and J.-P. Wigneron (2002), Simulating L-band emission of forests in view of future satellite applications. *IEEE Transactions on Geoscience and Remote Sensing*, 40(12), 2700–2708.
- Kerr, Y., P. Waldteufel, J.-P. Wigneron, J.-M. Martinuzzi, J. Font, and M. Berger (2001), Soil moisture retrieval from space : The soil moisture and ocean salinity (SMOS) mission. *IEEE Transactions on Geoscience and Remote Sensing*, 39(8), 1729–1735.
- Kerr, Y. and P. Waldteufel (2003), Note on SMOS calibration and validation. Cesbio Technical Report, [www.cesbio.ups-tlse.fr/data\\_all/SMOS-doc/SO2b.pdf](http://www.cesbio.ups-tlse.fr/data_all/SMOS-doc/SO2b.pdf), last accessed on 23 March 2009
- Macelloni, G., M. Brogioni, P. Pampaloni, M. Drinkwater, and A. Cagnati (2006), DOMEX 2004: An experimental campaign at Dome-C Antarctica for the calibration of space-borne low-frequency microwave radiometers. *IEEE Transactions on Geoscience and Remote Sensing*, 44(10), 2642–2653.
- Macelloni, G., M. Brogioni, P. Pampaloni, and A. Cagnati (2007), Multifrequency microwave emission from the Dome-C area on the East Antarctic Plateau: Temporal and Spatial Variability. *IEEE Transactions on Geoscience and Remote Sensing*, 45(7), 2029–2039.
- Prigent, C., W.B. Rossow, E. Matthews, and B. Marticorena (1999), Microwave radiometric signatures of different surface types in deserts. *Journal of Geophysical Research*, 104, 12147-12158, doi: 10.1029/1999JD900153.
- Wentz, F.J., C. Gentemann, and P. Ashcroft, On-orbit calibration of AMSR-E and the retrieval of ocean products. *Proceedings of the 83<sup>rd</sup> American Meteorological Society Annual Meeting*, Long Beach, CA.